UNIVERSITY OF BIRMINGHAM

Understanding and assessing the probability of oat lodging with respect to current and future climates

By

Mohammadreza Mohammadi

A thesis submitted to the University of Birmingham for the degree of

DOCTOR OF PHILOSOPHY

School of Civil Engineering

College of Engineering and Physical Sciences

University of Birmingham

Edgbaston, Birmingham

B15 2TT

United Kingdom August 2021

Abstract

This research aims to examine lodging (the failure of crops by wind and rain) in oats and hence to improve the understanding of lodging resistance for this particular crop. The applicability of a lodging model combining meteorology, agronomy, and engineering to describe lodging in oats is examined and the assumptions embodied in the model are evaluated. In order to provide supporting data to examine the lodging model, a number of field experiments were undertaken which were carried out in the Republic of Ireland to investigate the dynamic/aerodynamic parameters (natural frequency, damping ratio, and drag area). Moreover, standard husbandry treatments were applied on crops to provide realistic conditions for growing oats and to ensure that the outcomes are broadly applicable. A number of agronomic measurements were undertaken to provide the required input data for the lodging model. Consequently, the results of agronomic and dynamic/aerodynamic data enabled the lodging model to be modified/calibrated for oats and systematic parametric analysis of influential parameters was undertaken. It is demonstrated that the drag area is the most influential factor for both stem and root lodging. Additionally, stem yield stress and the number of stems per plant in the case of stem lodging, and the root diameter for root lodging, are identified to

have crucial roles. Furthermore, through calibrating anchorage system failure models, it is found that both root diameter and depth are influential in the failure anchorage resistance in oats. This research also shows crop growth and panicle interlocking in the last growth stages, causes a decrease in the natural frequency and damping ratio but increases the drag area, which results in a higher probability of lodging in the growth stages before the harvest. Moreover, using a combination of resistant variety with low seeding rate, low nitrogen rate and Plant Growth Regulator (PGR) application, are found to effectively reduce the lodging likelihood.

The lodging model was also used to evaluate the lodging probability by using the wind and rainfall cumulative density functions (CDFs). In order to evaluate the wind and rainfall CDFs, the historical data for June and July (the period corresponding to key lodging season) from 38 meteorological stations in the British Isles, are studied. Additionally, climate projections for the next six decades in the United Kingdom and the Irish Republic generated by the UK climate change projections (UKCP18) are examined and future wind and rainfall CDFs are identified. Results show that the projected climate changes during the peak growing period (June to July) in the next three decades are in the range which might occur as a result of different management/plant varieties.

Acknowledgements

I wish to express my sincere gratitude to my supervisors Professor Mark Sterling and Professor Chris Baker for their consistent support and guidance during the running of this project. I have greatly benefitted from their knowledge and supervision, which has inspired and encouraged me through this process. They graciously contributed their time, which has always ended up as a key element of my research and has greatly improved this work. I also wish to express my gratitude to Dr Pete Berry, Professor Nigel Wright, Dr Mike Jesson and Dr John Owen for their insightful comments and supports.

Further I would like to thank my supervisor from Teagasc, Dr John Finnan, who passed away in an aircraft accident last October. His expertise and input were instrumental in the agricultural elements of the research. His generous availability, during the field test, helped me to overcome all challenges in the experiments. I would like to thank Mr. John Spink for his support during the last years and accepting to supervise the project.

Thanks, are expressed to Teagasc and Walsh Fellowship for funding the project and creating a welcoming environment. I am thankful to Meteorological office and Met Éireann that provided their data free of charge.

And my biggest thanks to my wife, Maedeh, to have her patience and love throughout my life. To Mum and Dad, for all their unconditional support. To Moona, Hoda, and Alireza, my dear siblings for their kindness and help.

Thank you everyone!

Dedication

To my wife

Maedeh

For your love, patience and heart-warming words

To my family

For your constant support and reassurance over the years.

Contents

List of Figures

List of Tables

1.Introduction

1.1.The Problem and motivations

Lodging, the failure of plants either at the roots or along the stem, is a significant problem for the agricultural sector worldwide. (Baker et al., 2014; Berry et al., 2004; Kendall et al., 2017; Sterling et al., 2003; van Heerden, 2015; Zhang et al., 2014). The losses that can arise from lodging can be considerable. For example, the annual loss attributed to lodging in maize is about 40% of the worldwide yield (Flint-Garcia et al., 2003). The cost of lodging in winter wheat is ~£65m each year (Berry et al., 1998; Berry and Spink, 2012) whilst the average annual loss in cereals and oil seed rape is estimated to be ~£50m and can increase to ~£170m if adverse weather conditions occur (Berry et al., 2004).

Yield loss can occur in lodging through a number of different mechanisms. For example, lodging decreases the photosynthetic capacity of the crops and therefore reduces biomass production (Wu and Ma, 2019). A lodged canopy inhibits the regular transportation of nutrients and water through organic vessels and receives less solar radiation, both resulting in a higher risk of diseases and pests (Jellum, 1962; Berry et al., 2004; Wu et al., 2012; Wu and Ma, 2016; Wu and Ma, 2019). In addition to yield loss, lodging reduces grain quality, raises drying costs, and increases the harvest time (Berry et al., 2004; Crook and Ennos, 1993, Baker et al., 2014). Thus, the impacts of lodging are manifold.

A common way to reduce lodging is through the application of Plant Growth Regulators (PGRs) – a series of treatments that can either inhibit or enhance the plant's growth. In the

UK, almost 90% of wheat and more than 50% of oil seed rape is subject to PGRs (Berry et al., 2004). PGR chemical applications are expensive (£15-20m is spent annually in the UK) and extensive application increases the risk of chemicals remaining in the final yield (Berry et al., 2004).

Lodging is not a simple process and crop varieties (which represent a group of plants from a crop species with a common set of characteristics (United Nations Information Portal, 2021)) can have varying degrees of susceptibility to lodging. Furthermore, different agronomic husbandry techniques (e.g., seed rate and Nitrogen applications) can also positively and negatively affect a plant's likelihood to lodge (Berry et al., 2002). In order to guide effective agronomic husbandry techniques, accurate information about the probability of lodging in different meteorological and agronomic conditions is required. Furthermore, it is also unclear how different plant parameters affect the lodging process, particularly for oats, hence the focus of this study.

Although oats have a tendency to lodge (White et al., 2003; Wu and Ma, 2019), the crop has attracted considerable attention when it was discovered as a good source of vitamins, minerals, and antioxidants, reducing cholesterol level and lowering blood sugar (Rasane et al., 2015; Wu and Ma, 2019). Due to this high demand, approximately 9% of crop tillage areas in Ireland are cultivated for oats, producing 7-8 tons per hectare (Gillespie et al, 2016).

Oat lodging can occur due to adverse weather conditions, i.e. high rainfall and strong winds (Baker et al., 2014), the likelihood of which may change in the future (Meteorological Office, 2019). Nevertheless, it is unknown how changes in the climate might affect the lodging likelihood (Baker et al., 2014). The effect of such changes is examined in this research.

1.2.Aim and objectives

The aim of this research is to examine lodging in oats and hence to improve the understanding of lodging resistance for this particular crop through the application of an analytical model. In relation to this five objectives were devised:

1. To conduct a critical literature review focusing on crop lodging and modelling, and to evaluate the agronomic factors which might influence the likelihood of lodging.
2. To explore the lodging process in oats and, if appropriate, to assess, modify and calibrate an existing lodging model (i.e. Baker et al., 2014) through the collection and application of experimental data obtained from fieldwork.
3. To undertake a parametric analysis in order to understand the crop parameters that influence lodging the most.
4. To apply the modified and calibrated oat lodging model, to understand the potential impact of climate change on lodging resistance.
5. To identify the most appropriate plant parameters in order to reduce the likelihood of lodging in oats and to provide recommendations concerning the appropriate husbandry techniques which may result in such plant parameters.

1.3.Methodology

To achieve the objectives mentioned in Section 1.2, this research has been split into various steps.

First, a critical literature review was undertaken to consider the lodging models adopted for other types of crops and to identify any influential factors in lodging. Later, the existing crop lodging model (Baker et al. 2014), was critically examined for the assumptions embodied within it. Subsequently, an extensive meteorological data analysis was undertaken to examine

the probabilistic assumptions in the theoretical lodging model (Baker et al. 2014) and to find more accurate representative mathematical expressions.

Following the above work and in order to calibrate the model an extensive database was obtained from field trials. Hence, several experimental campaigns were developed to collect extensive agronomic data and to observe the crops for lodging events. This stage enabled the development of a database of agronomic data grown in a wide range of husbandry techniques as well as a record of the lodging events. Next, a non-intrusive method was designed to 'observe' the interaction of wind with crops without disturbing the natural condition of the canopy and hence to evaluate the parameters related to the dynamic movement of the plant. Subsequently, the agronomic database and the parameters related to the dynamic movement of the crop were incorporated into the model to assess the ability of the model to predict lodging specially and temporally, in comparison to the lodging observations.

Finally, the modified and calibrated model was used together with the latest climate projections (obtained from the UKCP18 climate projector) to evaluate the plausible variation of lodging probability in the future climate conditions and to compare it with the range of variations in the current climatic conditions. Additionally, the updated oat lodging model enabled a parametric analysis to be undertaken which eventually provided practical recommendations for the agronomic sector through the identification of the most influential plant parameters and husbandry techniques to avoid lodging.

1.4.Layout of the thesis

The chapters and contents of this thesis are organized as follows:

- Chapter 2 outlines the current literature and provides the relevant background information, including wind interaction with plants, the theory of turbulent flow over

plant canopies, lodging models, parameters associated with oat lodging, and the fundamental information about climate change and its potential effect on lodging.

- Chapter 3 describes the methodology used for the experiments including the experimental setup, field site information, and the agronomic measurements.
- Chapter 4 presents the experimental data in terms of velocity spectra and plant displacements due to the action of the wind as well as data analysis to obtain parameters related to dynamic movement of the crop including damping ratio, natural frequency and drag coefficient.
- Chapter 5 outlines the meteorological parameters (wind and rain) and discusses how historical data were analysed to obtain wind and rainfall cumulative density functions (CDF) and presents the future projections for climate conditions in the British Isles and potential changes in the lodging probability.
- Chapter 6 integrates the model and the experimental data obtained via the field trials, and in doing so identifies the most influential parameters in oat lodging.
- Chapter 7 presents a number of conclusions that have been made in support of the overall aim and objectives. Additionally, it highlights further aspects of the research which can be further developed in the future and provides some recommendations for future works.

2.Literature review

2.1. Introduction

This chapter provides a critical review of the existing literature relevant to the research undertaken. Section 2.2 introduces lodging models which have been used for different crops. Section 2.3 discusses how wind flows over plant canopies and Section 2.4 discusses statistical methods to analyse the turbulent flow over plant canopies. Section 2.5 focuses on relevant research relating to climate change and explores the meteorological parameters which can potentially influence lodging in oats, and introduces the latest climate change projectors for the British Isles. Finally, Section 2.6 provides conclusions and identifies relevant gaps in the literature.

2.2.Modelling Lodging

2.2.1.Theoretical lodging models

2.2.1.1.Lodging fundamentals

Although lodging has been studied for more than 40 years (Berry et al., 2004), this has only been analytically modelled by a small number of researchers - Baker (1995) and Baker et al. (2014). The main concept of these models was to consider the crop to act as a damped harmonic oscillator that interacts with both the wind and soil. In both models, the bending

moment applied on the plant by the action of the wind was compared with stem or anchorage resistance provided by the plant or the soil/root interaction. Stem lodging occurs when the applied bending moment at a particular point along the stem exceeds the natural bending resistance provided by the plant. In wheat and oat, stem lodging typically occurs at the bottom (first) internode which causes the stem to lie horizontally (Berry et al., 2004). It is worth noting that in both crops, the stem tends to contain between 4 and 6 solid points called nodes connected by internodes which are hollow cylindrical sections of the stem. In most plants, lodging tends to occur at the middle of the first (bottom) internode, which is the most susceptible point at the stem. However, in barley, lodging can occur at either the top, middle, or bottom of the stem as the structure of the stem is different from that of oat and wheat. Root lodging occurs when the applied bending moment exceeds the anchorage resistance (Baker, 1995; Baker et al., 1998). The influential parameters on both stem and anchorage (root/soil interaction) resistance are described in Section 2.2.1.2.

Comparing these models, the most recent lodging model, also known as the generalized model (Baker et al., 2014), used a number of more realistic assumptions (described later in this paragraph) which made it potentially suitable to be applied to different kinds of crops including wheat, oat, oil seed rape (OSR) and barley. Firstly, in the generalized model, the interactions of crops in canopies have been considered, while Baker (1995) assumed plants to act as single shoots. In the 1995 model, Baker represented turbulence by a simple step change in the velocity which was taken to be representative of the maximum gust that would be expected every hour. In the generalised model, the velocity spectrum was calculated to ensure a greater scale of turbulent fluctuations could be taken into account. Using the velocity spectrum, the bending moment spectrum was ultimately established. Finally, the generalised model was not based on meteorological data from a specific site (unlike the 1995 model) and therefore could use a wide range of climate data from different geographic locations.

2.2.1.2. The generalized lodging model

The generalised crop lodging model developed by Baker et al. (2014) is illustrated schematically in Figure 2.1. The model evaluates the influence of interactions of an interlocked canopy in the calculations and uses the wind fluctuations to solve the dynamic equation of motion, which gives the bending moment values along the stem. Using the determined values of plant/soil properties and the wind loading (see below), the model can be provided to identify the theoretical value of bending moment. If the identified bending moment exceeds anchorage/stem resistance, then root/stem lodging will happen.

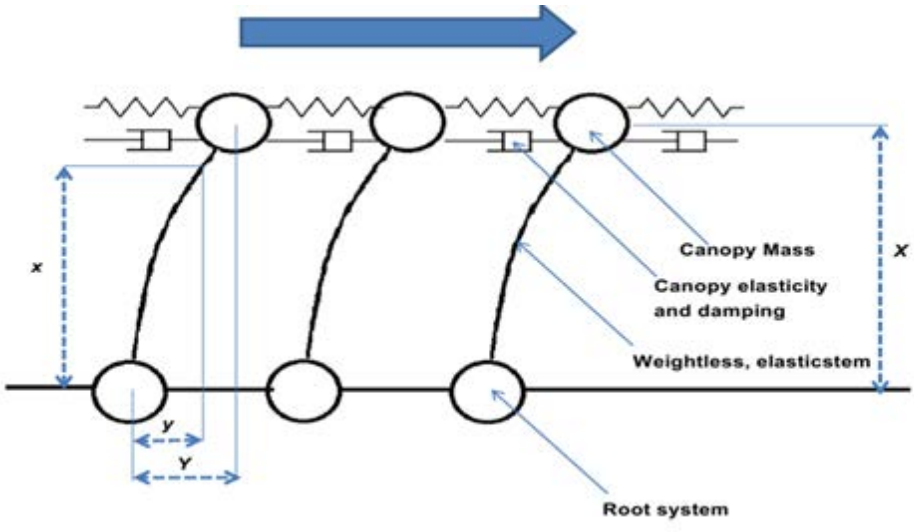

Figure 2.1. System model in the generalized model (Baker et al., 2014)

Wind is a deterministic factor in lodging as it applies a drag force on the canopy which can cause failure from the stem or root. The drag force applied on a plant can be expressed as follows (Baker et al., 2014; Gardiner, 2016):

$$\bar{F} = \frac{1}{2} A C_F \rho \bar{U}^2 \quad (2\text{-}1)$$

Where $\bar{F}$ is the mean drag force, A is the projected area of the plant, C_F is the drag coefficient, $\bar{U}$ is the mean wind speed and ρ is the air density. It is difficult to measure the drag coefficient and plant area separately due to the deflection of the plant under wind loading, hence these two parameters are often reported as a single parameter, i.e., AC_F (Gardiner, 2016).

Baker et al. (2014) showed that the mean bending moment ($\bar{M}$) can be expressed as:

$$\bar{M} = \frac{\left(1+\omega_n^2\left(\frac{X}{g}\right)\right)(0.5\rho AC_F X)\left(\cos\left(\alpha\frac{x}{l}\right)-cot\alpha\,\sin\left(\alpha\frac{x}{l}\right)\right)}{\omega_n^2\left(\frac{X}{g}\right)}\,\bar{U}^2 \tag{2-2}$$

where ω_n ($= 2\pi f_n$, f_n is the natural frequency) is the angular frequency, X is the height of the centre of mass of the canopy, g is the gravitational acceleration, x is the distance up the stem from the ground, ρ is the air density, AC_F is the plant drag area, l is the length of stem, and α is a constant determined from the following equation:

$$\alpha = \frac{3}{\omega_n^2\left(\frac{X}{g}\right)} \tag{2-3}$$

Additionally, the peak bending moment ($\widehat{M}$) can be described as the mean bending moment ($\bar{M}$) plus two components of fluctuations, a broadband component, which follows the fluctuating wind and a resonance component which happens when the plant is oscillating at frequencies near natural frequency as follows:

$$\widehat{M} = \bar{M} + ((g_{MB}\sigma_{MB})^2 + (g_{MR}\sigma_{MR})^2)^{0.5} \tag{2-4}$$

Where, g_{MB} and g_{MR} are the peak factor of the broad banded moment and the peak factor of the resonant moment respectively. Additionally, σ_{MB} and σ_{MR} are the standard deviation of the broad band moment and the resonant moment respectively. Baker et al., (2014) suggested the following expressions for these parameters:

$$g_{MB} = 0.42I \ln(\frac{3600}{\tau}) \quad (2\text{-}5)$$

$$g_{MR} = (2\ln(3600f_n))^{0.5} + \frac{0.577}{(2\ln(3600f_n))^{0.5}} \quad (2\text{-}6)$$

$$\sigma_{MR}^2 = \bar{M}^2 I^2 (\frac{\pi}{4\theta}) \quad (2\text{-}7)$$

$$\sigma_{MB}^2 = 4\bar{M}^2 I^2 \quad (2\text{-}8)$$

Where I is the turbulence intensity, θ is the damping ratio, and τ is the averaging time. The peak bending moment was later compared with stem strength (S_s) for stem lodging or anchorage resistance (R_s) for root lodging and if the moment exceeds stem resistance the plant was considered as 'lodged' from stem or root. Thus, lodging happens if $\widehat{M} > S_s$ for stem lodging and $\widehat{M} > R_s$ for root lodging, where S_s and R_s were proposed to be calculated as in equation 2-9, 2-10 and 2-11:

$$S_s = (\frac{\sigma\pi a^3}{4})(1 - \left(\frac{(a-t)}{a}\right)^4)n \quad (2\text{-}9)$$

Where σ is the stem yield stress, a is the stem radius, t is the stem wall thickness and n is the number of stems per plant. Equation 2-9 is calculated based on the bending moment for a hollow cylinder.

$$R_s = \gamma S d^3 \quad (2\text{-}10)$$

In equation 2-10 d is the effective root diameter, which is the point where most of the rigid roots end (Berry et al., 2000), S is the soil shear strength and γ is a constant and is unique for each crop (Baker et al., 2014). Additionally, there is an alternative expression for root anchorage model as follows:

$$R_s = \gamma S d^2 L \quad (2\text{-}11)$$

Where L is the root depth and the rest of the parameters are as mentioned in equation 2-10. These two expressions (equations 2-10 and 2-11) were proposed by Crook and Ennos, (1993) and Goodman et al. (2001) respectively. The earlier expression assumed the root plate moves downwards into the soil so the anchorage failure moment can be derived through multiplying the soil reaction force by *d/2*. Alternatively, Goodman et al. (2001) suggested the anchorage system failure causes soil compaction around the root and the anchorage system failure moment can be obtained by multiplying this reaction force by the root depth. In both cases, the soil reaction force was assumed to be proportional with d^2. From a mathematical/physical perspective in both equations, the failure anchorage moment is proportional to the volume of the root system, while in equation 2-10 the anchorage system has a spherical shape, and in the equation 2-11, the root system is assumed in a conical shape.

Crook and Ennos (1993) stated a relatively low coefficient of determination (R^2=0.41) between the root diameter and the anchorage failure moment and concluded other parameters

might be important to anchorage. The simplicity of the expression was also emphasized by Baker et al. (1998), Berry et al. (2006), and Sposaro et al. (2010). Nonetheless, an alternative expression (equation 2-11 or any other expression) has been never examined in a lodging model and Section 4.6 examines this through collected data for oat samples.

In order to obtain expressions for lodging velocities, Baker et al. (2014) assumed, τ=1s in stem lodging (based on lodging observations by Sterling et al. (2003)), I=1 and f_n=0.8. Consequently, the peak factors could be assumed as: g_{MR}=4.15 and g_{MB}=3.43. Similarly, root lodging observations by Sterling et al., (2003) showed root lodging happens over a timescale of minutes (i.e. τ=60s). The resonant component is not applicable here and the broadband peak factor denominates and was assumed as g_{MB}=1.72, where I=1. Consequently, the stem and root lodging velocities were derived as:

$$\overline{U}_{Ls} = \left(\frac{\omega_n^2\left(\frac{X}{g}\right) S_S}{\left(1+\omega_n^2\left(\frac{X}{g}\right)\right)(0.5\rho A C_F X)\left(\cos\left(\alpha\frac{x}{l}\right)-cot\alpha\,\sin\left(\alpha\frac{x}{l}\right)\right)(1+\,6.86I\,\left(1+0.366\left(\frac{\pi}{4\theta}\right)\right)^{0.5}}\right)^{0.5} \quad (2\text{-}12)$$

$$\overline{U}_{LR} = \left(\frac{R_S}{\frac{((1+\omega_n^2\left(\frac{X}{g}\right))}{\omega_n^2\left(\frac{X}{g}\right)}(0.5\rho A C_F X)(1+3.44I)}\right)^{0.5} \quad (2\text{-}13)$$

Chapter 4 will show the values assumed for natural frequency and the turbulence intensity are potentially crop-specific and appropriate values need to be taken into account for different crops. Section 3.2 will suggest alternative expressions for stem and root lodging velocities.

Equations 2-12 and 2-13 appears complex, however, it shows the stem failure wind speed is based on factors which can physically be determined and summarized as follows:

$\overline{U}_{Ls}$=Function $(\sigma, a, t, n, X, l, f_n, AC_F, I, \theta)$ (2-14)

$\overline{U}_{LR}$ =Function $(S, d, L, f_n, X, AC_F, I, \gamma)$ (2-15)

Parameters such as the stem yield stress (σ), the stem radius (a), the stem wall thickness (t) and the number of stems per plant (n), the centre of gravity (X), the length of stem (l), the root diameter (d), the root depth (L) can be calculated through agronomic methods proposed by Berry et al. (2000), which will be described in Chapter 3. However, the natural frequency, the damping coefficient, the turbulence intensity, and the plant drag area have to be determined from more complicated methods related to the flow over the canopy, the dynamic motion of the crop, and the interaction of wind with crops, which will be described in Chapter 4.

Baker et al. (2014) showed the contribution of wind and rainfall in the lodging process can be represented as a curve to determine lodging/no lodging occurrence as follows (this equation is derived from equation 2-4 and the calculation procedure is fully presented in Appendix A):

$$i = (1 - \frac{\overline{U}^2}{\overline{U}_{LR}^2}) i_0 \quad (2\text{-}16)$$

Where i is daily rainfall, i_0 is reference rainfall corresponding to zero wind speed. Figure 2.2 demonstrates graphically the probabilistic framework and the curve (equation 2-16) where the vertical axis shows the daily rainfall (i) and the horizontal axis is the hourly mean wind speed ($\overline{U}$) (Baker et al., 2014). The figure shows if the wind speed is less than saturation velocity ($\overline{U}_s$), equation 2-17, lodging will not typically occur. In higher wind speeds,

depending on the wind and rainfall conditions, root/stem lodging or both are likely to occur (Baker et al., 2014).

$$\overline{U}_s = \overline{U}_{LR}(1 - \frac{i_s}{i_0})^{0.5} \quad (2\text{-}17)$$

Where $\overline{U}$ represents the hourly mean wind speed and i represents the rainfall – the subscripts s and 0 represent the saturation rainfall and daily rainfall respectively. Equation 2-16 is represented graphically in Figure 2.2 and is dependent on a variety of dynamic/aerodynamic and biological parameters, i.e., the dashed lines should be viewed as illustrative only.

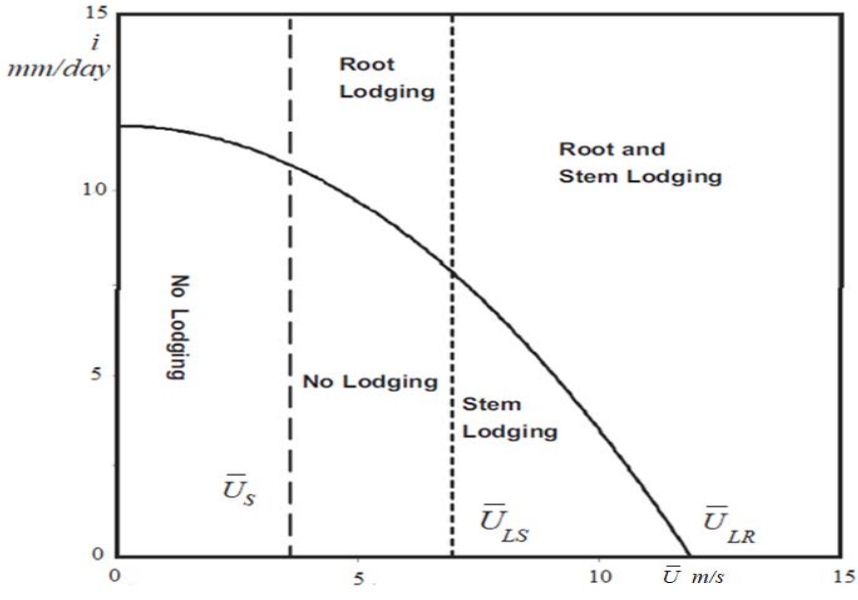

Figure 2.2. Lodging conditions in different daily rainfall and hourly mean wind speed conditions for a sample oat plant

In order to obtain the lodging probability expressions for rainfall and wind probability density functions (PDFs), Baker et al. (2014) suggested Rayleigh and the exponential distributions for wind and rainfall PDFs respectively (equations 2-18 and 2-19).

$$p(\bar{U}) = (\frac{2}{\lambda})(\frac{U}{\lambda})e^{-(\bar{U}^2/\lambda)} \quad (2\text{-}18)$$

$$p(i) = (\frac{1}{m})e^{-(i/m)} \quad (2\text{-}19)$$

In these equations, $P(\bar{U})$ and $P(i)$ are the PDFs for the mean hourly wind speed and (daily rainfall) respectively. In addition, λ is a parameter that is related to the wind climate and m is the mean daily rainfall (Baker et al., 2014).

Although at the time, both equations 2-18 and 2-19 were appropriate representations, Baker et al. (2014) acknowledged the necessity of further investigations to check if these expressions are convenient functions for wind and rainfall PDFs. Chapter 5 will show these expressions are not as accurate as first thought, although these expressions have implications for the analytical form of lodging probability (Baker et al., 2014). Alternatively, when a calibrated lodging model is available and representative PDFs (or the integrated form-Cumulative Density Functions, CDFs) are available the probability of lodging can be derived numerically. The procedure is described in Section 5.5.1.

2.2.2.Lodging in wheat

2.2.2.1.Modelling and agronomic approaches

Studying lodging in wheat attracted considerable attention in the 1990s and 2000s in the UK. As previously discussed, in Baker's 1995 model (Baker, 1995) plants were considered as

single shoots, which could represent wheat canopies. The work was followed by a variety of agronomic research in the UK, for example, Griffin (1998), Berry (1998), and Berry et al. (2000), as well as a study on aerodynamic properties of wheat by Sterling et al. (2003). These data were used to calibrate the model for wheat by Baker et al. (1998) and Berry et al. (2003). It is worth noting that Baker's model was also used to calibrate a lodging model for wheat in Mexico by Pinera-Chavez et al. (2016).

Berry (1998) and Berry et al. (2000) investigated the effect of using different treatments including sowing time, seed rate, soil nitrogen rate, PGR application, and Nitrogen timing on the wheat lodging. Results of this research showed that various husbandries can affect lodging-related parameters in the crops. Moreover, agronomic measurements (measuring lodging-related plant parameters including stem radius, stem diameter wall thickness, etc.) before the peak lodging season can provide the data needed to predict future lodging-related parameters and hence to anticipate the lodging likelihood. Additionally, these researchers provided methods and protocols to measure natural frequency, root diameter, stem yield strength, etc. for the first time. These protocols for agronomic measurements are used in the current research and will be described in Chapter 3.

Baker et al. (1998) was one of the primary studies to calibrate the lodging model for wheat, where supporting agronomic measurement data were supplied by Griffin (1998), while dynamic/aerodynamic parameters were not experimentally measured and were mainly estimated. Nevertheless, it was the first time that the outputs of Baker's model (Baker, 1995) were compared with experimental data to rank different treatments applied on crops. The research also developed a probabilistic framework based on PDFs for wind and rainfall. As real meteorological data was not available at the time, Monte Carlo simulations were used to

generate random wind and rain data based on Weibull and exponential distributions for wind and rainfall PDFs respectively. In the current research, the methods described in Baker et al., (1998) are used in Chapter 6 to evaluate the capability of the lodging model to rank different husbandry techniques based on susceptibility to lodging. Additionally, real meteorological data have been used to evaluate wind and rainfall probabilities and consequently the probability of lodging.

2.2.2.2.Aerodynamic approach to study lodging in wheat

Sterling et al. (2003) was the only work to study the crops from an aerodynamic perspective. Sterling et al. (2003) undertook full-scale wind tunnel experiments in a naturally grown wheat field to study the crop's dynamic movements. Although the method provided the opportunity to observe lodging for the first time and successfully calculated some parameters related to the dynamic movement of the crop such as natural frequency, damping ratio, and drag coefficient, the research had some limitations. Firstly, the method used to measure natural frequency involved isolating the plant's stem and displacing it in the field. The number of oscillations in time could indicate the natural frequency. Nevertheless, such a field test must be undertaken in a calm, isolated condition and could be disturbed by surrounding conditions.

An alternative method to measure this parameter was using the dynamic response of the plant due to the action of wind loading. Accordingly, strain gauges were attached to the plant's stem and the associated spectra were analysed to obtain both natural frequency and damping ratio. Despite the difficulties associated with attaching strain gauges to sensitive structures like crops, the research successfully determined both parameters through the spectra and the transfer function. Although such a method might not be appropriate for other crops which

create interlocked canopies like oat. Also, attaching strain gauges might affect the dynamic movement of crops.

Moreover, the research provided some data to compare turbulent flow conditions generated in the wind tunnel versus natural conditions, which showed several turbulent flow characteristics including longitudinal, lateral, and vertical turbulence intensities as well as the ratio of maximum to mean velocity measured in the wind tunnel are lower than those measured in natural conditions. The results showed the gust plays a less important role in the wind tunnel in comparison to real conditions, the maximum gust values are lower than natural conditions and the lateral fluctuations are not well produced in the wind tunnel. Nonetheless, comparing these values with Finnigan (2000) indicated values measured in the wind tunnel were in the correct order of magnitude. Finally, in order to identify the dynamic loading on the plants, strain gauges were attached to the stem shoots. In order to attach the strain gauges, not only were the surrounding plants inevitably disturbed but changes to the local properties of the stem could have resulted – the stem's surface was roughened, and strain gauges were subsequently glued. Thus, there is the possibility that this could have affected the dynamic movement of the crop. Overall, the study was important in lodging research as it proved the oscillatory nature of crops experimentally and observed the lodging occurrence for the first time. Subsequently, the non-intrusive approach which is used in this research (Section 3.4) can cause less disturbance to the natural movement of crops in comparison to the approach used by Sterling et al. (2003).

2.2.2.3.Calibration and application of lodging models for wheat

Berry et al. (2003) calibrated a lodging model for wheat. The model outputs were compared with experimental lodging observations to consider the spatial dissimilarity between wheat plants and temporal variation in the crop structure through the peak lodging season. Results

showed an encouraging agreement in the percentage of lodged area predicted by the model through the season and the lodging observations. The model was also capable of appropriately ranking different agronomic treatments applied on wheat, based on their susceptibility to lodging. These methods are used in this research (Chapter 6) to evaluate the lodging model outputs. A parametric analysis showed stem diameter and root diameter are the major influencing parameters in stem and root lodging respectively. Nevertheless, the results from the model were not ideal: the model generally under-predicted the root lodging and over-predicted the lodging for the low lodging risk crops.

In a similar work with Berry et al. (2003), Pinera-Chavez et al. (2016) calibrated a model for wheat in Mexico. The model and the approach used were mainly the same as those used in the UK. Accordingly, crops were grown under different treatments, their agronomic parameters (stem wall thickness, root diameter, etc.) were measured and meteorological conditions in the site were monitored. All the collected data were used to calibrate Baker's 1995 model. It is worth noting that the dynamic/aerodynamic parameters (damping ratio and drag coefficient) were assumed the same as measured by Sterling et al. (2003). Nevertheless, due to differences in geographic locations and meteorological conditions, this assumption might not be correct.

2.2.3.Application of lodging for barley

Baker's lodging model (Baker, 1995) was also applied and calibrated for barley by Berry et al. (2006), which particularly focused on stem failure from middle internodes (brackling) and from failure near the ear (necking). Nevertheless, this research developed Baker's 1995 model mainly from an agronomic perspective and relied on estimations (based on values obtained for wheat) for dynamic/aerodynamic parameters. Moreover, despite the earlier work

for wheat (Berry et al., 2003), this paper did not provide any results to show if the model was capable of predicting lodging throughout the growing season or whether the model can rank different treatments. Results of this research indicated the stem lodging velocity on average is lowest at the middle of barley stem (the stem structure in barley is very unusual and is more susceptible from middle and top rather than the stem base as other plants) and the root anchorage system has major similarities with wheat in both shape and size. The parametric analysis showed stem diameter is the major agronomic parameter affecting stem lodging, however, the plant tends to be more vulnerable at the middle of the stem rather than stem base. Nevertheless, the research did not investigate parameters related to dynamic motion including drag coefficient and damping ratio and relied on estimates for these parameters.

2.2.4.Application of lodging for sunflower

Sposaro et al. (2010) used Baker's model (Baker, 1995) for sunflowers. However, the crop has morphological differences with wheat and barley including a large disc shape head and very large leaves both of which are likely to affect the drag coefficient. Additionally, the process of drag area calculation is complicated due to the transformation in leaves and the plant's top, in different growth stages and in various genotypes. Moreover, the plant shape during different growth stages and between different genotypes was considerably different. The research showed the thickness of the epidermis plus cortex tissues and root diameter are the major parameters influencing stem/root lodging.

The model used in Sposaro et al. (2010) was originally developed for wheat and all of the dynamic/aerodynamic parameters (drag coefficient, damping ratio, etc.), as well as agronomic parameters (root diameter, stem wall thickness, etc.), had to be investigated for the new case study. Due to the considerable different shape between crops, Sposaro et al. (2010)

assumed that the top 1/3 of the plant experienced significant wind loading and, consequently, the point of wind loading application was assumed as 5l/6 where l is the plant height, rather than centre of gravity as used for wheat. In order to provide supporting input data for the model, the research measured agronomic parameters for a range of different treatments, plant varieties, and weather conditions. The approach used to measure the natural frequency was to isolate each plant and count the number of oscillations in a certain time once displaced (the same method as used for wheat (Sterling et al., 2003) and barley (Berry et al., 2006), which as previously stated can be affected by surrounding factors like wind or nearby plants. The damping ratio was assumed to be the same as wheat (0.08), as both plants grow as isolated shoots. Finally, the drag ratio was assumed as 0.5 which was based on the drag ratio values of same shape objects. The lack of experiments for identifying more accurate values for damping ratio and drag coefficient are major shortcomings in the research. This issue becomes more important knowing that the drag area (A) was found one of the major effective parameters and the value of this parameter can affect the order of most influential parameters in the lodging process for the plant.

2.3.Turbulent flow over plant canopies

2.3.1. Overview

Wind is a substantial factor in the mechanical loading of crops (Gardiner, 2016; De Langre, 2008; Baker et al. 2014). As noted by a number of researchers, (e.g., Holmes (2001), Baker et al. (2014) and Aly (2014) to name but a few), turbulence within the wind can play a major role in the overall wind loading on structures (and plants). Hence, it is essential to study the turbulent flow over the crop canopy to provide an insight into the process of wind-induced loading and the dynamic response of the plant. Studying the turbulent flow over the oat canopy has a number of benefits. Firstly, such an analysis can show how momentum and

kinetic energy is transferred in the flow and consequently to the canopy. Such insight can be compared with the previous findings of turbulent flow characteristics over the plant canopies to examine the consistency of the results with the literature. This is particularly important as the lodging velocities in the lodging model have been developed for a 'typical' flow over a crop canopy, which was defined by Finnigan (2000)-see Section 4.2.2. Section 2.3.2 discusses selected research that made a major contribution in the area and presents the key findings. Additionally, methods to study the momentum transfer and the kinetic energy over crop canopies are presented in Section 2.4, and the comparison between the collected data and the literature will be made in Chapter 4. Secondly, the main aim of such an investigation is to identify the parameters related to the 'loading' on crops such as plant drag area and turbulence intensity (the earlier is influential in the mean bending moment, (equation 2-2) and the latter is influential in the bending moment fluctuations, which are related to peak factors (equation 2-4 to 2-8)). Finally, using spectral analysis (discussed further in Section 2.4.3 and Chapter 4) not only enables a number of key parameters to be obtained (e.g., damping ratio and natural frequency) but enables these parameters to be understood in the context of the distribution of energy within the flow.

2.3.2. Wind flow over plant canopies

Over the last 30 years, knowledge of the flow over plant canopies has slowly developed (Finnigan, 2000). This approach was reasonable as the knowledge about the turbulence flow over and around the plant canopies is essential for agronomic, biological, and ecological studies (Brunet, 2020; De Langre, 2008). Moreover, the wind flow over canopies can affect the rate of heat exchange, water vapour, and carbon dioxide and can influence the biological/ecological factors associated with plant growth and diseases (Brunet, 2000). From a wind engineering perspective, the presence of vegetation influences the characteristics of

wind close to the canopy, so the data used in human-made structures are mainly not applicable and useful for plants (De Langre, 2008).

Raupach et al. (1996) and Finnigan (2000) provided a coherent picture and a clear interpretation of the turbulent flow over plant canopies based on experimental research in the 1980s and 1990s. The main finding of this research was that the turbulence structures (introduced later in this section) are dominated and scaled by the canopy elements. This research also discussed the structure of the turbulent flow over vegetation and showed that the canopy elements impact the turbulent flow in the boundary layer over plant canopies (see below). Moreover, the momentum transfer and turbulent kinetic energy (TKE) profiles were found to be different from boundary layer flow over non-vegetated surfaces, largely due to the levels of momentum absorbed, the flow structures generated, and the dissipation of TKE. Additionally, the region which is influenced by the crop elements was found to be ~2-3 canopy height above the canopy. Finally, the highest momentum transfer in the flow was found in the downward high momentum movements of air into the plant canopy (further discussed in Section 2.4.2).

The mean wind profile above the canopy can be represented by the logarithmic profile (equation 2-20), while the wind profile within the canopy can be represented in an exponential form (Raupach et al., 1996; Finnigan 2000). Thus, a point of inflection occurs in the horizontal velocity profile either in or near the top of the canopy, which causes instabilities in the interface between two flows known as mixing layer instabilities. These instabilities result in the formation of large-scale coherent structures in the flow which continue to develop and break up over the canopy. The mixing layer instabilities and coherent structures enhance the momentum transfer in the flow, which in turn cause the canopy to displace allowing the flow to either penetrate further into the canopy or get ejected from it (Raupach et al., 1996; Finnigan 2000; Gardiner, 2016). Due to the nature of coherent

structures, momentum transfer and deformation of the canopy etc. the instability/inflection point noted above is highly unstable which in turn will influence the turbulence flow (Py et al., 2006).

Figure 2.3 shows a comparison between boundary layer flow over a non-vegetated surface (Figure 2.3.a) and boundary layer over plant canopy (Figure 2.3.b), where *Z* is the height from the ground, *f* is the frequency. Figure 2.3.a shows when there is no vegetation on the ground, the logarithmic wind velocity profile starts from the ground, while the presence of vegetation changes the wind profile (Figure 2.3.b).

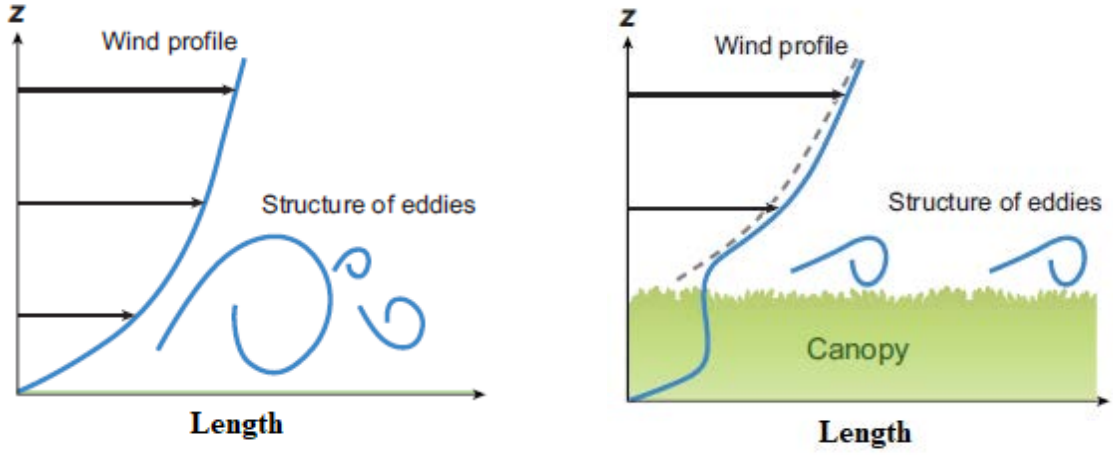

a) b)

Figure 2.3. The wind profile variation with height in a) the boundary layer flow b) a canopy layer flow (De Langre, 2008)

The logarithmic wind profile can be expressed as follows: (Holmes, 2001; Marshall, 1998; Garratt, 1994):

$$\overline{U} = \frac{u_*}{k} \ln \left(\frac{Z-d_0}{Z_0}\right) \quad (2\text{-}20)$$

where $\overline{U}$ is the time-averaged horizontal wind velocity, k is the Von Karman constant (~ 0.41), Z is the height from the ground and Z_0 is the surface roughness length (is the height at which the wind speed is zero and estimates the average roughness of the surface) and d_0 is the displacement height (the height at which wind speed is zero if the logarithmic wind profile being extrapolated downward). u_* is the surface friction velocity defined as (Sutton,1953):

$$u_* = \sqrt{\overline{u'w'}} \quad (2\text{-}21)$$

Where u' and w' are the fluctuating velocity components (the difference between instantaneous velocity and the mean velocity, see equation 2-26 and 2-28 below) in the streamwise and vertical directions respectively

Kaimal and Finnigan (1994) and Finnigan (2000) showed that for flow over plant canopies, the Eulerian integral length scale - a parameter which quantifies the size of the large energy containing eddies (Stephan, 2000) - was reported to be of the order of crop height ($1h$ - $2h$, where h is the crop canopy height) and the vertical length scale to be around 1/3 of the crop height for a wide range of vegetation, from grass canopies to forest trees (Py et al., 2006). This will be examined on the wind velocity data collected in this research (Section 4.2.2) to examine the consistency of the collected data with the literature. Such a turbulence length scale can be obtained from the use of single-point velocity autocorrelation function and as such corresponded to a fixed location, i.e., Eulerian analysis uses a stationary frame of

analysis to examine how the flow varies with respect to time. Formally, the autocorrelation function is defined as follows (Finnigan, 2000):

$$R_i(t) = \frac{\overline{u_i'(t)\, u_i'(t+T)}}{\sigma_i^2} \tag{2-22}$$

where t is time, T is the time lag, σ_i is the standard deviation of velocity component, i represents either streamwise, cross stream or vertical directions and u_i' is the fluctuating velocity component (the difference between instantaneous velocity and the mean velocity, see equation 2-26 to 2-28 below), i.e., either u (streamwise), v (lateral) or w (vertical). The Eulerian integral length scale can be derived as:

$$L_i = \overline{U} \int_0^\infty R_i(t)\, dt \tag{2-23}$$

Consequently, the streamwise and vertical turbulence length scales can be written as:

$$L_u = \frac{\overline{U}}{\sigma_u^2} \int_0^\infty \overline{u'(t)u'(t+T)}\, dT \tag{2-24}$$

$$L_w = \frac{\overline{U}}{\sigma_w^2} \int_0^\infty \overline{w'(t)w'(t+T)}\, dT \tag{2-25}$$

where L_u and L_w are the turbulence length scales in streamwise and vertical directions and σ_u and σ_w are standard deviation of streamwise and vertical velocities respectively (Finnigan, 2000). Formally, the velocity fluctuations are defined as follows:

$$u' = u(t) - \bar{u} \tag{2-26}$$

$$v' = v(t) - \bar{v} \tag{2-27}$$

$$w' = w(t) - \bar{w} \tag{2-28}$$

where $u(t)$, $v(t)$ and $w(t)$ are the instantaneous streamwise, lateral, vertical velocities respectively and $\bar{u}$, $\bar{v}$and $\bar{w}$ are mean velocities in the same orthogonal directions respectively and are related to $\bar{U}$ as follows:

$$\bar{U} = ((\bar{u})^2 + (\bar{v})^2 + (\bar{w})^2)^{1/2} \tag{2-29}$$

2.4. Statistical methods to study turbulent flows

2.4.1. Overview

Turbulent flows are known as a complex phenomenon with a random behaviour locally and spatially (Tsinober, 2009), however, there are some statistical methods that can be used to effectively describe the kinetic energy and momentum transfer in the flow (Finnigan, 2000). In this section, two statistical methods, i.e. Quadrant-hole analysis (Section 2.4.2) and spectral analysis (2.4.3) are introduced to study the flow. These methods together with the turbulence length scale complement each other and provide an insight into the wind loading process. The integral length scale quantifies the average size of the large energy-containing eddies which are produced by shear/buoyancy and are particularly important for their major contribution to the wind loading process, e.g., a small length scale implies that only a small

part of a plant/canopy will (on average) be loaded at any point in time whereas a large length scale suggests the opposite. The use of length scales in the current research is to check the consistency of the values with a 'typical' flow over the canopy (see Section 4.2.2), which is an initial assumption used for the lodging model.

The Q-H can illustrate how the high-energy eddies move in the flow and interact with the crop canopy which is important from a wind loading perspective. This issue is further discussed in Section 4.2.1 to justify the initial framework used by Baker et al. (2014) to model the wind loading process on crops. In addition to the scale, and momentum transfer, it is essential to understand how the energy within the flow is distributed with respect to frequency. Such an approach can indicate the amount of kinetic energy transferred between eddies and eventually to the plant through the wind loading process. The ratio between the kinetic energy of the flow and the plant, which can be obtained through spectral analysis (see Section 4.3.1.2) can also reveal the dynamic parameters of the oscillator, i.e. damping ratio and natural frequency, which are particularly important from a modelling perspective.

2.4.2. Quadrant-hole analysis

The Quadrant-hole analysis was first introduced by Lu and Willmarth (1973) and is a method to study how the momentum is transferred in the turbulent flow (Lu and Willmarth, 1973; Finnigan, 1979).

The key elements in the Quadrant-hole (Q-H) method are the streamwise and vertical velocity fluctuations ($u'$and w'respectively) which are defined in equation 2-26 and 2-28 and are used to determine how momentum is transferred in the flow above the canopy.

Based on signs of $u'$and w' the Q-H analysis classifies the u'-w'plane into four type events also known as quadrants:

- The first quadrant (Q_1) shows outward interactions where $u' > 0$ and $w' > 0$.
- The second quadrant (Q_2) shows ejections where $u' < 0$ and $w' > 0$.
- The third quadrant (Q_3) shows inward interactions where $u' < 0$ and $w' < 0$.
- The fourth quadrant (Q_4) shows sweeps where $u' > 0$ and $w' < 0$.

The first and the second quarters represent flows moving upward ($w' > 0$), while the former, shows a flow with high momentum (as the instantaneous velocity is higher than average wind speed i.e. $u' > 0$) and the latter shows a low momentum flow ($u' < 0$).

Similarly, the third and fourth quarters show downward movements ($w' < 0$), while the third quarter shows a low momentum flow ($u' < 0$) and the fourth quarter shows a high momentum flow ($u' > 0$).

Besides the sign of velocity fluctuations, the value of $|u'w'|$ can demonstrate values that have a strong contribution in overall momentum transfer. Accordingly, the fifth region is set as the Hole (*J*), the hyperbolic hatched area as shown in Figure 2.4, which is represented as by $|u'w'|$ =constant. When *J*=0, the hole is zero and all the events are considered. However, as *J* increases, the low momentum events (low values of $u'w'$) are neglected and high momentum events are considered. Hence, the hole is used as a filter and is useful from a visualization perspective.

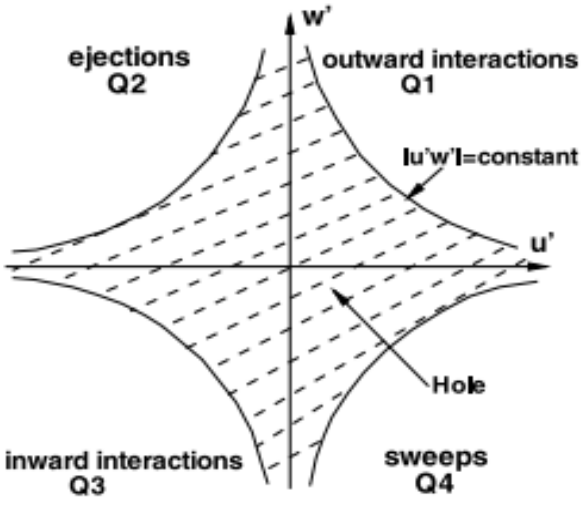

Figure 2.4. Streamwise and vertical velocity fluctuations showing the four quadrants and hyperbolic region known as hole, i.e. hatched area and different events (Lu and Willmarth, 1973)

An indicator ($I_{i,J}$) is defined by Lu and Willmarth (1973) to determine the contribution of $u'w'$ in each quadrant, where *i* represents the number of the quarter (*i*=1,2,3,4). Additionally, if (u', w') is in quadrant *i* and $|u'w'| \geq J\sigma_u\sigma_w$, then $I_{i,J} = 1$, otherwise, $I_{i,J} = 0$. Where σ_u and σ_w are the standard deviation of u and w respectively and the normalized conditional shear stress, $S_{i,j}$ is calculated as (Lu and Willmarth, 1973):

$$S_{i,J} = \frac{1}{\sigma_u\sigma_w T}\int_0^T u'(t)w'(t)\, I_{i,J}\, dt \qquad (2\text{-}30)$$

where *T* is measurement time.

Quadrant-hole analysis has consistently demonstrated that sweeps (downward high momentum movements of air into the plant canopy) and ejections (also known as burst, the

movement of upward, low momentum flow) dominate momentum transfer just above the plant canopies (Finnigan, 2000; Brunet, 2020). These results were consistent in a wide range of plants, e.g., in wheat canopies (Finnigan, 1979), wind tunnel models for different vegetation (Raupach et al., 1986, Sterling et al., 2003), corn canopies (Shaw et al., 1983), and even forests (Baldocchi and Meyers 1988; Gardiner, 1994). Additionally, Kline et al. (1967) has reported that ejections play a major role in outward vertical momentum transfer and consequently the production of turbulent kinetic energy (Wallace, 2016).

Using the Q-H analysis in this research is beneficial for two main reasons. First, the analysis provides an insight into how energy is transferred in the turbulence flow and ultimately to crops. Second, due to the consistency of the Q-H analysis results in a wide range of vegetation, it is worth investigating the momentum transfer in oats for the first time to examine the consistency of findings with the literature. Nevertheless, this method does not provide any information about other essential factors in the boundary layer flow such as the size of eddies or "*coherent patterns of velocity, vorticity and pressure spread over a wide range of sizes*" (Kaimal and Finnigan, 1994) - and how these eddies are produced and disappear to heat. These understandings can be provided by other methods such as spectral analysis and the measurement of turbulence length scale.

2.4.3. Spectral analysis

The turbulent flow over a vegetation canopy is highly influenced by the interactions of eddies with each other and the mean flow (Kaimal and Finnigan, 1994). In order to understand how turbulent kinetic energy is transferred between eddies at different scales, spectral analysis can be used (Kaimal and Finnigan, 1994), which uses Fast Fourier Transform (FFT) to convert velocity fluctuations from the time domain to the frequency domain (Kaimal and Finnigan,

1994). It is also used as an approach to study the amount of kinetic energy in the flow at different frequencies (Kaimal and Finnigan, 1994). Although spectral analysis is a common method in wind engineering and has been used to study a wide range of different plant canopies, e.g. corn (Shaw et al., 1983; Wilson et al., 1982), forests (Baldocchi and Meyers, 1988; Gardiner, 1994) and wheat (Sterling et al., 2003), both the time and frequency domain data must be used and interpreted carefully.

Similar to traditional boundary layers, the energy spectrum includes energy-containing range, inertial subrange, and dissipation range. In the energy-containing range, the energy is produced by buoyancy and shear, while in the inertial subrange energy is not produced or dissipated and is just transferred to smaller scales. Finally, in the dissipation range, the kinetic energy is transformed to heat (Kaimal and Finnigan, 1994). According to the Kolmogorov theory, in the inertial subrange, the velocity spectra are proportional to $f^{-5/3}$, where f is the frequency. The -5/3 power law is well known and has been reported frequently by different researchers (Stephan, 2000; Finnigan, 2000; Tennekes and Lumley, 1972). Moreover, the theory states there is a relationship between the spectra for the orthogonal components of velocity in the inertial subrange (where the spectrum is falling in Figure 2.5) as follows (Kaimal and Finnigan, 1994):

$$S_v = S_w = \frac{4}{3} S_u \tag{2-31}$$

Figure 2.5 shows a schematic of the velocity spectra against frequency where both axes are in logarithmic scales. The figure shows all streamwise, lateral and vertical velocity spectra fall off as $f^{-5/3}$ (Kaimal and Finnigan, 1994).

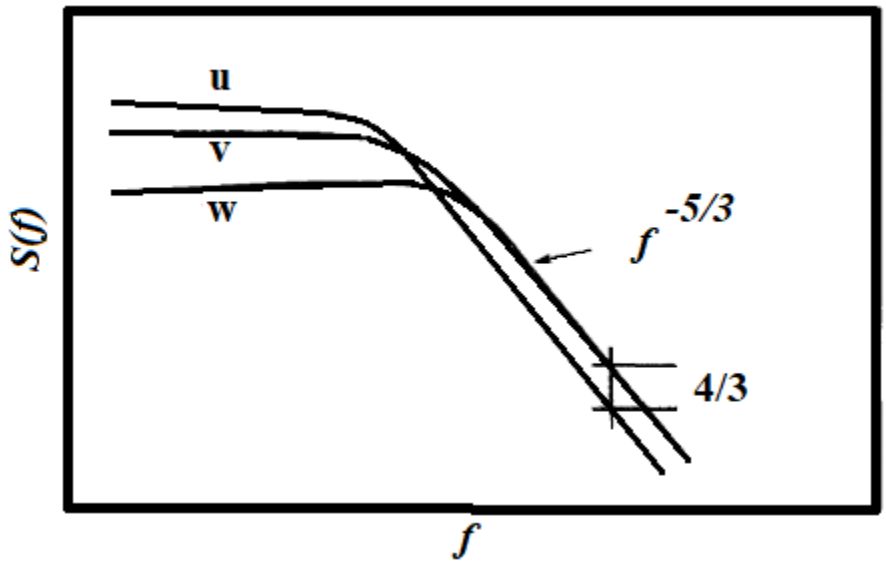

Figure 2.5. Idealized velocity spectra in the inertial subrange, axes are both in logarithmic scales (Kaimal and Finnigan, 1994).

Analytical expressions have been used to represent the velocity spectrum (Kaimal and Finnigan, 1994). The most commonly used of these representations for the longitudinal velocity component is the Von-Karman spectrum as follows (Holmes, 2001):

$$\frac{fS_u(f)}{\sigma_u^2} = \frac{4fL_u/\bar{U}}{(1+70.8\,(\frac{fL_u}{\bar{U}})^2)^{5/6}} \qquad (2\text{-}32)$$

Where L_u is the turbulent integral-length scale in the streamwise direction (the parameter is defined in Section 2.3.2).

Spectral analysis is a useful tool for this research as it can show the energy cascade in the velocity spectra over an oat canopy which can be compared with theory. Additionally, spectral analysis can be applied on crop displacement data to determine the natural frequency

(the frequency in which the oscillator shows the highest energy – see Section 4.3.2). Moreover, using the Von-Karman spectrum can be an alternative method to evaluate the turbulence length scale (besides using the autocorrelation function described in Section 2.3).

2.5. The potential effect of the climate change on oat lodging

2.5.1. Overview

Climate change, which is caused by considerable human-related greenhouse emissions, is a major international issue and is expected to affect meteorological conditions worldwide (Saboohi et al., 2012). As an example, the global temperature has increased by 0.74º C in the 20th century and rainfall patterns have changed globally (Gohari et al., 2013). The agricultural sector is highly dependent on weather conditions including temperature, sunshine, rainfall, etc. and can be influenced by changes in the climate (Masud et al., 2017). Nevertheless, the influence is not necessarily negative and might be different in various geographic locations. For instance, the projected changes in the future Irish climate are expected to reduce the cereal production in Ireland (Hennessy, 2010), while the future meteorological conditions are projected to have a positive effect on the agricultural sector in the northern regions of Alberta province (Masud et al., 2017). Nonetheless, it is unclear how severe problems in the agricultural industry like lodging, might change in the future climate conditions (Martinez-Vasquez, 2016).

Previous research has shown a rise in average rainfall of 0.5%–1% per decade in most of the middle and high latitudes in the northern hemisphere (Soltani et al., 2012). However, historical data in England and Wales show that the annual mean rainfall has not changed considerably since 1766 and seasonal precipitation demonstrates a reduction in summer

(Jenkins et al., 2009). Furthermore, data shows that the total precipitation in winter months has increased (Maisey et al., 2018). Furthermore, historical data also show the annual rainfall in the North and West of the country has increased while, there is a decline or small increase in the South and East of the country (McElwain and Sweeney, 2007).

Future climate projections show a rise of 1°C to 1.6°C and up to 2.3°C by 2100 in mean annual temperatures in the British Isles (Nolan, 2015; Meteorological Office, 2019). Moreover, the mean spring and summer precipitation amounts in the Republic of Ireland are expected to decrease by mid-century, and a higher number of droughts is expected during autumn and summer (Nolan et al., 2017). Similarly, UK summer precipitation is expected to decrease by 47% by 2070, however, winter precipitation is projected to increase by 35% (Meteorological Office, 2019). Additionally, future climate simulations have shown a decrease in the energy content of the wind in all the year except winter in the British Isles (Met Éireann, 2019).

It is well documented that strong winds and high rainfall are the major influential factors in lodging (Easson et al., 1993; Baker et al., 1998; Baker et al., 2014). Accordingly, several researchers have investigated the relationship between adverse weather conditions and lodging occurrences. Easson et al. (1993) showed lodging is likely to happen, not only in the presence of strong gusts (greater than 25km/h (7m/s)) but also in low wind speeds (16km/h (4m/s) or less). Nevertheless, Berry et al. (2002) showed if crops receive appropriate husbandry, lodging is preventable even in adverse weather conditions.

In order to consider the effect of meteorological parameters in a systematic manner, Baker et al. (1998 and 2014) proposed probabilistic frameworks, where the probability of lodging can be quantified. This framework can be used to evaluate the potential effect of climate change on lodging. Martinez-Vasquez (2016) used this framework together with climate projections

from UKCP09 to assess the lodging likelihood for oat, barley, wheat, and OSR in the future. However, this work had major assumptions which call into questions the reliability of the results and conclusions. First, at the time of publication, some of the data required to calibrate the lodging model was unavailable and the author produced the data through estimations. Consequently, the lodging models used for oat and osr were not calibrated while Sterling et al. (2003) showed that an incorrect estimation of effective parameters in lodging could cause 51% over-estimation in lodging wind speeds. Moreover, the paper used some of the UKCP09 parameter outputs (e.g. evapotranspiration, temperature, and solar radiation) and the data was extracted from 24-h FAO Penman-Monteith equation (equation 2-33 below) and was downscaled to estimate hourly winds. Nevertheless, an analysis (undertaken by the author of this thesis but not included for the sake of brevity) on the same output and studied location showed ~40% of the results are questionable and result in either negative or very large values of wind speed. The 24-h FAO Penman-Monteith equation is an empirical relationship between climatological parameters such as solar radiation, air temperature, humidity, and wind speed with reference evapotranspiration. Evapotranspiration (ET) refers to two water loss processes, evaporation and transpiration, and both processes are the conversion of water liquid to vapour. The earlier occurs on soil surfaces, wet plants, etc. while, the latter happens within the plant and causes water loss through leaves (Zotarelli, 2010). Reference evapotranspiration (ET_0) is a concept to consider the rate of evaporation regardless of the effect of crop type, crop development and management practices (Zotarelli, 2010) and is defined as: "*the rate at which readily available soil water is vaporized from specified vegetated surfaces*" (Zotarelli, 2010). The 24-h FAO Penman-Monteith equation is defined as (Allen et al., 1998):

$$ET_0 = \frac{0.408\Delta(R_n - G) + \gamma \frac{900}{T+273} u_2 (e_a - e_d)}{\Delta + \gamma(1 + 0.34u_2)} \quad (2\text{-}33)$$

where ET_0 is the grass reference evapotranspiration (mm /day^{-1}), Δ is the slope of the vapour pressure curve (kPa◦C^{-1}) , u_2 is the wind speed measured 2m above the ground (m/s), R_n is net radiation at crop surface (MJ m^{-2}day^{-1}), G is soil heat flux (MJ m^{-2}day^{-1}), γ is psychrometric constant (KPa$^{\circ}$ C^{-1}), e_d is the actual vapour pressure (kPa), e_a is the saturation vapour pressure and T is the mean temperature at 2m height (◦C) (Allen et al., 1998).

An alternative (and more robust) way to produce future wind speed data is using the climate change projections. Interestingly, the latest version of UK climate projections includes both rainfall and wind speed data, which will be briefly introduced in Section 2.5.2 and fully discussed and used in Chapter 5. Additionally, this research will enable a calibrated lodging model for the first time, which can be used to assess future lodging probability in oats.

2.5.2 Future climate projectors

UKCP09 and UKCP18 are two climate projection simulators showing possible climate change scenarios for the UK inland and marine regions. Both models include a number of variables, e.g., data source, emission scenario, and time and location. The UKCP09 projector was closed in December 2018 due to the release of UKCP18.

Emission scenarios used in UKCP09 and 18 are slightly different. In the UKCP09, three low, medium, and high emission scenarios were applied based on SRES, Special Report on Emissions Scenarios (AR4 Climate Change, 2007). While the UKCP18 employs Representative Concentration Pathways (RCPs), which determine the amount of greenhouse gases causing certain radiative forcing at the high altitude of earth's atmosphere by 2100, in

comparison to pre-industrial levels (The Intergovernmental Panel on Climate Change, 2018). Four forcing levels are determined: 2.6, 4.5, 6.0, and 8.5 W/m^2, which are defined as RCP 2.6, RCP 4.5, RCP 6.0, and RCP 8.5 scenarios (Meteorological Office, 2019). Table 2.1 shows a comparison between emissions scenarios used in two climate projections.

Table 2.1. A comparison between Representative Concentration Pathways (RCPs) used in UKCP 18 and emission scenarios used in UKCP 09 and their associated temperature increase (Meteorological Office, 2019)

RCP	Most similar scenario in UKCP09	Increase in Global mean surface temperature (°C) by 2081-2100
RCP 2.6	None	1.6 (0.9-2.3)
RCP 4.5	Low emission	2.4 (1.7-3.2)
RCP 6.0	between the low and medium emission scenarios	2.8 (2.0-3.7)
RCP 8.5	High emission	4.3 (3.2-5.4)

One of the main features of UKCP09 was a weather generator (WG), which was able to use a long-term training historical data set for a determined region and could fit a baseline on historical observations. Later, using change factors possible time series of future climate conditions could be projected. The WG was capable of providing samples of future projections for a minimum period of 30 years. Moreover, the UKCP09 could provide

probabilistic projections to show how meteorological parameters might change in monthly, seasonal, and annual timeframes.

In the UKCP18, the WG is substituted by global and regional projections which are based on many different and updated climate models (described further in Chapter 5) and provide a wider variety of outputs (UK climate projections website, 2018). Moreover, the probabilistic projection component is mainly the same as used in the UKCP09, while the historical data and emission scenarios have been updated.

2.6. Summary and identified gaps in the literature review

This chapter critically discussed the literature relating to lodging in crops. To date, the analysis of lodging has largely been based on the work of Baker (Baker, 1995; Baker et al., 2014). However, as noted above, there are a number of untested assumptions embodied within the work of Baker et al. (2014) which were primarily used to obtain an analytical form of lodging probability. For example, the PDFs used to represent both the wind and rainfall need to be explored for their general suitability. In addition, if their suitability is proven then the impact of geography on the fitting parameters also needs to be examined since this could have a considerable impact on the likelihood of lodging.

Furthermore, whilst it is understandable that Baker et al. (2014) developed an analytical solution to their model, there is no need for such a solution as the integration can be easily and rapidly be calculated numerically.

Lodging in oats has hitherto not been investigated and as such the agronomic and dynamic/aerodynamic parameters which govern lodging in other types of crops are unknown. Importantly, the actual mechanism by which lodging may occur has not been verified and

may be different from that found elsewhere. In addition, the impact (or not) that plant interlocking may have throughout the growing season is an open question. Hence, there are no data that could be used to either elucidate the lodging process in oats or validate and calibrate any models which are developed.

Even if the above was known and a suitable lodging model developed, the impact that climate change may have on lodging likelihood has never been investigated in a systematic and rigorous manner and as such is simply unknown. Given the importance of oats to the Irish economy (~10% of Irish cereal production is oat (Teagasc, 2021) and the annual export of crop products worth ~£25m (European commission, 2021)) this could have a considerable impact in the future.

3. Methods

3.1.Introduction

This chapter describes the experimental setup and the methods used for the research. The motivation for undertaking the experiments and measurements is described in Section 3.2 followed by a description of the agronomic measurements in Section 3.3. Section 3.4 is focused on aerodynamic experiments and describes the experimental setup and how video tracking was developed to record and interpret the motion of a crop. Finally, Section 3.5 provides a number of conclusions relating to the work contained in this chapter.

3.2.Motivation of the experiments and measurements

In Chapter 2 it was shown that the peak bending moment from the Baker et al. (2014) model can be written in the form of lodging velocities. Thus, the key failure criteria in terms of stem lodging velocity ($\overline{U}_{Ls}$) and root lodging velocity ($\overline{U}_{LR}$) are:

$$\overline{U}_{Ls} = \left(\frac{\omega_n^2\left(\frac{X}{g}\right) S_s}{\left(1+\omega_n^2\left(\frac{X}{g}\right)\right)(0.5\rho AC_F X)(\cos\left(\alpha\frac{x}{l}\right)-cot\alpha\sin\left(\alpha\frac{x}{l}\right))(1+I\left(4g_{MB}^2+g_{MR}^2(\frac{\pi}{4\theta})\right)^{0.5}}\right)^{0.5} \quad (3\text{-}1)$$

$$\overline{U}_{LR} = \left(\frac{R_S}{\frac{((1+\omega_n^2\left(\frac{X}{g}\right))}{\omega_n^2(\frac{x}{g})}(0.5\rho AC_F X)(1+2Ig_{MB})}\right)^{0.5} \quad (3\text{-}2)$$

These expressions are somewhat different to what is written in Baker et al. (2014) since they incorporate the general form of the gust factors (g_{MB} and g_{MR}). All of the parameters in equations 3-1 and 3-2 can be classified as either agronomic (related to plant properties), dynamic/aerodynamic (related to the plant's movement interacting with the wind), or soil properties. Table 3.1 presents these parameters, abbreviations, and the type of method to determine the parameter.

Agronomic parameters are the plant traits that are influential in the lodging process and can be quantified through standard protocols such as those developed by Berry et al. (2000 and 2003). These factors can be controlled by different husbandry techniques applied to crops (see Section 3.3.2 for a detailed explanation). Additionally, from the grower's perspective, agronomic terms are targeted, controlled, and varied. Consequently, this research aims to identify the effect of the agronomic husbandry techniques and agronomic factors on lodging velocity and probability (see Chapter 6). In addition to the measurement of crop characteristics, lodging occurrence in crops grown under different techniques has to be monitored to enable the comparison of the model output with lodging observations being made.

Table 3.1. Influential parameters in the stem/root lodging velocity, their abbreviations and the type of measurement method.

Parameter	abbreviation	parameter classification
Centre of gravity	X	Agronomic
Stem radius	a	Agronomic
Stem wall thickness	t	Agronomic
Stem height	l	Agronomic
the stem yield stress	σ	Agronomic
Number of stems per plant	n	Agronomic
Root diameter	d	Agronomic
Root depth	L	Agronomic
Soil shear strength	S	Agronomic (soil)
Natural frequency	f_n	Dynamic
Damping ratio	θ	Dynamic
Turbulent intensity	I	Aerodynamic
Plant drag area	AC_F	Aerodynamic

The other type of parameter in Table 3.1 can be thought of as dynamic/aerodynamic terms, which cannot be controlled in full-scale measurements and are dependent on the environmental conditions and agronomic factors. Despite the importance of these parameters (which determine the wind loading on crops), the only research which actually measured these factors for a crop (wheat) was Sterling et al. (2003) which involved a complex, time-consuming, and relatively expensive approach. Moreover, Sterling et al. (2003) reported differences in the turbulent flow characteristics in the wind tunnel in comparison to the

natural conditions (particularly in terms of the turbulent length scales generated). Furthermore, it was noted that the method of determining the force on the plants (by attaching strain gauges to the crops) had the potential to not only disturb large parts of the canopy, but also the plant's structure (and hence its ability to move naturally in the wind).

Determination of these factors in Table 3.1 are crucial, because from a modelling perspective oats are more complicated than, say wheat, due to their interactions with nearby crops and the structural changes they undergo through their growth cycles. For example, at the panicle emergence stage, oat canopies act as single shoots, while as time progresses and the plant grows, they create interlocked canopies. Nevertheless, it is unknown how this change in the canopy affects the dynamic movement, and forces applied to the crops. Moreover, the flow over oat canopies has not been studied before, and wind loading parameter such as the drag area is unknown. Additionally, as experiments have uncertainties associated with the roots and soil, the results would be more realistic if the parameters are investigated under field conditions (Sterling et al., 2003).

The only experimental method found in the literature to investigate the dynamic/aerodynamic parameters of crops was developed by Sterling et al. (2003), i.e., using a portable wind tunnel installed over the crop canopy and attaching strain gauges to the crops to monitor their dynamic response. However, this method is not applicable for interlocking crops like oats for a number of reasons outlined above. In order to address such issues, a non-intrusive approach was developed for the current research, based on tracking the movement of the plants whilst simultaneously measuring the wind directly above the crops which is described in Section 3.4.

3.3.Agronomic measurements

3.3.1. Oat plants

An oat plant is a kind of Gramineae family grass, which includes the root system, the stem, and the panicle (Magness et al., 1971). The oat plant produces up to five stems and in the mature stage of plant growth, a panicle emerges at the top of the stem including a group of branches and spikelet (Agriculture, Forestry and Fisheries, 2020).

Figure 3.1 demonstrates an oat plant's main parts and characteristics including, stem, nodes, leaf, root, and spikelet. Nodes are known as bud holders, producing new leaves and are generally solid and thicker than stem parts between two nodes (Agriculture, Forestry and Fisheries, 2020).

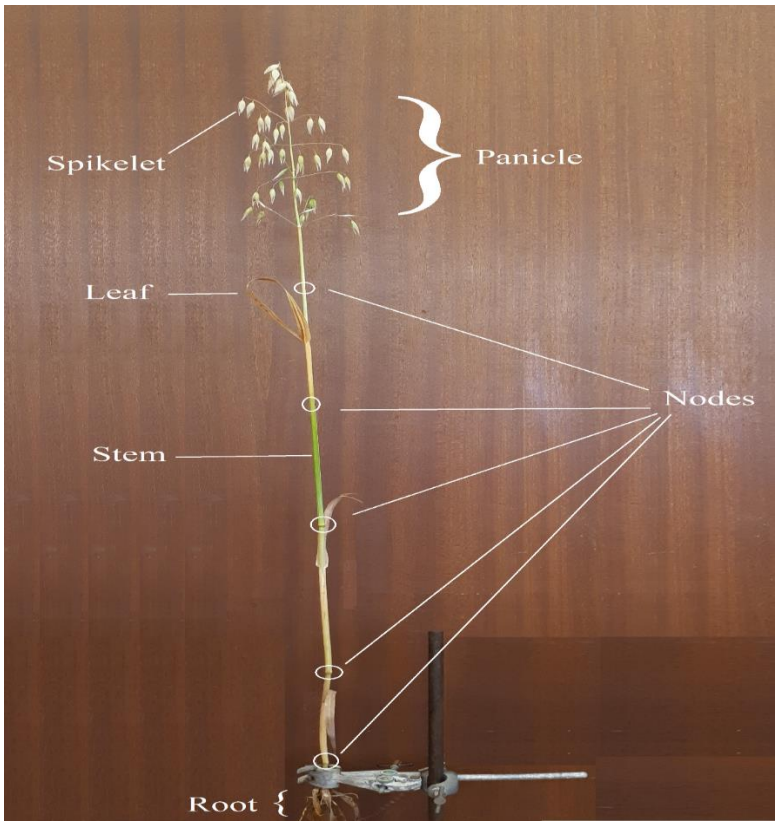

Figure 3.1. Oat plant main elements at the last stage of growing (before the harvest).

Historical evidence shows oats tillage in Ireland since the Bronze Age. Although oat usage was mainly horse feed prior 20th century, the crop attracted attention as a good source of vitamins, minerals, and antioxidants, reducing cholesterol level and lowering blood sugar (Baker et al., 2018; Rasane et al., 2015; Wu and Ma, 2019).

Oat plant growth can be divided into three main phases: foundation, construction, and production. The foundation phase is referred to the period of sowing to the start of stem extension. The length of the phase is affected by weather temperature and the amount of sunshine. The construction phase begins from the time the first node on the stem appears and the plant extends deep roots and yield delivering leaves. The production stage is after flowering to ripening and grain filling (Yara[1], 2019). Oats can differ from other cereals since in their initial growth phases (i.e., around panicle emergence) they can act as individual shoots, whereas as time progresses and the plant grows, they have the propensity to entangle with one another as shown in Figure 3.2 (Mohammadi et al., 2020b).

.

[1] Yara is an international environmental and agronomic company active in over 60 countries.

(a)

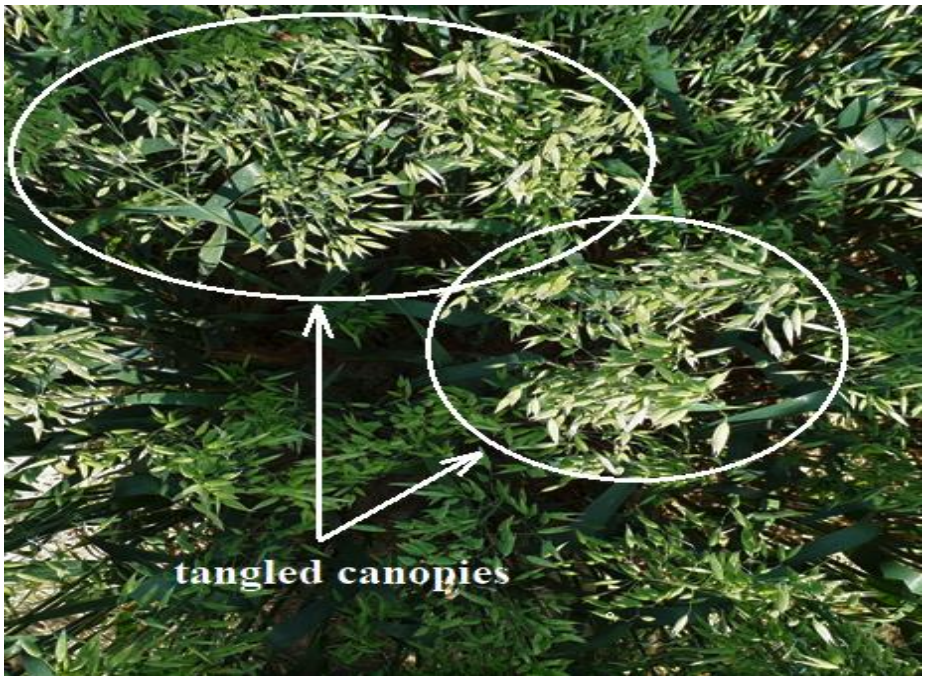

(b)

Figure 3.2. Oat canopies a) at beginning of the lodging season (just after panicle appearance) b) at the middle of the lodging season (Mohammadi et al., 2020b)

3.3.2. The experimental crops

The experiments were undertaken at two sites in the Republic of Ireland approximately 1.5km apart, i.e., Knockbeg, County Laois (52.86 °N, 6.94 °E, 54 MSL) and Oak Park

Research Centre, County Carlow (52.86 °N, 6.92 °E, 57 MSL). Figure 3.3 shows the location of experiments in two years. The former site was used for the 2017 experiments whilst the latter was used for the experiments undertaken in 2018. The sites are sufficiently close to be considered adjacent.

Figure 3.3. The location of study sites near Teagasc in 2017 and 2018 (Google Earth, 2021).

In order to ensure consistency and to enable comparisons to be undertaken, the same experimental agronomic protocols (see below) were used on each occasion. Plants were grown under a number of husbandry techniques as described below and summarized in Table 3.2. These techniques can control the agronomic parameters (Berry et al. 2000), which are considered as independent variables in this study and can ensure the findings of this research are widely applicable elsewhere :

1. Crop variety: Barra or Husky. Barra was chosen for its propensity to lodge whilst Husky is generally accepted to have moderate lodging resistance as it has a larger root

diameter, stem radius, and stem wall thickness (DAFM, 2019). Both varieties are winter oats and are sown in autumn.

2. Seeding rate: two seed rates were used: 200/500 seeds per m^2. The lower seed rate increases the space for the plant to grow, consequently, a low seed rate increases root diameter, root depth, and stem diameter (Berry et al., 2000).
3. Plant Growth Regulators (PGR): the presence or absence of a PGR program was examined. The chemical used was 1l/ha of 'Ceraid' (Taminco BVBA) at the GS30/31, followed by 2l/ha of 'CeCeCe 750' (BASF Plc) at GS32. PGR application reduces the height of the plant and the stem centre of gravity (Berry et al., 2000).
4. Nitrogen rate: Low (90Kg/ha, i.e., kilogram per hectare) and high (180Kg/ha) Nitrogen rates. High Nitrogen rate causes excessive growth (higher plant height and centre of gravity and reduces the stem diameter and stem wall thickness which causes weaker stem strength (Berry et al. 2000).
5. Nitrogen timing: the early Nitrogen was applied at GS30 and GS32, and the late Nitrogen was applied at GS32 and GS39. Early Nitrogen application increases the number of stems per plant but will also influence the number of shoots death rate (as more shoots compete for the given Nitrogen). Late Nitrogen application was found not influence the number of stems per plant in wheat (Berry, 1998).

Table 3. 2. Agronomic husbandry techniques as applied on the studied crops

husbandry	Choices	
Seed rate	Low (200 seeds per m^2)	High (500 seeds per m^2)
PGR application	Yes	No
Nitrogen timing	Early	Late
Nitrogen rate	90 Kg/ha	180Kg/ha

Plants were grown in 12m long and 2.1m wide plots. Each plot received one specific combination of husbandry techniques giving 32 different combinations and plots were laid in two parallel rows (16 plots on each row). For example, the husky variety, low seed rate, PGR application, early Nitrogen, and low nitrogen rate was applied to one plot. All combination of husbandry techniques are abbreviated and listed in Table 3.3, where H/B are the plant varieties (Husky/ Barra), 200/500 are the low/high seed rate (200/500 seeds per m^2), Y/N refer to PGR application (Yes/No), 90/180 indicate Nitrogen rate (90/180Kg/ha) and E/L refer to early or late Nitrogen timing.

Table 3.3. The combination of husbandry techniques applied on studied plots

Plot no.	Husbandry technique	Plot no.	Husbandry technique
1	B-200-N-90-E	17	H-200-N-90-E
2	B-200-N-180-E	18	H-200-N-180-E
3	B-200-N-90-L	19	H-200-N-90-L
4	B-200-N-180-L	20	H-200-N-180-L
5	B-200-Y-90-E	21	H-200-Y-90-E
6	B-200-Y-180-E	22	H-200-Y-180-E
7	B-200-Y-90-L	23	H-200-Y-90-L
8	B-200-Y-180-L	24	H-200-Y-180-L
9	B-500-N-90-E	25	H-500-N-90-E
10	B-500-N-180-E	26	H-500-N-180-E
11	B-500-N-90-L	27	H-500-N-90-L
12	B-500-N-180-L	28	H-500-N-180-L
13	B-500-Y-90-E	29	H-500-Y-90-E
14	B-500-Y-180-E	30	H-500-Y-180-E
15	B-500-Y-90-L	31	H-500-Y-90-L
16	B-500-Y-180-L	32	H-500-Y-180-L

In order to investigate the agronomic parameters of each plot, a sampling process was undertaken based on protocols developed by Berry et al. (2000). Accordingly, sampling was undertaken three times, and each time seven plants were taken from each plot (21 samples). Altogether, 1344 samples were collected to measure agronomic parameters (i.e., number of stems per plant, stem radius, stem wall thickness, stem height, root diameter, and root depth): 32 husbandry technique plots × 7 samples from each plot × 3 sampling times each year × 2 years of experimental data. In practice, some of the samples were damaged in the process of collection and storage, and the exact number of measurements for each parameter is presented in Table 4.8 in Chapter 4. Additionally, for the measurement of centre of gravity and natural frequency, the shoot had to remain unbroken. Consequently, in each sampling

event, 1 sample from each plot was kept unbroken and brought to the laboratory for the purpose of measurements. The sampling process was undertaken in the first, second and third week of June (GS51-GS83).

In addition to the sampling process, plots were monitored for lodging events during the period between panicle emergence (growth stage GS51, Zadoks et al., 1974) and before the final harvest (growth stage GS93). Additionally, the weather conditions (hourly mean wind speed and 24-hours rainfall) were monitored in both years using the Oak Park weather station located approximately 1.5 Km and 200m from the experimental locations in 2017 and 2018 respectively; the corresponding data is available at the Irish Meteorological Service (Met Éireann, 2019). The weather conditions in the period between the panicle emergence and harvest time (June and July) were very different in the two years studied. Figure 3.4 shows the daily rainfall and mean daily wind speed in two years. It is worth noting that the lodging model is formulated based on the mean hourly wind speed (equation 3-1 and 3-2) and the figure is provided to show the comparison of weather conditions in two years of experiments. As the figure shows, in the first year (2017), a higher amount of rainfall was recorded while the second year was relatively dry. Moreover, although a number of windy days were recorded in the middle of June 2018, the overall lodging season in 2018 was less windy than in 2017. As a consequence, five lodging occurrences were recorded in 2017, while in the second year no lodging events were observed.

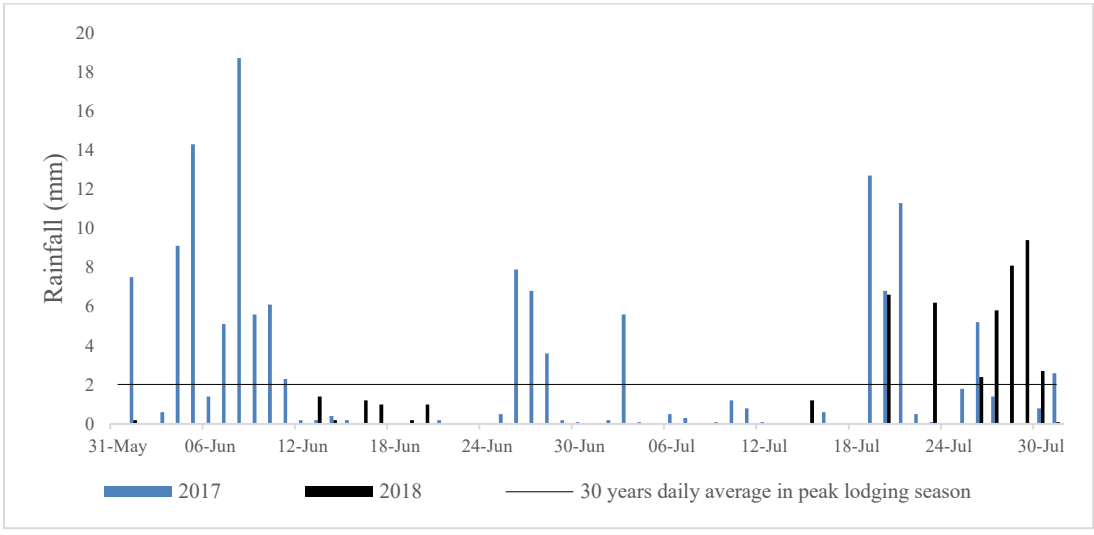

(a)

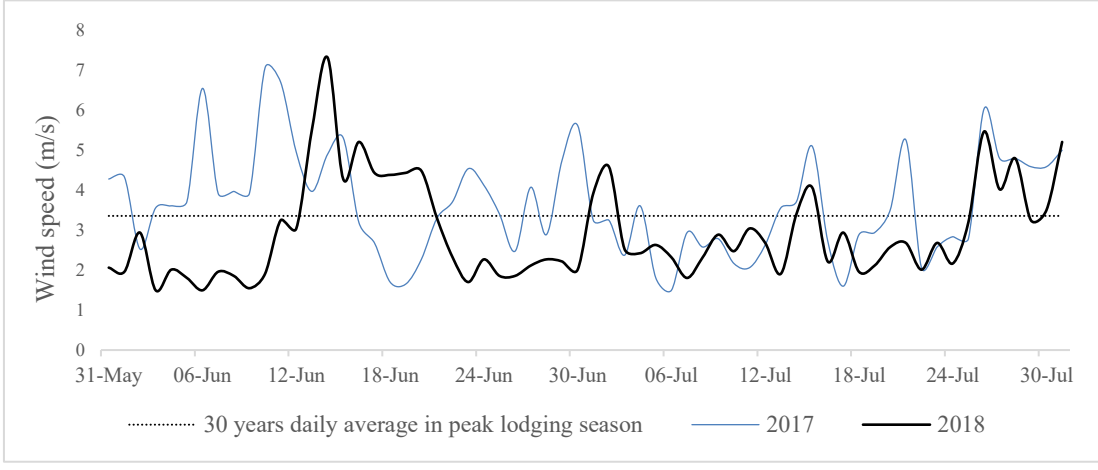

(b)

Figure 3.4. (a) The daily rainfall (b) the mean daily wind speed in the peak lodging season in 2017 and 2018 as recorded in Oak Park meteorological station (Met Éireann, 2019).

3.3.3. Measurements of stem and root parameters

The protocol for determination of the number of stems associated with the experimental crops and the relevant root parameters can be found in Berry et al. (2000):

The panicle per plant (n) is the ratio of the number of panicles per square meter to the number of plants per square meter. The former was counted in early June and the latter was measured in February after sowing (GS12-13)

For the root measurements, plant samples (at GS53-GS93) were chosen from each plot and were carefully excavated. The samples were soaked for some hours in the water in the laboratory, so the soil could be washed easily without damaging the roots. Later, the root diameter and depth were measured using a calliper. Based on the protocol developed by Berry et al. (2000), the root parameters were measured on a solid rigid portion of the root. It is worth noting that as roots do not grow uniformly, the largest and the smallest root diameter were measured, and their values were averaged for each sample.

In order to determine the centre of gravity, the stem of a sample plant was balanced on a ruler and the height of the balance point was measured. The plant height and length of each internode (the distance between two nodes) were determined using a tape measure. Finally, the stem diameter and wall thickness were measured using a calliper. These measurements were undertaken between GS53 and GS83.

3.3.4. Measurements of natural frequency

Once the plants had been removed from the field, Berry et al.'s method for measuring the natural frequency was adopted (Berry et al., 2000). This involved placing the shoot in a clamp and displacing it by approximately 0.10m and the time was taken for two or three oscillations was recorded.

Although this approach can be useful to provide an estimation of the plant's natural frequency, the method has a number of uncertainties. First, this method neglects the potential effect of entanglement or soil-root interactions on the natural frequency. Secondly, 2-3 oscillations are recorded which take ~ 1-second, and consequently, errors with respect to recording the times can be introduced (the time recording for each sample was repeated at least 10 times to minimize the uncertainties with the measurement). In order to measure the

parameter in the natural environment, an alternative method (Section 4.3.2) was used to determine the natural frequency through displacement spectrum in which displacement fluctuations are transformed from the time domain to the frequency domain and a graph of displacement versus frequency can be derived (Holmes, 2001). An example from this approach is shown in Figure 3.5 where the horizontal axis shows frequency and the vertical axis shows the crop displacement spectrum normalized by corresponding variance and the peak in the plot is associated with the natural frequency (this will be fully discussed in Section 4.3.2).

Overall, although Berry's method (Berry et al., 2000) is not as accurate as spectral analysis, it is considered the standard agronomic approach to measure natural frequency, and it has been used in this research for the sake of completeness in the adopted methods.

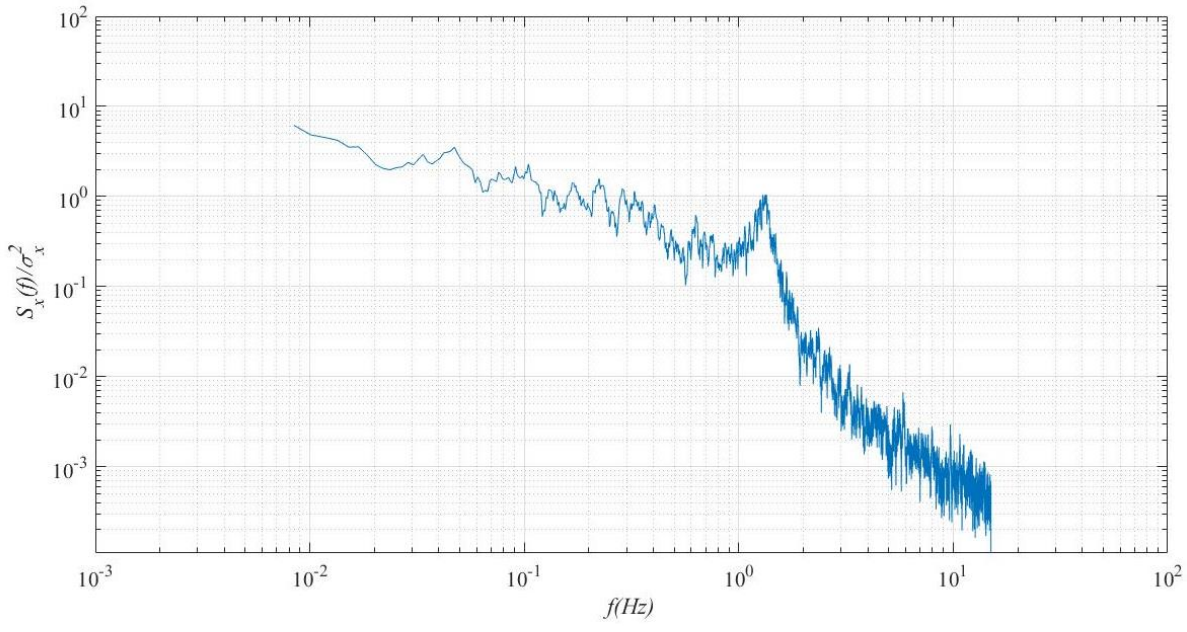

Figure 3.5. Crop displacement spectrum normalized by variance; data collected on 1 June 2018 (GS53)

3.3.5. Stem strength measurements

In order to obtain the stem yield stress and the root failure moment, 100 samples were taken at GS83. The test was undertaken when samples were fresh as the dried plants can have different mechanical properties. The number of samples was determined through the statistical formulation provided in Appendix B in which based on the statistical parameters of a previous measurement (Berry et al., 2003), the sample size can be determined. The stem yield stress can be calculated from the following equation (Berry et al., 2000):

$$\sigma = \frac{F_S h a}{\pi(a^4-(a-t)^4)} \tag{3-3}$$

In the equation F_S is applied force normal to the stem and h is the internode length and a, t and σ are as outlined in Chapter 2.

To determine the F_s, the relevant internode of the stem is supported at the nodes and the force required to break the stem is applied at the middle of the internode. Table 3.4 shows the mean values, standard deviation, random uncertainty and fractional uncertainties of the influential parameters to calculate the stem yield stress, where δ is the uncertainty, i.e., the ratio of standard deviation to the number of samples (100), and the fractional uncertainty is the ratio of δ to the mean value.

Table 3.4. Mean, standard deviation and uncertainties for parameters in stem yield stress test

	a (cm)	t (cm)	h (cm)	F_s (N)
mean	0.296	0.069	12.387	15.470
S_d	0.051	0.022	3.251	4.093
δ (±)	0.0005	0.0002	0.0325	0.0409
Fractional uncertainty	0.002	0.003	0.002	0.003

According to Taylor (1997), when a parameter is product and quotient of a number of other parameters as:

$$q = \frac{a_1 \times a_2 \times \ldots \times a_n}{b_1 \times b_2 \times \ldots \times b_n} \tag{3-4}$$

Then:

$$\frac{\delta_q}{|q|} \leq \frac{\delta_{a_1}}{|a_1|} + \frac{\delta_{a_2}}{|a_2|} + \cdots + \frac{\delta_{a_n}}{|a_n|} + \frac{\delta_{b_1}}{|b_1|} \ldots + \frac{\delta_{b_n}}{|b_n|} \tag{3-5}$$

Where δ_q is the uncertainty of parameter q and $|q|, |a_1|, \ldots, |b_n|$ are the mean values of the parameters. Additionally, Taylor (1997) showed, when $q = x^n$ then:

$$\frac{\delta_q}{|q|} = n\frac{\delta_x}{|x|} \tag{3-6}$$

Consequently, the fractional uncertainty for stem yield stress, is smaller or equal to summation of the uncertainties in parameters, which gives:

$$\frac{\delta_\sigma}{|\sigma|} \leq \frac{\delta_a}{|a|} + \frac{\delta_t}{|t|} + \frac{\delta_h}{|h|} + \frac{\delta_{F_S}}{|F_S|} \tag{3-7}$$

$$\frac{\delta_\sigma}{|\sigma|} \leq 0.01 \tag{3-8}$$

This uncertainty will be used in Chapter 4, where through an uncertainty analysis it will be shown that the uncertainty in this measurement is considered sufficiently accurate enough to be used in the lodging velocity calculation.

3.3.6. Anchorage system failure measurements

As described in Section 2.2.1.2, two expressions have been proposed for root anchorage system as follows:

$$R_s = \gamma S d^3 \tag{2-10}$$

$$R_s = \gamma S d^2 L \tag{2-11}$$

In order to evaluate the root strength, the following approach and protocol used by Griffin, (1998); Baker et al., (1998); Berry et al., (2003) and Berry et al. (2006) was used as follows:
The selected samples (oat plants) should be three rows or more from the plot edge to avoid the possible effect of plot edge soil on the experiment (as the pathways between the plots usually have more compacted soil, due to farmers and vehicles passing). Later, three plants

from each plot were selected and it was appropriate to ensure that the ground was wet otherwise failure may not occur. At this stage, a torque meter (Mecmesin, Advanced Force and Torque Indicator (AFTI)) was used to push the shoot to the anchorage failure point and the torque was recorded in Nm. The torque meter included a Mecmesin Smart torque cell attached to a metal rod with 20cm length to push the shoot to the anchorage failure point and a torque indicator. Later, the soil shear strength was measured by a shear vane near the plant (~5 cm away) using a PILCON shear vane fitted with a 1.9 cm vane. The data about this experiment and associated uncertainty analysis is provided in Section 4.6.

In the current research 50 samples were examined. This compared favourably with previous work by Griffin (1998) and Berry et al. (2006) who considered 12 and 37 samples respectively to be sufficient. Table 3.5 shows the mean, standard deviation and uncertainties of the influential parameters.

Table 3.5. Mean, standard deviation and uncertainties for parameters in stem yield stress test

	d (cm)	L (cm)	S (K pa)	R_s(N. m)
mean	5.18	5.86	9.04	0.13
S_d	0.80	1.36	0.61	0.06
δ (±)	0.11	0.19	0.09	0.009
Fractional uncertainty	0.02	0.03	0.01	0.07

3.4.Aerodynamic experiments

3.4.1. Aerodynamic setup

As described in Section 3.2, a non-intrusive approach is required to measure the dynamic/aerodynamic parameters of oats. In aerodynamic experiments, meteorological (wind and precipitation) parameters were recorded in the peak lodging season (GS51-GS93) to identify the influence of these factors on the movement of the oat crop. Accordingly, two 100Hz (the sampling rate is further discussed later in this section) sonic anemometers were mounted to record wind velocity in three perpendicular directions; one installed at 3m height from the ground and the other at the crop height (1.5m (in 2017), 1m (in 2018) from the ground and 0.5m from the pole). The crop height is the level where the flow loads the canopy and as such the wind velocity data is important. Moreover, a region ~2-3 canopy height above the canopy is the flow layer which interacts with the canopy (see Section 2.3.2) and the wind speed data at this level can provide an insight into the turbulent flow characteristics.

Moreover, one precipitation monitor was installed at a height of 2.5 m above the ground to collect rainfall data as shown in Figure 3.6. The setup was powered by a 12V 65Ah deep cycle lead acid battery (Mohammadi et al., 2018, Mohammadi et al., 2020b).

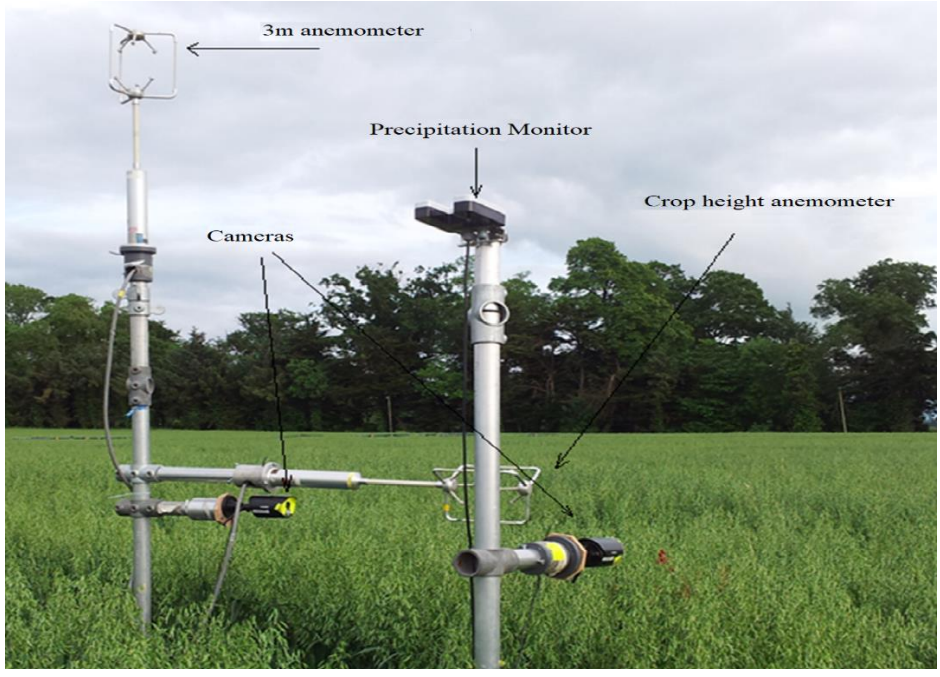

Figure 3.6. The experimental setup to measure dynamic/aerodynamic parameters of oat plant (Mohammadi et al., 2020b)

To monitor crop displacement two video cameras (Lorex, LW2770 series), with 30 frames per second sampling rate (the sampling rate is further discussed later in this section), were installed. The first camera was placed at the crop height above the ground on the same pole as the 3m anemometer and observed the movements in the East-West plane. The other camera was installed at the same height but captured the movements in the North-South plane. The wind/rainfall measurement equipment as well as cameras were linked to a watertight box where the power supply and data logging devices were located. In order to detect the displacements of a specific crop, a single oat panicle was coloured red (Figure 3.7) and the recorded video files were post processed with a video tracking code written in MATLAB (the code is presented in Appendix C and is discussed, verified and validated in Section 3.4.5).

The collected data from sonic anemometers and the displacement data (which is obtained from analyzing the video footages by MATLAB code) are a series of discrete points recorded in time. In the data analysis stage (Chapter 4), a Fast Fourier Transform (FFT) is used to represent the data mathematically. There is a theoretical limit for the number of points required to ensure an accurate reconstruction which is given by Nyquist-Shannon sampling theorem as follows:

"*The minimum sampling frequency of a signal that it will not distort its underlying information, should be double the frequency of its highest frequency component*" (Polikar, 2006). If a time series is not sampled through adequate sampling rate (i.e. enough data points), its frequency will be underestimated and the FFT might reconstruct the data with the wrong representations, which is called aliasing (Polikar, 2006). The range of crop natural frequency is 0.5-2 Hz (Baker et al., 2014) and the frequency of eddies over crop canopies is less than 10 Hz (Finnigan, 2000), thus, in this research the sampling frequency of 30Hz was used to avoid aliasing.

While choosing the target plant, a typical plant- a plant with visual similarities (height, number of spikes etc.) with average crops in the field. In order to ensure the measurements are independent from the selection of target, the test was undertaken on different targets at the same day and the measured values of damping ratio and natural frequency were compared. These tests were repeated during the season, while one the of panicles was continuously monitored to identify the variation of parameters through the season. Altogether, 10 samples (3 samples in 2017 and 7 samples in 2018) were examined. The result of target independence tests and the agronomic measurement of samples is provided in Appendix D. Moreover, at the end of each year's experiments the targets were excavated, carried to the laboratory and its agronomic parameters were measured and compared with average values of agronomic

measurements (Chapter 4, Table 4.8) to ensure it is a typical plant from an agronomic perspective (Appendix D, Table D-1).

Figure 3.7. Oat target position in front of cameras (Mohammadi et al., 2020b)

3.4.2. Ultrasonic anemometers

The accurate measurement of turbulent fluctuations is a crucial step to develop a deep understanding of the flow over canopies and to evaluate dynamic/aerodynamic parameters. The wind velocity can be measured by mechanical instruments (e.g., cup wheel and vane anemometers), in steady wind conditions. Nevertheless, such devices cannot accurately detect the turbulent fluctuations, due to the slow response time. Alternatively, non-mechanical anemometers (e.g. ultrasonic anemometers and hot-wires) can detect the wind fluctuation and rapid changes in the turbulent flow, in horizontal and vertical directions (Whelpdale, 1967).

The advantage of ultrasonic anemometers is the capability to reflect rapid changes in wind speed and direction to study the turbulent flow, something that cannot be detected by mechanical anemometers. Hot-wire anemometers use a short delicate wire heated by a

current. As the flow around the wire has a cooling effect, the temperature difference in the wire is used to measure the wind speed (Whelpdale, 1967). The hot-wire anemometer is not an appropriate choice for the current experimental setup as it must be cleaned and calibrated regularly and cannot be used in rain (Whelpdale, 1967). Thus, this instrument is appropriate for a laboratory study rather than a fieldwork with an unattended experimental setup. However, the ultrasonic anemometer is suitable for fieldwork as the instrument can work in a variety of weather conditions and does not need calibration (Gill manual, 2021). Consequently, in this research R3-100 ultrasonic anemometers were used to measure wind velocity. This device is designed to record the wind speed data in high frequency and accuracy which is essential for the spectral analysis used in this research (Chapter 4). This instrument has a sampling frequency of 100Hz while the frequency of eddies over crop canopies is less than 10 Hz (Finnigan, 2000). Consequently, the device is able to detect the energy cascade in the turbulent flow over the crop.

The ultrasonic anemometer has three pairs of transducers, which can send and receive pulses (Figure 3.8). The travel time of a pulse from upper to lower transducer depends on the distance between the transducers, the speed of sound and the wind speed between the transducers which can be represented as follows:

$$T = \frac{\Delta L}{C_s + V_{air}} \tag{3-9}$$

Where T is time, ΔL is the distance between transducers, C_s is the speed of sound, and V_{air} is the airspeed along the transducer axis (Gill manual, 2021). Each transducer acts both as a

transmitter and receiver, consequently, pulses travel in both directions between the transducers. The airspeed can be calculated from the pulse travel time in each direction as follows:

$$V_{air} = \frac{1}{2} V_{air}(\frac{1}{t_1} - \frac{1}{t_2}) \quad (3\text{-}10)$$

The probe has a spar to point to the North direction, so the output velocity can be interpreted. Accordingly, the output data is provided in three columns where the first, second, and third columns represent the wind velocity components in the North, West, and upward directions. Having the velocity components in the three directions the velocity components in the streamwise, cross-stream and vertical directions can be identified as follows:

$$u = (u_{North} cos\theta + u_{west} sin\theta) cos\varphi + u_{up} sin\varphi \quad (3\text{-}11)$$

$$v = -u_{North} sin\theta + u_{west} cos\theta \quad (3\text{-}12)$$

$$w = u_{up} cos\varphi - (u_{North} cos\theta + u_{west} sin\theta) sin\varphi \quad (3\text{-}13)$$

Where the angles are given by:

$$tan\theta = \frac{\bar{v}}{\bar{u}} \quad (3\text{-}14)$$

$$tan\varphi = \frac{\bar{w}}{\sqrt{\bar{v}^2 + \bar{u}^2}} \quad (3\text{-}15)$$

Where $\bar{u}$, $\bar{v}$ and $\bar{v}$ are the mean values of streamwise, cross stream and vertical velocities.
The working condition for this device is between -40ºC to +60 ºC and precipitation of 300 mm/hr. The environmental conditions (wind, temperature, and rainfall) of study locations are within these ranges, and as such, this device is suitable for the measurements. The range of anemometers detection was 0-45m/s with a resolution of 0.01m/s. Moreover, and the measurable direction range is range 0-359° with a resolution of 1° to an accuracy of ±1° RMS. The effect of these uncertainties is considered in Appendix E, which shows such small uncertainties has a negligible effect on the projected streamwise wind speed. It is worth noting that, as the mean wind speed is used to evaluate drag area parameter, the effect of wind speed uncertainty, together with other influential parameters must be taken into the account (Section 4.3.3).

While using ultrasonic anemometers, limitations and disadvantages of the device must be considered as well. The instrument is relatively expensive, and the electronic components are complex, and can be only calibrated by the manufacturer. In the case of considerable temperature field in the passes of pulses, the travel time might be affected, and errors can be introduced in the output data (Whelpdale, 1967), however, this is not the case in the current experiment. Finally, the elements of the instrument can potentially affect the turbulent flow characteristics, although such an effect is neglected (Whelpdale, 1967).

The device has an alignment spar which must be used to enable the data to be interpreted. The spar must be pointed north when the device is positioned vertically (3m height anemometer) and downward when positioned horizontally (crop height anemometer).

The ultrasonic anemometer is calibrated by the manufacturer and does not need a further calibration unless the measuring head is distorted, which causes false data even when the

wind speed is zero. In such conditions, the device must be returned to the manufacturer to be recalibrated in a wind tunnel. In order to ensure the instrument was calibrated, the output data in a still condition was checked before the field experiments each year, which showed the probe can accurately measure the zero wind speed and the device is calibrated.

Although the device does not need any calibration, the output data from anemometers was checked for any unreasonable very large values. Additionally, the averaged wind speeds from two sonic anemometers over different period of times were compared with each other and with other wind speed devices at the field (i.e., a 10Hz sonic anemometer installed on field in 2017 and with the wind speed data from the meteorological station in 2018). Finally, the velocity fluctuations were used in Q-H and spectral analysis to examine if the turbulent flow characteristic as measured by these instruments are consistent with the literature. Figure 3.8 shows an ultrasonic anemometer dimensions and alignment spar.

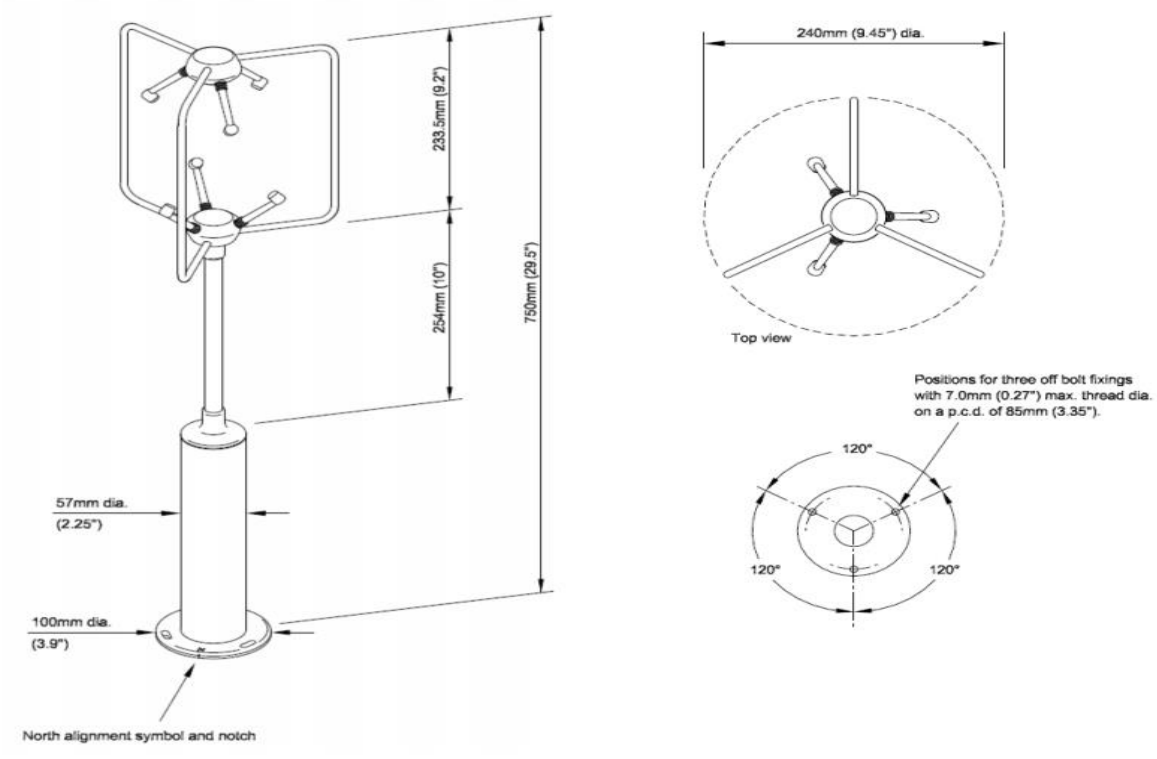

Figure 3.8. R3-100 North Spar Alignment and Dimensions (Gill manual, 2021)

3.4.3. Data logging device

The experimental setup described in Section 3.3.1 was installed in a remote place and the data was recorded for many hours and several days through the lodging season and it was not feasible to log the data through a PC or a laptop. Consequently, an antilog manufactured by Anticyclone Systems Ltd was used to receive and record data from ultra-sonic anemometers. This device was selected due to its capability to log the data in two channels from two sonic anemometers without the need for a PC or Laptop. Moreover, the data logger was small (pocket size) and could be easily placed in a watertight box, besides other logging and power supply equipment. Additionally, the device can log a large amount of data (~1 TByte) for several hours/days and does not need continuous checking. The device is also easy to connect to a PC and can be reconfigured easily. Figure 3.9 shows a sample antilog used in the setup (AntiLog RS232 Data Logging System User Guide, 2017).

Although the device has many advantages as mentioned above, it has some limitations which must be considered when used. First, the device is not waterproof, and it was placed in the water tight box which was always kept dry. Additionally, although the device was supported by a 12 Volts DC power, an internal battery was required to ensure about the power supply for a long time, as the DC power cannot supply all the connected devices for more than ~24 hours. Moreover, the internal battery showed a significant drop in voltage (tested by a voltmeter) after 2-3 days, so the internal battery had to be changed repeatedly.

Figure 3.9. AntiLog RS232 data logger

The following steps are the standard procedure advised by the manufacturer to ensure the device functions correctly:

1. The Antilog should be connected to a PC or laptop using the provided cable with the device and the manufacturer software (alternatively other antilog software e.g. PUTTY or Windows Command Prompt, Microsoft Windows 10 app, can be used to operate the device)
2. The green LED must light after pressing the ‘On’ button
3. The software terminal should show the device name, serial number, time and date, memory used, and setting options (The time and date is automatically updated when the device is connected to a PC)
4. Based on LED colours and flashing, it can be determined if the device works correctly. Accordingly, in order to use the device to record the data (record mode), the ‘On’ button should be pressed for a very short period (~1 second), and the LED should flash red following by a number green and/or yellow flashes to show Antilog

is writing the data. Additionally, the LED light must light briefly when the 'Off' button is be held for seconds to confirm power down before the button released. If the LED does not flash as above, the problem-solving procedure must be undertaken.

In addition to the above steps, the Antilog was attached to an ultrasonic anemometer in still conditions and the recording and logging the data was examined which showed correct output data when the anemometer was tested in still conditions and when it was exposed to a flow at a certain time and period.

3.4.4. Precipitation Monitor

The precipitation monitor was used to detect the beginning and the end time of precipitations on the field. Such data can be important as heavy rainfall can influence the data quality of ultrasonic anemometers (Gill manual, 2021). Consequently, knowing the start and the end time of the heavy rainfall, the relevant wind speed data can be excluded from the analysis.

It is worth noting that this device does not provide any information about the amount of rainfall during 24 hours (as required by the lodging model) and this information was collected by the meteorological stations near the experimental site. Moreover, the placement of the device must be done carefully, as it should be above other devices, away from dripping and condensation from other instruments. Additionally, the data logger for the device is not waterproof and was placed in a watertight box.

The precipitation monitor can detect different forms of precipitations including drizzle, rain, snow or hail using infrared light barrier system and produces a signal in the electronics in the device. The device can filter environmental incidents such as leaves, bird dropping; insects,

etc. as the device considers a 50 second time window to ensure the incident detected is a form of precipitation (OMC-270 Precipitation Monitor, 2017). To log the precipitation output data the OM-CP-Process101A data logger was used. The data logger has an internal battery lasting for 4 years and can be connected to a computer for starting/stopping the data logging and operating the internal memory. The device has a mode to detect a number of drops at a time, which was used to test the device before installed in the setup. Additionally, the device was tested by pouring water in a certain time period, and the output data was checked to ensure the device is capable to detect the beginning and the end of the incident.

Although the device was used in the setup to ensure precipitation does not affect ultrasonic anemometer outputs, in practice the data analysed in this research were collected on dry days, and the output of the precipitation monitor was zero. Consequently, the uncertainties associated with the measurement by this device are not influential on the results explained in the next chapters. Figures 3.10a and 3.10b show a Precipitation Monitor and a data logger respectively (OM-CP SERIES manual, 2017).

(a) (b)

Figure 3.10. (a) OMC-270 Precipitation Monitor (OMC-270 Precipitation Monitor) (b) OM-CP-PROCESS101A

3.4.5. Camera and video tracking

Two cameras were used to observe plant movements, in two planes i.e. North-South and East-West planes. Both cameras were connected to a rechargeable touch panel LCD receiver/recorder by relevant cables (Lorex user guide, 2017). The LCD receiver / recorder is the user interface with cameras and can record videos if using an SD memory card. Figure 3.11 demonstrates the camera system components. This device was chosen, as it could record video in 30 Hz frequency which is quick enough to detect the natural frequency of the crop (Section 3.4.1).

Figure 3. 11. Camera system main components (a) camera (b) rechargeable touch panel LCD receiver/recorder (c) Power adapters for receiver and cameras (d) SD memory card (Lorex user guide, 2017).

The cameras were calibrated to eliminate the potential effect of lens distortion and to make a relationship between dimensions in the real world and the pixels. Accordingly, two types of

parameters were determined, extrinsic and intrinsic parameters, where the former transforms the real dimensions to camera coordinates and the latter adjusts the camera coordinates to the image plane using the camera characteristics such as focal length of the lens, optical centre, and lens distortion coefficients. In order to undertake the camera calibration, 20 images from a checkerboard from different angles but the same distance were inserted into the Camera Calibrator App in MATLAB. Knowing the size of each checkerboard square, the software can show the extrinsic and intrinsic parameters of the camera.

A video tracking MATLAB code (Appendix C) was developed to analyse recorded video files and to detect the red target position in each video frame. The target could be painted in other colours however red was chosen to provide a significant contrast with the background plants and the blue sky. Accordingly, the imported video was analysed by MATLAB code where thresholds for the image's hue, saturation and colour were defined to detect the red target and the centroid of the red pixels was calculated.

The tracking program considers the video file frame by frame and provides an array of centroid coordinates through time. The pixel coordinates can be converted to real stem displacement using the focal length of the camera lens, the optical centre, and the distance from the target to each camera lens. Moreover, the zero displacement point can be identified based on the pixel in which the centroid of the target stays in a still (no wind) condition.

Each camera detected the displacement at a different plane, i.e. North-South (X_{NS}) and West-East (X_{WE}) planes. Later, based on the direction of streamwise velocity, the streamwise direction (X_s) is determined. Consequently, the streamwise and cross stream directions can be obtained as follows:

$$X_s = X_{NS}\, cos\theta + X_{WE}\, sin\theta \tag{3-16}$$

$$X_{cs} = -\, X_{NS}\, sin\theta + X_{WE} cos\theta \tag{3-17}$$

Where X_s is the displacement of the target in the direction of the streamwise velocity, X_{cs} is the displacement of the target in the cross-stream direction, X_{NS} and X_{WE} are the observed displacement of the target in North-South and East-West planes and θ is as defined in equation 3-14. Figure 3.12 shows a schematic of the position of target in front of cameras and the displacement planes (θ is not shown as it determined by streamwise wind speed).

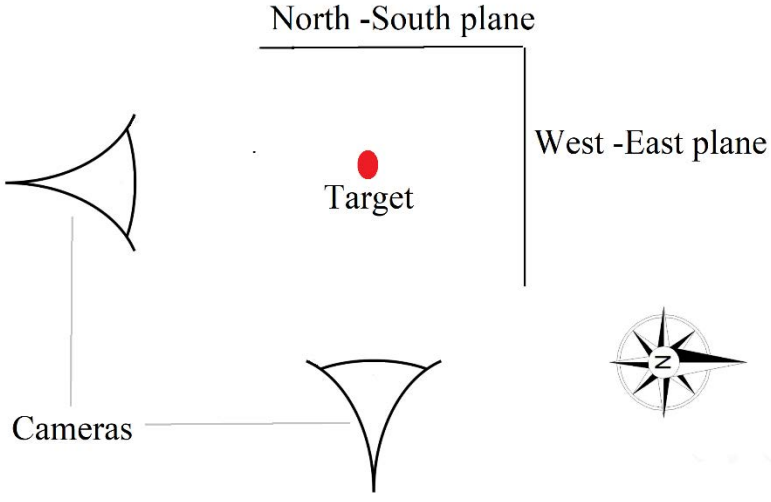

Figure 3.12. The position of target in front of cameras and the displacement planes

In addition to the camera calibration, the MATLAB code must be verified to ensure the designed setup and the code are capable to meet the requirements and track the target accurate enough. Accordingly, a target red dot was placed in front of cameras (a similar position as shown in Figure 3.12) and was moved at a given rate and direction. This test was

repeated 20 times and the results show measurement uncertainty δ = ±1.6mm and S_d = 0.007mm in 1m travel distance of the target, where δ is the random uncertainty which is the ratio of standard deviation to the number of tests. The test was repeated with targets in different sizes and movement directions and in all cases the code was capable to detect the movement with the same order of uncertainty.

In order to ensure if the accuracy of the code is enough for aerodynamic measurements (Section 4.3.3 will describe the mean displacement used together with the mean velocity to determine the drag area factor), an uncertainty analysis is undertaken on the displacement equations 3-16 and 3-17. Accordingly, the following expressions can be derived:

$$\frac{dX_s}{X_s} = \left(\frac{\partial X_s}{\partial X_{NS}}\right) dX_{NS} + \left(\frac{\partial X_s}{\partial X_{WE}}\right) dX_{WE} + \left(\frac{\partial X_s}{\partial \theta}\right) d\theta \tag{3-18}$$

$$\frac{dX_s}{X_s} = \frac{(cos\theta)dX_{NS} + (sin\theta)dX_{WE} - X_{NS}\, sin\theta\, d\theta + X_{WE}\, cos\theta\, d\theta}{X_{NS}\, cos\theta + X_{WE}\, sin\theta} \tag{3-19}$$

And

$$\frac{dX_{cs}}{X_{cs}} = \left(\frac{\partial X_{cs}}{\partial X_{NS}}\right) dX_{NS} + \left(\frac{\partial X_{cs}}{\partial X_{WE}}\right) dX_{WE} + \left(\frac{\partial X_{cs}}{\partial \theta}\right) d\theta \tag{3-20}$$

$$\frac{dX_{cs}}{X_{cs}} = \frac{(-sin\theta)dX_{NS} + (cos\theta)dX_{WE} + (-X_{NS}cos\theta)d\theta + (-X_{WE}sin\theta)d\theta}{-X_{NS}\, sin\theta + X_{WE}cos\theta} \tag{3-21}$$

From the aforementioned experiment $dX_{NS} = 0.0016m$, $dX_{WE} \cong 0m$ when $\theta = 0$. Additionally, the direction of streamwise displacement is determined by the streamwise velocity. Thus, from sonic anemometer $d\theta$=1°=0.017 radian. Inserting these values in equation 3-19 and 3-21 gives the fractional uncertainty of streamwise and cross stream

displacements. Results for test for different θ angles, the fractional uncertainties are of the order of -3 and -4. Section 4.3.3 will use this finding and evaluate the uncertainty analysis for the drag area parameter. In addition to the above experiment, a wind tunnel test to measure the target crop static deflection where at a constant wind speed (3m/s) the displacement of a red painted target plant δ= 2mm and S_d = 0.01mm. These tests showed, regardless of size and shape of the targets, tracking the centroid of the object gives an accurate indication of object movement.

As mentioned above the cameras recorded the displacement of the target crop at two orthogonal planes. Using the data from the ultrasonic anemometer, the streamwise mean velocity can be obtained. Subsequently, the displacement at two planes can be converted to the mean streamwise displacement and mean cross-stream displacement. It is expected that over a time period (i.e. 10 minutes) the mean streamwise displacement be proportional to mean streamwise velocity (further described in Section 4.3.3) and the mean cross-stream displacement to be near zero. The former can be used to evaluate drag area and the latter can be employed as a validation to ensure the tracking code is accurate enough. It is worth noting that in all the analysed videos, the cross-stream displacement was an order of -4. Given that the uncertainties in 1m displacement in the aforementioned test are an order of -3, it is not surprising to see a lower uncertainty in the cross-stream displacement in the field conditions, as the displacement of the crop is lower.

.

Although the visual method developed to study the dynamic/aerodynamic parameters has the advantage of being non-intrusive and is appropriate to study interlocked canopies like oats, it has some limitations. The method is highly dependent on out-of-control environmental conditions, i.e. daylight to enable the target to be detected and windy weather to move the

target. Consequently, there are limited times when both conditions, especially the latter occurs and the method is not efficient from a timing perspective as long field measurements are required and only a small part of the collected data meet the criteria and can be used for the data analysis and post-processing stage. The other limitation of the method was the number of targets that can be tracked simultaneously. The MATLAB code could track one panicle in a specific colour. Consequently, having two red targets in one frame was not feasible, while other detectable colours were already in the environment and could not be used. Consequently, in order to examine different targets, the whole setup had to be displaced, which was time and energy-consuming.

3.5.Conclusions

This chapter presented the methods used in this research to measure agronomic and dynamic/aerodynamic parameters. Following conclusions can be made:

Crops were grown under a number of husbandry techniques, which enables the research to investigate the effect of such environmental conditions on the lodging susceptibility of crops. The methods to undertake agronomic measurements were adopted from standard agronomic protocols developed in the late 1990s and early 2000s.

The novel method introduced for dynamic/aerodynamic parameter measurements enables parameters like natural frequency, damping ratio, and drag area to be investigated in a natural condition through the lodging season with the least possible interference. Moreover, as the wind measurements are undertaken in natural condition, the constraints of wind tunnel simulation to produce a realistic wind condition is not applicable. The main instruments used in the experimental setup were the ultrasonic anemometers and video cameras. The ultrasonic anemometers were used to enable accurate recording with a high sampling rate. The cameras

used in the aerodynamic measurements were not specially designed for this application. Nevertheless, it was shown that the camera is quick enough to detect the natural frequency of crops at the post-processing stage. Moreover, the camera was calibrated through a standard method to remove potential distortions. A video tracking code was developed in MATLAB to track the displacement of the crop and it was shown that it can accurately and precisely track a moving sample target. Moreover, the analysis of the output displacement data verified the code as the output agreed with the physics of the wind/plant interactions.

4. Field data and analysis

4.1. Introduction

This chapter presents the data collected from the experimental campaigns as well as the analysis undertaken to study the turbulence flow over the crop canopy and the dynamic response of the crops when displaced by wind-induced forces. Section 4.2 presents data analysis concerning the wind flow over an oat canopy where the momentum transfer in the flow, the turbulence length scale, the velocity spectra, and other turbulence flow parameters (e.g. turbulence intensity) are investigated and discussed. Additionally, the crop's dynamic/aerodynamic parameters including damping ratio, natural frequency, and the drag area have been studied in Section 4.3. Section 4.4 presents displacement time histories produced by the model and compares them with the observed displacement. Section 4.5 and 4.6 focus on the agronomic results, where the former presents the data collected in agronomic measurements and the latter presents and discusses the results of experiments on the anchorage system. Section 4.7 brings together all the uncertainties presented in the current and the previous chapter in order to evaluate the overall effect of these uncertainties on lodging velocities. Finally, brief conclusions relating to this chapter are presented in Section 4.8.

4.2. Turbulent Flow over the canopy

This section gives an insight into the turbulent flow over the canopy and provides an opportunity to compare the results obtained with those in the literature. Section 4.2.1 presents the results of Q-H analysis and shows how momentum is transferred in the flow. Section 4.2.2 presents the results relating to the size of eddies which dominate the flow over the plant canopy, whilst Section 4.2.3 uses spectral analysis in order to obtain an insight into the wind field. Finally, Section 4.2.4 presents some data analysis relating to other turbulent flow parameters.

4.2.1. Quadrant-hole analysis

The Q-H analysis was fully described in Section 2.4.2 and the results of the analysis are provided in this section. This analysis gives an insight into the momentum transfer from the flow to the canopy and thus enables the fundamental mechanism which drives lodging to be ascertained – such behaviours form a key component of the lodging model. Accordingly, the velocity data collected by ultrasonic anemometers are used in this analysis to find an indication of the flow structure over the canopy.

As described in Section 2.4.1, the Q-H analysis considers the flow momentum based on the signs of streamwise and vertical velocity fluctuations and normalized conditional shear stress, $S_{i,j}$ as follows:

$$S_{i,j} = \frac{1}{\sigma_u \sigma_w T} \int_0^T u'(t) w'(t)\, I_{i,j} dt \qquad (2\text{-}30)$$

Figures 4.1, 4.2 and 4.3 are based on the velocity data as collected on 15th June 2017 (GS87) for 10 minutes, above the oat canopy for two different heights. It is worth noting that results were found to be consistent from 10 minute to 1 hour recordings (see Appendix F).

Figure 4.1 demonstrates the distribution of velocity fluctuations in four quadrants at two measurement heights (each point represents a velocity measurement) and illustrates the percentage of each quadrant in the total points. The horizontal and vertical axes are the streamwise and vertical velocity fluctuations normalized by corresponding standard deviations. This figure shows the highest percentage of interactions in the ejections quadrant (sweeps and ejections are defined in Section 2.4.1), followed by sweeps, while the latter seems to have a higher magnitude and consequently a higher contribution in momentum transfer. This finding can be also noticed from Figure 4.2 which shows the joint probability of velocity fluctuations. Results from Figure 4.1 and figure 4.2 show despite the higher probability of ejection interactions, the velocity fluctuations in the sweeps quadrant have higher values (and consequently higher contributions in the momentum transfer) than those in the ejections quadrant.

Finally, the variation of normalized conditional shear stress, $S_{i,j}$ is plotted versus j (both defined in Section 2.4.1) is demonstrated in Figure 4.3, where sweeps and ejections ($S_{2,0}$ and $S_{4,0}$ respectively) are much larger than inward and outward contributions ($S_{1,0}$ and $S_{3,0}$ respectively) at both heights (the $S_{i,j}$ in the second and third quadrant are multiplied by -1 to make the visual comparison between figure 4.1, 4.2 and 4.3 easier). It is also noticeable that sweeps, which represent a downward movement of flow into (and ultimately the force acting on) the canopy, are the dominant event to transfer the momentum in both heights. Moreover, ejections, which represent an upward movement are the second major event in both levels.

Consequently, although a higher number of velocity fluctuations recorded in the ejection quadrant (Figure 4.1 and 4.2), sweeps have a higher contribution in the momentum transfer (Figure 4.3). These findings provide an insight into how the turbulent flow and the canopy interact with respect to the momentum transfer. Through the interaction of the flow with the canopy, shear is produced which eventually loads the plant. In addition to the momentum transferred from the flow to the canopy, the sweeps and ejections (coupled with the dynamic movement of the plants) gives rise to the coherent waving of the canopy.

The results of the Q-H analysis, which provides an insight into the wind loading mechanism on crops, are consistent with the finding in other plant canopies as similar results were reported for wheat canopies (Finnigan, 1979), wind tunnel models for different vegetation (Raupach et al., 1986, Sterling et al., 2003) and corn canopies (Shaw et al., 1983). This consistency shows the wind loading mechanism is similar in oat loading in comparison to other crops. Moreover, the results showed the results are consistent between different data sets when a 10-minute averaging period is used. The length of the averaging period was varied from 10 minutes to 1 hour (see Appendix F) and the findings remain consistent. A 10-minute sampling period was chosen since it ensured that the number of sets of data available for analysis was maximised. Consequently, 10-minutes is an appropriate averaging time to consider the flow/crop momentum transfer and wind loading (which is used in Section 4.3.3 to evaluate drag area parameter). Additionally, this finding suggests the approach proposed by Baker et al. (2014) to evaluate the mean drag force over a period of time is appropriate and applicable to study oat canopies.

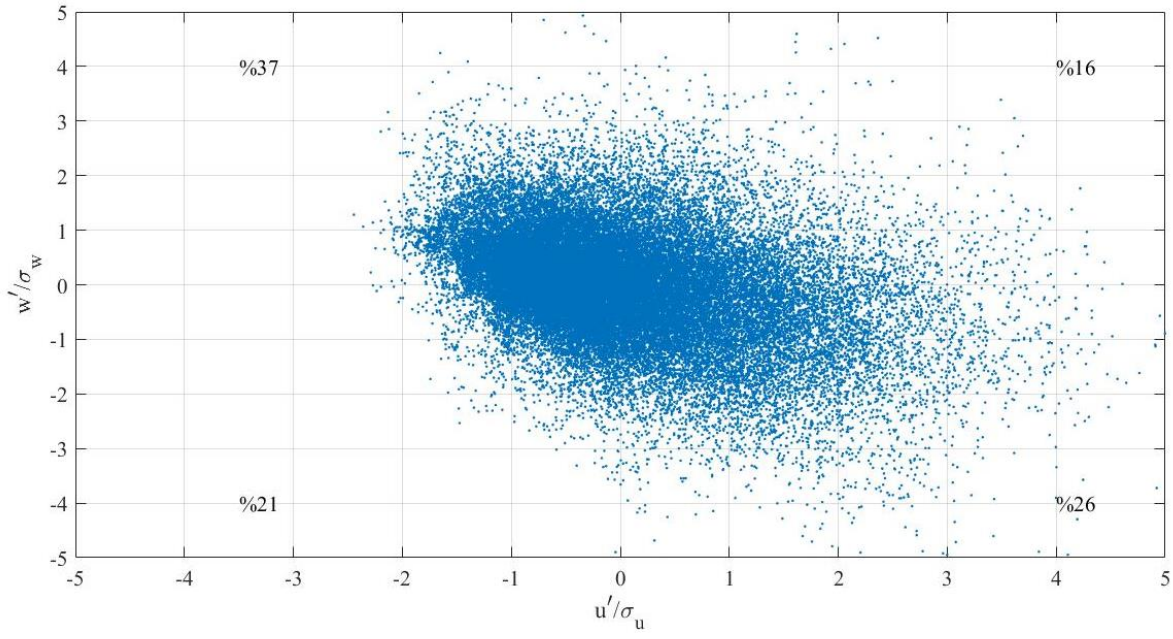

(a) The distribution of normalized velocity fluctuations at oat crop height (1.5m)

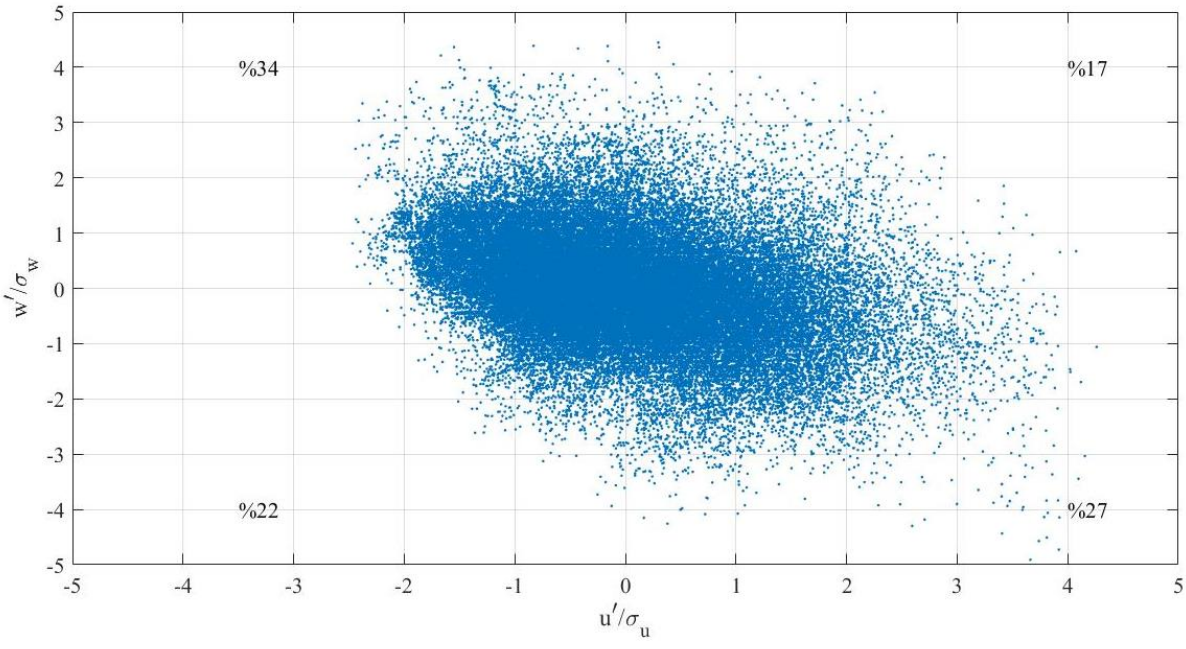

(b) The distribution of normalized velocity fluctuations at 3m height

Figure 4.1. Normalised instantaneous velocities fluctuations in the $u' - w'$ plane (standard deviations are used to normalise the velocity components). The percentages in both figures illustrate the total number of data points which fall into each quadrant.

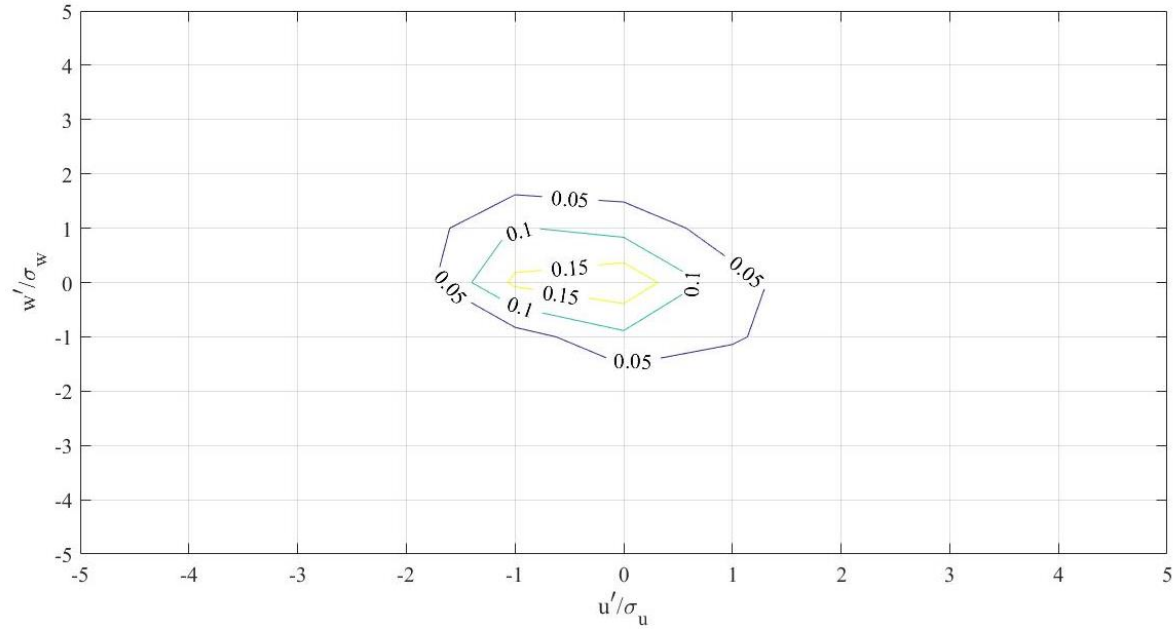

(a) Joint probability density function at the crop height (1.5m)

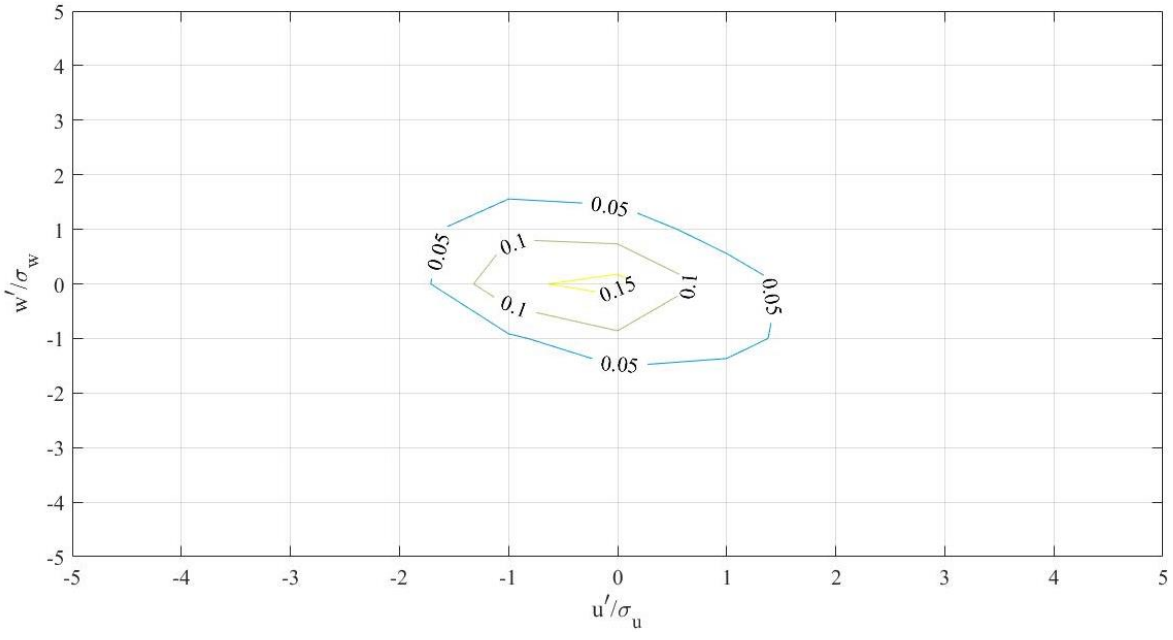

(b) Joint probability density function at 3m height

Figure 4.2. Joint probability density function in two different heights

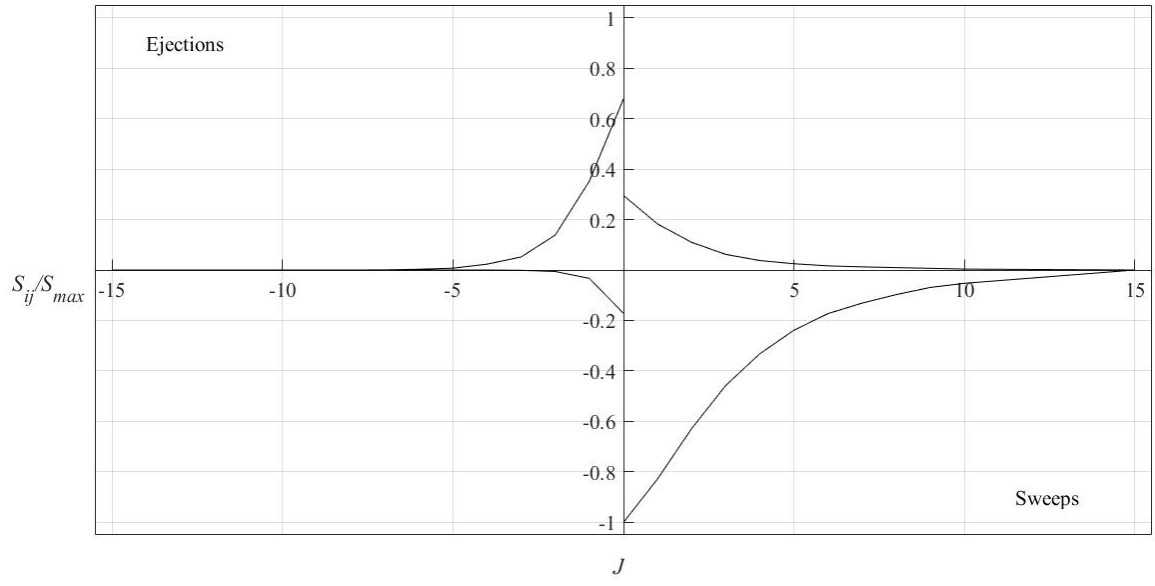

(a) Quadrant-hole analysis results for the data at the crop height (1.5m)

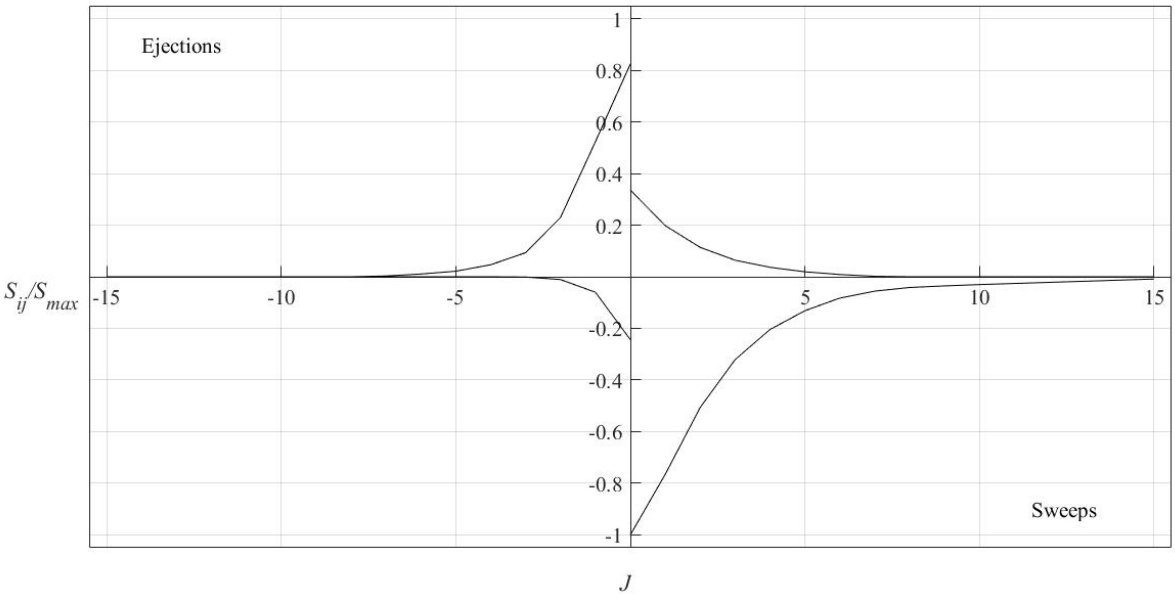

(b) Quadrant-hole analysis results for the data at the 3m height

Figure 4.3. Quadrant-hole analysis results for the data as collected data as collected on 15th June 2017 (GS87)

4.2.2. Determining the Turbulence length scales

The crop failure criteria used in Baker et al.'s lodging model are derived for a 'typical' flow over a 'typical' crop (based on the earlier work defined by Finnigan (2000)). The following analysis explores the assumption of the turbulence length scale which is one of the assumptions made.

As mentioned in the literature review (Section 2.3.2), coherent structures are important elements of the turbulent flow. The length scale of eddies with the highest energy (and consequently important from wind loading perspective) is known as the integral turbulence length scale and in the flow over crops, this parameter is related to the crop height (see Section 2.3.2). Consequently, a good test on the collected turbulent flow data is to check the consistency of the value of this parameter with the literature. The integral turbulence length scale can be defined using the autocorrelation function (equation 2-22), assuming that eddies are transported by the mean velocity of the flow stream (known as Taylor's frozen turbulence hypothesis), without changes in their properties (Hill, 1996). Although the turbulent flow is time-dependent and not frozen, the assumption can be widely used in practice as the eddy lifetime is usually much higher than their travel time across the sensor (Hill, 1996). Moreover, a wide range of experiments supports the applicability of the hypothesis in the turbulent flow over canopies (Kaimal and Finnigan, 1994; Finnigan, 2000). Taylor's frozen turbulence hypothesis enables the integral turbulent length scale to be derived from the velocity measurements at a single point as following equations:

$$L_u = \frac{\bar{U}}{\sigma_u^2} \int_0^\infty \overline{u'(t)u'(t+T)}\, dT \qquad (2\text{-}24)$$

$$L_w = \frac{\bar{U}}{\sigma_w^2} \int_0^{\infty} \overline{w'(t)w'(t+T)}\, dT \qquad (2\text{-}25)$$

Where L_u and L_w are the turbulence length scales in streamwise and vertical directions, $\bar{U}$ is the mean wind speed, σ_u is and σ_w are the standard deviation of streamwise and vertical velocities (Finnigan, 2000).

In order to determine the integral turbulence length scale, the autocorrelation function (equation 2-22) is usually integrated up to the smallest value where the autocorrelation function is zero (Benedict and Gould, 1998). However, due to random variations, the autocorrelation function might not cross the horizontal axis and cause inaccuracies in the results (Benedict and Gould, 1998; Trush et al. 2020). Figure 4.4 demonstrates an example result of streamwise and vertical velocity autocorrelation functions for the velocity data collected on 13th June 2018 (GS83).

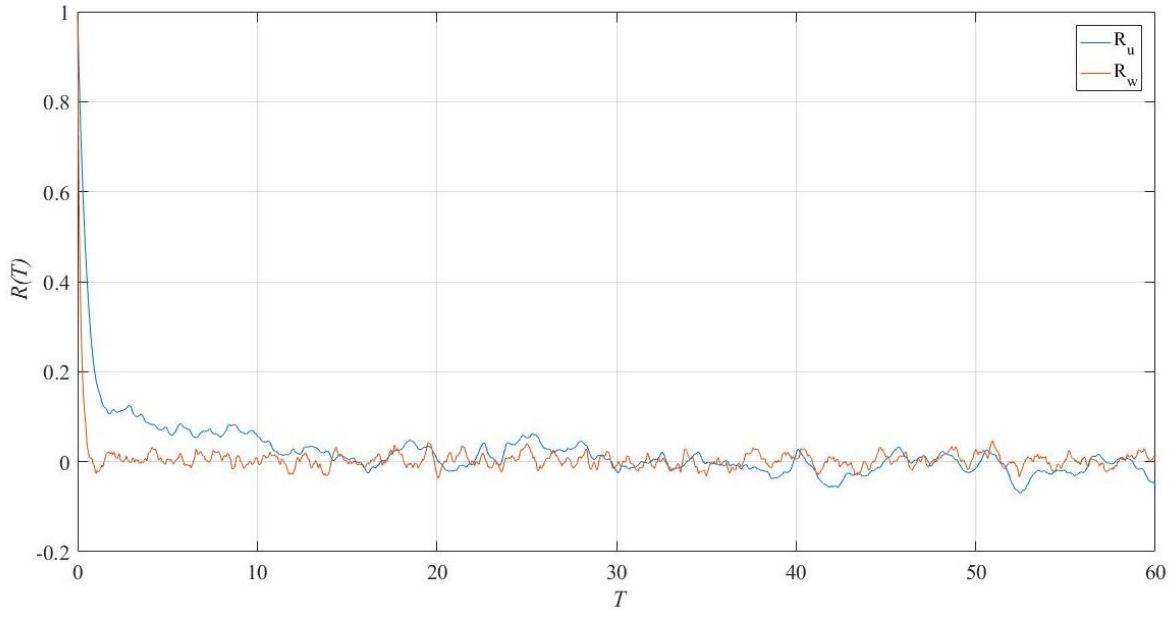

Figure 4.4. Streamwise (R_u) and vertical (R_w) velocity autocorrelation functions (equation 2-22) versus time lag (T)

In order to calculate the turbulence length scale through the autocorrelation method, 20 individual records were studied each 10 minutes in length. The range, mean and standard deviation values are shown in Table 4.1.

Table 4.1. Range, mean values, standard deviations of non-dimensionalised length scales calculated from the autocorrelation method

	range	mean	S_d
L_u/h	1.16-4.26	2.01	0.73
L_v/h	0.92-4.71	2.26	1.12
L_w/h	0.22-0.34	0.28	0.04

An alternative method to determine the turbulence length scale, as described in Section 2.4.2, is based on Von Karman's power spectral density. From a mathematical perspective, the power spectral density is the Fourier transform of the autocorrelation function and this should give identical results to those obtained above. Homes (2001) notes that the following expression is widely used for the Von Karman spectral density:

$$\frac{fS_u(f)}{\sigma_u^2} = \frac{4fL_u/\overline{U}}{(1+70.8(\frac{fL_u}{\overline{U}})^2)^{5/6}} \tag{2-32}$$

Using the values of other parameters in the above equation from the experimental data, L_u can be determined through a curve fitting process (see below) and the Curve Fitting tool in MATLAB was used for this purpose. This tool provides both visual and numerical outputs to show the goodness of fit. Once a curve is fitted in this manner, it is possible to view the fitted curve alongside the actual data which provides a final, visual check as to the goodness of fit.

However, the numerical factors focus on the statistical aspect (introduced later in this section) of the curve fitting. Overall, both types of measures are useful for the curve fitting process.

In order to undertake the curve-fitting, the frequency values (*f*) and the left side of equation 2-32 was entered as the variable and function respectively (based on data obtained from the experiments). Next, the right side of equations 2-32 was entered in the Curve Fitting tool in MATLAB as a customized equation and the curve fitting tool was used to find the best fit based on variable L_u value. Figure 4.5 shows an example curve fitting for 10-minute data collected on 13th June 2018 (GS83), which shows the curve is visually a good fit for the data.

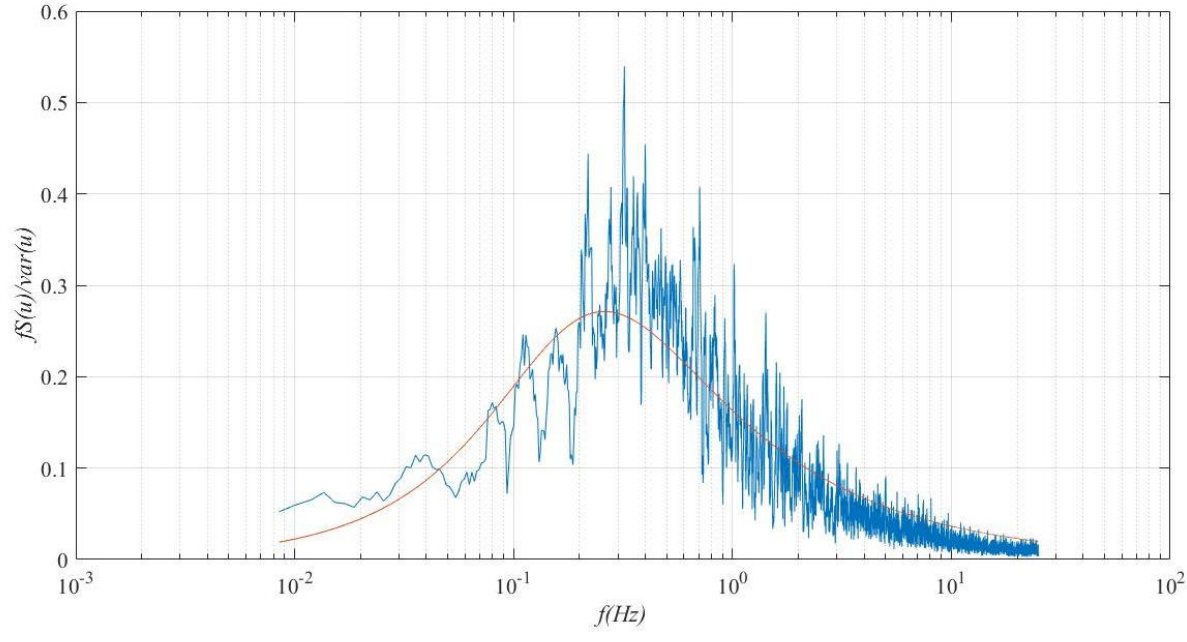

Figure 4.5. Von-Karman spectral curves for the wind in the streamwise direction for velocity data collected at crop height on 13th June 2018 (GS83).

Table 4.2 shows the statistical parameters about the goodness of fit for all considered records in the curve fitting process. In this Table, L_u/h is the turbulence length scale normalized by the crop height and the R^2 is defined as follows (MATLAB help, 2021):

$$R^2 = 1 - \frac{SSE}{SST} \quad (4\text{-}1)$$

Where *SSE* is the summation of squares due to error and *SST* is the summation of squares about the mean. These parameters are defined as follows (MATLAB help, 2021):

$$SSE = \sum_{i=1}^{n}(y_i - Y_i)^2 \quad (4\text{-}2)$$

$$SST = \sum_{i=1}^{i_{max}}(y_i - \bar{y})^2 \quad (4\text{-}3)$$

Where y_i represents the values of the data (here the left side of equation 2-32), Y_i is the corresponding value as calculated by the curve (i is the order of values in the database), and $\bar{y}$ represents the mean value of y_i.

The R^2 value can take any value between 0 and 1 and as the value is closer to 1, a higher proportion of variance is accounted by the model. For example, in the fitted curve in Figure 4.5, the R^2=0.84, which means that the fit explains 84% of the total variation in the data about the average.

Another useful statistical term to assess the goodness of the fit is the root mean square error (RMSE) which is defined as follows (MATLAB help, 2021):

$$\text{RMSE}=\sqrt{\frac{SSE}{z}} \quad (4\text{-}4)$$

where z is the number of data points (number of population). Table 4.2 show the records used in the curved fitting process, the fitted L_u/h and the corresponding curve fitting statistics.

Using the turbulence length scale values from the two mentioned methods, it is possible to compare the results with the literature. Table 4.3 shows a summary of results from two methods used in this research as well as results from Sterling et al. (2003) and Finnigan (2000) to study the flow over wheat canopies. It is worth noting that both methods considered 20 wind data records at the crop height and the period of each record was 10 minutes.

The results show that the Von Karman method provides a lower range of variation than the autocorrelation method. Moreover, the values from the earlier method are closer to $L_u = h$ as suggested by Finnigan (2000) for crop canopies. These differences are in some cases due to the integration of the autocorrelation function – in some cases the function does cross the horizontal axis.

The results from both methods show L_u and L_w are scaled with the canopy height as suggested by the literature (Kaimal and Finnigan, 1994; Finnigan, 2000; Py et al., 2006), although the autocorrelation method shows higher values due to aforementioned issue in the method. The results also agree Finnigan's (2000) experimental data and L_u/h values calculated based on auto correlation approach, are closer to values reported by Sterling et al. (2003).

Based on these results, it can be concluded that the flow over an oat canopy is similar to the flow over other plant canopies and suggests that some of the underlying assumptions present in the lodging model are applicable to oat lodging.

Table 4.2. The statistical parameters for the goodness of fitted curves

Record No.	L_u/h	R^2	RMSE	Date
1	1.17	0.88	0.009	15 June 2017
2	1.19	0.88	0.009	15 June 2017
3	1.13	0.87	0.008	15 June 2017
4	1.15	0.85	0.010	31 May 2018
5	1.16	0.85	0.010	31 May 2018
6	1.08	0.85	0.010	31 May 2018
7	1.58	0.83	0.009	01 June 2018
8	1.58	0.84	0.010	01 June 2018
9	1.62	0.85	0.008	01 June 2018
10	1.67	0.82	0.010	11 June 2018
11	1.56	0.84	0.008	12 June 2018
12	1.44	0.87	0.011	13 June 2018
13	1.16	0.82	0.013	14 June 2018
14	1.65	0.85	0.008	15 June 2018
15	1.47	0.82	0.010	18-June 2018
16	1.5	0.83	0.009	18 June 2018
17	1.26	0.8	0.011	19 June 2018
18	1.13	0.81	0.009	20 June 2018
19	1.55	0.82	0.010	21 June 2018
20	1.11	0.8	0.009	21 June 2018
mean	1.36	0.84	0.009	

Table 4.3. Mean and ranges of non-dimensionalised turbulence length scales calculated from autocorrelation method and Von-Karman spectral form versus results from Sterling et al. (2003) and Finnigan (2000).

	Oat					
	L_u/h		L_v/h		L_w/h	
	mean	range	mean	range	mean	range
Autocorrelation	2.01	1.16-4.26	2.26	0.92-4.71	0.28	0.22-0.34
Von-Karman	1.36	1.08-1.67	-	-	-	-
	Wheat					
	L_u/h		L_w/h		L_v/h	
Sterling et al. (2003)	3.5 – 6.7		1.6 – 3.7		0.2 – 0.3	
Finnigan (2000)	0.8–1.8		-		0.1–0.7	

4.2.3. Velocity spectra

Another test to examine the consistency of the data with the background knowledge relating to turbulent flow is to compare the results with Kolmogorov's theory. This theory is not limited to the flow over the canopy and describes how the energy is cascaded at different scales of eddies (Kaimal and Finnigan, 1994). According to the theory, there are three scales of eddies, the energy-containing range, the inertial subrange, and the dissipation range. The theory states in the inertial subrange, the spectrum would diminish by -5/3 slope and the turbulence flow would be isotropic in the inertial subrange, which implies the following theoretical equation.

$$S_v(f) = S_w(f) = \frac{4}{3} S_u(f) \quad (4\text{-}5)$$

$$\beta = \frac{S_w(f)}{S_u(f)} \tag{4-6}$$

In practice, β changes in different plant canopies. β=0.94 for corn and dense deciduous forest, while in Moga forest β=1.7 and in Aspen, pine and spruce canopies, β= 1±0.15 (Finnigan, 2000). Spectrum ratio results for the current research shows β=1.05 which is consistent with data from other plant canopies.

Figure 4.6 shows the velocity spectra of wind at crop height non-dimensionalised by the variance versus the frequency. The data corresponding to this figure was collected on 15 June 2017 (GS87) for 10 minutes. It is worth noting that all the spectrums used in the data analysis process have been examined through Persival theorem (which compares the summation of the square of the velocity fluctuation in the time domain with the summation of the square of its Fourier transform) and it was found that the energy of the time domain and frequency domain signals are the same. In this figure, S_u is the streamwise velocity spectrum normalized by the variance of streamwise velocity and f is the frequency in Hz. The figure demonstrates significant energy at low frequency which diminishes in higher frequencies. The slope of the declining spectrum is -5/3 (the red line), which agrees with the Kolmogorov theory (Finnigan, 2000).

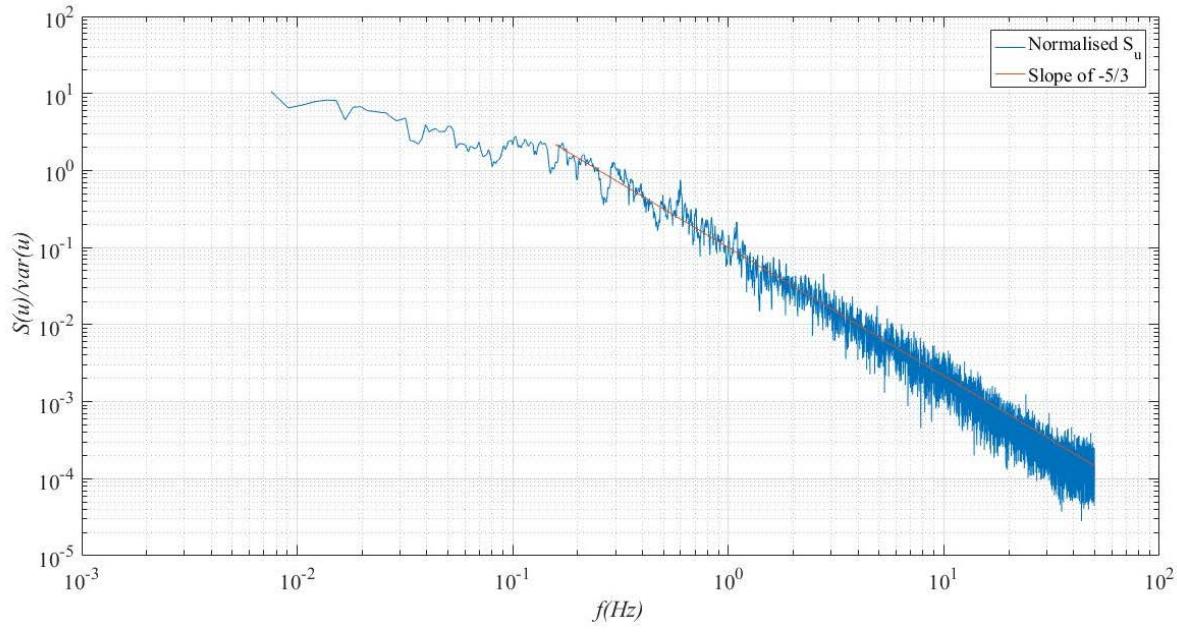

(a) Normalised streamwise velocity spectrum

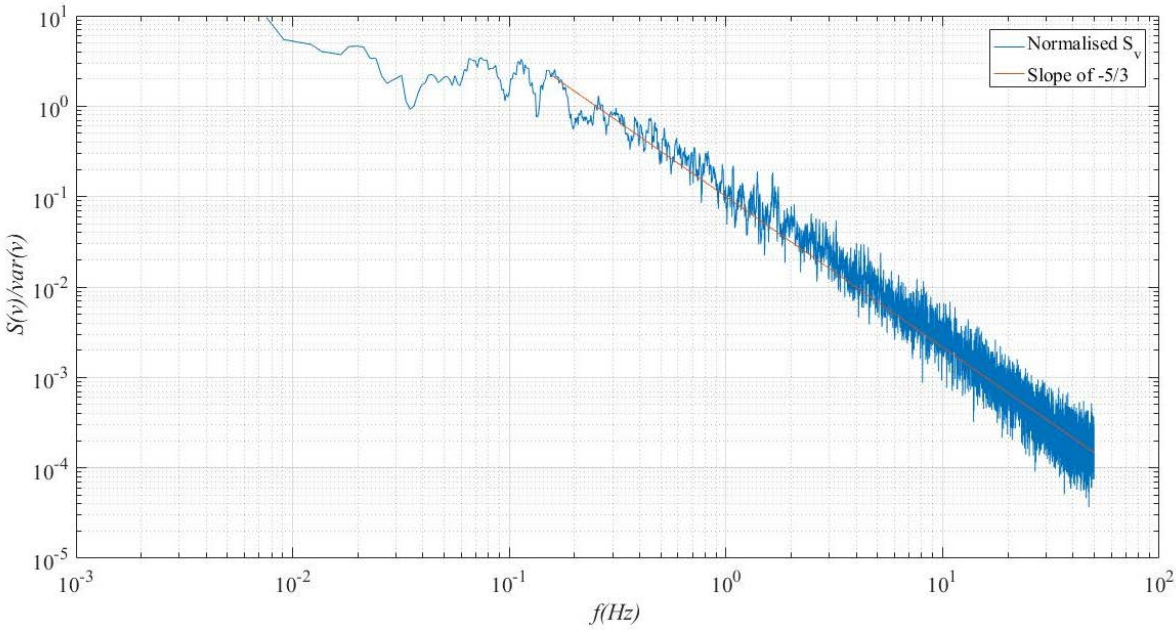

(b) Normalised cross stream (lateral) velocity spectrum

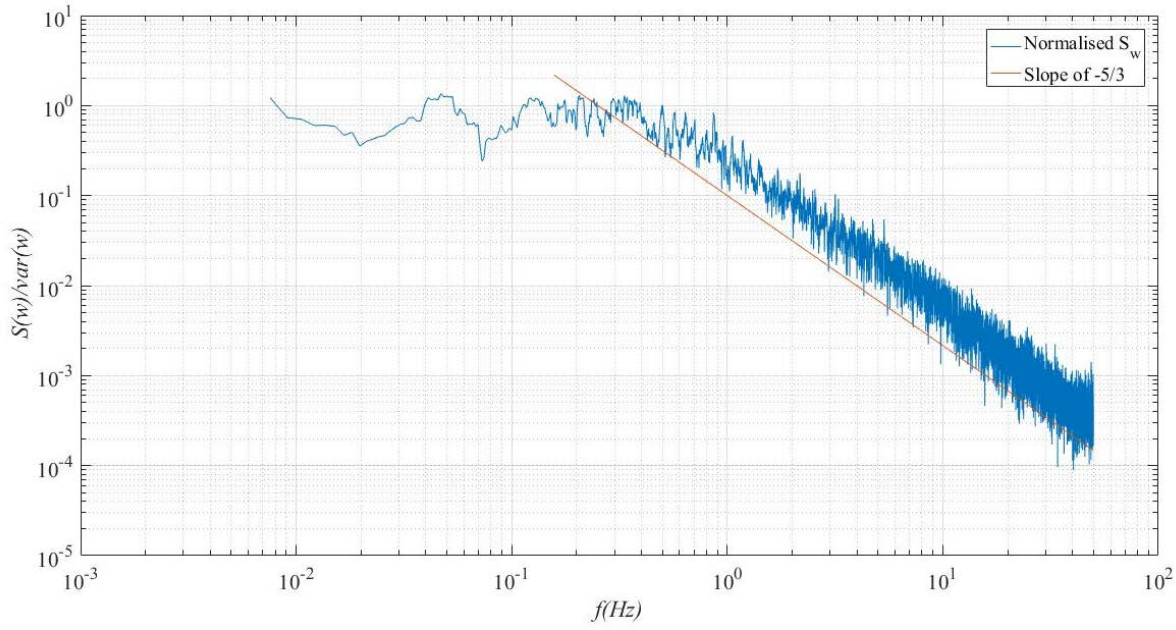

(c) Normalised vertical velocity spectrum

Figure 4.6. Velocity spectra at the crop height in three direction (a) streamwise, (b) cross stream and (c) vertical

4.2.4. Other turbulence parameters

The turbulence intensity (I_i) is defined as follows (Holmes, 2001):

$$I_i = \frac{\sigma_i}{\overline{U}} \tag{4-7}$$

Where σ_i is the standard deviation of wind velocity fluctuations and $\overline{U}$ is the mean wind speed and is defined as follows:

$$\bar{U} = ((\bar{u})^2 + (\bar{v})^2 + (\bar{w})^2)^{1/2} \quad (2\text{-}29)$$

In this section values of σ_i/u_* (σ_i is the standard deviation of the velocity component in the i^{th} direction and u_* is surface friction velocity (equation 2-21)) and the turbulence intensities have been averaged over 20 datasets (each record was 10 minutes) and presented in Table 4.4. (Appendix G shows an averaging period of 10 minutes is sufficient to capture the general trend and magnitude of this parameter). Equation 2-21 is as follows:

$$u_* = \sqrt{\overline{u'w'}} \quad (2\text{-}21)$$

Where u' is the streamwise velocity fluctuations, $v'$is the cross stream velocity fluctuations and w' are the vertical velocity fluctuations.

$$u' = u(t) - \bar{u} \quad (2\text{-}26)$$

$$v' = v(t) - \bar{v} \quad (2\text{-}27)$$

$$w' = w(t) - \bar{w} \quad (2\text{-}28)$$

Where $u(t)$, $v(t)$ and $w(t)$ are the instantaneous streamwise, cross stream, vertical velocities respectively and $\bar{u}$, $\bar{v}$ and $\bar{w}$ are mean velocities in the same orthogonal directions respectively.

Table 4.4 shows the values recorded in the measurements are in agreement with the values reported the previous research on wheat canopies and the turbulence intensity parameter values agree with what has been reported in previous research for wheat (Sterling et al., 2003).

These results show the range of values measured for streamwise turbulence intensity is much lower than I_u=1 as assumed by Baker et al. (2014) to calculate peak factors (equation 2-5) and illustrates the importance of undertaking this analysis in order to obtain the correct of lodging velocities (equation 3-1 and 3-2). Section 6.6 will show how these modifications influence the lodging velocity values as calculated by the model.

Table 4.4. Values of wind turbulence statistics for oats compared to those in the literature

				Panofsky and Dutton (1984)	Finnigan (2000)	Sterling et al. (2003)
	range	mean	S_d	mean	range	range
σ_u/u_*	1.18-3.33	2.26	0.75	2.39	1.7 – 2.4	2.11– 2.12
σ_v/u_*	0.95-2.94	1.94	0.55	1.92	-	-
σ_w/u_*	0.67-1.81	1.29	0.35	1.25	1.0 – 1.3	1.04 – 1.10
I_u	0.45-0.67	0.60	0.06	-	-	0.48 – 0.74
I_v	0.38-0.70	0.50	0.08	-	-	0.44 – 0.61
I_w	0.25-0.43	0.33	0.05	-	-	0.25 – 0.36

4.3. Measurements of dynamic/aerodynamic parameters

In this section, the collected data is used to determine the dynamic/aerodynamic parameters required for the lodging model. Accordingly, Sections 4.3.1, 4.3.2, and 4.3.3 consider damping ratio, natural frequency, and drag area parameters respectively.

4.3.1. Damping ratio

As discussed in Chapter 2, the lodging model considers the plant as an underdamped harmonic oscillator which is interacting with wind. When the plant is displaced by an external force it starts to oscillate about an equilibrium point with a diminishing displacement amplitude. The damping ratio is a dimensionless parameter describing how oscillations in a system decay after a disturbance (Clough and Penzien, 1993). In this section, the damping ratio is calculated from two methods. The first method, logarithmic decrement (Section 4.3.1.1), considers the displacement decrement in the time domain while the second method, transfer function (Section 4.3.1.2) considers the dynamic response of the plant in the frequency domain.

4.3.1.1 Logarithmic decrement

The logarithmic decrement method is a common tool to determine the damping ratio of an underdamped system, in the time domain. In this method, the logarithmic decrement (L_D), can be defined as the natural logarithm of the ratio of the amplitudes of any two successive peaks as below (Clough and Penzien, 1993):

$$L_D = (\frac{1}{k})(\ln(\frac{Y_1}{Y_{k+1}})) \quad (4\text{-}8)$$

Where k is the number of oscillations to decay from amplitude Y_1 to Y_{k+1}. The damping ratio (θ) can be calculated as (Clough and Penzien, 1993):

$$\theta = \frac{L_D}{\sqrt{(2\pi)^2 + {L_D}^2}} \tag{4-9}$$

In order to identify the variation of damping ratio on different days, 10 records for each day were studied (Appendix H shows higher number of samples does not affect the mean and standard deviation of the results). Figure 4.7 shows sample results of streamwise oat displacement variation in time for a 3.5s record on 15th June 2017 (GS87). (The zero-displacement reference point is the position where the target crop stays in a steady condition) and Table 4.5 presents a summary of results in the lodging season 2018.

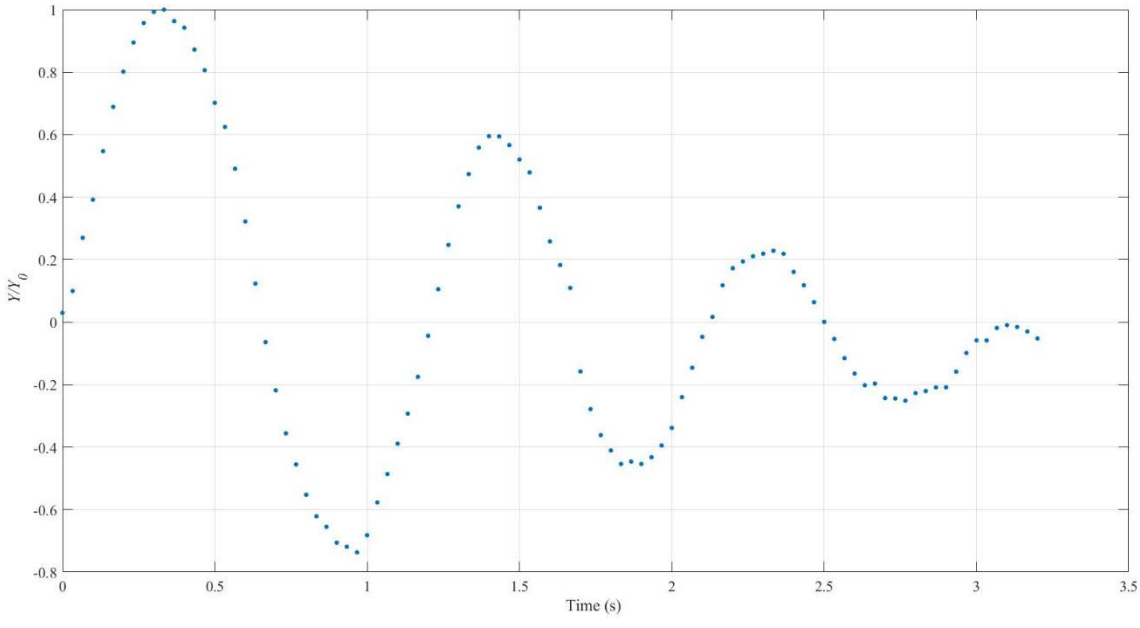

Figure 4.7. Streamwise oat displacement in time after an isolated gust (θ = 0.1)

4.3.1.2 Transfer function

While studying the dynamic response of a plant subject to a wind induced displacement, the normalized streamwise displacement spectrum can be related to the normalised velocity spectrum through a transfer function known as mechanical admittance $|H(f)^2|$ as follows (Holmes, 2001):

$$S_x(f)=\frac{4\bar{X}^2}{\bar{U}^2}\,|H(f)^2|S_u(f) \tag{4-10}$$

In this equation S_x and S_u are displacement and velocity spectra respectively, $\bar{U}$ is the mean velocity and $\bar{X}$ is the mean displacement. Consequently, the mechanical admittance can be determined if S_x, S_u , $\bar{X}$ and $\bar{U}$ are known. It is worth noting that the wind loading area of the plant is small in comparison to the turbulence length scale (see Section 4.2.2) and the aerodynamic admittance (another type of transfer function which relates the wind fluctuations to the cross-wind force fluctuations) is not applicable here (Holmes, 2001). The mechanical admittance function can be illustrated as (Holmes, 2001):

$$|H(f)|^2 = \left[\left(1-\left({}^{f}/_{f_n}\right)^2\right)^2 + 4\theta^2\left({}^{f}/_{f_n}\right)^2\right]^{-1} \tag{4-11}$$

Where f_n is the natural frequency and θ represents the plant's damping ratio. Consequently, equations 4-10 and 4-11 can be written as:

$$\frac{S_x(f)}{S_u(f)}\frac{\bar{U}^2}{4\bar{X}^2} = \left[\left(1-\left(\frac{f}{f_n}\right)^2\right)^2 + 4\theta^2\left(\frac{f}{f_n}\right)^2\right]^{-1} \quad (4\text{-}12)$$

The left hand side of equation 4-12 can be obtained from the experimental data, while the right side of equation can be used in the curve fitting process to estimate the natural frequency (f_n) and damping ratio (θ). The curve fitting process was undertaken in the MATLAB curve fitting tool, where the left hand side of the equation was entered as a function of variable *f*, and the right side expression was entered in the MATLAB curve fitting tool as a customised equation and the natural frequency (f_n) and damping ratio (θ) values were estimated through curve fitting process. Figure 4.8 shows sample results and compares the fitted curve and the experimental data. It is worth noting that the data corresponding to this figure was collected for a 10 minute period on the 15th June 2017 (GS87).

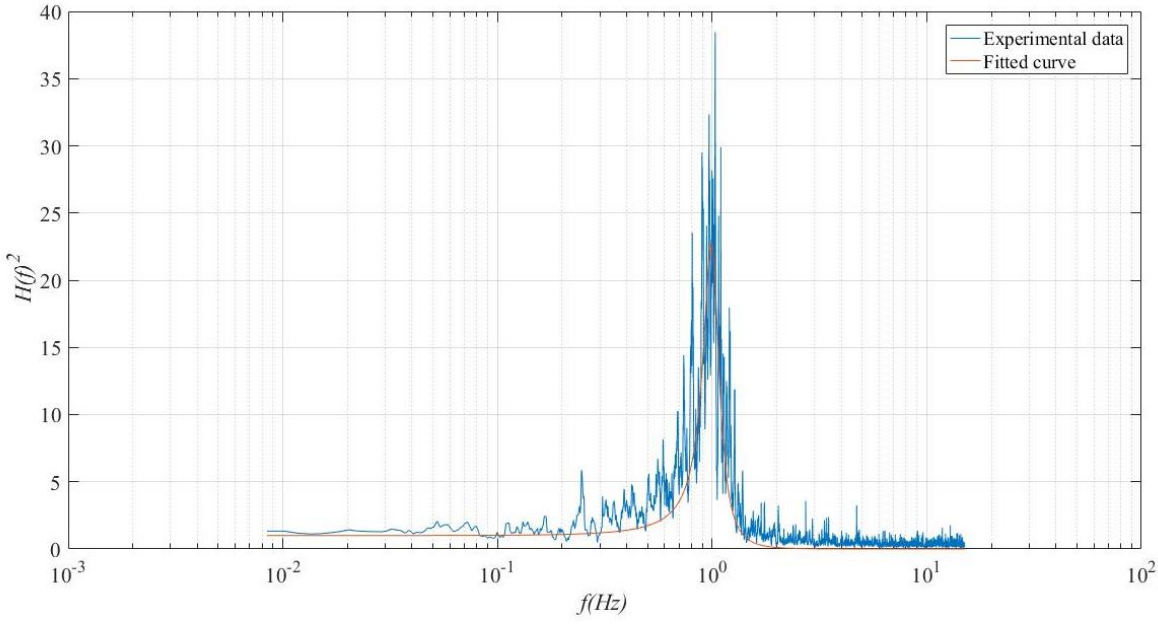

Figure 4.8. Transfer function (normalized ratio of displacement spectrum to wind spectrum) versus frequency (Natural frequency = 1Hz, damping ratio= 0.1) for data recorded on 15th June 2017 (GS87).

Table 4.5 presents the data from the two methods to determine the damping ratio. The results show, considering the uncertainties inherent in the data, there is a good agreement between obtained damping ratios from two different approaches, as they are in the same range of uncertainty. Moreover, the parameter shows an increasing trend in the mean values. At the beginning of the season, when the panicles have just emerged, the plants act like isolated shoots and the damping value is low, however, as plants grow the plants create interlocked canopies, and the damping ratio increases.

Table 4.5. Mean, standard deviation and random uncertainty of the damping ratio

	Logarithmic decrement			Transfer function		
	mean	S_d	δ (±)	mean	S_d	δ (±)
15 June 2017	0.113	0.027	0.009	0.108	0.004	0.002
31-May 2018	0.051	0.02	0.007	0.059	0.008	0.004
01-Jun 2018	0.053	0.019	0.006	0.062	0.003	0.002
07-Jun 2018	0.081	0.017	0.006	0.084	0.004	0.002
11-Jun 2018	0.111	0.028	0.009	0.108	0.006	0.004
12-Jun 2018	0.112	0.035	0.011	0.125	0.009	0.005
13-Jun 2018	0.121	0.032	0.011	0.135	0.009	0.005
14-Jun 2018	0.133	0.034	0.011	0.142	0.004	0.003
15-Jun 2018	0.133	0.044	0.014	0.144	0.014	0.008
18-Jun 2018	0.137	0.025	0.008	0.137	0.006	0.004
19-Jun 2018	0.142	0.024	0.008	0.134	0.001	0.001
20-Jun 2018	0.13	0.035	0.012	0.133	0.006	0.004
21-Jun 2018	0.129	0.017	0.006	0.136	0.008	0.005

4.3.2. Measurements of natural frequency (Frequency domain approach)

In addition to the method described in Section 3.4.4, the natural frequency can be calculated from spectral analysis (Holmes, 2001), where the displacement of the target plant in the time domain is transformed into the frequency domain using the FFT (Holmes, 2001). The displacement spectrum illustrates how the energy content in the oscillations changes with the frequency.

Figure 4.9 shows two samples of streamwise displacement spectra (S_x) over a 10-minute period (normalized by the variance). A peak associated with the plant's natural frequency can be detected in the range of 1Hz – 1.3Hz. A summary of results for the natural frequency values as well as random uncertainties are presented in Table 4.6. From comparing the displacement spectra at the beginning and the end of the experimental season (4.9.a and 4.9.b respectively), it can be observed that the peak in the displacement spectrum has shifted to the lower frequency values. Table 4.6 also shows a decline in the mean natural frequency values throughout the loading season in 2018. This is due to the biological changes in the plant during the season which is further discussed later in this section. It is worth noting that as the sampling frequency is 30 Hz (30 frames per second) and each recording was 10 minutes, the number of data would be 18000 recordings. Consequently, the difference between two frequencies in the spectrum (i.e. $\Delta f = \frac{sampling\ frequency}{number\ of\ samples}$) would be approximately 0.001, which is enough to avoid leakage to the adjacent frequencies at the natural frequency (Ferrero et al. 2015) . It is worth noting that spectral leakage occurs when the spectral content of a signal does not correspond to the available spectral line. Additionally, no window (also known as the uniform window) was used in the analysis, which has a higher frequency resolution in comparison to other windows and enables the natural frequency in the spectrum to be detected (Ferrero et al. 2015).

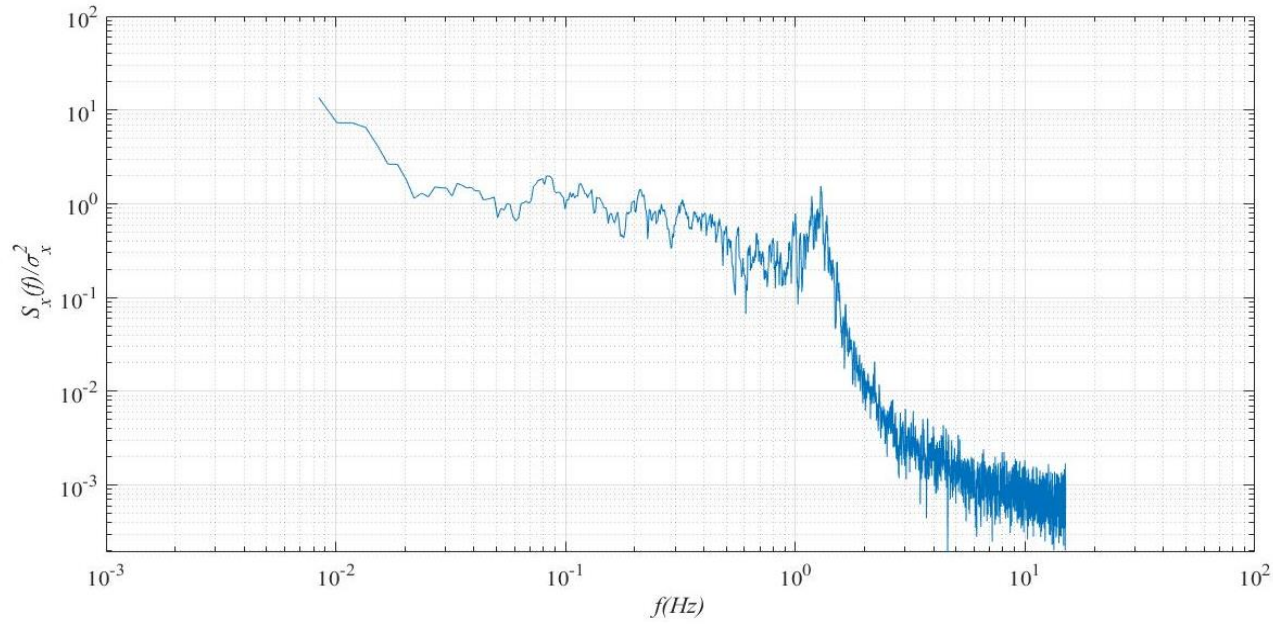

(a) Crop displacement spectrum normalized by variance for 10-minute interval in 31 May 2018 (GS53)

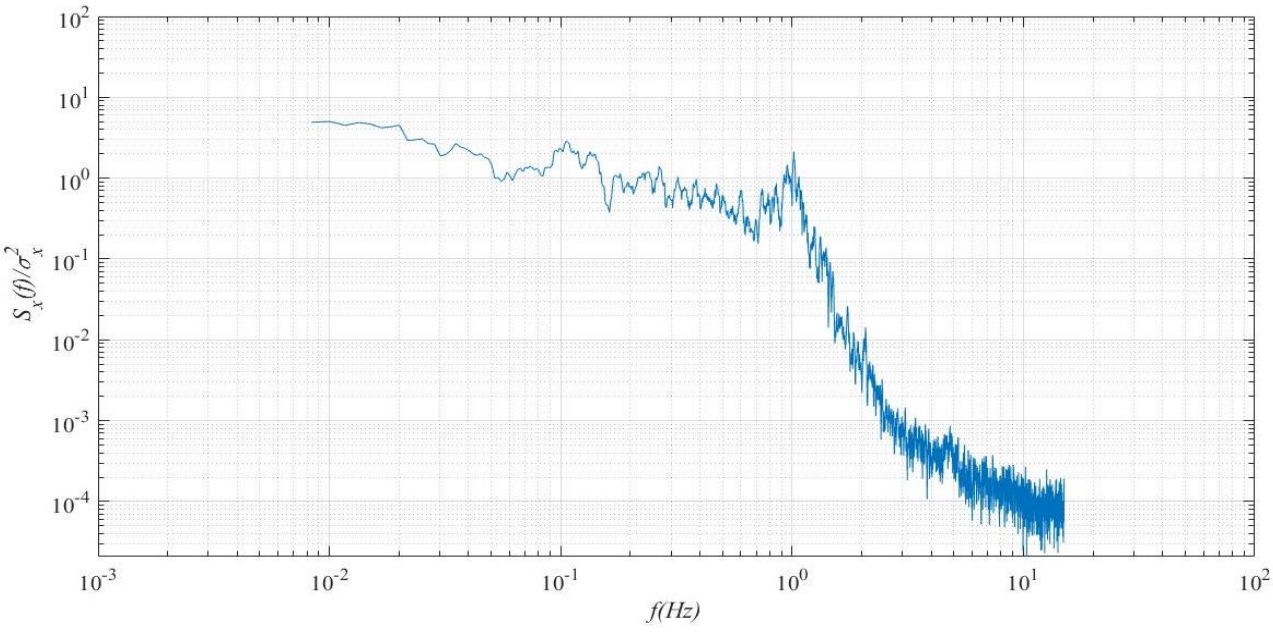

(b) Crop displacement spectrum normalized by variance for 10-minute interval on 21 June 2018 (GS87)

Figure 4.9. Crop displacement spectra normalized by variance (a) 31 May 2018 (GS53) (b) 21 June 2018 (GS53)

Table 4.6 presents the natural frequency values as well as random uncertainties throughout the lodging period in 2018. It is worth noting that on each day three, 10-minute records were analysed. Additionally, the results in Table 4.6 demonstrate demonstrates a considerable change in natural frequency over time.

Table 4.6. Natural frequency and damping ratio values as calculated in 2017 and 2018.

	mean	δ (±)
15 June 2017	0.98	0.017
31 May 2018	1.28	0.017
01 June 2018	1.31	0.019
07 June 2018	1.26	0.021
11 June 2018	1.07	0.006
12 June 2018	1.08	0.009
13 June 2018	1.08	0.012
14 June 2018	1.02	0.015
15 June2018	1.06	0.015
18 June 2018	1.03	0.008
19 June 2018	0.96	0.009
20 June 2018	0.99	0.007
21 June 2018	1	0.009

The natural frequency of the plant is the frequency at which the plant would tend to oscillate after being disturbed by isolated wind-induced force (Clough and Penzien, 1993). At the start of the lodging period the plants act like isolated shoots (31st May and 1st June, i.e. GS 53)), the natural frequency is at the highest level, ~1.3 Hz (Figure 4.9a). As the plants grow, the

plant height increases and the crop fills the grains, which increases the plant weight and reduces the natural frequency (Figure 4.9b).

From a mechanical perspective, the plant can be considered as a cantilever and is loaded by external forces including wind. The natural frequency f_n of the simple harmonic oscillator is given is given by:

$$f_n = \frac{1}{2\pi}\sqrt{\frac{k}{m}} = \frac{1}{2\pi}\sqrt{\frac{F}{mY}} \quad (4\text{-}13)$$

Where k is the stiffness of the oscillator, m is the mass, F is the external force and Y is the deflection. For a cantilever, Y is proportional with the length (plant height in this case), and consequently, as the plant height increases the natural frequency would decrease. Figure 4-10 shows this relationship between the plant height and the natural frequency as measured for different samples in 2017 and 2018. The figure shows as the plant height increases the natural frequency decreases, which supports the findings in Table 4.6, where the plant growth through the season causes a reduction in the natural frequency. Additionally, the peak lodging stage is associated with the panicles emergence stage until harvest. This period is known as the "grain filling" stage when the plant increases the weight of the panicle through accumulating the assimilate from photosynthesis in developing grains, which is another reason for the decrease in the natural frequency during the season.

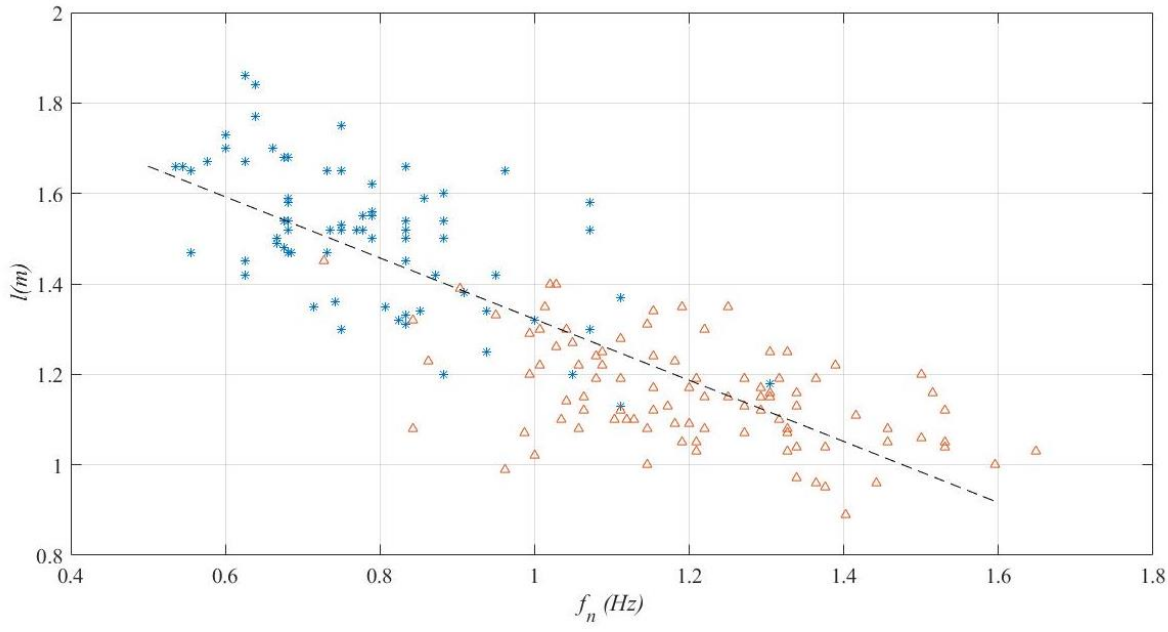

Figure 4.10. Relationship between plant height (l) and natural frequency (f_n) for main shoots in 2017 (*) and 2018 (Δ). The black line shows the linear trend line y = -0.67x + 1.99 (R^2=0.68)

4.3.3. Drag Area

The plant drag area (AC_F) is an influential parameter in the wind-induced drag force applied on the plant (see equation 2-1) and is determined by the plant area perpendicular to wind (A) multiplied by the drag coefficient (C_F). Baker et al. (2014) showed the plant drag area can be calculated from a relationship between the mean plant displacement ($\bar{Y}$) and the mean wind velocity ($\bar{U}$) as follows:

$$\bar{Y} = \left(\frac{0.5\rho/\mu}{(2\pi f_n)^2}\right) AC_F \bar{U}^2 \quad (4\text{-}14)$$

As described in Section 2.2.1.2, the upper ground canopy mass in the lodging model is assumed to be concentrated at the top of the canopy (see Figure 2.1) and μ in the above equation is the equivalent mass at the top of the plant, producing the equal moment as the total crop's mass does (further described below).

In the above equation, the mean plant displacement, the mean wind velocity and the natural frequency can be obtained from the video tracking method (Section 3.4.5) and corresponding sonic anemometer data (Section 3.4.2), and spectral analysis (Section 4.3.2) respectively. The equivalent mass at the top of the plant (μ) can be estimated based on agronomic measurements (see below). Accordingly, it can be assumed that the actual above ground plant mass (m) is applied on the centre of gravity (X), so knowing the height of centre of gravity, the plant mass, and the height of the plant, μ can be approximated as follow (Appendix I shows how this equation is derived):

$$\mu = mX/l \tag{4-15}$$

An alternative approach is to assume, the mass is equally distributed between the internodes with the same height which gives (Appendix I shows how this equation is derived):

$$\mu = \frac{m}{2} \tag{4-16}$$

In order to weight a plant and identify the centre of gravity, the plant has to be excavated, which is a destructive process. Alternatively, 100 samples from the area near the target,

where excavated and the plant height, centre of gravity and upper ground mass were measured (Table 4.7). Results show there is a reasonable agreement between μ values obtained from these two different approaches (~ 35 *gr*). Table 4.7 shows the statistics and random uncertainties in measurement of agronomic parameters used to determine μ. The fractional uncertainty of equivalent mass ($\frac{\delta_\mu}{|\mu|}$) can be derived as follows (see equation 3-5) :

$$\frac{\delta_\mu}{|\mu|} \leq \frac{\delta_m}{|m|} + \frac{\delta_l}{|l|} + \frac{\delta_X}{|X|} \tag{4-17}$$

Using the values in Table 4.3, $\frac{\delta_\mu}{|\mu|} \leq 0.013$. This value is used later in this section to evaluate the uncertainty of AC_F.

Table 4. 7. Mean, standard deviation and uncertainties for parameters in stem yield stress test

	m (gr)	l (cm)	X (cm)
mean	70.18	113.25	57.98
S_d	5.51	2.78	1.66
δ (±)	0.55	0.28	0.166
Fractional uncertainty	0.008	0.002	0.003

Figure 4.11 illustrates a graph where the changes of $K=(\frac{0.5\rho/\mu}{(2\pi f_n)^2})\overline{U}^2$ versus the mean displacement are plotted and where the linear trend line corresponds to drag area (AC_f~0.017m^2). Moreover, the figure demonstrates the experimental data and the linear

regression line with the 95% confidence intervals. The confidence intervals (*CI)* for the linear regressions were calculated from the following equations:

$$CI=y^* \pm t^* SE_y\sqrt{\frac{1}{z}+\frac{(K^*-\bar{K})}{\sum(K_i-\bar{K})}} \quad (4\text{-}18)$$

Where y^* is the estimated value of K based on the linear regression, $\bar{K}$ is the mean value, z is the number of points (samples), i represents the order of point in the database (i=1,2,3,..,z), SE_y is the standard error of linear estimate, and t^* is an statistic which can be determined based on the T-distribution for 95% confidence interval (see Appendix J).

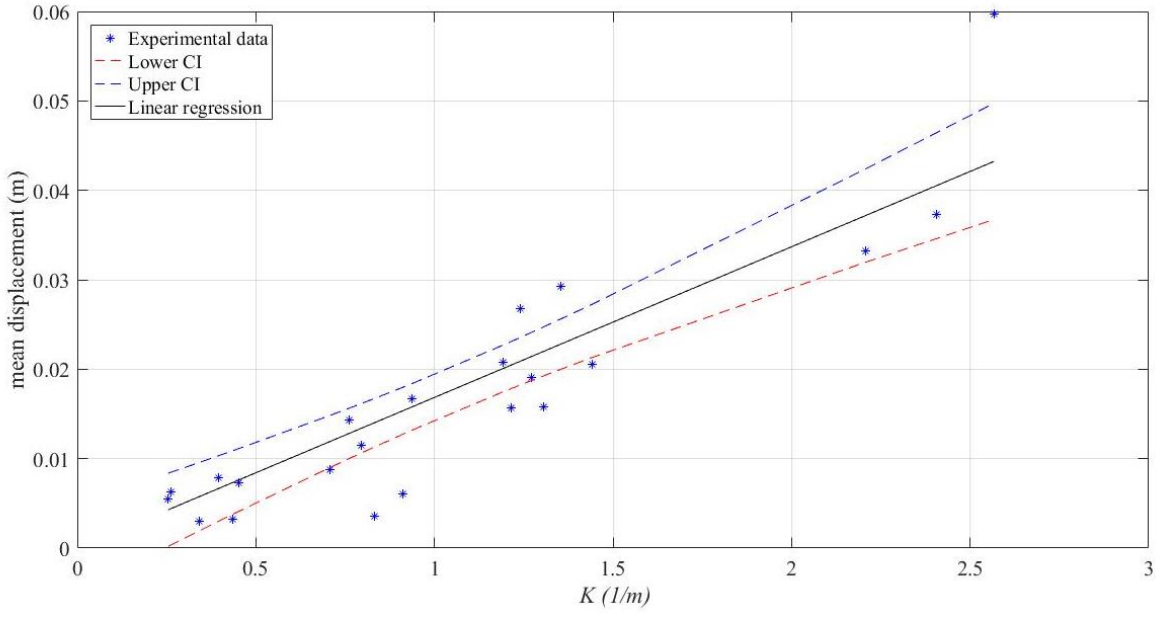

Figure 4.11. Mean displacement versus $K=(\frac{0.5\rho/\mu}{(2\pi f_n)^2})\bar{U}^2$, $R^2 = 0.83$

As the plant area perpendicular to wind (A) can change in an oscillation, equation 4-14 is a simplified relationship between the mean velocity and displacements which neglects the aero-

elastic behaviour of the plant. Section 4-4 investigates if such a simplification in the lodging model affects the ability of model to predict lodging.

In order to undertake the uncertainty analysis, equation 4-19 is written as follows:

$$AC_F = \frac{\bar{Y}\,\mu(2\pi f_n)^2}{0.5\rho\,\bar{U}^2} \tag{4-19}$$

Thus the fractional uncertainty of AC_F can be obtained as follows:

$$\frac{\delta_{AC_F}}{|AC_F|} \leq \frac{\delta_{\bar{Y}}}{|\bar{Y}|} + \frac{\delta_{\mu}}{|\mu|} + 2\frac{\delta_{\bar{U}}}{|\bar{U}|} + 2\frac{\delta_{f_n}}{|f_n|} \tag{4-20}$$

Using the values from Section 3.4.5, appendix E and Section 4.3.2 the fractional uncertainty of AC_F is:

$$\frac{\delta_{AC_F}}{|AC_F|} \leq 0.036 \tag{4-21}$$

These values are used and discussed in Section 4.7 for the propagation of uncertainty.

4.4. Displacement time histories

Section 4.3.1 to 4.3.3 presented the results and values for natural frequency, drag area, and the damping ratio as measured for oat plants through experiments. Based on these values it is now possible to evaluate the equation of motion as suggested by Baker et al. (2014) and compare it with the experimental displacement record in a given time seri. Such a comparison

can demonstrate how simplifications in generalized model, e.g. and neglecting the aeroelastic behaviour of the crop, can influence the model outputs. It is worth noting that aeroelastic behaviour refers to a condition in which the movement of the structural component, influences the aerodynamic properties of the structure, so the dynamic response becomes motion dependant and therefore nonlinear.

In the generalised lodging model (Baker et al., 2014) the motion equation of the crop is a second-order differential equation as follows:

$$\frac{1}{\omega_n^2}\frac{d^2Y}{dT^2} + \frac{2\theta}{\omega_n}\frac{dY}{dT} + Y = 0.5\rho A C_F/\omega_n^2\mu\,(U_T)^2 \qquad (4\text{-}22)$$

Where T is the time, U_T is the wind velocity as a function of time, and μ is the equivalent mass of a plant's canopy (Baker et al., 2014). This can be rewritten in the form of equation 4-14, if average terms are kept.

If the right-hand side parameters in equation 4-22, including variation of wind velocity with respect to time, are known, the equation can be solved numerically to determine crop displacement as a function of time, using the values of the natural frequency, damping ratio and the drag area (see previous sections). Figure 4.12 indicates an example of displacement results using Runge-Kutta method to solve the differential equation.

The figure shows a general agreement between the experimental data and the model output. Although the predicted displacement by the model does not match with the observed displacement temporally, the peak displacements are well predicted. This is an important finding as lodging occurs at peak displacement and the ability of the model to predict these

values is crucial and justifies using an average value for AC_F rather than adding the complexities of aeroelastic behaviour of the crop into the model.

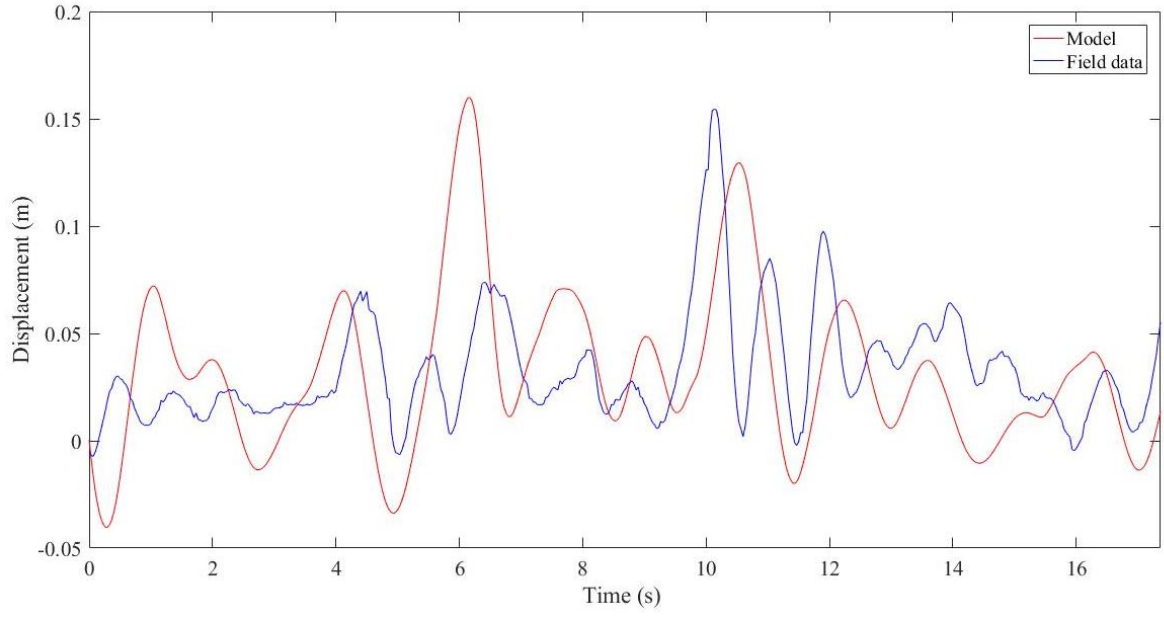

Figure 4.12. The model output and the experimental crop displacement data for oats

4.5. Agronomic parameters

Table 4.8 shows the plant parameters recorded in 2017 and 2018 with the measurement uncertainties defined as $\delta = \pm S_d/\sqrt{z}$ (Zwillinger, 1995). In this relationship δ is the random uncertainty, S_d is the standard deviation and z is the number of samples. It should be noted that the stem yield stress (σ) was examined in 2018 only. Moreover, the natural frequency values demonstrated in Table 4.8 are measured using the method described in Section 3.3.4 (counting the number of oscillations in time) which indicate $\pm$20% difference with what is calculated from crop displacement spectra (see Section 4.3.2), due to a number of uncertainties associated with the earlier method (as described in Section 3.3.4). Consequently, these values were not used in the lodging model. Nevertheless, investigating

the value of the parameter from two different methods enabled the uncertainties in the standard agronomic approach to be identified.

A deeper look at the data shows the mean values for agronomic parameters can change in different years. For example, the stem length (l) and the centre of gravity (X) values are higher in 2017 rather than 2018, while the root diameter (d) is lower in the first year (2017) in comparison to the second year (2018) and the stem wall thickness (t) has not changed considerably. The reason for these changes can be various meteorological conditions (e.g., sunshine, soil moisture, temperature, different sowing dates and potentially differences in plant establishment leading to different plant density) in different years before the peak lodging season. For example, if the number of sunny days is higher in a specific year, the photosynthesis in crops and consequently their growth would be encouraged (Vining, 1990).

Table 4.8. Mean and standard deviation for agronomic parameters measurements in 2017 and 2018 (Mohammadi et al., 2020b).

	2017				2018			
Agronomic parameters	mean	S_d	δ (±)	z	mean	S_d	δ (±)	z
a (cm)	0.32	0.08	0.003	672	0.28	0.07	0.002	672
t (cm)	0.09	0.03	0.001	672	0.09	0.36	0.014	672
l (cm)	149.18	16.08	0.63	649	112.40	12.53	0.48	672
X (cm)	70.19	8.24	0.92	81	62.54	6.94	0.70	96
d (cm)	4.97	0.57	0.07	623	5.29	1.29	0.04	672
L (cm)	7.2	3.14	0.12	623	5.56	2.56	0.1	672
f_n(Hz)	0.8	0.18	0.02	81	1.20	0.18	0.02	96
σ (MPa)	-	-	-	-	40.30	17.23	0.41	100

4.6. Soil and anchorage system parameters

In order to examine if equation 2-10 and 2-11 can represent the anchorage system resistance and root/soil structure, a number of tests were undertaken based on the methods (described in Section 3.3.6), where the root system failure torque, root diameter and soil shear strength were measured. Equation 2-10 and 2-11 are as follows:

$$R_s = \gamma S d^3 \quad (2\text{-}10)$$

$$R_s = \gamma S d^2 L \quad (2\text{-}11)$$

It is worth noting that the process presented here is not a simple curve fitting, but it is an investigation to check which physical expression better represents the root anchorage system. As mentioned in Section 3.3.6, equation 2-10, estimates the failure moment to be proportional with the volume of sphere while equation 2-11 considers the anchorage system in a conical shape.

Figure 4.13 demonstrates the relationship between the anchorage resistance and soil/root parameters and shows equation 2-11 (Figure 4.13.b) better represents the data (R^2=0.79) than equation 2-10 shown in Figure 4.13.a (R^2=0.55). In comparison to the previous similar experiments where the reported R^2 value varies between 0.41 (Crook and Ennos, 1993) to 0.69 (Berry et al. 2006), these results, especially the latter expression, show acceptable R^2 values. Moreover, the sample size used in this research is larger than previous experiments (see Section 3.3.6) and consequently more reliable.

This figure indicates the slope of the linear trend line in Figure 4.13.a and 4.13.b is associated with γ (~0.1). This value is lower than γ values for wheat (~0.4; Crook and Ennos, 1993; Baker et al. 1998), barley (~0.6; Berry et al. 2006) and sunflowers (~0.4, Sposaro et al. 2008), which means when the volume of the root system and the soil conditions are the same for different crops, oats (which have a lower value of γ) are more susceptible to root lodging. This can be due to less flexible roots, or lower number of roots, which reduces the ability of the anchorage system to 'hold' the soil volume. This is further discussed in Chapter 7.

It is noteworthy that the confidence intervals *CI* for linear regressions in Figure 4.13 were calculated from the following equations:

$$CI=y^* \pm t^* SE_y\sqrt{\frac{1}{z}+\frac{(V_S{}^*-\overline{V_S})}{\sum(V_{S_i}-\overline{V_S})}} \quad (4\text{-}23)$$

In the above equation $V_S = Sd^3$ in Figure 4.13.a and $V_S = Sd^2L$ in Figure 4.13b, y^* is the estimated value of $V_S{}^*$ based on the linear regression, $\overline{V_S}$ is the mean value of the entire dataset, z is the number of points (samples), i represents the order of point in the database (i=1,2,3,..,z), SE_y is the standard error of linear estimate, and t^* is an statistic which can be determined based on the T-distribution for 95% confidence interval (see Appendix J).

Given the variability of the data in Figure 4.13, the linear regression at best is indicative of the general trend.

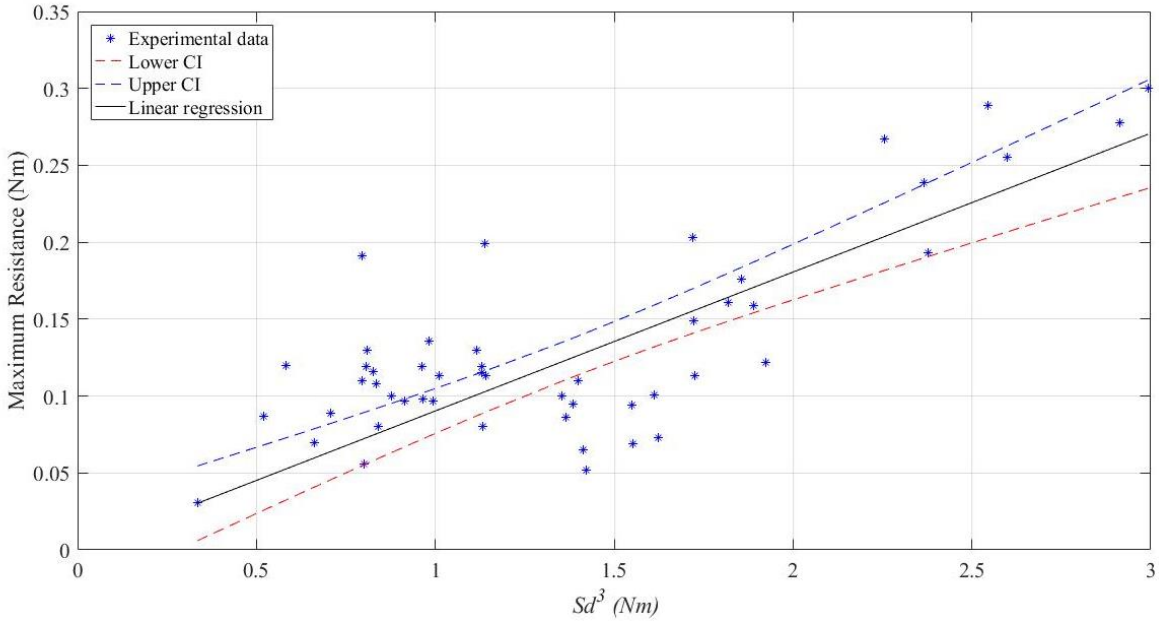

(a) The maximum resistance versus Sd^3

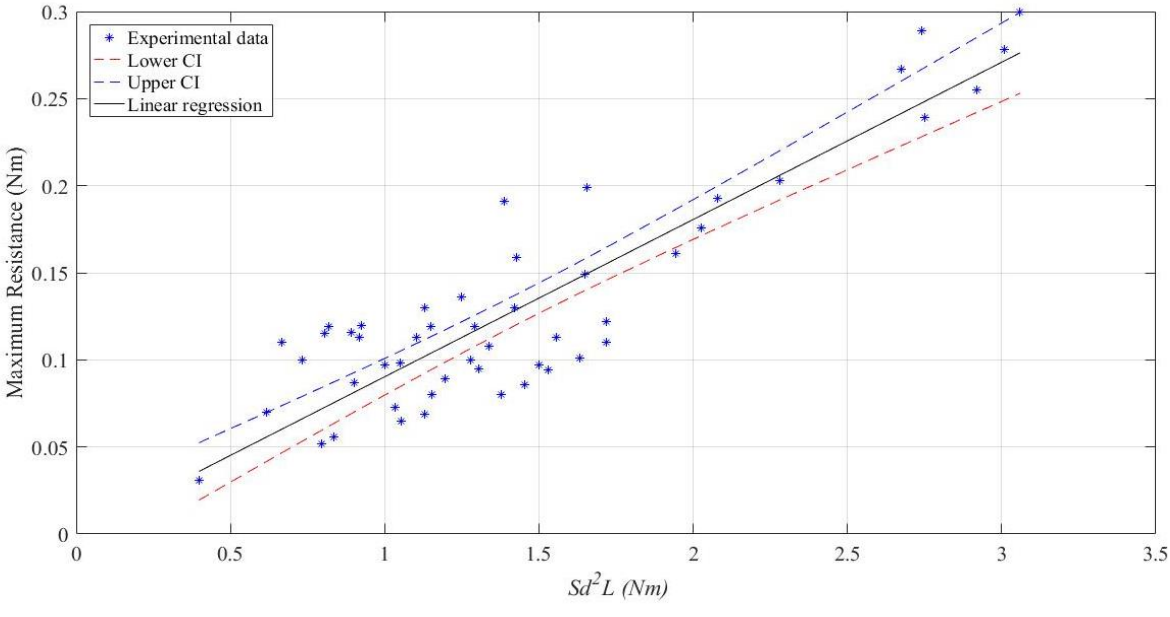

(b) The maximum resistance versus Sd^2L

Figure 4.13. The results of the experiments in 2018 to investigate equation 2-10 and 2-11

4.7. Propagation of uncertainty

In order to identify the uncertainty of the measurement for each parameters influences the overall lodging velocities calculated by the model; the propagation of uncertainty (Taylor, 1998) is presented in this section. As mentioned in Section 3.3.5, when a parameter is a product and quotient of a number of other parameters, e.g. :

$$q = \frac{a_1 \times a_2 \times \ldots \times a_n}{b_1 \times b_2 \times \ldots \times b_n} \tag{3-4}$$

Then the uncertainty can be expressed as:

$$\frac{\delta_q}{|q|} \leq \frac{\delta_{a_1}}{|a_1|} + \frac{\delta_{a_2}}{|a_2|} + \cdots + \frac{\delta_{a_n}}{|a_n|} + \frac{\delta_{b_1}}{|b_1|} \ldots + \frac{\delta_{b_n}}{|b_n|} \tag{3-5}$$

Taylor (1997) also showed that when $q = x^n$ then:

$$\frac{\delta_q}{|q|} = n\frac{\delta_x}{|x|} \tag{3-6}$$

Finally, if q is a function of the summation and differences between other parameters, i.e.:

$$q = a_1 + a_2 + \cdots + a_n - (b_1 + b_2 + \cdots + b_n) \tag{4-24}$$

Then the uncertainty is give as:

$$\delta_q \leq \delta_{a_1} + \delta_{a_2} + \cdots + \delta_{b_n} \tag{4-25}$$

The lodging velocity is a function of different parameters as follows:

$$\overline{U}_{Ls} = \left(\frac{\omega_n^2\left(\frac{X}{g}\right) S_s}{\left(1+\omega_n^2\left(\frac{X}{g}\right)\right)(0.5\rho A C_F X)\left(\cos\left(\alpha\frac{x}{l}\right) - cot\alpha \sin\left(\alpha\frac{x}{l}\right)\right)\left(1+ I\left(4g_{MB}^2+g_{MR}^2\left(\frac{\pi}{4\theta}\right)\right)^{0.5}\right.}\right)^{0.5} \tag{3-1}$$

Alternatively, this can be expressed as:

$$\overline{U}_{Ls} = \left(\frac{A_1 S_s}{A_2 B_1 B_2 B_3}\right)^{0.5} \tag{4-26}$$

Where A_1, S_s, A_2, B_1, B_2 and B_3 are:

$$A_1 = \omega_n^2 \frac{X}{g} \tag{4-27}$$

$$S_s = \left(\frac{\sigma\pi a^3}{4}\right)\left(1 - \left(\frac{(a-t)}{a}\right)^4\right)n \tag{2-9}$$

$$A_2 = 1 + \omega_n^2\left(\frac{X}{g}\right) \tag{4-28}$$

$$B_1 = (0.5\rho A C_F X) \tag{4-29}$$

$$B_2 = \left(\cos\left(\alpha\frac{x}{l}\right) - cot\alpha \sin\left(\alpha\frac{x}{l}\right)\right) = (\cos\beta - cot\alpha \sin\beta) \tag{4-30}$$

$$B_3 = (1 + I\left(4g_{MB}^2 + g_{MR}^2(\frac{\pi}{4\theta})\right)^{0.5} \quad (4\text{-}31)$$

And

$$\beta = \alpha\frac{x}{l} \quad (4\text{-}32)$$

$$\alpha = \frac{3}{\omega_n^2(\frac{X}{g})} = \frac{3}{A_1} \quad (4\text{-}33)$$

The fractional uncertainties of the above parameters can be written as:

$$\frac{\delta\bar{U}_{LS}}{\bar{U}_{LS}} \leq 0.5(\frac{\delta A_1}{A_1} + \frac{\delta A_2}{A_2} + \frac{\delta S_S}{S_S} + \frac{\delta B_1}{B_1} + \frac{\delta B_2}{B_2} + \frac{\delta B_3}{B_3}) \quad (4\text{-}34)$$

$$\frac{\delta A_1}{A_1} \leq \frac{2\delta f_n}{f_n} + \frac{\delta X}{X} \quad (4\text{-}35)$$

$$\frac{\delta A_2}{A_2} \leq (\frac{\omega_n^2\frac{X}{g}}{1+\omega_n^2\left(\frac{X}{g}\right)})(\frac{2\delta f_n}{f_n} + \frac{\delta X}{X}) \quad (4\text{-}36)$$

$$\frac{\delta S_S}{S_S} \leq \frac{\delta\sigma}{\sigma} + \frac{\delta n}{n} + \frac{3a^2\delta a + \left(4\left(\frac{\delta a+\delta t}{a-t}\right)+\frac{\delta a}{a}\right)\frac{(a-t)^4}{a}}{a^3(1-\frac{(a-t)^4}{a^4})} \quad (4\text{-}37)$$

$$\frac{\delta B_1}{B_1} = \frac{\delta AC_F}{AC_F} + \frac{\delta X}{X} \quad (4\text{-}38)$$

$$\frac{\delta B_2}{B_2} = \frac{-sin\beta\ \delta\beta + \left(\frac{sin\beta}{sin^2\alpha}\right)\delta\alpha - cot\alpha\ cos\beta\ \delta\beta}{(\cos\beta - cot\alpha\sin\beta)} \quad (4\text{-}39)$$

$$\frac{\delta B_3}{B_3} \leq (\frac{\delta I}{I} + 0.5(\frac{\delta\theta}{\theta} + 2\frac{\delta g_{MB}}{g_{MB}} + 2\frac{\delta g_{MR}}{g_{MR}}))(\frac{I\left(4g_{MB}^2+g_{MR}^2\left(\frac{\pi}{4\theta}\right)\right)^{0.5}}{(1+I\left(4g_{MB}^2+g_{MR}^2\left(\frac{\pi}{4\theta}\right)\right)^{0.5}}) \quad (4\text{-}40)$$

$$\frac{\delta g_{MB}}{g_{MB}} = \frac{\delta I}{I} \tag{4-41}$$

$$\frac{\delta g_{MB}}{g_{MB}} = \frac{1}{3600(2\ln(3600 f_n)+0.577)}\left(1 - \frac{0.577}{(2\ln(3600 f_n))^{0.5}}\right)\delta f_n \tag{4-42}$$

Similarly, the expression for root lodging velocity is as follows:

$$\overline{U}_{LR} = \left(\frac{R_S}{\frac{((1+\omega_n^2(\frac{X}{g}))}{\omega_n^2(\frac{X}{g})}(0.5\rho A C_F X)(1+2Ig_{MB})}\right)^{0.5} \tag{3-2}$$

The root lodging velocity can be written as:

$$\overline{U}_{LR} = \left(\frac{A_1 R_S}{A_2 B_1 B_4}\right)^{0.5} \tag{4-43}$$

Where all the parameters in the right hand side are defined above and B_4 is as follows:

$$B_4 = (1 + 2Ig_{MB}) \tag{4-44}$$

The fractional uncertainties of the above parameters can be written as:

$$\frac{\delta \overline{U}_{LR}}{\overline{U}_{LR}} \leq 0.5\left(\frac{\delta A_1}{A_1} + \frac{\delta A_2}{A_2} + \frac{\delta R_S}{R_S} + \frac{\delta B_1}{B_1} + \frac{\delta B_4}{B_4}\right) \tag{4-45}$$

Where

$$\frac{\delta B_4}{B_4} \leq 2\,\frac{\delta I}{I}\left(\frac{2Ig_{MB}}{1+2Ig_{MB}}\right) \tag{4-46}$$

Based on equations 4-34 and 4-45, it is now possible to consider the effect of uncertainties in measurements on the lodging velocities.

Table 4.9 presents the fractional uncertainties associated with the parameters and terms above. The results show the agronomic terms are the major source of uncertainty, which is not surprising as the agronomic uncertainties presented here are based on Table 4.8, which shows the variation between 32 treatments, while in practice, the model is applied to study a sample plant, or a group of plants that receive a certain treatment. Nevertheless, the results show even in such an exaggerated variation, the model has less than 10% fractional uncertainty, in root/stem lodging.

After the agronomic variations, the major source of uncertainty is drag area ($\frac{\delta_{AC_F}}{|AC_F|} \leq 0.036$, see equation 4-21). The parameter was measured through the relationship between mean velocity measured by an anemometer (Section 3.4.2) and mean displacement measured by the camera and video tracking (Section 3.4.5) and it might be expected that the uncertainty of measurement from these devices would affect the drag area parameter significantly. Nevertheless, both $\frac{\delta_{\bar{Y}}}{|\bar{Y}|}$ and $\frac{\delta_{\bar{U}}}{|\bar{U}|}$ were an order of 10^{-3}, and the equivalent mass ($\frac{\delta_{\mu}}{|\mu|}$) and natural frequency are the most influential factors (see equation 4-20 and 4-21). This is particularly interesting as it shows despite the potential sources of measurement error and limitations in the video tracking method (e.g. the visibility of the target, using the centroid trajectory, etc.) the uncertainty is very low in comparison to other parameters.

Table 4.9. The fractional uncertainty of different parameters in stem/root lodging

Aerodynamic parameters		Agronomic parameters/terms	
$\frac{\delta f_n}{f_n}$	0.01	$\frac{\delta R_s}{R_s}$	0.07
$\frac{\delta ACF}{ACF}$	0.036	$\frac{\delta S_s}{S_s}$	0.053
$\frac{\delta \theta}{\theta}$	0.018	$\frac{\delta X}{X}$	0.01
$\frac{\delta I}{I}$	0.02		
Lodging velocities			
$\frac{\delta \overline{U}_{Ls}}{\overline{U}_{Ls}}$	0.09	$\frac{\delta \overline{U}_{LR}}{\overline{U}_{LR}}$	0.098

4.8. Conclusions

Results of this chapter showed the turbulence flow parameters over the canopy were in agreement with what has been reported in the literature (Finnigan, 2000, Sterling et al., 2003) and justified some of the assumptions in the lodging model. The wind loading process through the momentum transfer was understood through quadrant-hole analysis which also showed an appropriate averaging time (10 minutes) to study the wind loading process. Moreover, the lodging model (Baker et al., 2014) was developed for 'typical' crop canopies where the turbulence length scale is of the order of 1h - 2h (h is the canopy height), and the results of this chapter showed consistency of the results with the literature. Furthermore, it was shown that the streamwise velocity spectra over the oat canopy declined at -5/3 slope at high frequencies which agreed with Kolmogorov theory relating to energy cascade in the inertial subrange (which gives extra assurance about the validity of the data collected in the experiments). Finally, the turbulence intensity results showed the range of values measured in the experiments is much lower than what was assumed by Baker et al. (2014) and justified

the necessity of using the modified expression of lodging velocities (equation 3-1 and 3-2) rather than what was suggested by Baker et al. (2014), i.e. equation 2-12 and 2-13.

The field measurements enabled the dynamic/aerodynamic parameters of oats, i.e., natural frequency, damping ratio and the drag area to be estimated. Although the interlocking of the crop later in the season influences the crop's movement, a peak in the displacement spectra (which is associated with the natural frequency) can be detected throughout the peak lodging season, which gradually reduces to lower values through the season due to plant growth.

The experiments on the anchorage system showed the root diameter and depth are both important in anchorage resistance and the oat root system is better represented by a cone rather than a spherical shape.

This chapter also showed uncertainties associated with the measurements have a negligible effect on lodging velocities and the results. It was found that the uncertainties with the video tracking method are very low in comparison to the other sources of uncertainties including the agronomic terms which shows the novel method developed in this research is accurate enough for evaluating the dynamic/aerodynamic parameters of the crops.

5. The meteorological parameters and the potential impact of climate change

In what follows, certain sections have been adapted from the following paper for which the author can claim considerable intellectual input:

- Mohammadi, M., Finnan, J., Baker, C., Sterling, M. (2020a) The potential impact of climate change on oat lodging in the UK and Republic of Ireland, Advances in Meteorology, Volume 2020

5.1 Introduction

This chapter considers the possible influence of climate change on oat lodging in the UK and the Republic of Ireland. Long-term historical data has been analysed to find representative wind and rainfall CDFs. Details relating to the meteorological stations from which the data were obtained are provided in Section 5.2. Section 5.3 presents the methodology used to project future climate conditions, whilst Section 5.4 outlines the development of wind and rainfall probability distributions which were from historical data. Finally, Section 5.5 presents an analysis of the probability of lodging, both for the current situation and for the projected future climate.

5.2 Historical data

To evaluate historical data for the last 30 years, data from 38 stations were collected from the national meteorological service in Ireland, Met Éireann (Met Éireann, 2019), the Meteorological Office Integrated Data Archive System (MIDAS) Land and the Marine Surface Stations (Ceda Archive, 2016) and the Met office National Meteorological Archive. Table 5.1 outlines the meteorological stations used, their location, and the type of data obtained.

These specific stations were selected based on the availability of long-term data (1987-2016). Additionally, meteorological stations were chosen in regions where the soil conditions are suitable for tillage and oats are commercially grown, i.e. mainly eastern and southern parts of Ireland (Figure 5.1), Eastern Scotland as well as Western and Southern England (Tillage Sector Development Plan, 2012; RSK ADAS Ltd, personal communication, 2016). Figure 5.2 demonstrates the geographic distribution of studied meteorological stations.

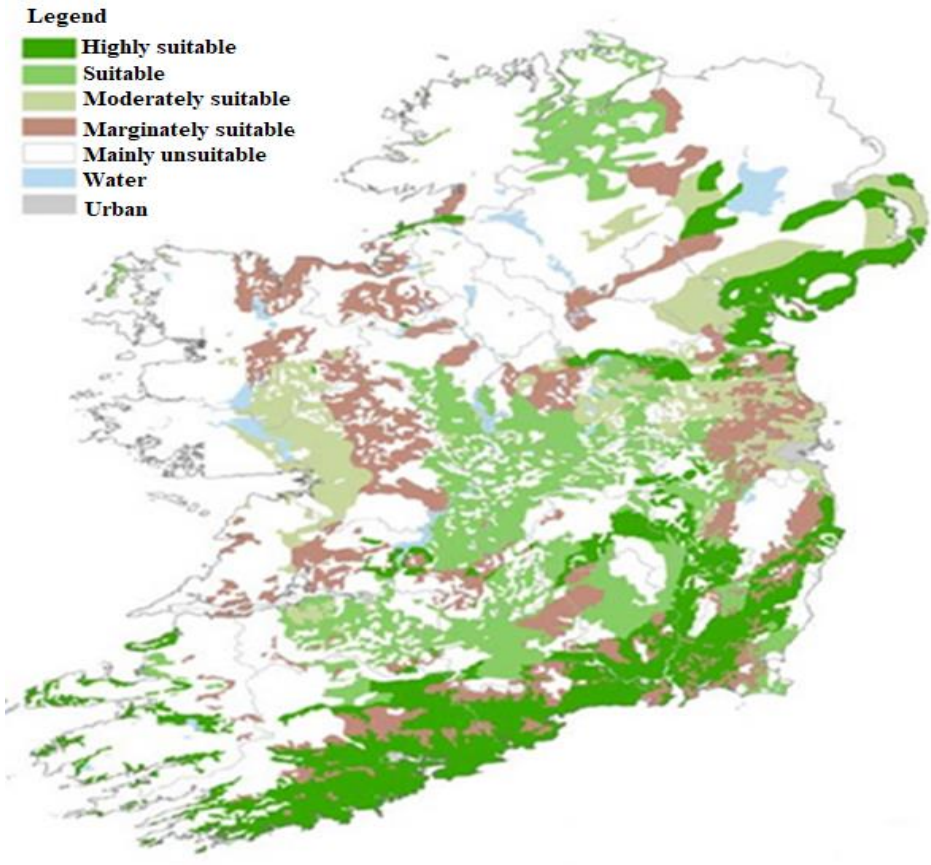

Figure 5.1. Soil suitability for tillage in Ireland (Tillage Sector Development Plan, 2012).

(a) Stations across the Republic of Ireland

(b) Stations across the UK

Figure 5.2. Spatial distribution of studied meteorological stations in the British Isles (Google Map, 2019; Met Éireann, 2019; Meteorological Office, 2019).

Table 5.1. Weather stations with geographical coordinates located in Ireland and the UK.

Order number	Station	County (Country)	Latitude (° *N*)	Longitude[2] (° *W*/ ° *E*)	Height (m)	Daily rainfall	Hourly wind
1	Hacketstown	Carlow (IR)	52.857	-6.552	189	✓	✓
2	Derrygreenagh	Offaly (IR)	53.388	-7.255	90	✓	✓
3	Lavistown house II	Kilkenny (IR)	52.636	-7.192	52	✓	×
4	Montenotte	Cork (IR)	51.903	-8.441	94	✓	×
5	Foulksmills	Wexford (IR)	52.306	-6.760	71	✓	×
6	Aherla More	Cork (IR)	51.843	-8.722	122	✓	×
7	Bansha	Tipperary (IR)	52.404	-8.120	128	✓	×
8	Casement Aerodrome	Dublin (IR)	53.303	-6.437	91	✓	✓
9	Mullingar	Westmeath (IR)	53.536	-7.357	101	✓	✓
10	Kingscourt	Meath (IR)	53.870	-6.803	67	✓	×
11	Castledermot	Kildare (IR)	52.934	-6.888	85	×	✓
12	Malin head	Donegal (IR)	55.370	-7.337	20	✓	×
13	Cork airport	Cork (IR)	51.842	-8.485	155	✓	✓
14	Dublin Airport	Dublin (IR)	53.423	-6.238	71	×	✓
15	Hereford	Herefordshire (UK)	52.052	-2.735	73	✓	×
16	Old Storridge Worcester	Worcestershire (UK)	52.16	-2.37	84	✓	×
17	Preston Montford for Shrewsbury	Shropshire (UK)	52.72	-2.84	71	×	✓
18	Wilton House Salisbury	Wiltshire (UK)	51.08	-1.86	53	✓	×
19	Lyneham	Wiltshire (UK)	51.502	-1.990	145	×	✓
20	Haslemere	Surrey (UK)	51.08	-0.74	117	✓	×
21	Strongford	Staffordshire (UK)	52.949	-2.179	95	✓	×
22	Alton Edward Road	Hampshire (UK)	51.155	-0.968	114	✓	×
23	Testwood	Hampshire (UK)	50.933	-1.495	7	✓	×
24	Shawbury	Shropshire (UK)	52.794	-2.663	72	×	✓
25	South Farnborough	Hampshire (UK)	51.279	-0.771	65	×	✓
26	Barnhorn	East Sussex (UK)	50.844	0.412	29	✓	×
27	Boundstone	Surrey (UK)	51.189	-0.803	113	✓	×
28	Camberley	Surrey (UK)	51.327	-0.765	60	✓	×
29	Kent Hatch Resr	Surrey (UK)	51.244	0.057	202	✓	×
30	Capenoch	Dumfriesshire (UK)	55.226	-3.815	52	✓	×
31	Rawburn filters	Berwickshire (UK)	55.799	-2.513	244	✓	×
32	Evelix	Sutherland (UK)	57.889	-4.082	37	✓	×
33	Tullynessle	Aberdeenshire (UK)	57.261	-2.729	191	✓	×
34	Coldstream	Berwickshire (UK)	55.664	-2.225	37	✓	×
35	Threave Castle	Dumfries Galloway (UK)	54.93	-3.95	73	✓	×
36	Leuchars	Fife (UK)	56.377	-2.860	142	×	✓
37	Dyce	Aberdeenshire (UK)	57.205	-2.203	110	×	✓
38	Lossiemouth	Moray (UK)	57.72	-3.28	22	×	✓

[2] Negative values represent west of Prime Meridian.

5.3 Future scenarios projection

UKCP18 provides the most recent projections for future climate conditions in the coming decades based on a number of data sources and emission scenarios for different periods and locations (UK climate projections website, 2018).

Although international efforts aim to reduce greenhouse gas emissions, different scenarios are plausible based on the decisions countries make and their commitment to international agreements. Consequently, UKCP18 has devised a range of different scenarios which are defined as Representative Concentration Pathways (RCPs), which determine the amount of greenhouse gases causing certain radiative forcing at the high altitude of the Earth's atmosphere by 2100, in comparison to pre-industrial levels (the Intergovernmental Panel on Climate Change, 2018). Four forcing levels are used: 2.6, 4.5, 6.0, and 8.5 W/m^2, which are defined as RCP 2.6, RCP 4.5, RCP 6.0, and RCP 8.5 scenarios (Meteorological Office, 2019).

Projections in the UKCP18 include probabilistic, global, and regional outcomes. Each type of projection is based on a number of climate change models and grid resolutions (UK climate projections website, 2018). These models simulate physical processes related to the transfer of mass and energy in the Earth's climate. In a climate model, the Earth's surface is composed of a three-dimensional grid of cells and relevant equations corresponding to the relevant climate models are solved for each cell (National Oceanic and Atmospheric Administration, 2021). Table 5.2 shows different models used in each type of projection and the corresponding grid resolution.

In addition to the climate models used for each type of projection, the probabilistic, global, and regional projections also provide different types of output. Despite the probabilistic projections, the regional and global projections do not provide any probability distribution of

model response, however, these two projections can provide a wider range of alternative future climate conditions (UK climate projections website, 2018).

Table 5.2. Models, grid resolution, RCP and geographic output for probabilistic, global and regional projections in UKCP18

	Probabilistic	Global	Regional
Climate Model	HadCM3 and CMIP5-ESM	HadGEM3-GC3.05 (15 simulations) CMIP5-13 (13 models as listed in Table 5.3)	12 outputs from HadGEM3-GC3.05
Grid resolution	25km	60km	12km
RCP	RCP 2.6, 4.5, 6.0 and 8.5	RCP 8.5	RCP 8.5
Geographic output	UK	British Isles	British Isles

Probabilistic projections are designed to demonstrate the ranges of uncertainty in the outputs for a certain period, location (region), and different emission scenarios. These projections merge historical weather data with climate models (HadCM3 and CMIP5-ESM) and statistics at a 25km grid resolution to provide outputs for different emission scenarios. Thus, they are considered to be an appropriate tool to study the effect of different RCPs on precipitation anomalies. However, the tool provides data only for UK areas and does not include projections for the Republic of Ireland.

Global projections are based on 28 climate models at 60km grid resolution including 15 simulations of the Met Office Hadley Centre model (HadGEM3-GC3.05) and 13 other

outputs adopted from the Intergovernmental Panel on Climate Change's Fifth Assessment Report, CMIP5-13 (Maisey et al., 2018).

The HadGEM3-GC3.05 is a coupled atmosphere-ocean configuration, including different levels of the stratosphere, atmospheric chemistry, vegetation, and ocean biology (Meteorological Office, 2019). In each model's output, all plausible variables are perturbed in the given climate model configuration, building a Perturbed Parameter Ensemble (PPE) (Murphy et al., 2018). These plausible variants account for a variety of different effects, e.g., convection parameters, mountain effects, atmospheric boundary layer conditions, cloud radiation, and aerosols parameters which can be found in Murphy et al. (2018). PPEs have subsequently been filtered to provide the highest plausibility and diversity of outputs, producing 15 simulations (Murphy et al., 2018).

In order to add diversity to the projections, 13 CMIP5 models (CMIP5-13) are also provided simulating global and zonal mean temperatures in Earth surface, global trend of sea surface temperature (SST) bias, Atlantic Meridional Overturning Circulation (AMOC) as well as climatological conditions over the North Atlantic and Europe (Murphy et al, 2018). Table 5.3 shows models incorporating in CMIP5-13 and associated modelling groups.

Table 5.3. The CMIP5-13 models used in UKCP18 under the RCP8.5 scenario (Murphy et al., 2018).

Model designation	Modelling group
CMCC-CM	Centro Euro-Mediterraneo per I Cambiamenti Climatici
BCC-CSM1	Beijing Climate Centre, China Meteorological Administration
CanESM2	Canadian Centre for Climate Modelling and Analysis
ACCESS1-3	Commonwealth Scientific and Industrial Research Organization (CSIRO) and Bureau of Meteorology (BOM), Australia
CESM1-BGC	Community Earth System Model Contributors
CNRM-CM5	Centre National de Recherches Météorologiques / Centre Européen de Recherche et Formation Avancée en Calcul Scientifique
EC-EARTH	EC-EARTH consortium
GFDL-ESM2G	NOAA Geophysical Fluid Dynamics Laboratory
HadGEM2-ES	Met Office Hadley Centre
IPSL-CM5A-MR	Institute Pierre-Simon Laplace
MPI-ESM-MR	Max-Planck-Institut für Meteorologie
MRI-CGCM3	Meteorological Research Institute
CCSM4	National Centre for Atmospheric Research

Regional projections are based on HadGEM3-GC3.05 and use 12 PPEs in a downscaled the results (i.e., transform from the large grid used in the model to a small grid closer to the ground) in comparison to the global projection which enables the effect of physiographic

features including mountains, coasts, urban areas, lakes and rivers being considered. It is worth noting that the global and regional projection use the worst emission scenario (RCP 8.5) while, the probabilistic uses all the plausible scenarios (Fung et al., 2018).

5.4 Climate data and projections

5.4.1 Wind and rainfall probabilities

Figure 5.3 shows sample data relating to cumulative density functions (CDFs) for a selected station in England (Hereford). These are for the months of June and July when lodging events are known to occur. In Figure 5.3, the horizontal axis illustrates rainfall and the vertical axis shows the correspondent cumulative probability.

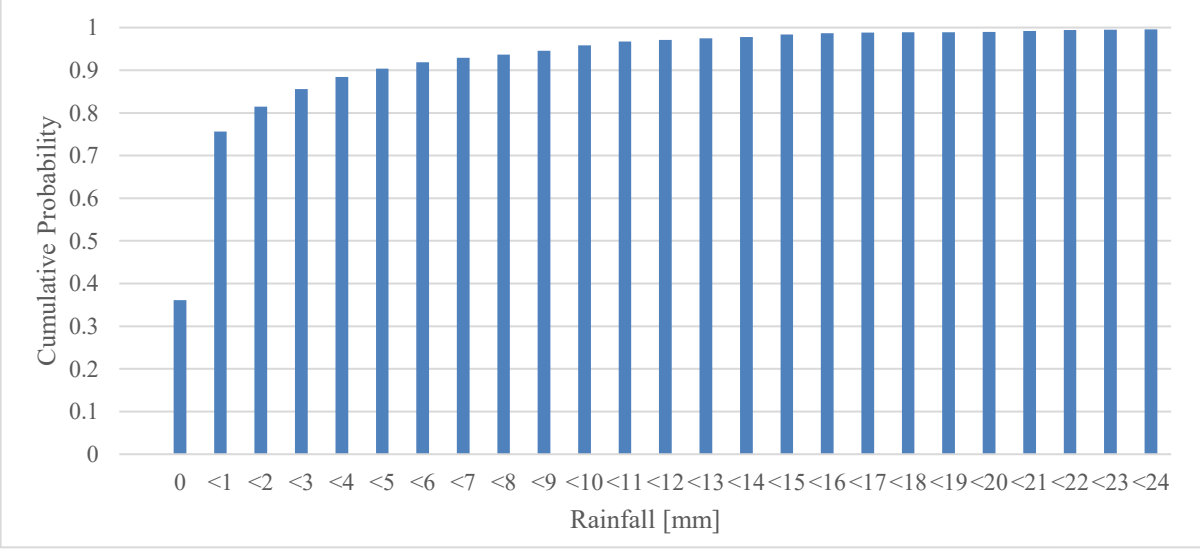

Figure 5.3. Rainfall CDF for Hereford meteorological station in the period from 1987 to 2016 for June and July (Ceda Archive, 2016).

Although the CDF is a discrete function, finding a representative continuous function to predict the values in the discrete ranges can be helpful for the calculation procedure for the probability of lodging (the procedure is fully described in Section 5.5.1). Accordingly, to identify representative functions, equation 2-19 which was assumed by Baker et al. (2014) was examined versus historical data from the studied stations. Figure 5.4 shows a sample comparison between CDF obtained from Cork airport meteorological data (no. 13 in Table 5.1) and the CDF obtained from integrating equation 2-19). As the figure shows, this assumption cannot be considered as a good fit on the meteorological data, due to remarkable difference especially at low rainfall values.

$$p(i) = (\frac{1}{m})e^{-(i/m)} \qquad (2\text{-}19)$$

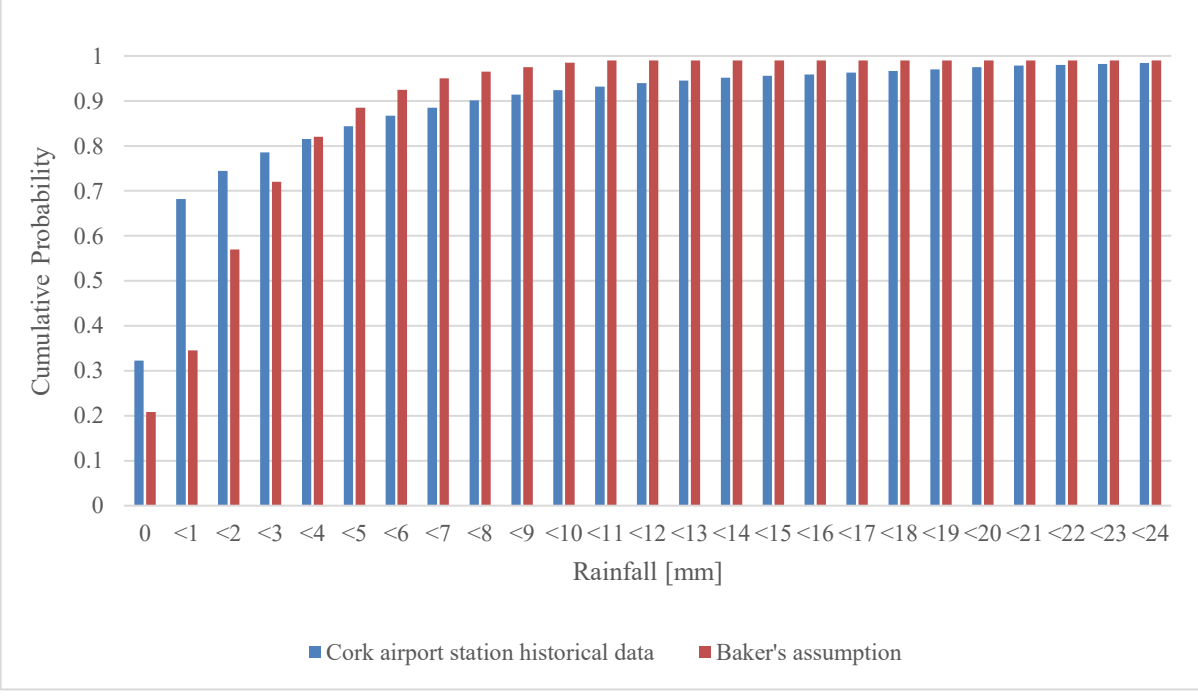

Figure 5.4. A sample comparison between CDF obtained from Baker's assumption (Baker et al. 2014) for rainfall CDF and the real meteorological data for Cork Airport station.

In order to find a better mathematical representation of rainfall CDF a number of curves as suggested by MATLAB curve fitting tool were examined on the data and the summation of two exponential functions was found to be the best representative function (equation 5-1). It is noted that the mean-square error (Table 5.4) and Quantile-Quantile (Q-Q) plot (explained later in the chapter) were used to evaluate the goodness of fit.

$$CDF(i) = ae^{-bi} + ce^{-di} \tag{5-1}$$

Where i is amount of daily rainfall, CDF(i) is the cumulative probability and a, b, c and d are site dependent coefficients. Despite the geographic variation of rainfall, it was found that the overall CDFs can be defined at regional scales for Ireland, Scotland and England (Table 5.4). Furthermore, it was observed that through appropriate selection of the values of a, b, c and d, an overall curve could be obtained which represented all of the data irrespective of location to a reasonable degree of accuracy, i.e., 0.2%. The fitted curve parameters for all studied stations are presented in Table 5.5.

Table 5.4. Coefficients for regional and overall representative curves for rainfall PDFs and corresponding curve difference with actual data.

	a	*b*	*c*	*d*	Mean-squared error
Ireland	0.966	0.0002	-0.594	-0.378	0.001
England	0.955	0.0004	-0.535	-0.440	0.002
Scotland	0.982	0.0002	-0.607	-0.390	0.002
Overall	0.981	0.0002	-0.059	-0.390	0.002

Table 5.5. The best fit for rainfall CDF curve coefficients for studied stations

Station	County (Country)	a	b	c	d
Hacketstown	Carlow (IR)	0.975	0.0003	-0.609	-0.396
Derrygreenagh	Offaly (IR)	0.977	0.0003	-0.609	-0.373
Lavistown house II	Kilkenny (IR)	0.966	0.0005	-0.570	-0.416
Montenotte	Cork (IR)	0.973	0.0003	-0.553	-0.382
Foulksmills	Wexford (IR)	0.968	0.0004	-0.572	-0.391
Aherla More	Cork (IR)	0.967	0.0004	-0.545	-0.310
Bansha	Tipperary (IR)	0.968	0.0004	-0.572	-0.280
Casement Aerodrome	Dublin (IR)	0.978	0.0003	-0.607	-0.496
Mullingar	Westmeath (IR)	0.984	0.0002	-0.629	-0.332
Kingscourt	Meath (IR)	0.981	0.0002	-0.606	-0.352
Castledermot	Kildare (IR)	0.978	0.0003	-0.597	-0.436
Malin head	Donegal (IR)	0.990	0.0001	-0.654	-0.307
Cork airport	Cork (IR)	0.970	0.0004	-0.560	-0.340
Hereford	Herefordshire (UK)	0.978	0.0003	-0.575	-0.599
Old Storridge Worcester	Worcestershire (UK)	0.972	0.0003	-0.569	-0.456
Preston Montford for Shrewsbury	Shropshire (UK)	0.976	0.0003	-0.599	-0.452
Wilton House Salisbury	Wiltshire (UK)	0.977	0.0003	-0.575	-0.520
Haslemere	Surrey (UK)	0.973	0.0003	-0.562	-0.468
Strongford	Staffordshire (UK)	0.978	0.0003	-0.577	-0.463
Alton Edward Road	Hampshire (UK)	0.975	0.0003	-0.568	-0.487
Testwood	Hampshire (UK)	0.973	0.0004	-0.562	-0.607
Barnhorn	East Sussex (UK)	0.972	0.0004	-0.558	-0.703
Boundstone	Surrey (UK)	0.977	0.0003	-0.574	-0.594
Camberley	Surrey (UK)	0.975	0.0003	-0.581	-0.495
Kent Hatch Resr	Surrey (UK)	0.978	0.0003	-0.570	-0.531
Capenoch	Dumfriesshire (UK)	0.978	0.0003	-0.585	-0.294
Rawburn filters	Berwickshire (UK)	0.977	0.0003	-0.602	-0.384
Evelix	Sutherland (UK)	0.981	0.0003	-0.609	-0.468
Tullynessle	Aberdeenshire (UK)	0.975	0.0003	-0.611	-0.444
Coldstream	Berwickshire (UK)	0.974	0.0004	-0.587	-0.524
Threave Castle	Dumfries Galloway (UK)	0.980	0.0003	-0.584	-0.268

Additionally, these functions were assessed by Quantile-Quantile (Q-Q) plot which examines if two data series have the same distribution. A quantile splits the data into groups that contain the same data points. The Q-Q plot gives each point a quantile and adds the same number of quantile on the studied curve and plots the data from the dataset versus the associated quantile from the curve. If the historical data has the same distribution as equation 5-1, most data points would be close the line, this means both the historical data and the distribution (equation 5-1) have comparable quantiles (NIST/SEMATECH, 2020). Figure 5.5 shows the Q-Q plot for the curve fitted for Ireland, England, Scotland and the overall function fitted for all the studied stations. Figure 5.5 shows that the historical data quantile points are very close to the line and there is a reasonable agreement between the fitted curves and meteorological data across most of the data range, which means the selected distribution is a good fit.

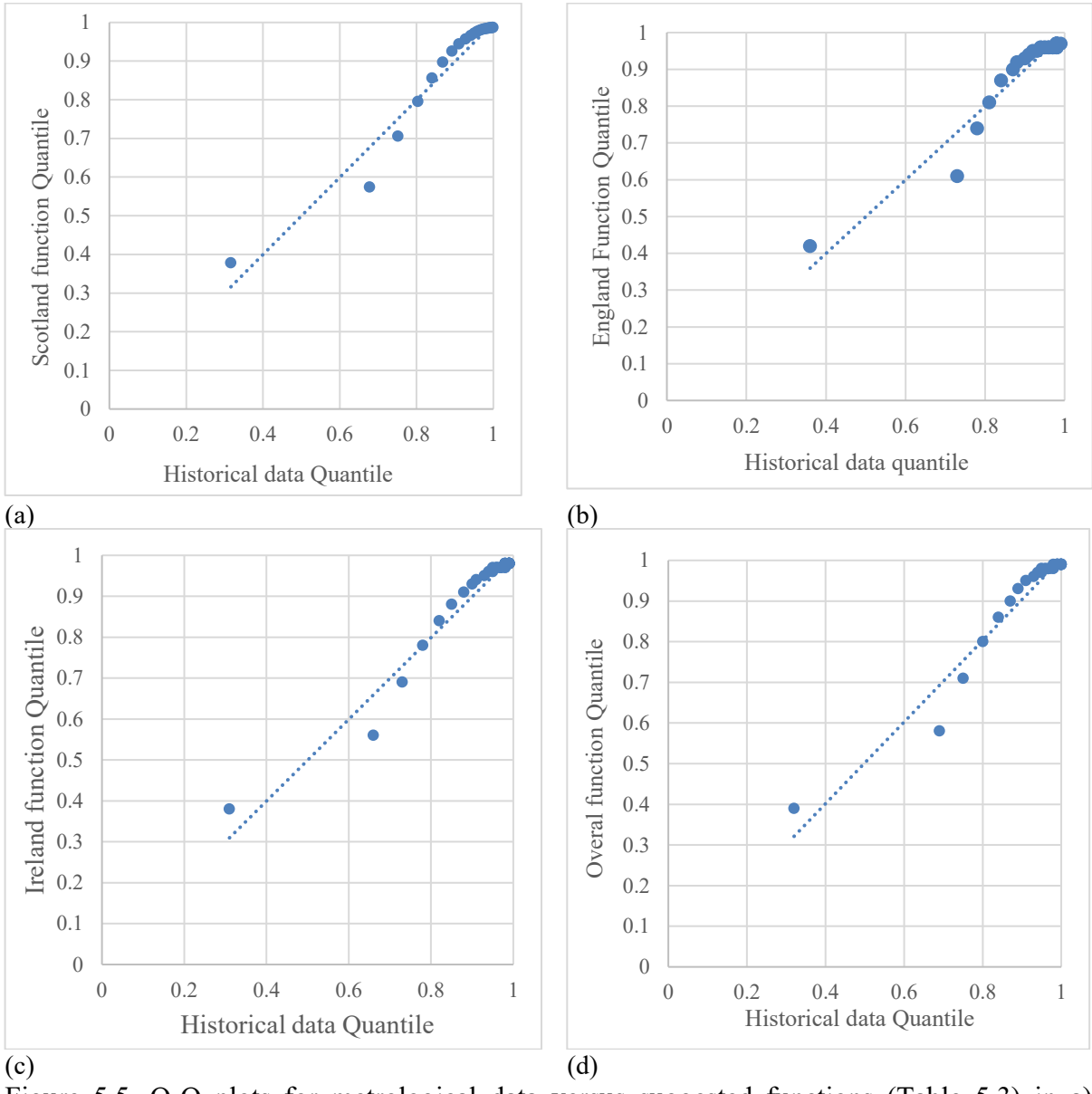

Figure 5.5. Q-Q plots for metrological data versus suggested functions (Table 5.3) in a) Scotland b) England c) Ireland d) all the studied stations

A similar analysis was undertaken for the wind speed to investigate representative functions to be used in the lodging probability calculation. First, the assumption used by Baker et al. (2014), i.e. the Rayleigh distribution was examined versus the meteorological data (Table 5.1). Figure 5.6 shows a comparison between a sample meteorological data and the Rayleigh

distribution fitted by MATLAB curve fitting tool. As the figure shows the curve is not a good fit particularly for wind speeds less than 6 m/s.

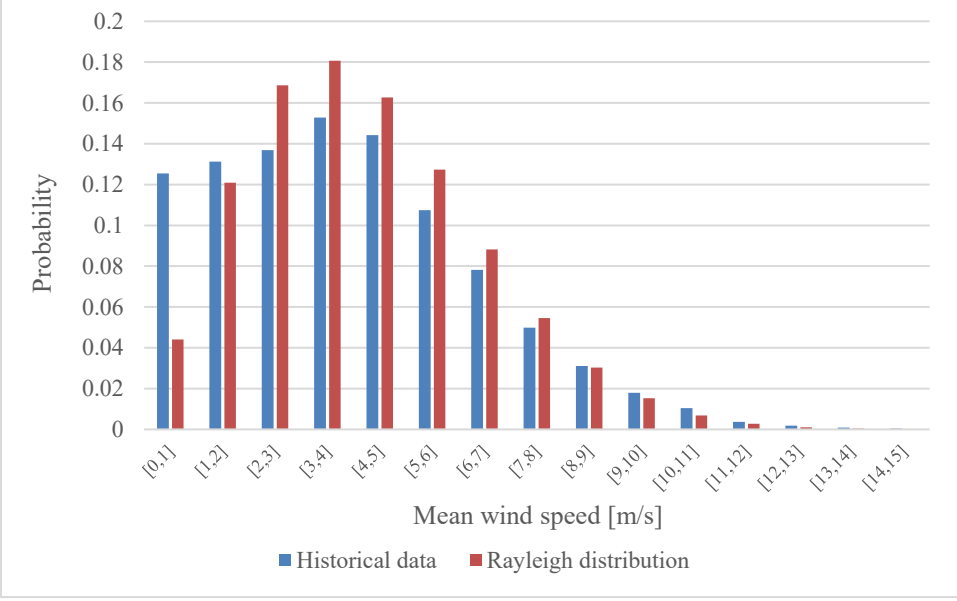

Figure 5.6. A sample comparison between Rayleigh distributions assumed by Baker et al. (2014) for hourly mean wind speed PDF and the real meteorological data for Leuchars station (no.36 in Table 5.1). The measurement height is 10m above the ground.

In order to find a representative function to be used in the lodging probability calculation, CDF functions for studied stations were plotted and it was found that the Weibull distribution (equation 5-2) can represent all the stations with less than 0.2% mean squared error. Weibull is a well-known distribution to represent wind speed data collected over a long period of time and the CDF version of the distribution is given in equation 5-2 (Klaver, 1996).

$$P(U) = 1 - e^{-(\frac{U}{\lambda})^k} \quad (5\text{-}2)$$

Here, λ and k are parameters governing the scale and shape of the distribution respectively. Although the Weibull distribution is well known and widely used to represent the wind PDF and CDF (Klaver, 1996) , Baker et al. (2014) used Rayleigh to enable an analytical form of the lodging probability to be derived. Nevertheless, when representative probability functions (e.g. equations 5.1 and 5.2) are available the lodging probability can be derived numerically and there is no need for the analytical solution. Table 5.6 shows the scale and shape factors for the best fits on the data from studied stations.

Table 5.6. The best fit curve coefficients for studied stations

Station	λ	k
Casement Aerodrome	5.12	1.89
Dublin Airport	5.35	2.13
Mullingar	3.96	2.00
Cork airport	5.30	2.28
Shawbury	4.52	1.88
Lyneham	4.50	2.20
South Farnborough	4.02	1.84
Leuchars	4.51	1.55
Dyce	4.50	1.75
Lossiemouth	4.51	1.55
Overall function	4.50	1.92

Figure 5.7 shows the Q-Q plot for the Weibull distribution and the meteorological data for Shawbury station (no.24 in Table 5.1) and the historical data quintile points show a reasonable agreement between the fitted curves and meteorological data. Moreover, while considering different curves suggested by MATLAB curve fitting tool (including exponential and summation of two exponentials), the Weibull distribution showed the lowest mean squared error between the meteorological data and fitted curve. Finally as mentioned earlier in this section, the Weibull distribution has been widely used in the literature (Cook, 1985; Klaver, 1996) to represent the wind data.

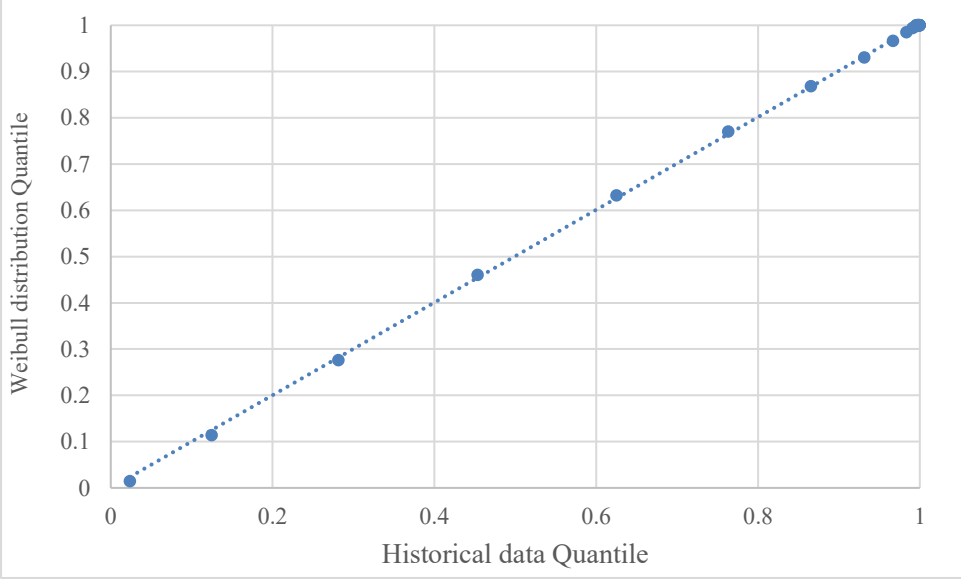

Figure 5.7. Q-Q plots for metrological data for Shawbury station (no.24 in Table 5.1) versus Weibull distribution.

5.4.2 Future Climate projection

Projections of UKCP18 show warmer, wetter winters and hotter, drier summers for the UK (UK climate projections website, 2018). All the regions of the UK are projected to face higher temperatures and the increase is greater in summers rather than in winters. Perhaps not

surprisingly, geographic and seasonal variation of precipitation are likely to continue to exist in future. This section discusses results from the UKCP18 where probabilistic, global and regional projections are presented in Section 5.4.2.1 to 5.4.2.3.

5.4.2.1 Probabilistic projections (25km resolution)

Figure 5.8 illustrates precipitation rate anomalies in June and July respectively in all the UK areas using the 1981-2010 baseline and geographic variations in precipitation (rainfall) anomalies can be clearly observed. The figure includes three images for the 10^{th}, 50^{th}, and 90^{th} percentiles and each square indicates the range of change in the area. For example, a grid showing a 10% precipitation anomaly rate (i.e., the difference when compared to the average monthly rainfall in a specific month for the 1981-2010 period) corresponding to the 50^{th} percentile represents the probability that 0.5 of the monthly rainfall will increase by less than 10% (UK climate projections, 2018). It means 10% is the projected anomaly while the percentile shows the probability that this change to occur. As all RCPs show similar outcomes, only data corresponding to RCP 2.6 is presented here. Figure 5.8 shows drier conditions for southern regions of England in June and July, while western regions of Scotland are projected to experience a wetter climate in June. Overall, the probabilistic projections show a higher probability of wetter conditions in June and July.

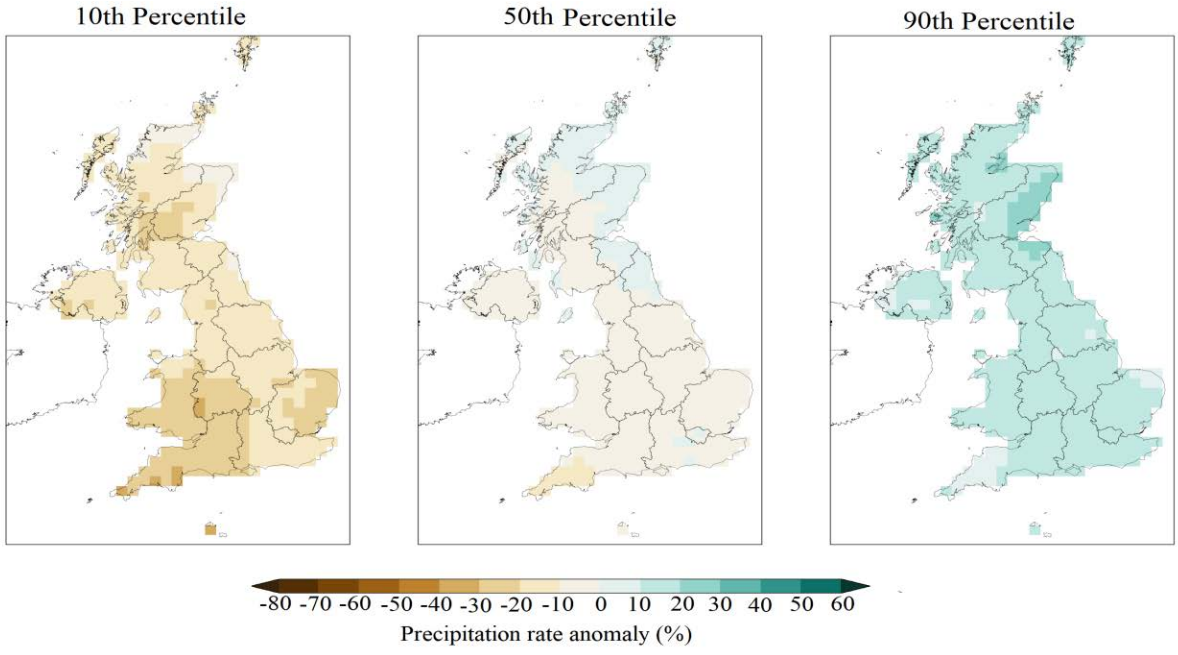

(a) Data corresponding to June

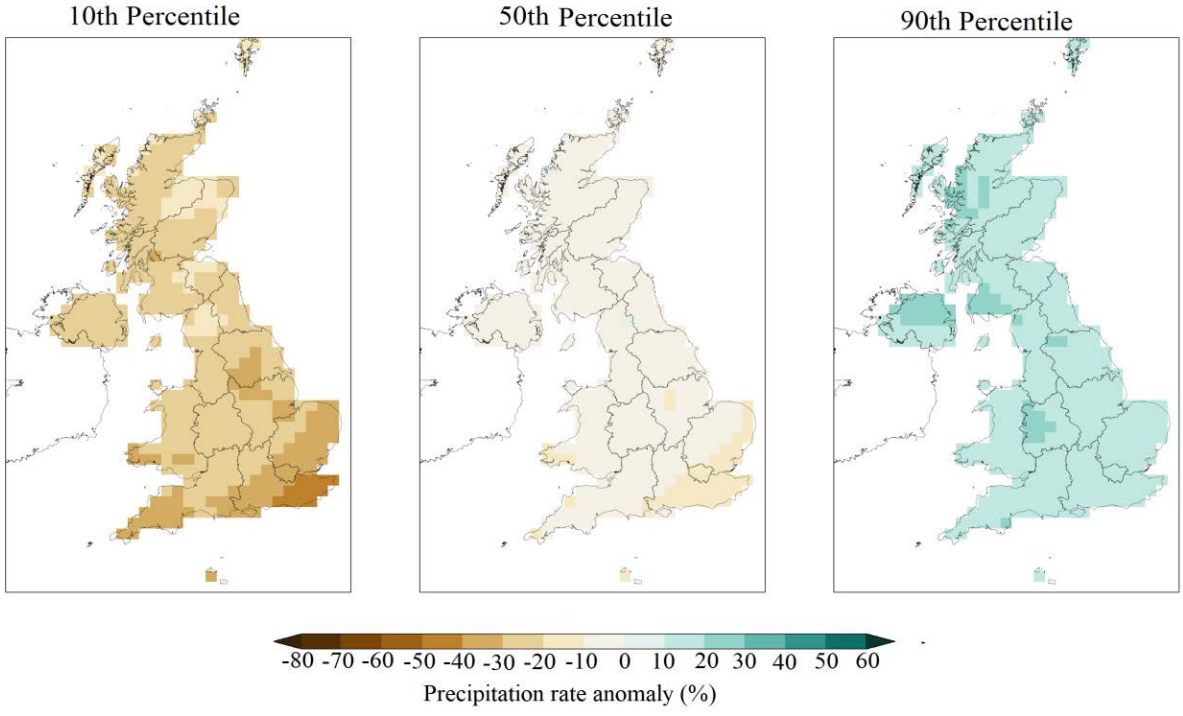

(b) Data corresponding to July

Figure 5.8. Monthly average precipitation rate anomaly (%) in 2020 to 2049 using baseline 1981-2010 and Scenario RCP 2.6

The probabilistic projection tool from UKCP18 (described in Section 5.3) was employed to analyse data at 16 stations across Southern and Western areas of England as well as Eastern and Southern regions of Scotland (areas where oats are commercially grown). Results illustrate that for all stations, different emission scenarios have only a slight effect on precipitation rate anomaly (%), although the difference between emission scenarios plots is larger in July. Figure 5.9 illustrates an example of a CDF for monthly rainfall changes at a sample weather station (Hereford, England) for different emission scenarios. More details regarding the anomaly range from the 10th percentile to the 90th percentile are presented in Table 5.7 (Section 5.4.2.4). As illustrated in Figure 5.9, different RCP results in different CDFs, which is perhaps not too surprising given the complexity of the climate model and the uncertainty associated with this particular area.

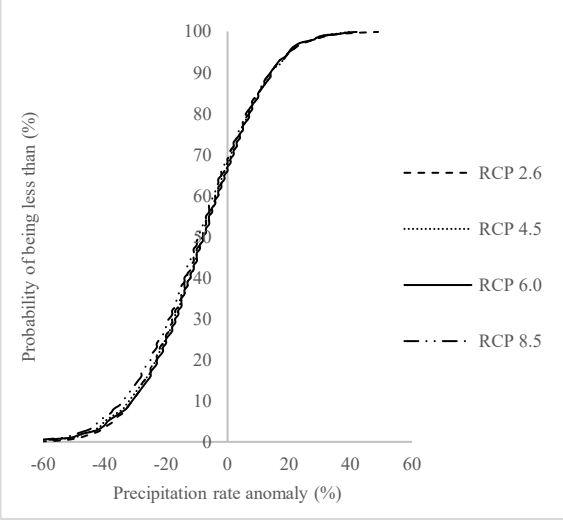

(a) Data corresponding to June

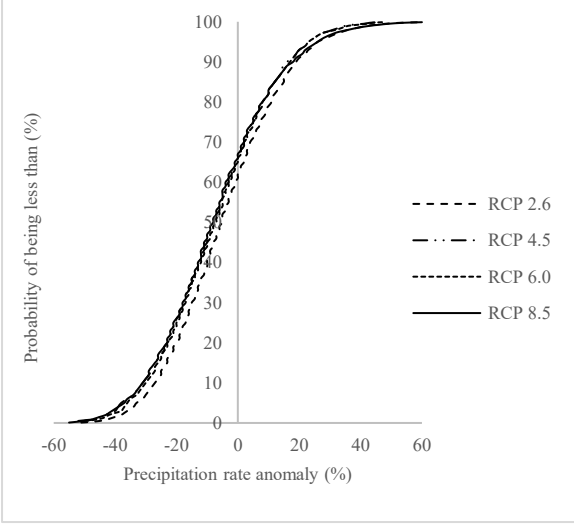

(b) Data corresponding to July

Figure 5.9. Cumulative Distribution Function for precipitation rate anomaly in Hereford England for RCPs used in the UKCP18.

5.4.2.2 Global projections (60km resolution)

Figure 5.10 shows the results of global projections from these 28 climate models at a 60 km resolution. In addition to model designations described in Table 5.3, 15 PPEs from HadGEM3-GC3.05 are presented as five-digit numbers. These numbers are allocated to denote selected PPEs by UKCP18 researchers and do not have any significance (Meteorological Office, personal communication, 2019). The results illustrate that in the most severe projections, Southern regions of Ireland might witness up to 30-40% drier conditions in June and July. However, some models project a different trend suggesting an increase of precipitation of up to 40%. In general, the majority of the models show a projected difference of ± 20% in June and July.

With respect to England, the majority of the projections suggest that June will be 10% to 30% drier, although regions in the South could experience up to 30% increase in rainfall. In July, most models show drier conditions (up to 60% especially in Southern parts) whilst the extreme cases suggest a 40% increase in rainfall. Finally, precipitation in Scotland is expected to experience ± 30% and ± 20% in June in July, respectively.

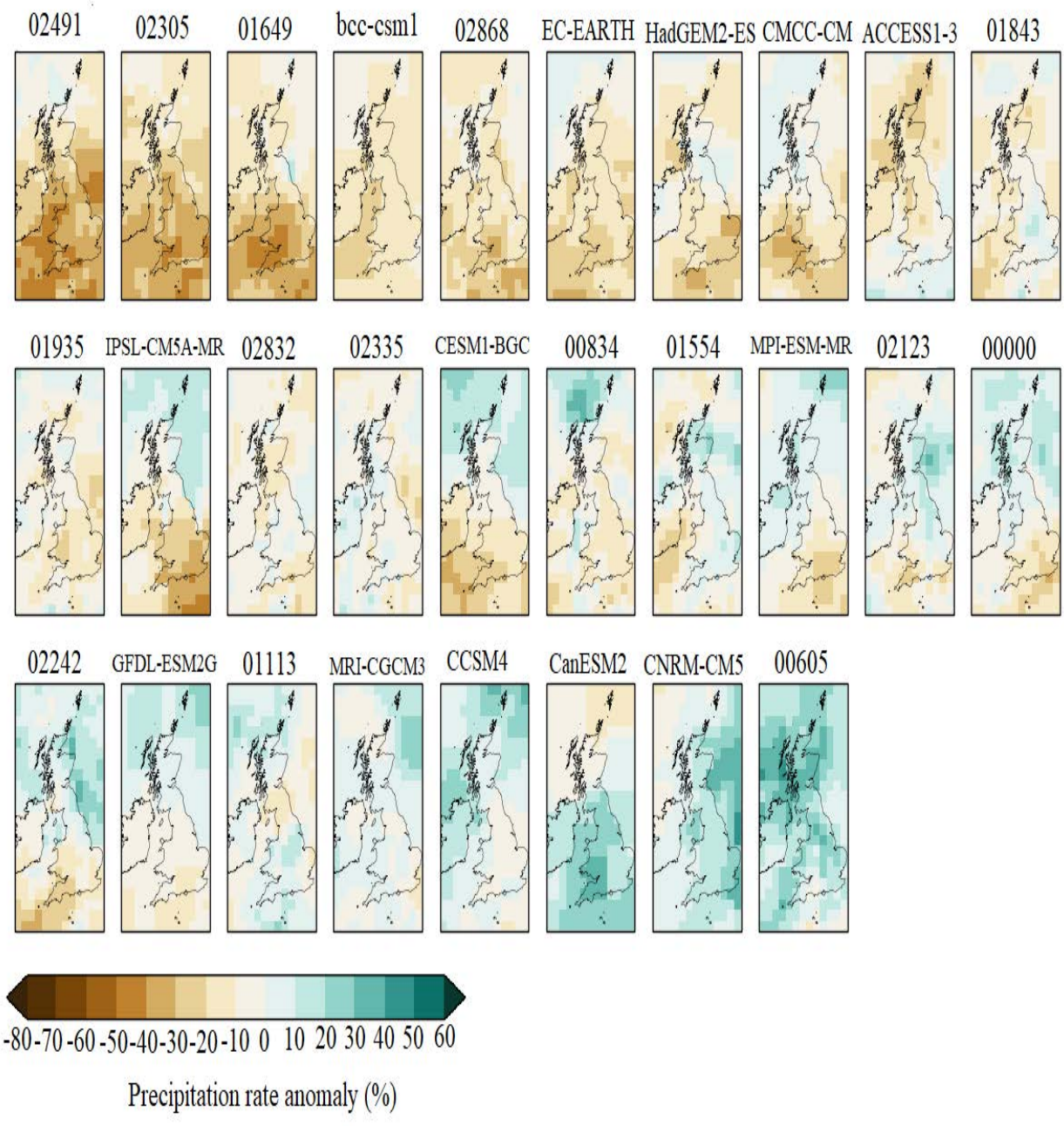

(a) Data corresponding to June.

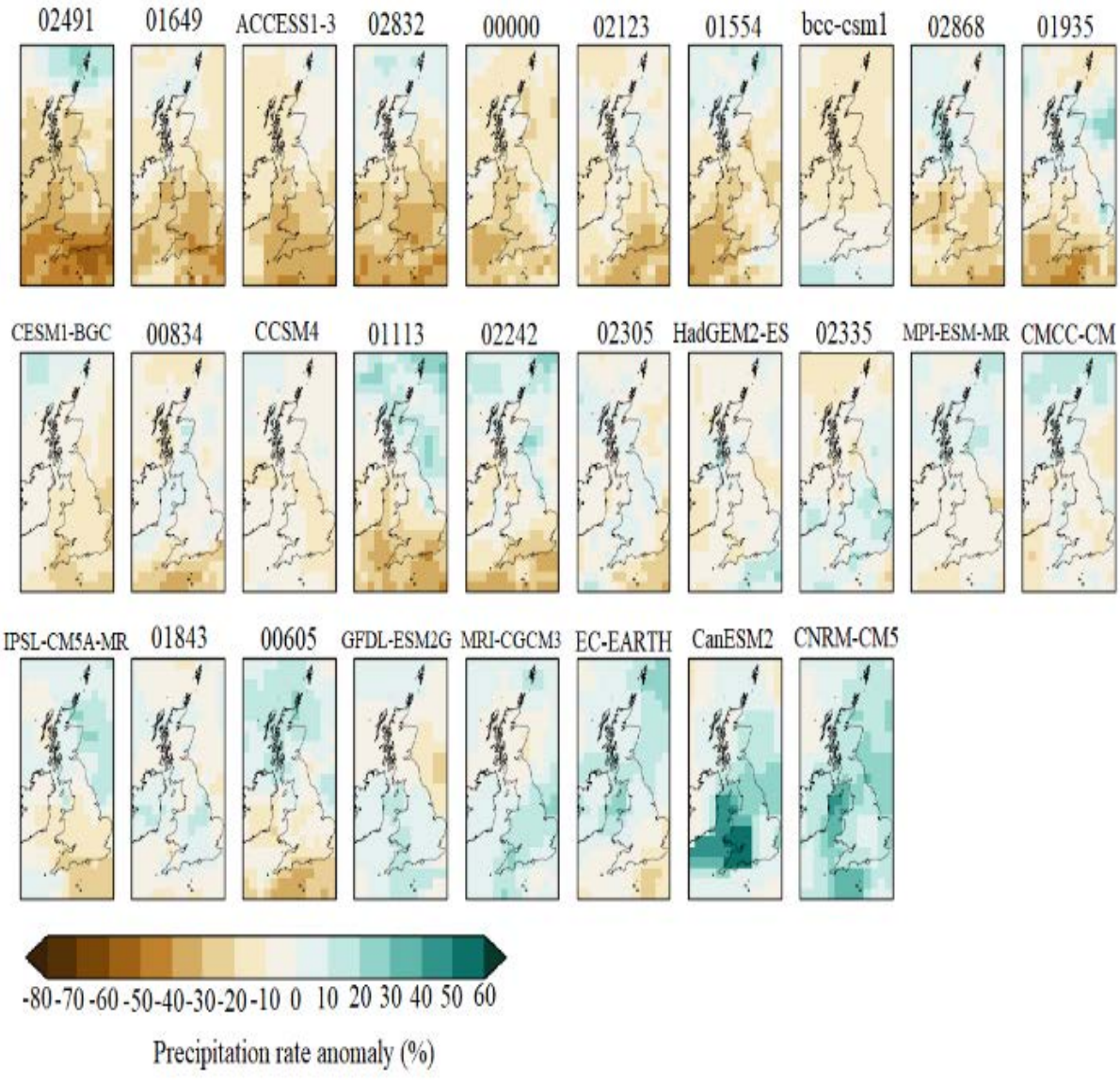

(b) Data corresponding to July

Figure 5.10. Monthly average precipitation rate anomaly (%) in 2020 to 2049 using baseline 1981-2010 and scenario RCP 8.5. (The four digit number/letters above the projections correspond to the relevant models used for the projections.)

5.4.2.3 Regional projections (12km resolution)

Figure 5.11 illustrates precipitation maps of anomalies for regional projections for the RCP8.5 scenario. These outputs are generated by 12 projections from the Met Office Hadley

Centre model at 12km scale resolution. In general, most models show the UK and Ireland will tend to experience drier conditions in June and July with variations corresponding to Ireland of between ±20% and up to 50% reduction in the monthly rainfall in Southern regions. Furthermore, the majority of the models imply Southern and Western regions of England will become drier in June and July while the variation of projections in Eastern parts is from 40% drier to 50% wetter condition. Finally, Scottish areas are projected to experience mainly ± 30% anomaly in precipitation.

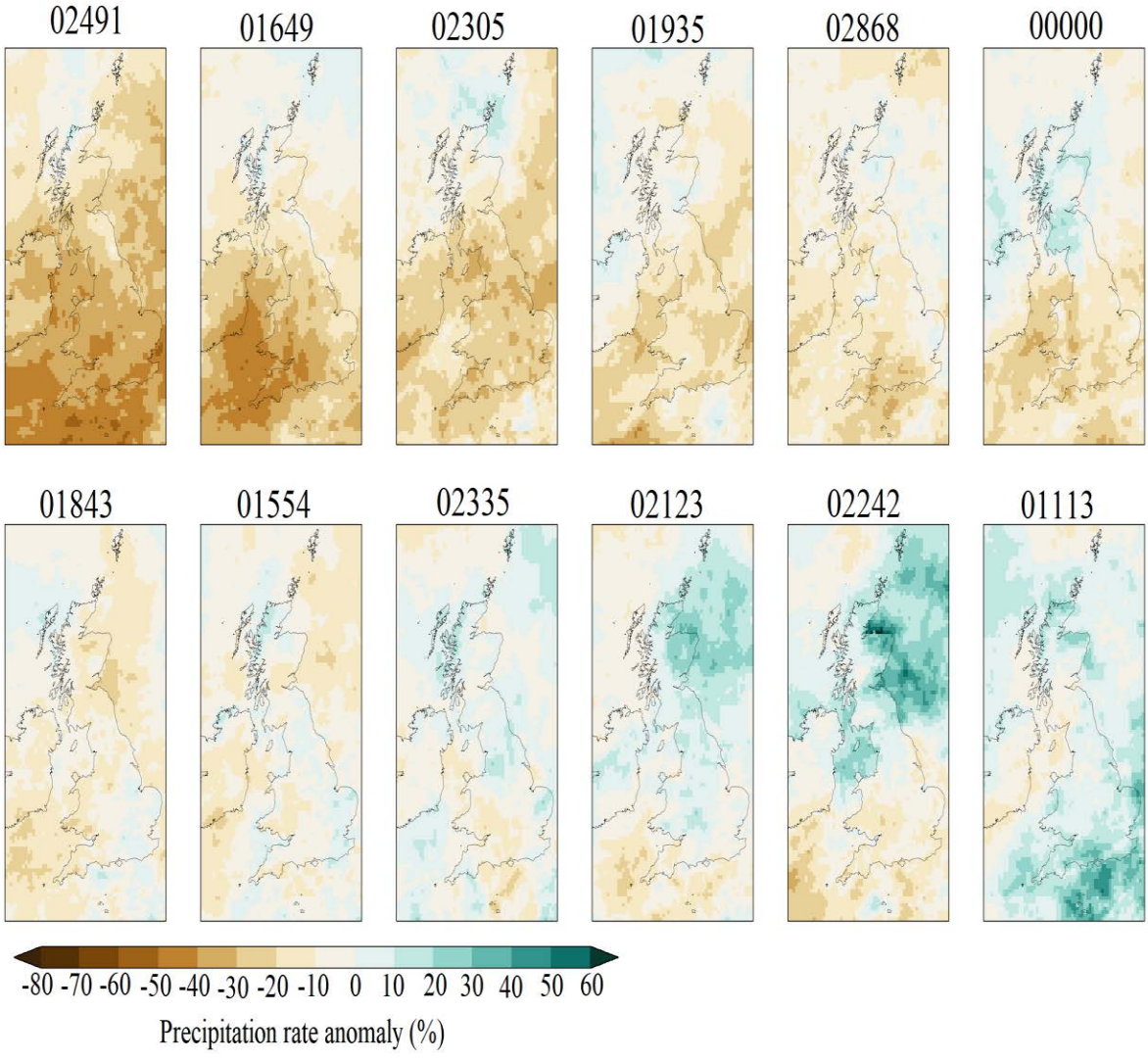

(a) Data corresponding to June.

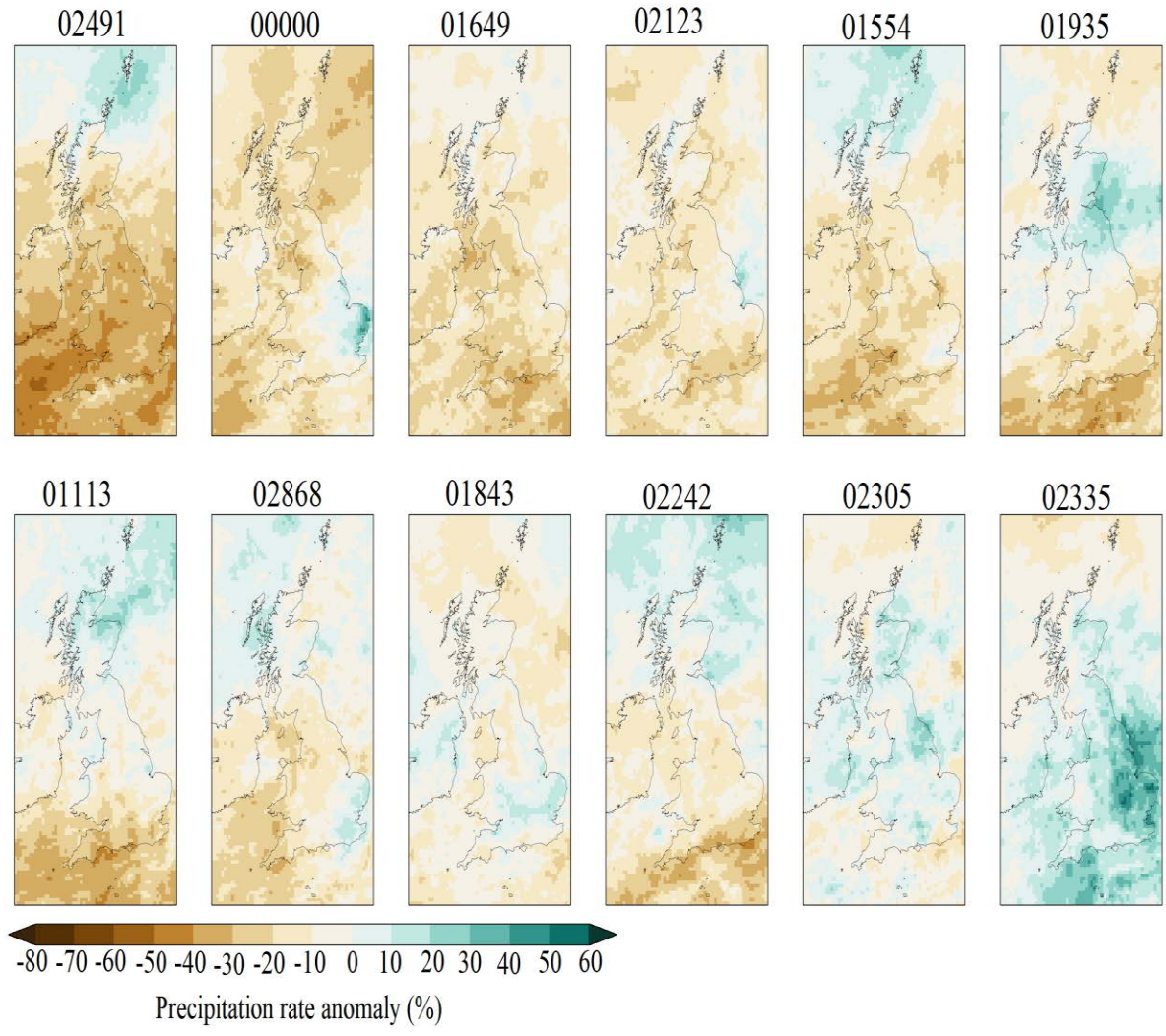

(b) Data corresponding to July.

Figure 5.11. Monthly average precipitation rate anomaly (%) in the period from 2020 to 2049 using baseline 1981-2010 and scenario RCP 8.5. (The five-digit number above each map indicate the PPE model used for the projection).

Figure 5.12 shows the monthly average wind speed anomaly at 10m above the ground in 2020 to 2049 for June and July. This figure illustrates the wind speed change in both England and Ireland is ±1m/s, i.e., a relatively small change. A slight increase is observed in Scotland, but again this projected increase is small and from a lodging perspective is unlikely to be significant. It is noted that these outputs correspond to a 10m height which is the standard

wind speed measurement and consequently the most appropriate height to use (Meteorological Office, 2019). Moreover, the data represents anomalies in June and July, the period associated with peak lodging season and therefore considered to be most important period to focus on. Finally, the output provided by UKCP18 is the mean wind speed rather than gust which agrees with what is used in the calibrated model.

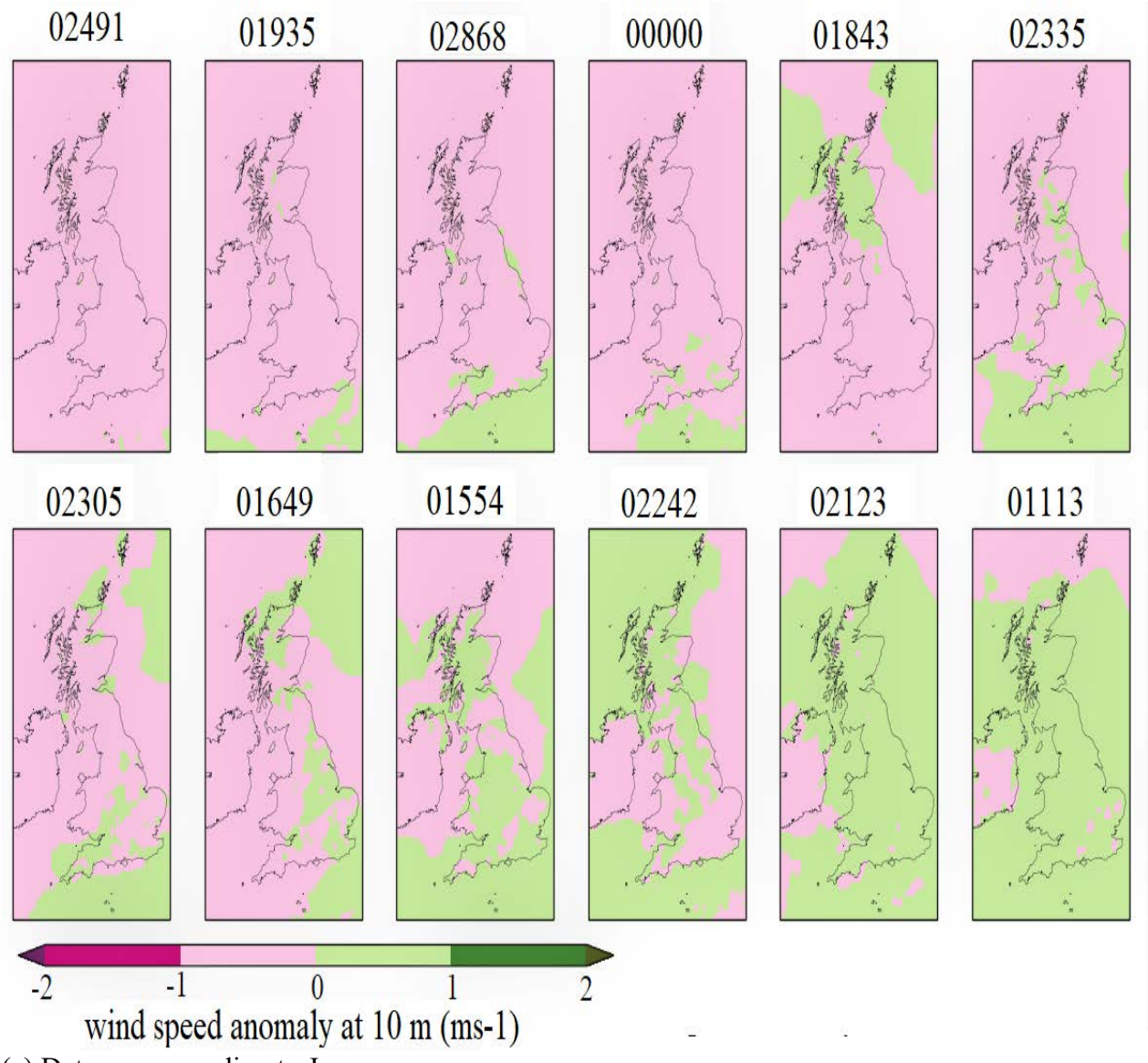

(a) Data corresponding to June.

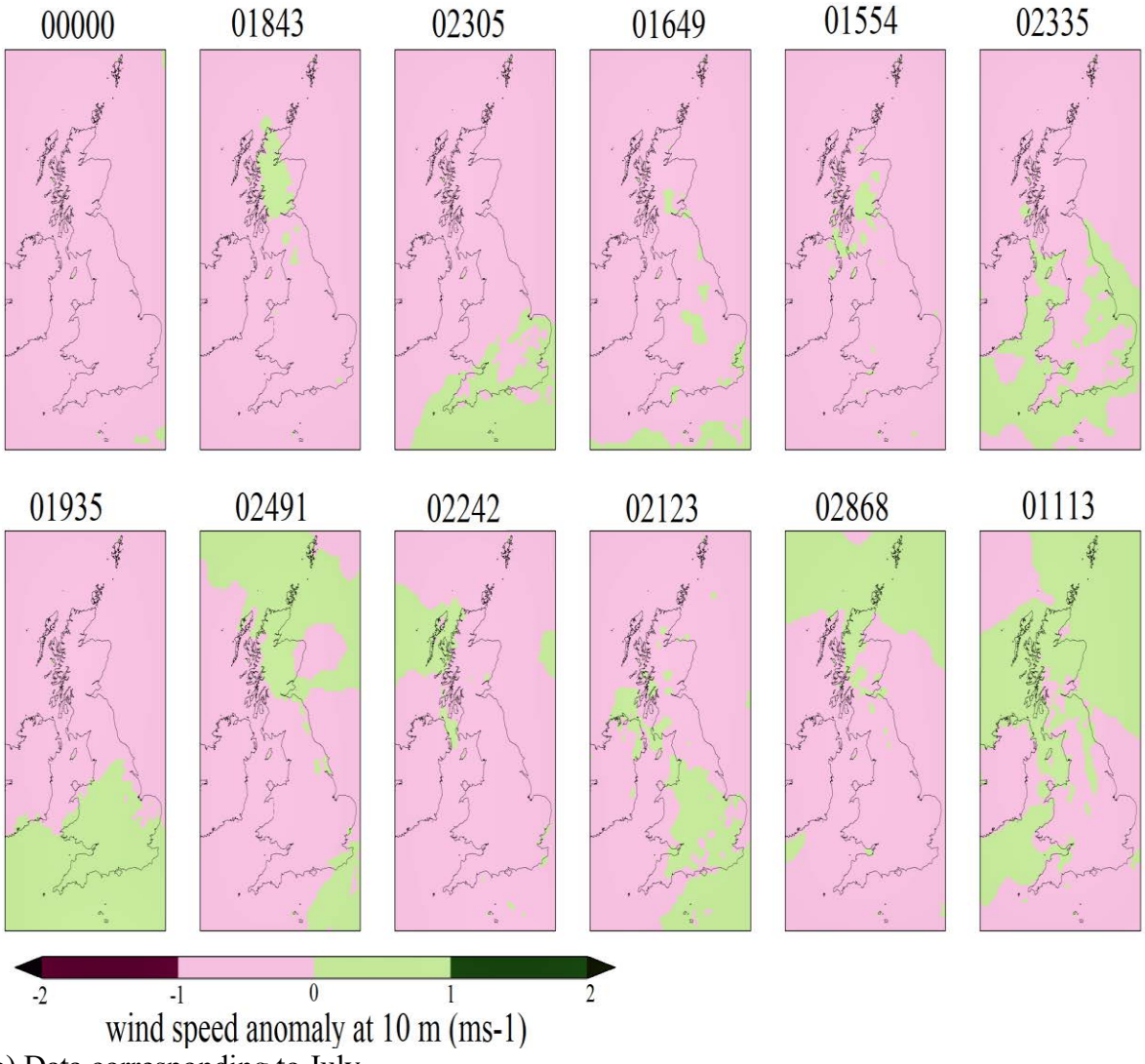

(b) Data corresponding to July.

Figure 5.12. Monthly average wind speed anomaly at 10 m in 2020 to 2049 using baseline 1981-2010 and scenario RCP 8.5.

5.4.2.4 Summary of projections

UKCP18 outputs produced by different models are summarized in Table 5.7, where results are presented for the 2020-2049 and the 2050-2079 periods. Probabilistic projections (Section 5.3) demonstrate anomaly ranges from the 10th percentile to the 90th percentile, while regional and global variations represent the largest anomaly projected. It is worth noting that the global and regional projection include a higher range of models and different PPEs and

include a wide range of plausible climate conditions, while the probabilistic projections are based on one climate change model. Consequently, the ranges of rainfall anomalies from the probabilistic projection is smaller than regional and global projections. For the same periods (2020-2049 and 2050-2079), wind projections show ±1 m/s change in all studied areas, while the rainfall anomalies show a wide range of projections from different models (see Table 5.7). The Republic of Ireland is mainly projected to face a reduction in average wind speed except in a few areas on the Northern and Southern coasts. Results for the UK appear to be spatially variable. Next sections will evaluate how these variations might impact the probability of lodging.

Table 5.7. Monthly average precipitation rate anomaly (%) using baseline 1981-2010 in June and July

Month	Region	Projection	2020-2049				2050-2079			
			RCP2.6	RCP4.5	RCP6	RCP8.5	RCP2.6	RCP4.5	RCP6	RCP8.5
June	South England	Probabilistic	-26% to +17%	-24% to +19%	-24% to +19%	-27% to +19%	-37% to +3%	-42% to 2%	-43% to +2%	-50% to +4%
		regional				-50% to +50%				-70% to +20%
		global				-40% to +40%				-70% to +20%
	West England	Probabilistic	-31% to +22%	-30% to +22%	-29% to +22%	-32% to +21%	-38% to +4%	-43% to +3%	-44% to +3%	-51% to +4%
		regional				-50% to +30%				-70% to +10%
		global				-40% to +40%				-70% to +20%
	Scotland	Probabilistic	-18% to +22%	-17% to +22%	-17% to +23%	-17% to +22%	-25% to +14%	-27% to +14%	-27% to +14%	-29% to +14%
		regional				-30% to +60%				-40% to +30%
		global				-40% to +40%				-50% to +30%
	Ireland	regional				-50% to +20%				-70% to 0%
		global				-40% to +30%				-60% to +20%
July	South England	Probabilistic	-43% to +16%	-44% to +16%	-44% to +17%	-47% to +14%	-44% to +12%	-49% to +9%	-49% to 10%	-56% to +7%
		regional				-40% to +50%				-60% to +10%
		global				-50% to +50%				-70% to +30%
	West England	Probabilistic	-27% to +19%	-29% to +19%	-28% to +19%	-31% to +18%	-37% to +9%	-41% to +8%	-40% to +8%	-47% to +5%
		regional				-40% to +20%				-60% to +10%
		global				-30% to +50%				-60% to +30%
	Scotland	Probabilistic	-28% to +22%	-28% to +22%	-28% to +22%	-30% to +21%	-38% to +15%	-40% to +17%	-40% to +17%	-47% to +19%
		regional				-40% to +30%				-50% to +10%
		global				-30% to +40%				-50% to +20%
	Ireland	regional				-50% to +30%				-60% to -10%
		global				-40% to +40%				-60% to +40%

5.5 Lodging probabilities in current and future conditions

5.5.1. Calculating the lodging probability

Lodging occurs when the wind speed exceeds the stem or root resistance for any given plant. It is known that rainfall can influence the soil strength which in turn can affect the plant's anchorage (root) resistance (Baker et al., 2014; Berry et al., 2004). The probability of lodging can be identified by integrating PDF functions of wind and rainfall (or using the integrated forms, CDFs) in conditions when lodging is likely to happen (equation 5-3) as shown in the Figure 2.2 for a sample plant.

$$P_{Lodging=} \int_{U_s}^{\infty} P(\overline{U}) d\overline{U} \int_{i(\overline{U})}^{\infty} P(i) di \quad (5\text{-}3)$$

Figure 2.2 demonstrates graphically the probabilistic framework used by the lodging model, where the vertical axis shows the daily rainfall (i) and the horizontal axis is the hourly mean wind speed ($\overline{U}$). As mentioned in Chapter 2, in very low speed wind conditions (lower than the saturation velocity ($\overline{U}_s$)), lodging will not typically occur. Nevertheless, in higher wind speeds, the lodging occurrence depends on the wind and rainfall conditions, and root/stem lodging or both are likely to occur (Baker et al., 2014).

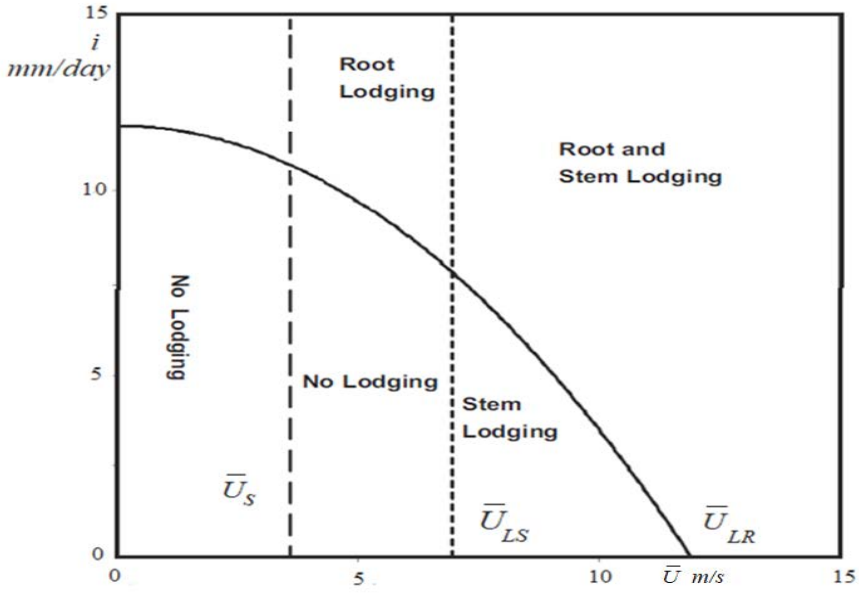

Figure 2.2. Lodging conditions in different daily rainfall and hourly mean wind speed conditions for a sample oat plant.

The following steps are typically undertaken to investigate the probability of lodging using the above approach:

1. Representative CDF functions for wind and rainfall are obtained (as discussed in Section 5.4.1).
2. The relevant plant properties and dynamic/aerodynamic characteristics ($a, t, X, AC_F, l, n, \theta, S, L, d, f_n, X, \sigma$) are obtained and used in the lodging model (see Chapter 3).
3. The model uses the input data to reproduce a plot similar to Figure 2.2 for each plant sample, by calculating the lodging/no lodging curve (equation 2-16), the saturation velocity (equation 2-17) and the lodging velocities (equation 3-1 and 3.2).
4. The wind/rainfall CDFs and the probability of lodging are calculated in boundaries where lodging is likely to happen.

$$i = (1 - \frac{\overline{U}^2}{\overline{U}_{LR}^2}) i_0 \quad (2\text{-}16)$$

$$\overline{U}_s = \overline{U}_{LR}(1 - \frac{i_s}{i_0})^{0.5} \quad (2\text{-}17)$$

$$\overline{U}_{Ls} = (\frac{\omega_n^2\left(\frac{X}{g}\right) S_s}{\left(1+\omega_n^2\left(\frac{X}{g}\right)\right)(0.5\rho A C_F X)(\cos\left(\alpha\frac{x}{l}\right) - cot\alpha \sin\left(\alpha\frac{x}{l}\right))(1+ I\left(4g_{MB}^2 + g_{MR}^2(\frac{\pi}{4\theta})\right)^{0.5}})^{0.5} \quad (3\text{-}1)$$

$$\overline{U}_{LR} = (\frac{R_S}{\frac{((1+\omega_n^2\left(\frac{X}{g}\right))}{\omega_n^2(\frac{X}{g})}(0.5\rho A C_F X)(1+2Ig_{MB})})^{0.5} \quad (3\text{-}2)$$

5.5.2. The probability of lodging in current climate conditions

To investigate the range of variation in the lodging probability in autumn sown oats in the current conditions, a database of 1000 'synthetic' plants was generated based on the mean values and standard deviations of various plant parameters including panicle area, stem radius, stem wall thickness, centre of gravity, root diameter, anchorage depth of the rooting system and the number of stems per plant provided in Table 5.8 (in keeping with the approach of Berry et al. 2003), i.e., for each synthetic sample, the plant parameters were randomly generated assuming a corresponding normal distribution (see Berry et al., 2003). Experience has shown that 1000 samples are sufficient to ensure that the results are statistically independent (Berry et al. 2003) and the normal distribution assumption is valid for such agronomic measurements[3] (Berry et al., 2003). In order to provide the input to the database, plant data (i.e., mean and standard deviations of above parameters) were obtained as part of the experiments undertaken in 2016-2017 at Knockbeg, County Laois, the Republic

[3] This assumption was also checked for the current work and found to be valid. However, the results are not reproduced in this thesis given that this is a well-documented approach.

of Ireland (52.86 °N, 6.94 °E, 54 MSL). As illustrated in Chapter 3, in addition to the agronomic parameters, the lodging model also relies on soil and dynamic/aerodynamic parameters provided in Table 5.8. The aerodynamic parameters were evaluated using the methods described in Section 4.3, while the soil shear strength was measured in the studied site.

Table 5.8. Agronomic, aerodynamic and soil parameters (Letter abbreviation for parameters used can be found in Section 2.2).

Agronomic parameters	mean	S_d
a (cm)	0.32	0.08
t (cm)	0.09	0.03
l (cm)	149.33	16.08
X (cm)	70.19	8.24
d (cm)	4.97	1.87
L (cm)	7.28	3.14
σ (MPa)	40.30	17.23
Aerodynamic/soil parameters		
f_n(Hz)	1.1	0.01
S (KPa)	35	5.1
AC_f	0.021	0.003
θ	0.1	0.04

In addition to the range of variation in the probability of lodging for different crops at a farm scale, the range of variations under different husbandry techniques can be investigated. As fully discussed in Chapter 3, the plants under consideration were raised from two varieties: an oat variety susceptible to lodging (Barra) and an oat variety with moderate resistance to

lodging (Husky). Both varieties were grown under different combinations of agronomic treatments designed to create a range of plants which varying lodging characteristics. Thus, four different synthetic databases were generated corresponding to variety/seed rate combinations. The mean and standard deviation values used to generate the database are presented in Table 5.9 (The soil and dynamic/aerodynamic factors can be found in Table 5.8). It is noted that Table 5.10 is provided to show the ranges of variation in the probability of lodging. Accordingly, the probability of lodging for each sample was calculated and the cumulative density functions of lodging probability values was calculated. The 10^{th}, 50^{th} and 90^{th} percentile can be easily derived from the CDF, where percentile means the value below which a percentage of data falls. For example, in the first group (susceptible and 200 seeds/m^2), 50% of calculated probabilities are less than 0.21. Additionally, the results show the probability of lodging at farm scale (the first database, generated based on Table 5.8) varies from 3% to 65% from the 10^{th} to the 90^{th} percentiles. These results show a relatively large spread of lodging probability in different husbandry techniques and at a farm scale can be observed and illustrates that different husbandry treatments/varieties can result in considerable differences in failure probabilities – this is an important result which will be discussed in the following sections.

Table 5.9. Parameters used to generate the agronomic databases for different husbandry techniques.

Treatments / Parameters	Barra 200		Barra 500		Husky 500		Husky 200	
	mean	S_d	mean	S_d	mean	S_d	mean	S_d
a (cm)	0.35	0.04	0.28	0.05	0.31	0.04	0.36	0.05
t (cm)	0.1	0.04	0.07	0.01	0.09	0.02	0.01	0.02
l (cm)	152.1	14.8	145.4	12.83	144.5	19.8	150.5	19.01
X (cm)	71.0	7.1	67.55	6.9	69.9	10.41	72.11	8.5
d (cm)	6.31	0.16	5.25	0.65	6.22	0.10	6.30	0.12
L (cm)	9.45	0.41	10.03	0.71	8.44	0.14	8.80	0.56

Table 5.10. Lodging probability variation in different treatments and seed rates

Variety	Seed Rate	lodging probability range (10^{th} - 90^{th} percentile)	50^{th} percentile probability
Susceptible	200 seeds/m^2	0.06-0.60	0.21
Susceptible	500 seeds/m^2	0.11-0.62	0.32
Moderate resistance	200 seeds/m^2	0.03-0.46	0.20
Moderate resistance	500 seeds/m^2	0.04-0.60	0.26

5.5.3. Lodging probability in future climate conditions

Based on the data of Table 5.7, Table 5.11 illustrates the possible variation in wind speed and rainfall in the future generated by most of the models. These ranges of variation will used in the analysis of probability that follows.

Table 5. 11. Monthly average wind and rainfall rate anomaly percentage generated by most of the models using baseline 1981-2010 in June and July.

Region	Most likely monthly anomaly to happen			
	2020-2049		2050-2079	
	rain	wind	rain	wind
South England	-30% to 10%	±1m/s	-40% to 0%	-1m/s to 0
West England	-30% to 10%	±1m/s	-40% to 0%	±1m/s
Ireland	±20%	-1m/s to 0 m/s	-40% to 0%	-1m/s to 0 m/s
Scotland	±20%	±1m/s	-40% to10%	±1m/s

Using the range of values of rainfall and wind speed calculated above, revised CDFs for these variables can be determined, corresponding to likely future climate conditions. These were calculated by applying the projected rainfall and wind anomalies to these CDFs. Typical values are shown in Figure 5.13 below. It should be noted that CDFs shown in this figure can be plotted as histograms similar to Figures 5.4 and 5.6. However, in Figure 5.13 the discrete values are presented as a curve to provide a better representation of changes in the CDFs.

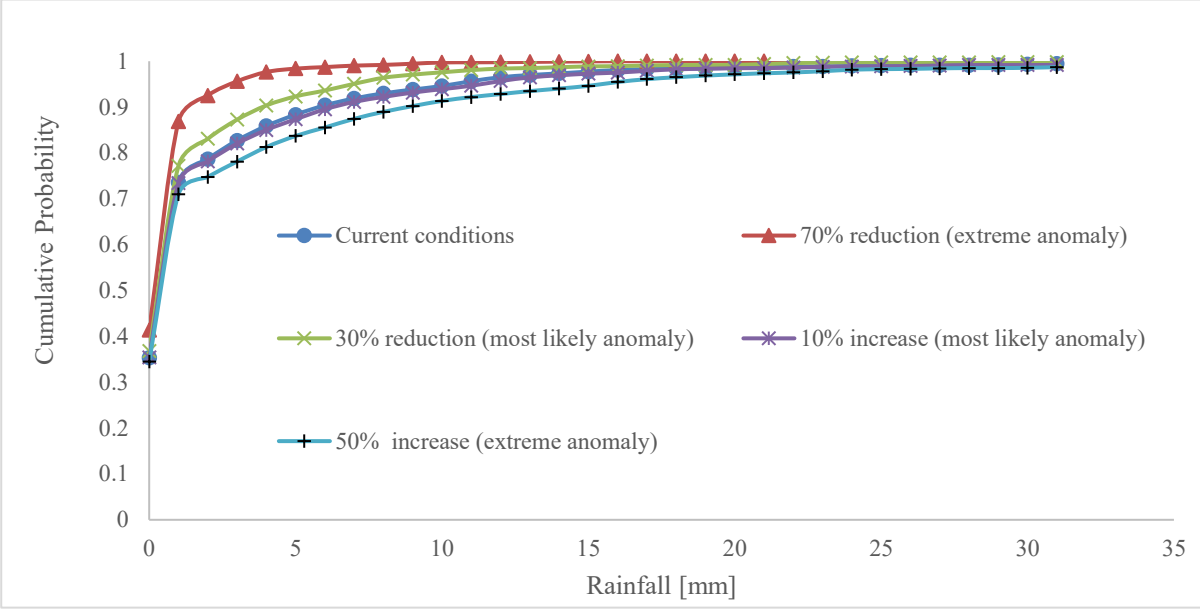

(a) Rainfall CDFs

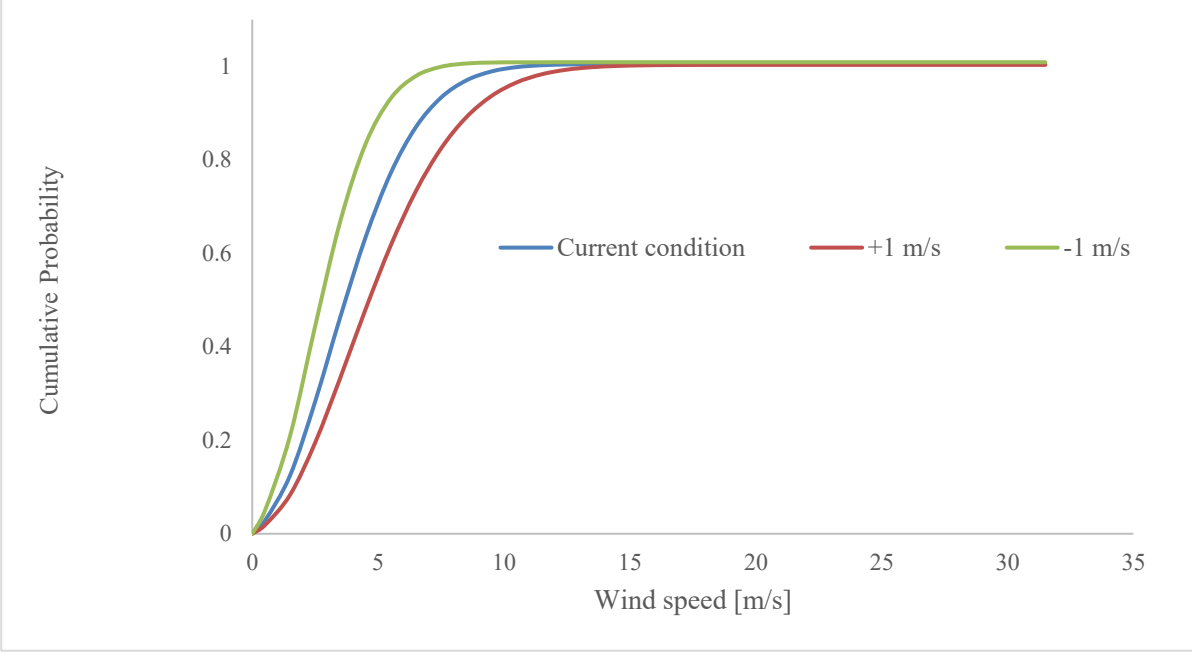

(b) wind CDFs

Figure 5.13. 24 hours rainfall and hourly wind CDFs in the current and future climate conditions for Haslemere station (South England).

Calculation of lodging probability for oats was then carried out using the lodging model described in Section 2.2. Using the new wind and rainfall CDFs and mean agronomic values (Table 5.8), the failure probability in each anomaly range is obtained. Figure 5.14a and 5.14b show the lodging probability variation vs wind changes (Figure 5.14a) and rainfall changes (Figure 5.14b) for the Haslemere station (no. 20 in Table 5.1), which is similar to what is found for Ireland, England, and Scotland. The figures shows if only one of the meteorological parameters i.e., wind or rain, changes (the red line in both figures) the ranges of variation due to wind variation is larger. Additionally, Figure 5.14a demonstrates if the average wind speed is reduced by 1m/s, the range of lodging probability would be less than 10% in any rainfall condition, while, if the average wind speed does not change, the probability of lodging will vary from ~15% to ~20% (irrespective of any change in rainfall). In the case of 1m/s increase in the average wind speed, the probability of lodging would be 25-30% for drier conditions and higher than 30% for wetter conditions. Figure 5.14b, shows the range of variation due to rainfall anomalies is much less than as the result of wind variation. For example, if the wind conditions do not change (the red line), the driest expected anomaly (-0.7, i.e., 70% reduction in rainfall) to wettest condition (+0.5, i.e., 50% increase in the rainfall) the probability of lodging varies between 14-18%. Consequently, the lodging probability is more affected by changes in the wind speed compared to the rainfall and if the wind conditions do not change considerably in the future, then the probability of lodging is unlikely to vary significantly from present conditions.

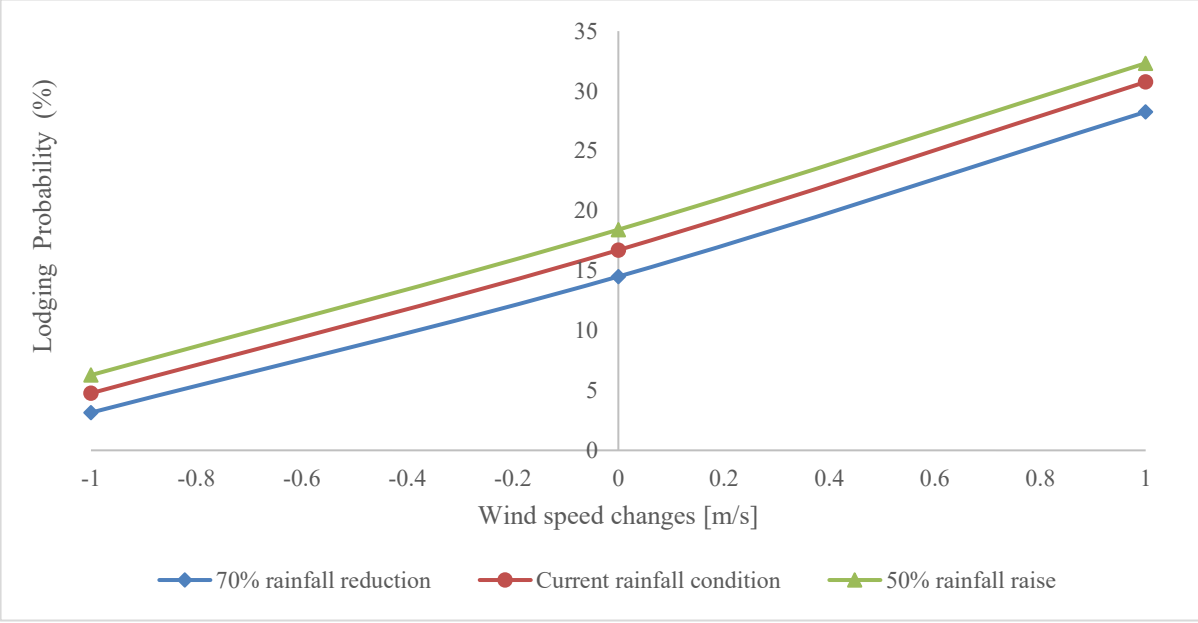

(a)

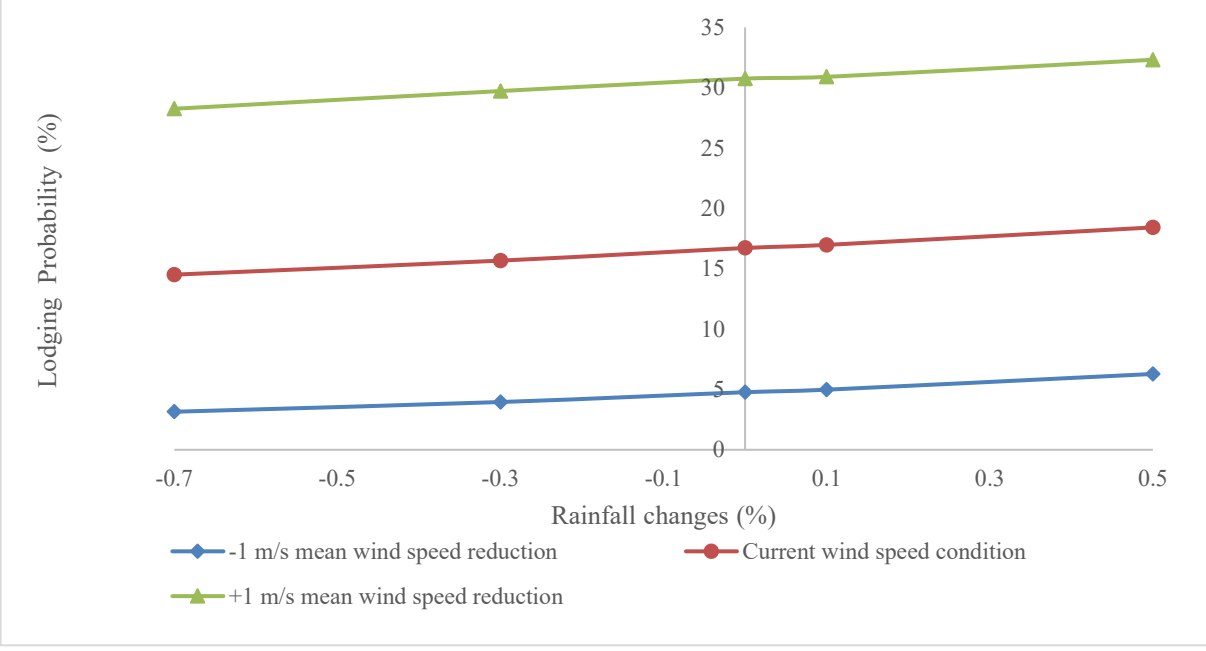

(b)

Figure 5.14. Lodging probability variation based on (a) wind and (b) rainfall anomalies

A flowchart of the comparison made between the range of lodging probability at a farm-scale and the different husbandry techniques (Section 5.5.2) and the range of plausible variation in the lodging probability due to climate change (Section 5.5.3) is presented in Figure 5.15. The

results presented in the aforementioned sections show both variations are in the same range and the effect of climate change on the probability of lodging is not significant.

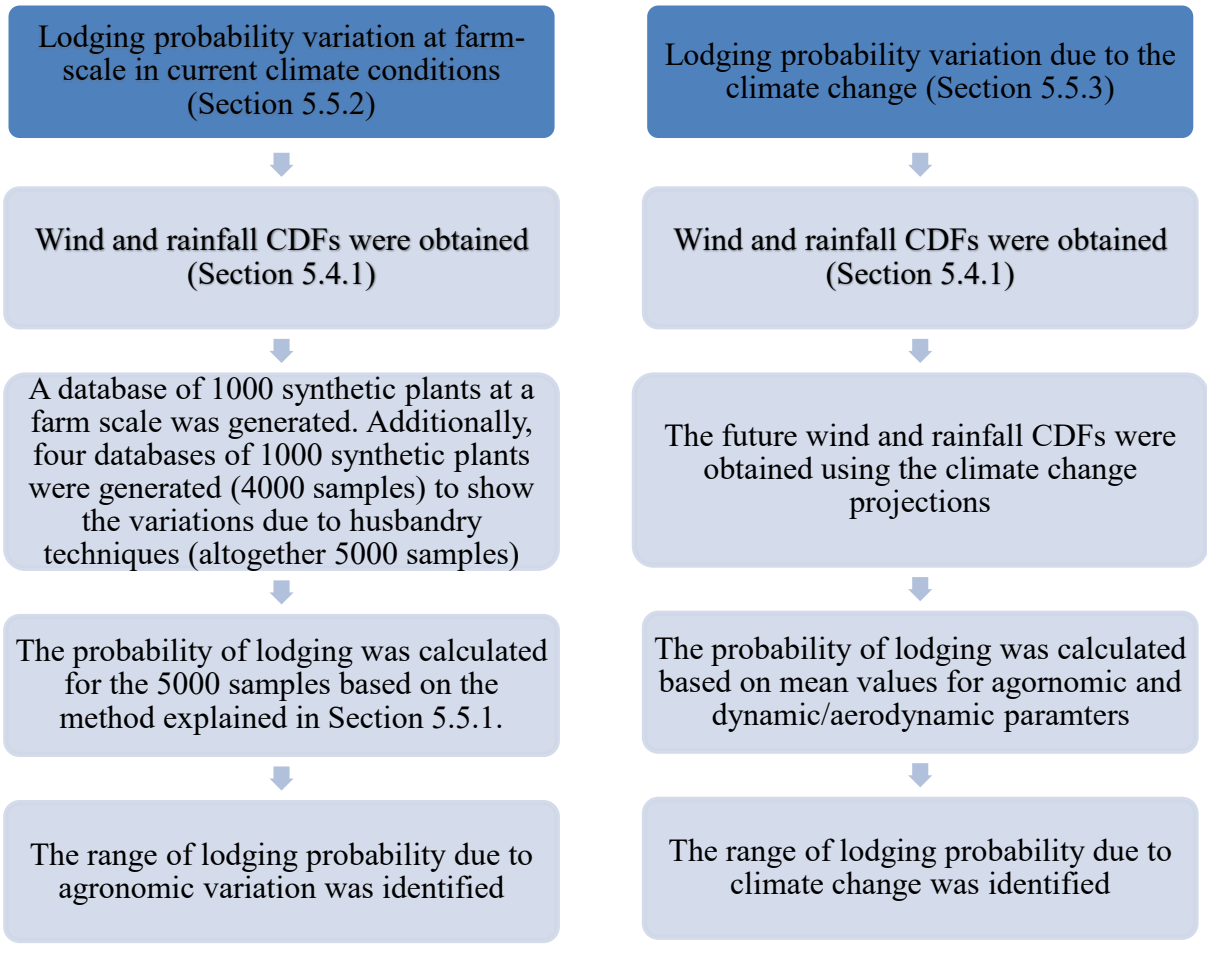

Figure 5.15. A comparison between the lodging probability variations due to agronomic variations versus the climate change variations

5.6 Conclusions

This chapter has examined the potential effect of climate change on lodging in oats. Based on the work undertaken in this chapter the following conclusions can be made:

1. It was found that the summation of two exponential functions can effectively represent the rainfall CDF. The accuracy of the representative functions was tested via the mean squared error method and quantile-quantile plots and it was shown that the representative functions are a reasonable fit to the historical data, although it is acknowledged that the variation is beyond what would typically be accepted in wind engineering terms. Similarly, it was found that the Weibull distribution can be used to represent the wind data which is consistent with the literature.
2. The projections of future rainfall conditions are unclear, with some climate models outputs showing that the rainfall will decrease in June and increase in July (and vice-versa). Nevertheless, most of the climate models show drier conditions will be experienced in the future during the critical lodging period, especially in England.
3. The climate model projections for wind speed for the peak lodging period (June and July) vary in different models. Nevertheless, the wind speed anomaly ranges are small ($\sim$1 m/s) and will not change the probability of lodging dramatically (the changes in lodging probabilities will remain 10-20% which is the range of variations that can be seen at a farm-scale).
4. It was shown that lodging is more affected by changes in wind speed rather than changes in rainfall (over the scale considered). Consequently, it is tempting to conclude that lodging will reduce in the future (if other things remain constant) in certain regions where most of the models show a reduction in the wind speed; however, taking the uncertainty associated with the wind speed projections into the account, this conclusion cannot be made with any degree of certainty.
5. The effect of climate change on the probability of lodging is not significant as the variations in the probability of lodging remain in the range which can be seen

through the impact of different husbandry. This is an interesting conclusion and is important for the agriculture sector.

6. Lodging model application

In what follows, certain sections are adapted from the following paper for which the author can claim considerable intellectual input.

- Mohammadi, M., Finnan, J., Sterling, M., Baker, C. (2020b) A calibrated oat lodging model compared with agronomic measurements, Field Crops Research, Volume 255, 107784.

6.1. Introduction

This chapter outlines the model and its applicability to assess lodging. The model is used to rank lodging in oats subject to various husbandry techniques and the results are compared to field observations (Section 6.2). Additionally, the model is used to predict the timing of lodging during the peak lodging season and its output is compared with the observed lodging events (Section 6.2). Section 6.3 contains a parametric analysis while Section 6.4 describes how different crop husbandry approaches can affect the lodging susceptibility of oats. Section 6.5 discusses the structural requirements to avoid lodging and Section 6.6 compares the modified model with the lodging model proposed by Baker et al. (2014). Finally Section 6.7 presents the conclusions which can be made from this chapter.

6.2. A comparison between model predictions with field observations

6.2.1. Model ranking

Experience has shown that different husbandry techniques can lead to improvements in lodging probability (Berry et al., 2002). In addition, it is also known that the crop variety (defined in Chapter 1) also influences the plant's susceptibility to lodging (Griffin, 1998). Work undertaken by (Berry et al., 1998; Griffin, 1998) has led to the concept of a lodging rank, where the impact of husbandry techniques, as well as the crop variety, are expressed in a simple system which indicates the plant's expected propensity to lodge – the lower the rank the more likely the plant is to lodge. Based on the method used by Berry (1998), Baker et al. (1998), and Berry et al. (2000), the oat plants outlined in Chapter 3 were grown under different husbandry techniques which were monitored and assessed for lodging susceptibility during the peak lodging season.

Having calibrated the lodging model for oats, it is possible to calculate the failure wind speed corresponding to the impact of different husbandry techniques and thus to obtain a model ranking. Accordingly, the model used the agronomic measurements for each husbandry approach to determine the failure stem/root velocity and to calculate the lodging probability.

As described in Section 3.3.1, different varieties of oats were grown subject to different husbandry techniques (seed rate, PGR application, Nitrogen rate, and Nitrogen timing; in total 32 different cases were grown). The probability of lodging for each technique was calculated as described in Section 5.5.1, while for the plant parameters, averaged values over each husbandry technique were used. Later these probabilities were arranged from the highest to lowest values, generating the model ranking, where the lower the rank, the higher probability of lodging.

The experimental ranking was evaluated using the method suggested by Baker et al. (1998) and (Berry et al. 2003) as follows:

For each husbandry technique adopted, the observed percentage of lodged area versus time was plotted, and the area under the curve was calculated, indicating accumulated lodged area. Accordingly, all husbandry applications were sorted and ranked based on highest (the most susceptible) to lowest (most resistant) lodged areas.

Figure 6.1 illustrates the model ranking against the experimental ranking. In order to evaluate how well the real lodging observations (experimental rankings) can be represented by the model ranking, the discrete points are compared versus Y=X line (which indicates perfect agreement) using coefficient of determination (R^2) which is calculated from the following equations:

$$R^2 = 1 - \frac{SSE}{SST} \tag{4-1}$$

Where SSE is a measure of the total deviation between the experimental and model rankings, and *SST* is the summation of squares about the mean. These parameters can be expressed as follows:

$$SSE = (y_1 - Y_1)^2 + (y_2 - Y_2)^2 + \cdots + (y_{32} - Y_{32})^2 \tag{6-1}$$

$$SST = (y_1 - \bar{y})^2 + (y_2 - \bar{y})^2 + \cdots + (y_{32} - \bar{y})^2 \tag{6-2}$$

Where y_i and X_i denotes the model and experimental rankings respectively (i = 1 to 32), and $\bar{y}$ is the mean value of y.

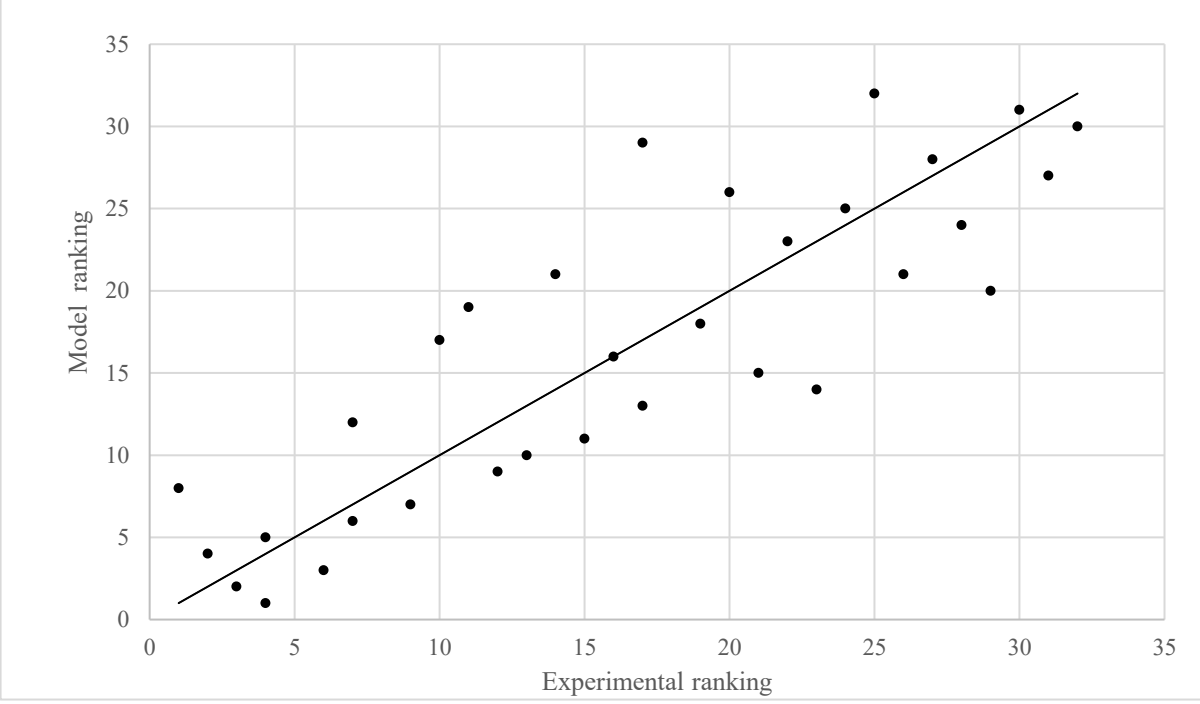

Figure 6.1. Experimental versus model predicted ranking of lodging susceptibility of 32 management of oat crops (rank 1 is the most susceptible).

It can be observed that there is, in general, a reasonable agreement (R^2 = 0.71) between the two processes. Whilst 0.71 may in other disciplines be considered a poor agreement, within the context of the current work this value is considered to be reasonable and consistent with that which has traditionally been obtained (Berry et al., 2003).

In order to calculate the probability of lodging from the model, it was assumed that the number of panicles (N) which interlock together through the season is, on average, five and that the mean soil shear strength is 20kPa. The soil shear strength was highly dependent on

the soil moisture and consequently the amount of rainfall. Whilst both of these assumptions are subjective, they are on average reasonable and consistent with the experimental data. In order to examine the impact of these assumptions, the soil strength was varied over the range of 10-30kPa (which was consistent with that observed during file conditions) and the number of panicles was also varied from 4 to 5. These changes resulted in R^2 varying between 0.67 to 0.72, which is considered not to be significant given the norms for the research and variations that occur in natural biological systems.

It is worth noting that despite all the potential variations associated with the input data into the model (for example average plant values were inserted into the model while plants are growing and interlocking during the season) the model successfully ranked the susceptibility of the husbandry techniques and distinguished the highly susceptible techniques from more resistant ones. Additionally, comparing these results with the previous lodging models calibrated for other crops shows the same or better levels of agreement. For example, the R^2 for winter wheat (Berry et al., 2003) and spring wheat (Pinera-Chavez, 2016) was 0.75 and 0.35 respectively were considered reasonable at the time.

6.2.1. Model timing

The generalised lodging model can also be used to predict the timing of lodging during the peak lodging season (i.e., through the known variations in model input data with respect to time). To compare the model outputs with observed lodging data (described in Section 3.1), all husbandry techniques were classified into four groups: highest observed lodging, moderate-high observed lodging, moderate-low observed lodging, and low observed lodging. This classification was based on the recorded accumulated lodged area through the season. Table 6.1 indicates the husbandry techniques and their agronomic values for each group. All

husbandry techniques are abbreviated in the Table, where H/B are the plant varieties (Husky/ Barra), 200/500 are the low/high seed rate (200/500 seeds per m^2), Y/N refer to PGR application (Yes/No), 90/180 indicate Nitrogen rate (90/180Kg/ha), and E/L refer to early or late Nitrogen timing.

In keeping with the approach of Berry et al. (2003), a database of 1000 plants was randomly generated based on mean values and standard deviations of agronomic parameters, assuming the parameter values are normally distributed. Experience has shown that 1000 samples are sufficient to ensure that the results are statistically independent (Berry et al. 2003) and the normal distribution assumption is valid for such agronomic measurements[4] (Berry et al., 2003). Additionally, plant parameter variations through the season were taken into the account and the lodging velocity for each plant was calculated. Next, weather data for the site was extracted from Oak Park weather station (Met Éireann, 2019) located at approx. 1.5 Km from the experimental site outlined in Section 3.3.2 and at each lodging event the maximum mean hourly wind speeds were extracted. It is worth noting that in each lodging event, the meteorological data was checked for 24 hours before the lodging observation and the highest mean hourly wind speed was considered as the condition when lodging has happened. Comparing this wind speed with stem/root lodging velocities would suggest if the plant would fail/resist in the lodging event. Later, the number of failed plants in the database was counted and expressed as a percentage of the total plants and can be compared with real observations.

[4] This assumption was also checked for the current work and found to be valid. However, the results are not reproduced in this thesis given that this is a well-documented approach.

Table 6.1. Agronomic husbandry techniques and parameters as measured in 2017 classified based on observed lodging.

	highest observed lodging		moderate-high observed lodging		moderate-low observed lodging		low observed lodging	
husbandry techniques	B-500-N-180-E		H-500-N-180-L		B-200-Y-180-L		B-500-Y-90-E	
	B-500-N-180-L		B-500-N-90-L		H-200-Y-180-E		H-200-N-90-L	
	B-200-N-180-E		B-500-N-90-E		B-200-Y-180-E		H-200-Y-90-E	
	B-500-Y-180-L		H-200-N-180-L		H-200-Y-180-L		B-200-Y-90-E	
	B-200-N-180-L		H-500-Y-180-E		H-500-N-90-L		B-200-Y-90-L	
	B-500-Y-180-E		B-200-N-90-E		H-200-N-90-E		H-500-Y-90-E	
	H-500-N-180-E		H-500-N-90-E		B-200-N-90-L		H-200-Y-90-L	
	H-200-N-180-E		H-500-Y-180-L		B-500-Y-90-L		H-500-Y-90-L	
Agronomic parameters	mean	S_d	mean	S_d	mean	S_d	mean	S_d
a (cm)	0.33	0.05	0.32	0.06	0.34	0.06	0.33	0.06
t (cm)	0.09	0.04	0.09	0.02	0.09	0.03	0.09	0.02
l (cm)	157.64	13.76	151.72	17.33	149.77	12.64	138.06	13.82
X (cm)	76.06	8.18	70.90	7.44	71.50	5.81	64.43	7.85
d (cm)	4.78	0.17	5.17	0.16	4.85	0.14	5.05	0.25

Figure 6.2 shows a comparison of the lodging percentage by the model and those observed in reality. As the panicles emerged at the beginning of June, panicles were not interlocked in the

first two lodging events (1st and 7th June) and the interlocking assumption (*N*=4, where *N* is the number of panicles which interlock together) was applied from the third lodging event (21th June). It is worth noting that, the soil shear strength through the season was estimated based on the daily rainfall and a number of measurements in June and July as described in Section 3.3.6. Due to the low amount of lodging in the two first lodging events and dry conditions in the third event, the value of soil shear strength can affect only the last two lodging events and the second event is high observed lodging group. Although, reducing the soil shear strength in a lodging event in a plausible range can change the overall lodged plants through the season by 3-7%. Similarly, changing the interlocked panicles from N=4 to 5, can increase the lodged plants in a single day by 16%, but is not influential on the conclusions made below. This is consistent with what is suggested by the model ranking and demonstrates the model can best represent lodging assessments assuming four/five panicles create a canopy during tangling period.

Figure 6.2 shows at the first two lodging events when panicles have just emerged and interact as single shoots with wind, the percentage of lodged area is low, and the model predictions are reasonably consistent with reality. The figure also indicates the total amount of lodging is reasonably well predicted in three higher observed lodging classes (the highest, moderate high and moderate low observed lodging groups) but over predicted in lowest observed lodging group (Low observed lodging group). Additionally, there are some under/over predictions in the middle of the season (third and fourth events). This is the time, when panicles interlock, which is a gradual process and does not happen for all the plants at the same time. Moreover, the number of panicles interlock is very variable in the middle of the season. Nevertheless, from the figure, it can be seen that despite these over/under predictions at the middle of the season, the accumulated amount of lodging at the end of the season is well predicted in three more susceptible groups to lodging (the highest, moderate high and

moderate low observed lodging groups). This finding is important to growers as these are plant groups that are most susceptible to lodging and require more attention from the grower's perspective.

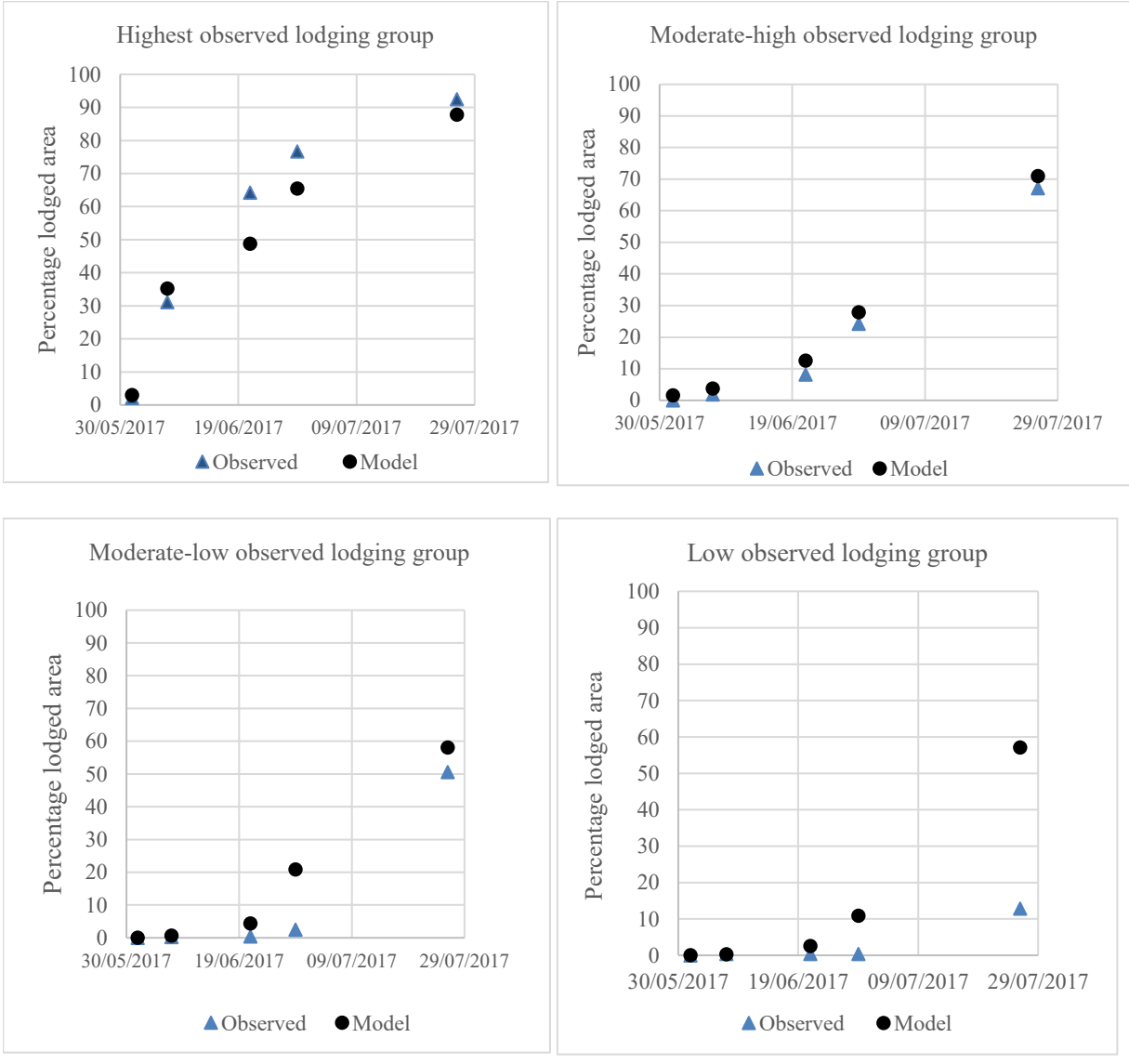

Figure 6.2. The percentage lodged area in five lodging events as observed experimentally and predicted by the model highest observed lodging, moderate-high observed lodging, moderate-low observed lodging and low observed lodging

6.3. Parametric analysis

Noting all of the various parameters used in the generalised model (and outlined in Chapter 2), it is worthwhile to examine their relative importance. Thus, Figures 6.3, 6.4, and 6.5 show the results of a parametric analysis that was undertaken to investigate the relative impact of different parameters on the failure wind speed. This method was first introduced in Berry et al. (2000) and was later used by Berry et al. (2003 and 2006) and Sposaro et al. (2010) to evaluate the most influential parameters in crop lodging. Accordingly, each parameter was varied from the lowest to the highest values which were observed during the measurement trials and the percentage of change in the stem/root lodging speed was compared with the mean stem/root failure velocity. Additionally, as agronomic parameters were measured in mid-June, the plant parameter variations during the season were also taken into the account to cover all plausible value ranges. Moreover, the panicle drag area was studied for the variations over six interlocked canopies (mean value of AC_f=0.001-0.023m^2), while, the parameter for a single panicle might change from 0.001-0.004m^2.

From Figure 6.3 it is evident that the plant drag area is the most influential parameter for both stem and root lodging, where the lodging velocity can reduce by three times as panicles become interlocked ($\overline{U}_{Ls}$ =4.5-16.3m/s, $\overline{U}_{LR}$ =5-18.1m/s). The lowest range of this parameter is associated with the early peak lodging season when plants have newly emerged panicles. At this time in the growing season, the drag area is low and plants oscillate independently like single shoots. Later during the growing season, as panicles grow and become tangled (interlocked), a higher drag force is exerted on plants, as a consequence, the plant becomes more susceptible to lodging. Notwithstanding this increase in the panicle drag area, the model shows that for the plausible variations associated with a single plant, the stem/root lodging velocity may vary by up to 5-6m/s: $\overline{U}_{Ls}$=11-16.3m/s and $\overline{U}_{LR}$=12.2-18.1m/s. Other critical parameters in stem lodging are those which contribute to stem strength

(equation 2-9) including the number of stems per plant, stem yield stress, radius, and wall thickness, respectively ordered by importance.

$$S_s = (\frac{\sigma\pi a^3}{4})(1 - \left(\frac{(a-t)}{a}\right)^4)n \quad (2\text{-}9)$$

where σ is the stem yield stress, a is the stem radius, t is the stem wall thickness and n is the number of stems per plant. Interestingly, the values of stem lodging velocity reduce significantly (~50%) when one of the three earlier parameters changes from the lowest to the highest range. Nevertheless, the latter parameter (stem wall thickness) has a relatively smaller impact (~24 %) on the lodging velocity.

Figure 6.5 shows the root diameter (d) and root depth (L) which have a direct effect on anchorage resistance are the second and third most important parameters in root lodging respectively, and, their effect on the percentage change in root lodging velocity (~67% and 63%) are lower than the change influenced by the lowest drag area (~166%). Finally, stem height, centre of gravity, natural frequency, and damping ratio have comparatively lower effects on stem/root lodging wind speed (Figures 6.4 and 6.5).

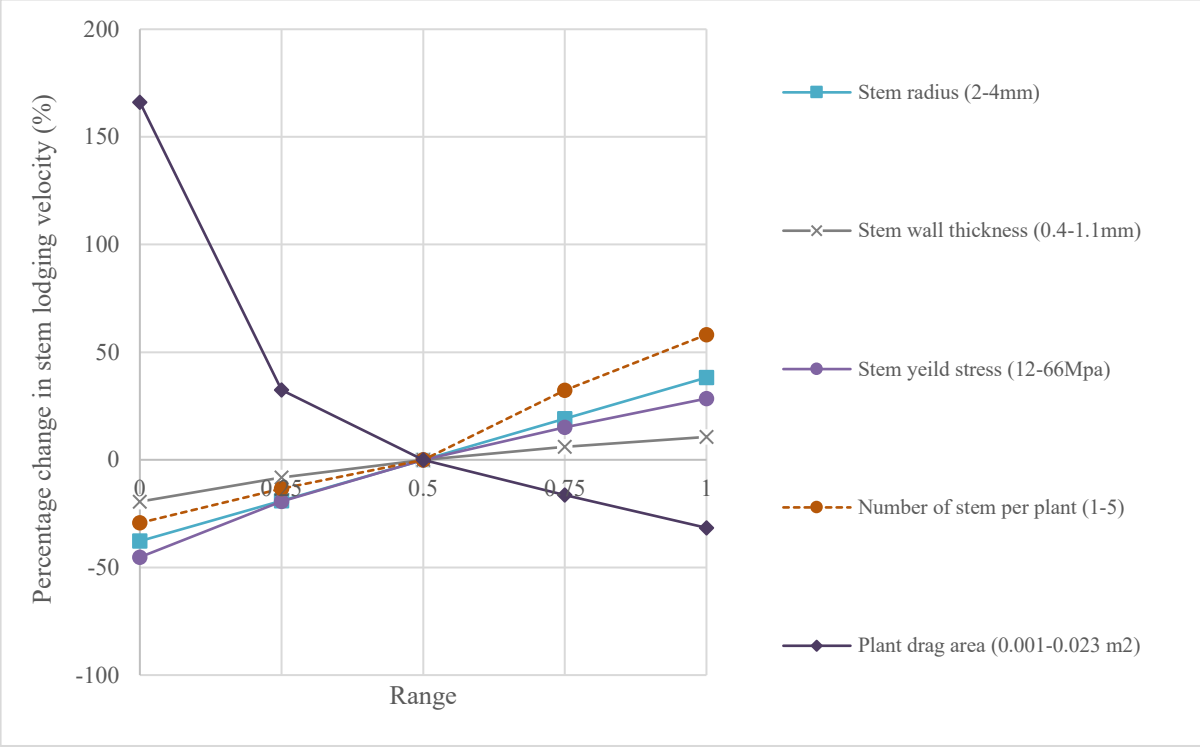

Figure 6.3. Stem lodging velocity changes with stem radius, stem wall thickness, number of stem per plant and plant drag area

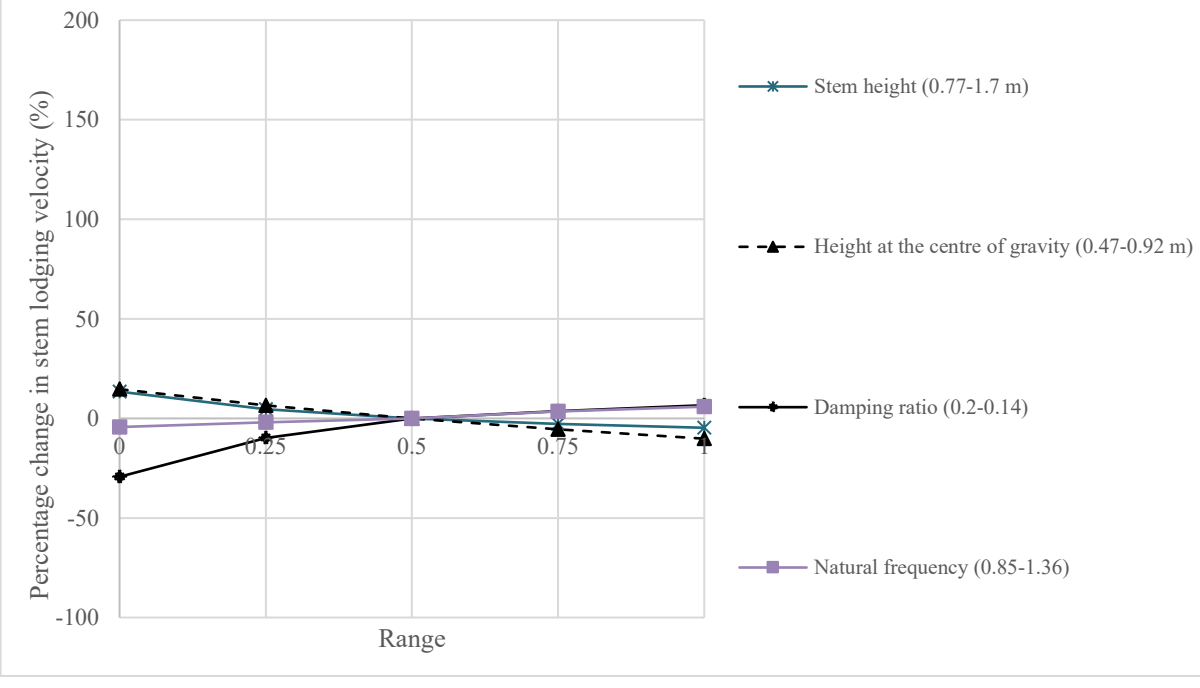

Figure 6.4. Stem lodging velocity changes with stem height, height at the centre of gravity, damping ratio and natural frequency

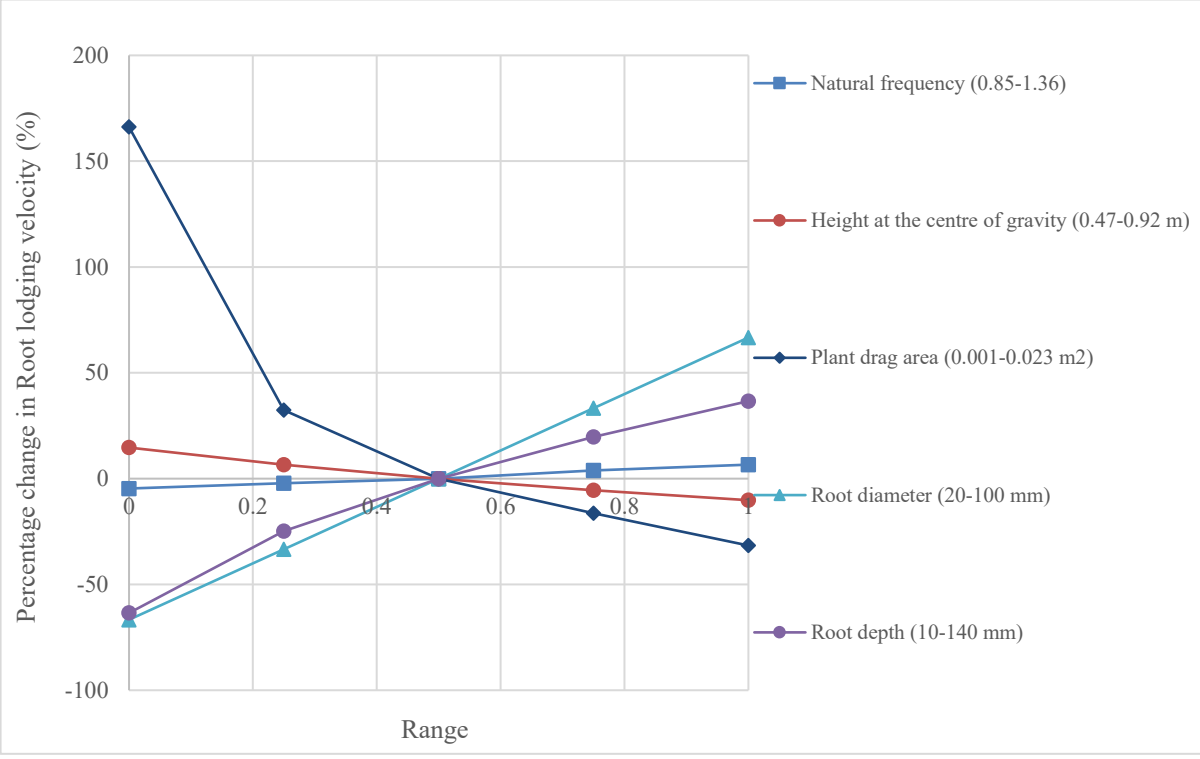

Figure 6.5. Root lodging velocity changes with natural frequency, height at the centre of gravity, plant drag area, root diameter and root depth

6.4. The effect of agronomic practice on lodging

In order to identify the effect of each husbandry factor (variety, seed rate, etc.) on agronomic characteristics and lodging susceptibility, root and stem resistance parameters (the averaged root plate diameter and stem strength), parameters associated to external bending moment applied on the crop (centre of gravity multiplied by panicle drag area) as well as lodged areas and lodging velocities for plots which received each specific husbandry factor is shown in Figure 6.6.

Figure 6.6a shows resistant variety (Husky) plants have a high root diameter, something which appears to be encouraged by a low seeding rate. Similarly, Figure 6.6b illustrates that

stem bending strength was much lower in the high seeding rate treatments than in the low seeding rate treatments and was greater in the resistant variety than in the susceptible (Barra) variety. On the other hand, the resistant variety and low seeding rate treatments (irrespective of variety) also increased panicle drag area to the same extent (Figure 6.6c). Nevertheless, choosing a resistant variety rather than a susceptible variety as well as a low seeding rate rather than a high seeding rate increased both root and stem lodging velocities (Figure 6.6e and 6.6f) and reduces the lodging area (Figure 6.6d).

PGR application and low Nitrogen rate increased the average root diameter (Figure 6.6a) but led to a decrease in the stem strength (Figure 6.6b). Nevertheless, as these husbandry treatments also reduced the panicle drag area and the external bending moment applied on the plant (Figure 6.6c), the stem lodging velocity was not greatly affected by the use of PGR or the rate of Nitrogen (Figure 6.6f), whereas the root lodging velocity was dramatically increased (Figure 6.6e). Thus, crops receiving PGRs had a lower lodged area than crops that did not receive PGR, and lodged areas in low Nitrogen rate crops were less than plants receiving high Nitrogen rate (Figure 6.6d). Additionally, changing the timing of Nitrogen fertilization did not have a large effect on lodging characteristics (Figure 6.6a-d), on lodging velocities (Figure 6.6e and Figure 6.6f) or on the incidence of lodging. Overall, using a resistant variety, a low seed rate, PGR application, and low Nitrogen rate can reduce the lodging (Figure 6.6d) which is consistent with the literature (Wu and Ma, 2019; Berry et al., 2000; Berry et al., 2004). Moreover, the amount of Nitrogen rate and Nitrogen timing are the most and the least influential husbandries to affect lodging susceptibility, respectively (Figure 6.6d).

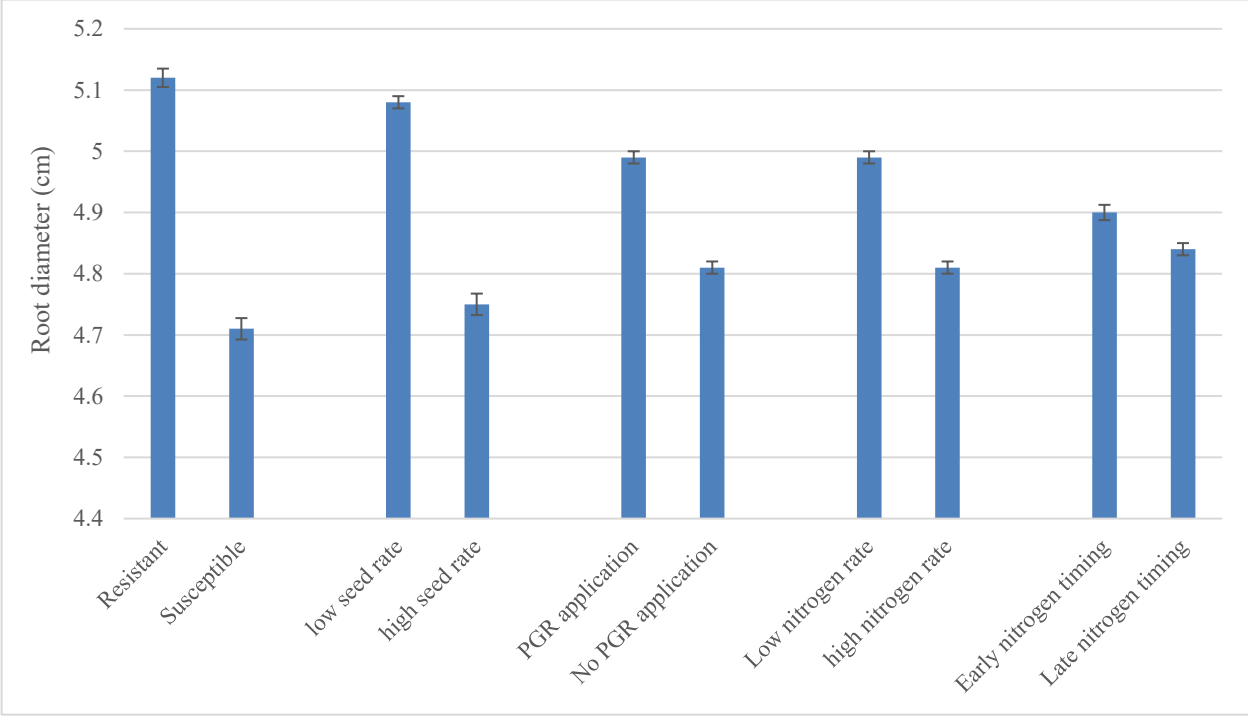

(a) Root diameter

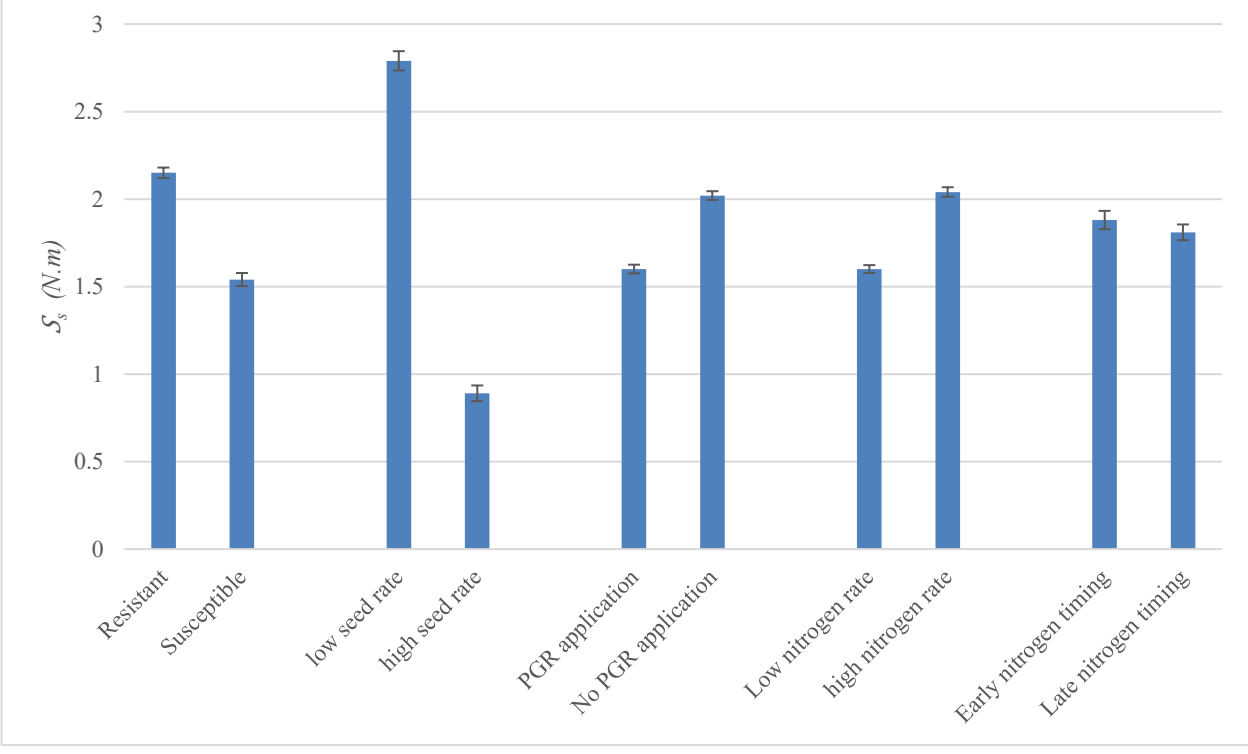

(b) Stem strength

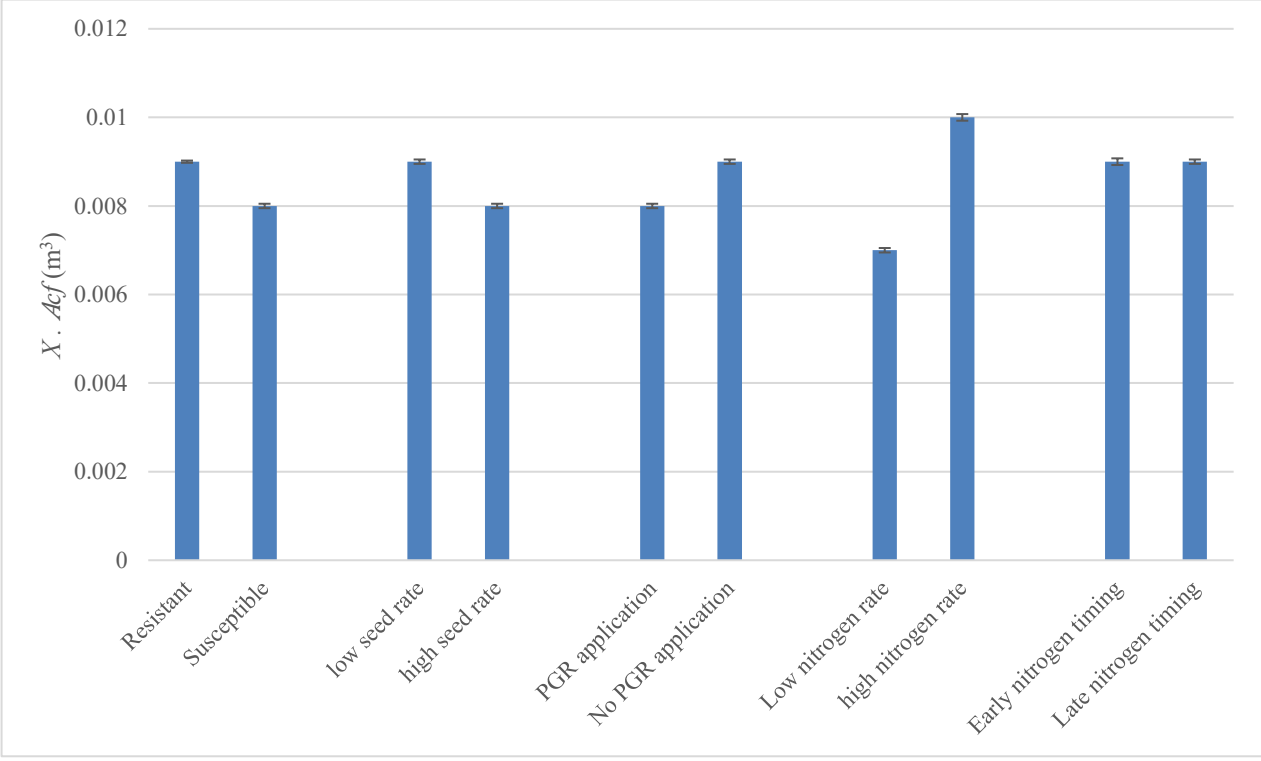

(c) Panicle drag area multiplied by centre of gravity

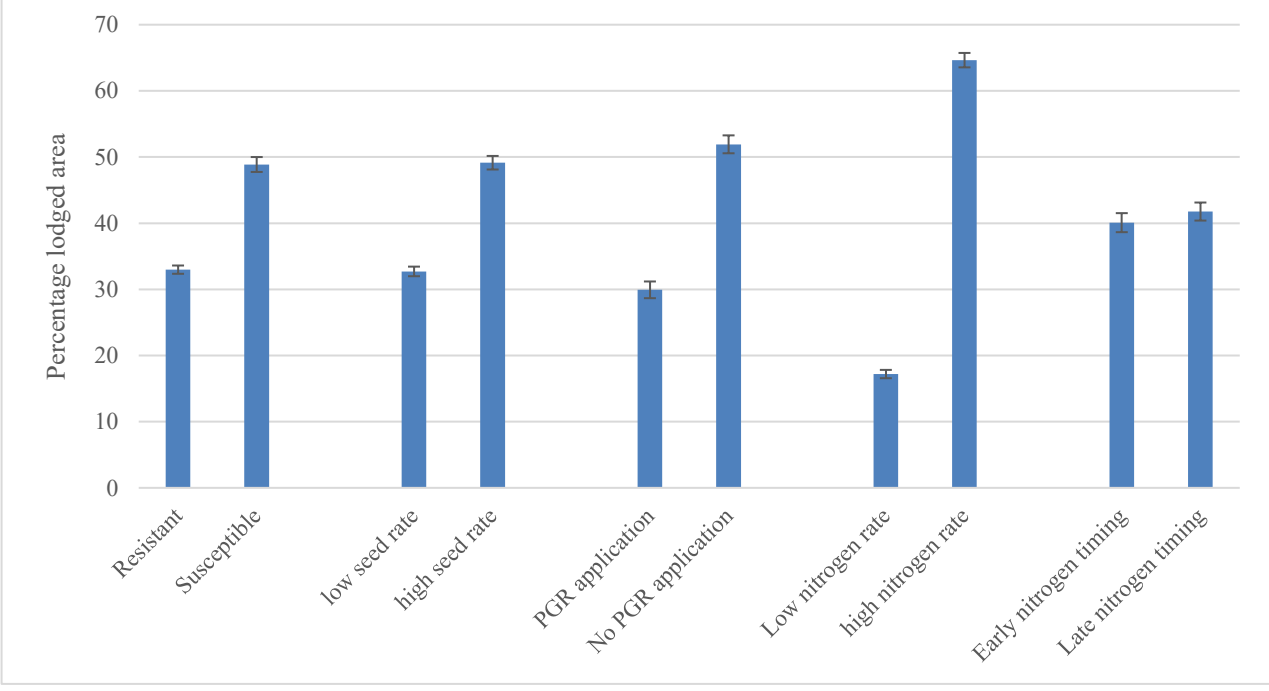

(d) Lodged area

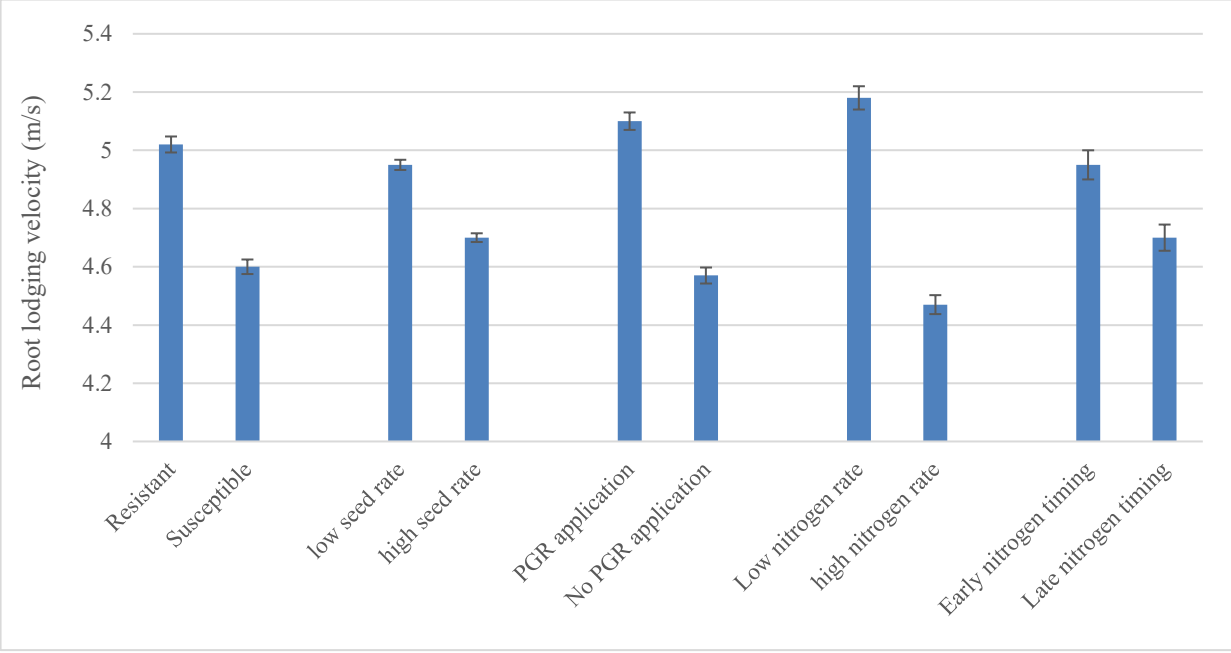

(e) Root lodging velocity

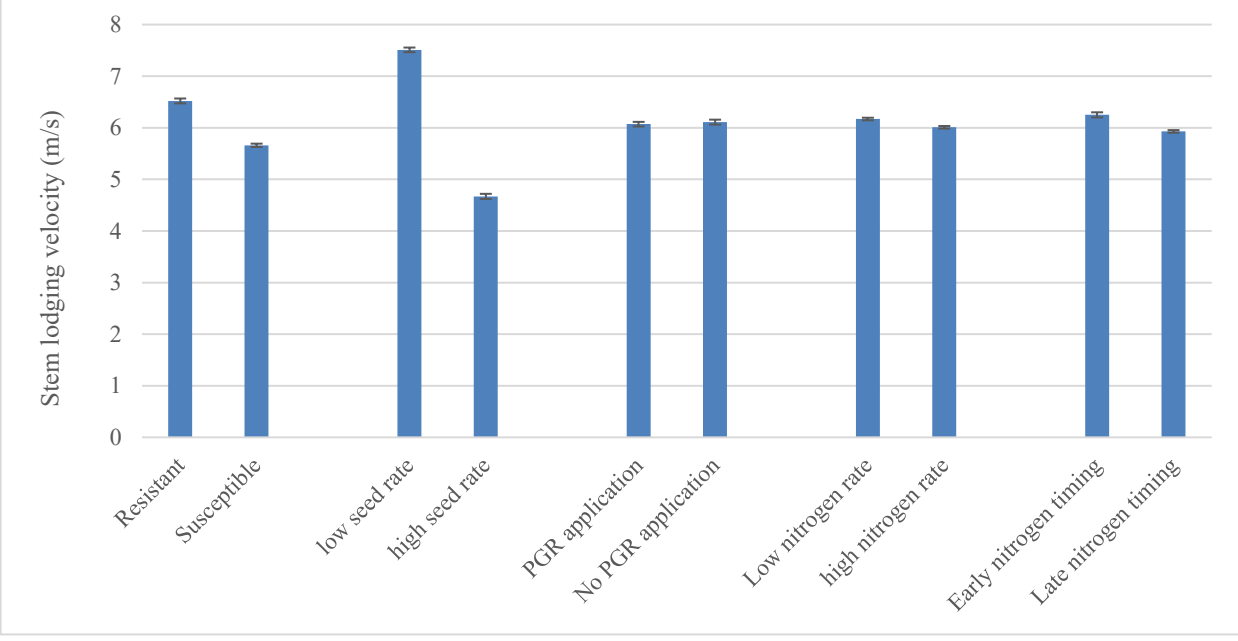

(f) Stem lodging velocity

Figure 6.6. The effect of different husbandries on the average (a) Lodging area (b) Stem lodging velocity (c) Root lodging velocity (d) root diameter, (e) stem strength, (f) panicle drag area multiplied by centre of gravity. Error bars show standard errors (±)

In order to examine if the difference between mean values of each two groups (Husky vs Barra, low seed rate vs high seed rate, high Nitrogen rate vs low Nitrogen rate etc.) is statistically significant, a t-test is used. The test considers a null hypothesis (H_0) that each two groups are the same, while the alternative hypothesis (H_a) is they are statistically different. The standard error of difference between two mean values can be obtained as follows:

$$SE_d = \sqrt{\frac{S_{d1}^2}{z} + \frac{S_{d2}^2}{z}} \quad (6\text{-}3)$$

Where $S_{d1}^2$and S_{d2}^2 are the variance of first and second husbandry techniques and z is the sample size, i.e. number of plots which received a specific husbandry (Parker, 2009), where z is the same for all techniques (z=16).

In order to investigate if the difference between two mean values was statistically significant a parameter, *t-value*, is calculated (equation 6-4) which is the ratio of the difference between the mean of samples and the variations within the samples. The higher the value of the *t-value* the larger difference exists between two samples.

$$t - value = \Delta M / SE_d \quad (6\text{-}4)$$

Where ΔM is the difference between two mean values (Parker, 2009). Later, a statistical parameter, degree of freedom (*df*) is calculated, which is *df=z-1* for one group and *df=z+z-2*, for two groups (the concept and meaning of the parameter is described in Appendix J). In this

analysis, as all the sample sizes are the same, *df*=30 for all cases. Having calculated the $t-value$ and the degree of freedom, it is possible to compare the $t-value$ with critical values at T-distribution Table (Appendix J). In summary, if 2.75< $t-value$ <3.65 the two samples are statistically significant at *P<0.01* (there is less than 1% probability if there is not a statistically significant difference between two groups, in other words, the null hypothesis is true) and if $t-value$ >3.65 the samples are statistically significant at *P<0.001* (there is less than 0.1% probability if there is not a statistically significant difference between two groups, in other words, the null hypothesis is true), while, $t-value$ <2.04 shows a significant difference cannot be observed at *P<0.05* and the husbandry techniques do not have a significant effect of the properties and two samples are the same (Parker, 2009).

The $t-values$ provided in Table 6.4 illustrate that the effect of PGR application and Nitrogen rate on stem lodging velocities were not significant. Similarly, the timing of Nitrogen application did not influence the plant parameters and the incidence of lodging. However, $t-values$ of crop characteristics and lodged areas/lodging velocities receiving other husbandry techniques showed their mean values are statistically significant ($P<0.01$ or $P<0.001$), which supports the conclusions drawn in relation to Figure 6.6. It is worth noting that, as the treatment plots were not replicated, there was the chance that the effect of husbandry techniques may be affected by spatial variation across the trial area, although this was minimised by taking an average for each treatment factor across several plots.

Table 6.2. Mean, values for different husbandry techniques

	Husky variety	Barra variety	Low seed rate	High seed rate	PGR application	No PGR application	Low Nitrogen rate	High Nitrogen rate	Early Nitrogen timing	Late Nitrogen timing
Lodged area	32.98	48.87	32.71	49.14	29.93	51.92	17.20	64.64	40.08	41.76
U_{LR} (m/s)	5.02	4.60	4.95	4.70	5.10	4.57	5.18	4.47	4.95	4.7
$\overline{U}_{LS}$(m/s)	6.52	5.66	7.51	4.67	6.07	6.11	6.17	6.01	6.25	5.93
d (m)	5.12	4.71	5.08	4.75	4.99	4.81	4.99	4.81	4.90	4.84
S_s (N.m)	2.15	1.54	2.79	0.89	1.60	2.02	1.60	2.04	1.88	1.81
X.A_{Cf} (m3)	0.009	0.008	0.009	0.008	0.008	0.009	0.007	0.010	0.009	0.009

Table 6.3. SE_d values for different husbandry techniques

	Husky/Barra	Low/high seed rate	PGR/No PGR application	Low/High Nitrogen rate	Early/Late Nitrogen rate
Lodged area	5.14	5.02	7.4	5.03	7.92
$\overline{U}_{LR}$ (m/s)	0.15	0.1	0.16	0.20	0.26
U_{LS}(m/s)	0.23	0.27	0.26	0.14	0.22
d (m)	0.09	0.08	0.06	0.06	0.06
S_s (N.m)	0.19	0.28	0.14	0.14	0.27
$X.A_{Cf}$(m3)	0.0002	0.0003	0.0003	0.0004	0.0004

Table 6.4. $t-$ values for different husbandry techniques

	Husky/Barra	Low/high seed rate	PGR/No PGR application	Low/High Nitrogen rate	Early/Late Nitrogen rate
Lodged area	3.09[1]	3.27[1]	2.97[1]	9.42[2]	0.21
$\overline{U}_{LR}$ (m/s)	2.82[1]	2.71[1]	3.25[1]	3.44[1]	0.92
$\overline{U}_{LS}$(m/s)	3.73[2]	10.55[2]	0.15	1.13	1.43
d (m)	4.44[2]	4.02[2]	3.18[1]	3.18[1]	0.93
S_s (N.m)	3.17[1]	6.68[2]	2.96[1]	3.09[1]	0.25
$X.A_{Cf}$(m3)	4.47[2]	3.53[1]	3.53[1]	7.5[2]	0

[1] statistically significant at $P < 0.01$

[2] statistically significant at $P < 0.001$

6.5. Structure requirements to avoid lodging

The lodging probability is dependent on both adverse weather conditions probability and plant susceptibility. Figure 6.7 shows the result of joint (wind and rain) probability density function for a sample station (Cork airport station, no.13 in Table 5.1) for June and July month in the 30 years period (1987-2016). Interestingly, the probability of wind speeds greater than 9m/s at 10m height from the ground is very low and any husbandry techniques used or different varieties planted which reduce the failure wind speed can have positive impact on the probability of lodging.

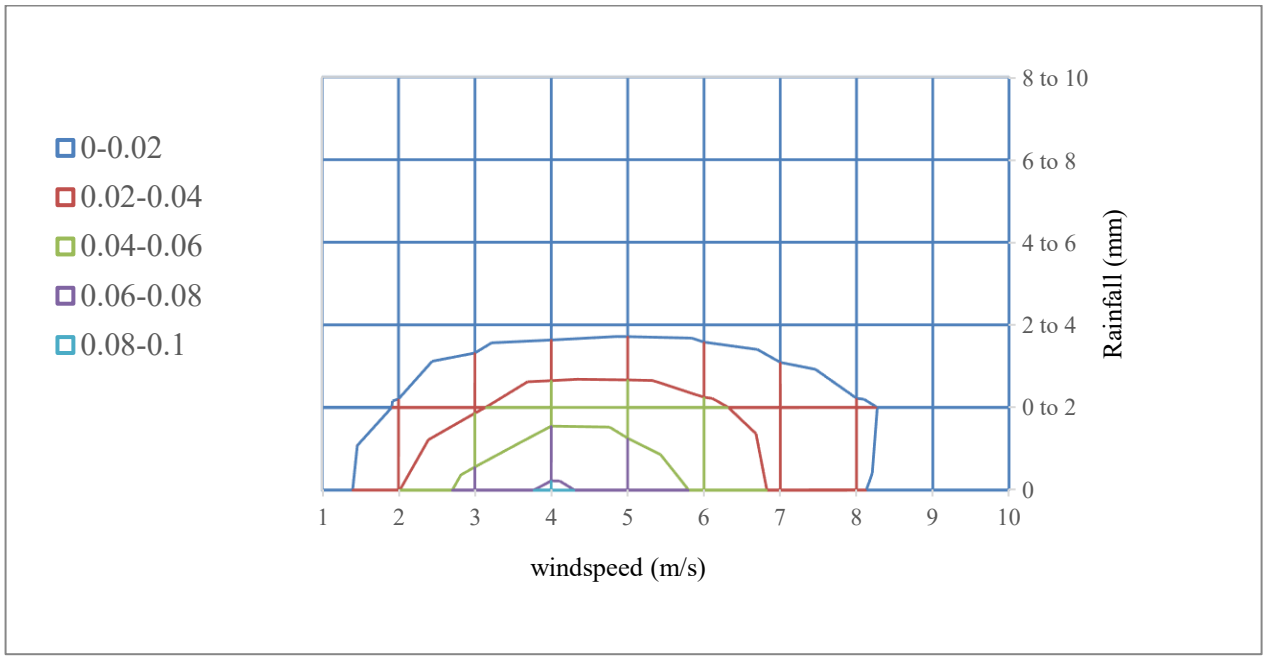

Figure 6.7. Joint (wind and rainfall) probability density function for Cork airport station in Ireland in the period from 1987 to 2016 for June and July.

Figure 6.8 shows lodging velocities (at 10m height) for different husbandry techniques in a suitable condition for lodging, i.e. the soil shear strength is low (S=10kpa), and the crops have formed a highly interlocked canopy (N=5). The figure shows the choice of variety and crop treatment could increase stem lodging velocity to values greater than 9m/s, while using these husbandry techniques, the highest root lodging velocity is 7 m/s. The abbreviations used in the figure are similar to those used in Table 6.1, where H/B are the plant varieties (Husky/ Barra), 200/500 are the low/high seed rate (200/500 seeds per m^2), Y/N refer to PGR application (Yes/No), 90/180 indicate Nitrogen rate (90/180Kg/ha) and E/L refer to early or late Nitrogen timing.

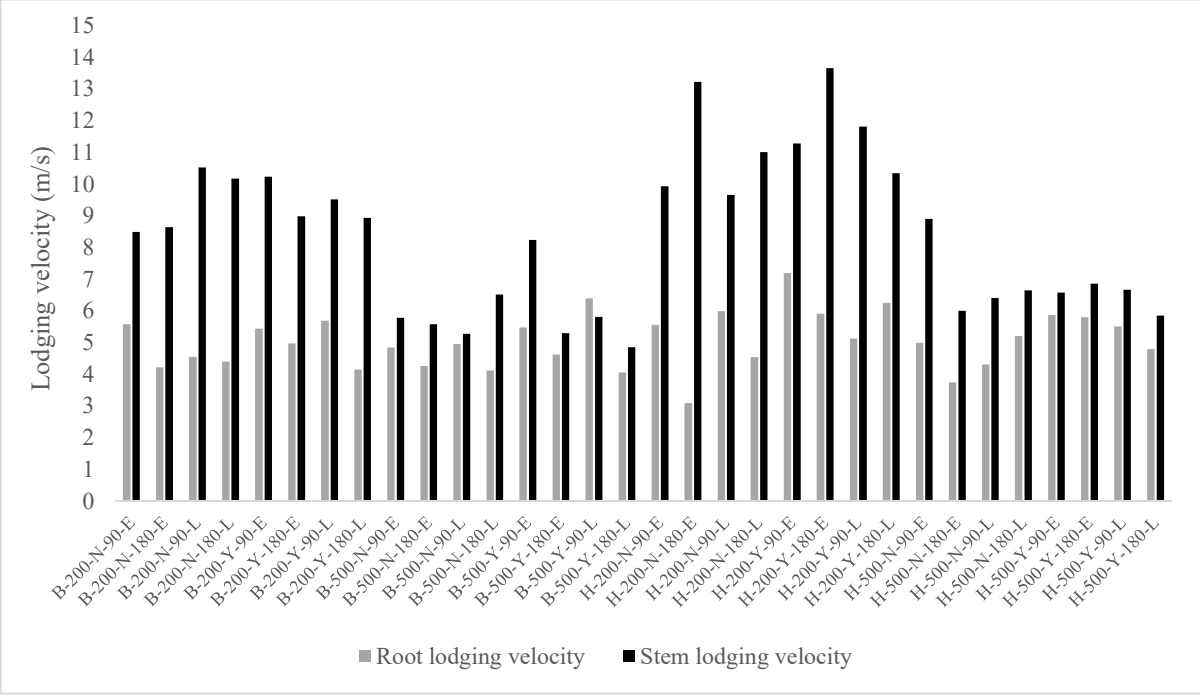

Figure 6.8. Stem and root lodging velocities for different husbandry techniques

In addition to husbandry techniques, plant characteristics with high lodging velocities could also be achieved through plant breeding (plant breeding is an approach to improve crops by selection and hybridization of desired genotypes (Lockhart and Wieseman, 1983)). The probability of lodging changes during the lodging season as plants become more susceptible to failure due to the increase in the panicle drag area, centre of gravity and stem length. Table 6.5 illustrates the lodging velocities (at 10m height) over the range of plausible values of parameters associated with the highest bending moment (AC_f=0.023m^2, X=0.92m) and highest/average/lowest measured values of stem/root resistance parameters, while other parameters were assumed constant.

Table 6.5. Stem and root resistance parameters and associated stem/root lodging values

Stem parameters				
n	1	2	5	
a (cm)	0.2	0.3	0.4	
t (cm)	0.04	0.07	0.1	
$\overline{U}_{LS}$ (m/s)	1.83	5.01	12.48	
Root parameters				
d (cm)	2	6	10	10
L (cm)	1	7.5	10	14
$\overline{U}_{LR}$ (m/s)	0.79	6.50	12.50	14.80

The table shows for the same bending moment experienced; the failure velocity can change from the most susceptible to most resistant plant. Thus, lodging proof ideotypes should have strong stems (stem radius of 0.4cm and stem wall thickness of 0.1cm) and wide and deep root systems (root diameter and depth10cm). The achievement of such breeding targets would represent an alternative means of minimising lodging in oat crops.

Another way to demonstrate the structural requirements of crops is to assume the highest bending moment is applied on the crop (AC_f=0.023m^2, X=0.92m) and to calculate the plant parameters which gives lodging velocities equal to 9m/s . Such a graph is shown in Figure 6.9 and 6.10 where the combination of stem (number of stem per plant, stem radius, and stem wall thickness) or anchorage (root diameter and depth) parameters result in $\overline{U}_{Ls}$ or $\overline{U}_{LR}$ =9m/s are identified as a critical curve. If the measured values in a sample plant (or average of values in a group of plants) are above the curve, the plants are highly resistance to lodging ($\overline{U}_{LR}$ or $\overline{U}_{Ls}$> 9m/s), while if the parameters are below the line, the plant are more likely to lodge.

Figure 6.9 shows the critical values for three parameters, number of stem per plant, stem wall thickness and the stem radius. For n=3,4 and 5 the critical value curves is shown in Figure 6.10 Similarly the critical values for root diameter and depth are shown in figure 6.10

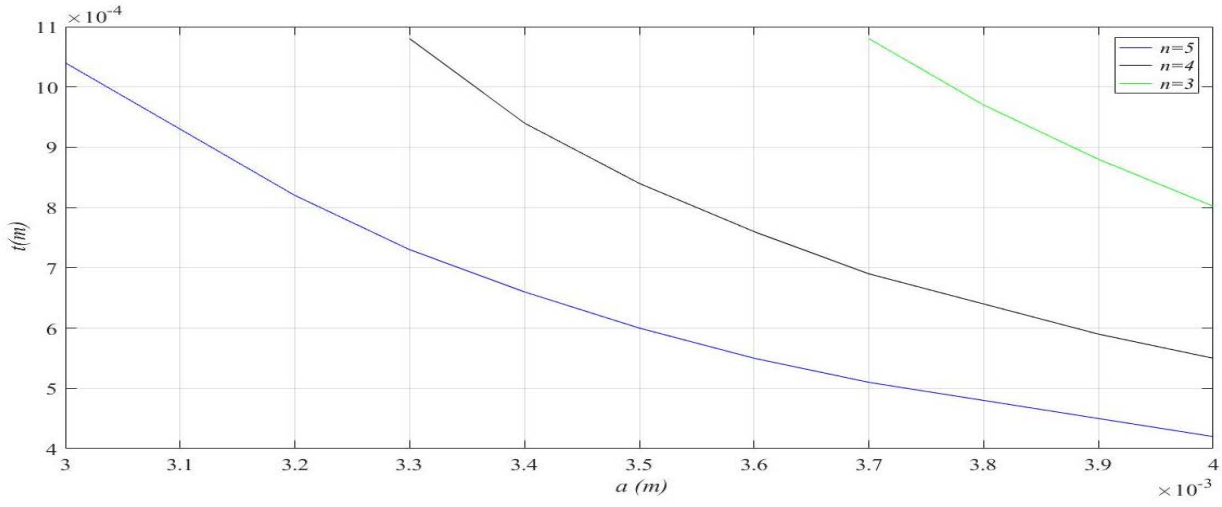

Figure 6.9. The combination of number of stem per plant (n), stem thickness (t) and stem radius (a) values which result in $\overline{U}_{Ls}$ =9m/s

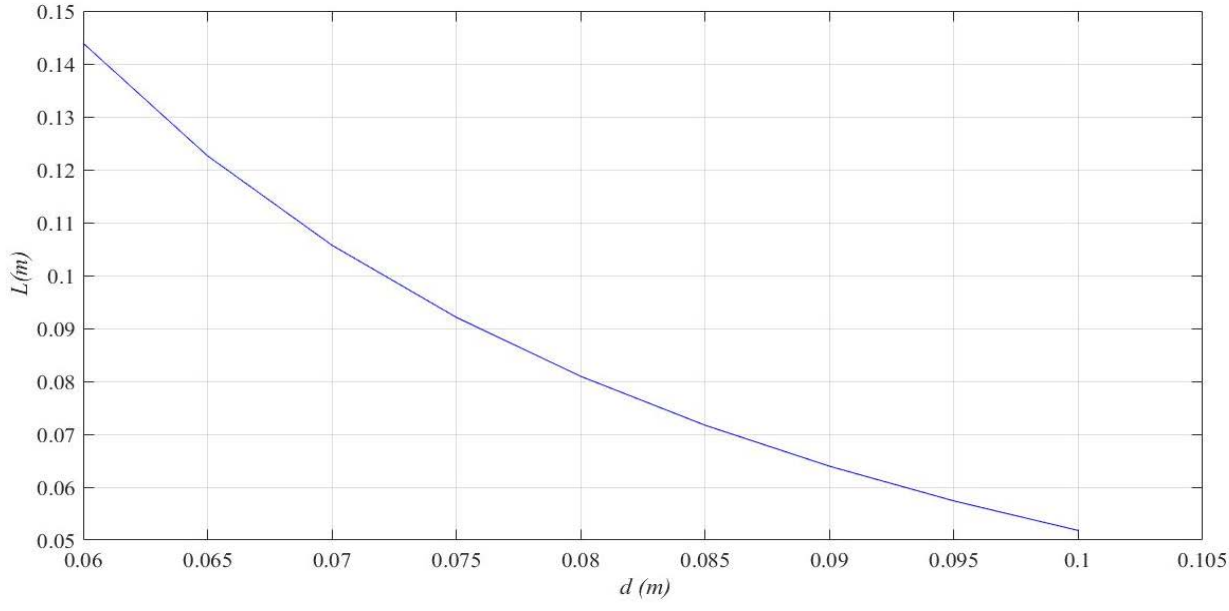

Figure 6.10. The combination of root plate diameter (d) and root depth (L) values which result in $\overline{U}_{LR}$ =9m/s

6.6. A comparison between the generalized lodging model and the modified model

In this research, a lodging model was modified and calibrated based on the generalized lodging model developed by Baker et al. (2014) and it is useful to compare the outputs of the modified model and the original model to show the importance of modification and calibration process. Figure 6.11 shows a flow chart of the generalized model (left) versus the steps undertaken in this research (right) to examine, modify and calibrate the model to use it in practice.

As the figure shows, at the first stage, the generalized model calculates the peak bending moment applied on the crop and compares it with stem/root resistance. This is a logical mechanical concept that is kept in the modified lodging model. In the next stage, the calculated bending moments are rewritten in the form of lodging velocities. As mentioned in Section 2.2.1.2, Baker et al. (2014) assumed various values for the broad branded and resonant peak factors: g_{MR}=4.15 and g_{MB}=3.43 for stem lodging and g_{MB}=1.72 for root lodging assuming I=1 and f_n=0.8. In Baker et al. (2014) these values were chosen for example purposes but, Chapter 4 proved they are crop dependent. The results from the lodging model show if the same input data is used for Baker's lodging velocity expression (equation 2-12 and 2-13) and the modified expressions (equation 3-1 and 3-2), the earlier shows ~30% error in both stem and root lodging velocity values. Consequently, this modification is an important step in lodging model modification and calibration.

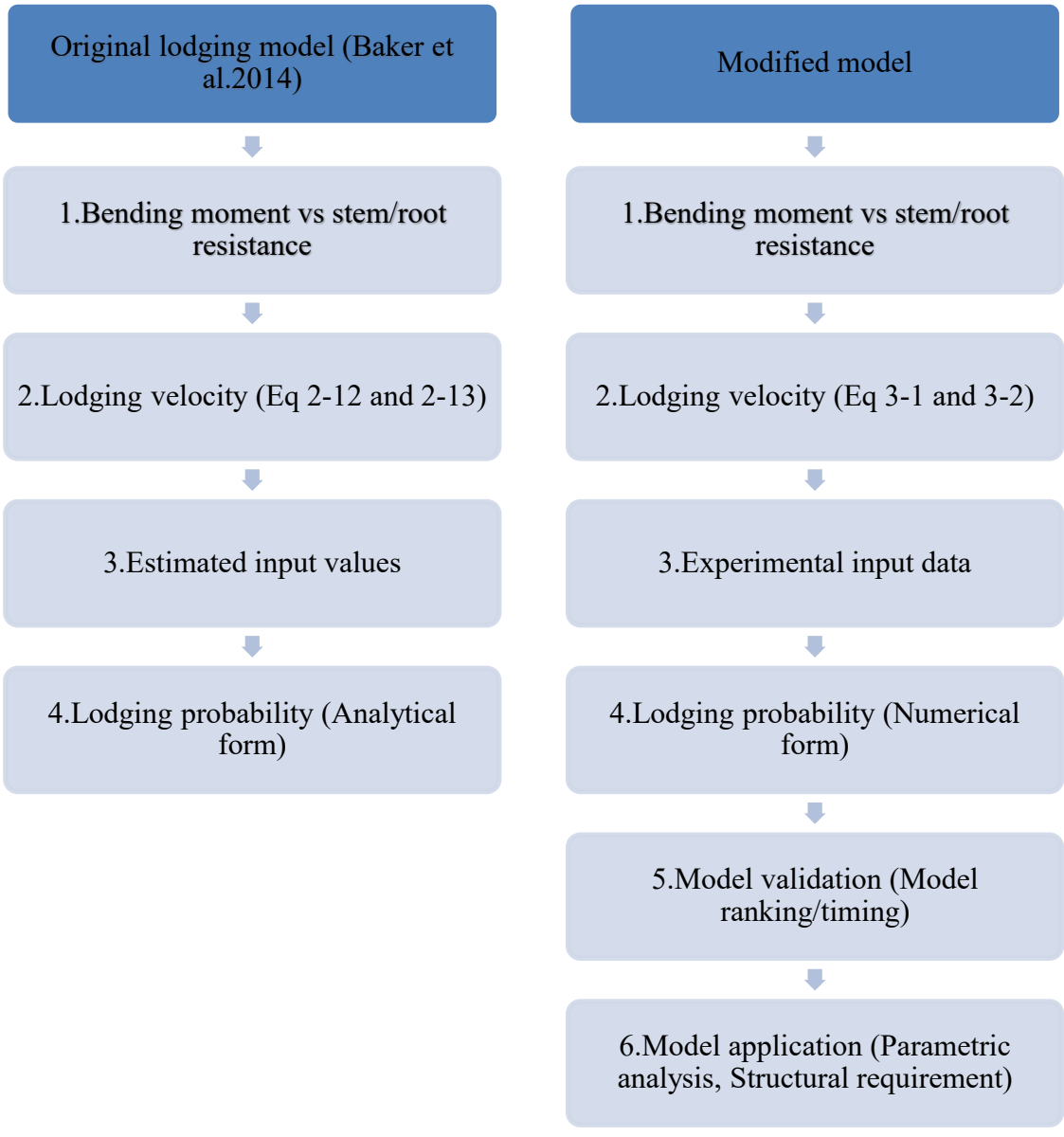

Figure 6.11. A comparison between Baker et al. (2014) and modified lodging model for oat

Both the bending moment and plant resistance expressions are based on agronomic, dynamic/aerodynamic, and soil parameters which are required as the input data for the model. Although Baker et al. (2014) used estimations for all the agronomic and dynamic/aerodynamic factors, Chapter 4 showed different values in comparison to what was assumed before. The results of lodging velocities calculated based on these assumptions show ~73% difference with the output of the modified/calibrated model. This finding supports the

conclusion made by Berry et al. (2003) and Sterling et al. (2003) about the importance of experiments before the application of a lodging model on any kind of crop.

The fourth stage in Figure 6.11 calculates the lodging probability which was fully described in Section 5.5.1. At this stage a major correction has been applied on the lodging model as alternative expressions for wind and rainfall probabilities functions were used and Chapter 5 showed a significant difference in the probabilities of wind and rainfall as calculated by Baker's assumptions (Baker et al. 2014) and the expressions found based on historical data analysis.

As Figure 6.11 shows, the last two stages (5 and 6), go beyond what Baker et al. (2014) could achieve, as a modified and calibrated model can be tested in practice and be used to produce practical ways to reduce lodging. Accordingly, in the 5th Stage, the modified and calibrated model output is compared with lodging observations to evaluate if the model is capable to predict lodging spatially and temporally (see Section 6.2). In the 6th stage (Figure 6.11) the most influential parameters and the structural requirements of oat to resist adverse weather conditions are determined (see Section 6.5).

Overall, the lodging model which was discussed in this research has used the principal concept of the generalized model (stage 1) and examined, modified and calibrated the other elements of the model. A major contribution was made through the experimental campaigns (described in the Chapter 3) which was necessary to calibrate a lodging model for any crop type. Additionally, the modification suggested in the model were found to impact the outputs dramatically, and consequently crucial. Finally, the modified lodging model is highly suggested for future studies about lodging on other crops, as its mathematical expressions and

the probabilistic assumptions were found to be much more accurate than Baker's model (This is further discussed in Chapter 7).

6.7. Conclusions from lodging model application

Based on the above analysis, the following conclusions can be made:

- The model output aligns with the lodging observations as it can rank the husbandry techniques based on their susceptibility to lodge and is capable to predict the lodging timing/quantity during the lodging season, although there is a sign of over prediction for least susceptible group. (See Figure 6.2)
- Oats become more susceptible when their panicles interlock and create a canopy (see Figure 6.5). This is because of an increase in the drag area and consequently wind-induced force on the plants. Additionally, the number of stems per plant, stem yield stress, stem radius and wall thickness for the stem lodging and the root diameter and root depth for the root lodging were also found to be important factors.
- It was found that if growers and breeders target specific stem and root resistance parameters in oats, the probability of lodging can be reduced. Moreover, the Husky variety, low seed rate, PGR application and low Nitrogen rate were found influential husbandry techniques to reduce lodging.

7. Conclusions

7.1. Introduction

The aim of this research was to examine lodging in oats and hence to improve the understanding of lodging resistance for this particular crop through the application of an analytical model. In this section, a number of conclusions have been made in support of the overall aim and objectives. For the sake of ease, Section 7.2 restates the objectives and discusses how each objective was met, whilst Section 7.3 presents some recommendations for future research which, it is hoped, others would find useful.

7.2. Conclusions

Objective 1: To conduct a critical literature review focusing on crop lodging and modelling, and to evaluate the agronomic factors which might influence the likelihood of lodging.

From the critical literature review (conducted in Chapter 2), it became evident that only two theoretical lodging models have been developed i.e., Baker (1995) and Baker et al. (2014). The latter was found to be more appropriate for oat canopies than the former (see Section 2.2.1.1). It was also found that a number of studies have been undertaken to adopt Baker (1995) on wheat, barley, and sunflower. The Baker et al. (2014) model has never been

adopted in practice and the embodied assumptions were never examined. The literature review also showed a number of influential agronomic factors in lodging which can be controlled by husbandry techniques. Although the effect of different husbandry techniques on the lodging probability has been documented elsewhere (e.g. wheat), such a study has not been conducted for oats. Consequently, the necessity of undertaking agronomic measurement to establish a database of the effect of husbandry techniques on plant properties was found a crucial step to study lodging in oats.

Although the parameters related to the dynamic movement of the crop (damping ratio, natural frequency, and the plant drag area), are crucial to determine the wind loading on the crops and the dynamic response of the plants, there was no previous research to study this in oat canopies. This is particularly important given the fact that oats create an interlocked canopy later in the growing season which can be expected to influence the dynamic movement of the crop (and ultimately lodging). Finally, it was discovered that the existing research about the effect of climate change on lodging was based on inaccurate methods and alternative methods were required to study the problem.

Objective 2. To explore the lodging process in oats and, if appropriate, to assess, modify and calibrate an existing lodging model (i.e. Baker et al., 2014) through the collection and application of experimental data obtained from fieldwork.

The lodging model developed by Baker et al. (2014) was presented in detail and discussed in Chapter 2. The model is based on a number of assumptions and estimations which had never been investigated prior to this research. Fundamentally, the model compares the peak bending moment against the stem/root resistance to decide if lodging is likely to happen. Nevertheless, the expression for peak bending moment is derived for a ‘typical’ flow over

crop canopy. The results presented in Chapter 4 showed the turbulence parameters in the flow over oat canopies are consistent with the values found elsewhere and hence the aforementioned assumption is valid. Nevertheless, while rewriting the peak bending moment expression in lodging velocity forms, Baker et al. (2014) made some assumptions for peak factors, which have been discovered to be crop specific (Chapter 4). Hence, the approach adopted by Baker et al (2014) was incorrect and alternative expressions for lodging velocities were presented (equation 3.1 and 3.2).

This research also examined the probabilistic expressions suggested by Baker et al. (2014) to calculate the lodging probabilities through evaluating the historical data from 38 meteorological stations in the British Isles where oats are commercially grown. The corresponding data analysis showed that the summation of two exponential functions can appropriately represent the rainfall CDF for the peak lodging period (June and July). It was also demonstrated that a slight difference in the considered lodging period would not change the evaluated functions. At the time, there was no investigation to suggest accurate and representative PDFs (or CDFs) to be used by Baker et al. (2014) in the lodging probability calculation process. Thus, Baker et al. used exponential and Rayleigh distributions to represent rainfall and wind PDFs respectively. A comparison between the 30 years' historical rainfall time series with what was assumed by Baker et al. (equation 2-19), shows a considerable difference. The current research shows that a Weibull distribution can be used in all studied stations although the scale and shape factor might vary locally. Nevertheless, a representative Weibull curve was found to be an appropriate distribution.

In addition to the above modifications, experimental campaigns were conducted to measure a number of agronomic and dynamic/aerodynamic factors and to calibrate the lodging model for oats. To evaluate the agronomic parameters which might influence the likelihood of lodging the following steps were followed:

- Crops were grown[5] under 32 different treatments for two subsequent years and their agronomic parameters were measured under standard protocols as described in Chapter 3.
- The collected data were used to calibrate the model and to evaluate the effect of different agronomic husbandry techniques on the probability of lodging. The results illustrate how various techniques (e.g., seed rate, PGR application, etc.) affect the agronomic parameters associated with lodging (as described in Chapter 6) and consequently the lodging velocities and probability. It was found that using a resistant variety, a low seed rate, PGR application, and low Nitrogen rate can reduce the lodging occurrence (average percentage lodged area =28.20) rather than using a susceptible, high seed rate, without PGR application, and high Nitrogen rate (average percentage lodged area =53.64). Further information was discussed in Section 6.5.

The agronomic parameters could be determined by measurements in the laboratory and/or in field (Section 3.3), while, evaluating the dynamic and aerodynamic parameters required associated experiments as described in Section 3.4. The experimental setup included ultrasonic anemometers to record wind velocities over the crop canopies and video cameras to observe the crops' movements. The cameras were appropriately calibrated (Section 3.4.5), and a bespoke video tracking program developed in MATLAB was used which enabled the motion of plants to be tracked in real-time and a variety of aerodynamic parameters to be determined. The output of the code was verified and validated through a number of experiments. Using obtained dynamic/aerodynamic and agronomic parameters, the model was calibrated for oat and the probability of lodging was derived based on the CDFs in

[5] Soil preparation, seeding, and chemical application were instructed by the author and undertaken by Teagasc technicians. The agronomic measurements and the aerodynamics experiments reported in this thesis were done by the author of this thesis.

conditions where lodging is likely to happen. Consequently, the probability of lodging could be derived for all the agronomic managements and was used to rank the treatments from the most susceptible to the most resistant. This theoretical ranking was finally compared with an experimental ranking, which was calculated based on the accumulated lodged area for each husbandry technique during the lodging season. The model output to rank the agronomic treatments based on the lodging probabilities agreed with the lodging observations in the field. Moreover, the calibrated model was able to anticipate the lodging timing and quantity during the lodging season.

Objective 3. To undertake a parametric analysis in order to understand the crop parameters that influence lodging the most.

The lodging model enabled a parametric analysis to be undertaken in order to identify the most influential agronomic and dynamic/aerodynamic parameters with respect to lodging. Accordingly, the drag area was found to be the most influential parameter for both the stem and root lodging where the lodging velocity can reduce by approximately three times as the panicle becomes interlocked ($\overline{U}_{Ls}$=4.5-16.3m/s, $\overline{U}_{LR}$=5-18.1m/s). This parameter is affected by panicle interlocking and increases during the season. Hence, the probability of lodging also increases from the time panicles emerge, until the harvest time. Moreover, the lodging model showed that other plant parameters relating to the stem bending strength (i.e. the number of stems per plant, stem yield stress, stem radius, and wall thickness) are highly influential parameters with respect to stem lodging. The most effective factor parameter with respect to stem lodging in oats (i.e. the drag area), contrasts with wheat (Berry et al., 2003), sunflowers (Sposaro et al., 2010), and barley (Berry et al., 2006) - other plant parameters were found of major importance for these plants (e.g., stem wall thickness, stem diameter,

etc.). Moreover, parameters such as natural frequency and the height of the centre of gravity were identified to have a relatively minor effect on the stem and root velocities in oats, which is in agreement with the existing literature for other crops (Berry et al., 2003; Sposaro et al., 2010). A comparison between agronomic values as measured for oats (Table 4.8) and those reported for wheat (Berry et al., 2003), shows on average, wheat have a higher number of stems per plant (3.2), but lower stem yield stress (30MPa), stem wall thickness (0.64mm) and the stem radius (1.67mm). Consequently, the lodging model shows that wheat is more susceptible to stem lodging than oats.

The root diameter and depth were the second and third most influential parameter (after drag area) in the oat root lodging while the root diameter was found to be the major important factor in root lodging for wheat (Berry et al., 2003), barley (Berry et al., 2006) and sunflower (Sposaro et al., 2010).

Objective 4.To apply the modified and calibrated oat lodging model, to understand the potential impact of climate change on lodging resistance.

Although both wind and rainfall have been reported to be influential factors on lodging, the current research showed wind has much more importance than precipitation. For example, climate change projections demonstrate up to 70% reduction in monthly rainfall after the 2050s and just ±1 m/s wind speed changes in the average monthly wind speed. However, the lodging model showed that such a dramatic change in rainfall reduces the probability of lodging by 5%, whereas an increase/decrease in wind speed of ±1m/s changes the lodging probability by more than 10%. Moreover, most of the climate projections demonstrate a reduction in the mean wind speed in Ireland. Thus, it can be assumed that, on average, the lodging probability will be reduced in Ireland over time. Nevertheless, the same conclusion

cannot be made for the UK. Finally, the outcome of the research for the agriculture sector was to show that the influence of climate change on lodging probability is the same as changes in the failure probability due to plant natural variation and different managements applied on crops.

Objective 5. To identify the most appropriate plant parameters in order to reduce the likelihood of lodging in oats and to provide recommendations concerning the appropriate husbandry techniques which may result in such plant parameters.

The lodging model was able to determine the values of influential agronomic parameters associated with the stem/root velocities that can affect the failure probability. These outcomes can assist the agricultural sector in growing more lodging resistant plants. Moreover, it was identified that using appropriate husbandry techniques can dramatically increase the stem lodging velocities to values higher than 9m/s (the highest 'expected' failure windspeed for a typical crop growing areas in Ireland). However, none of the treatments were identified to be sufficiently influential to enhance root lodging velocity to values higher than 8 or 9m/s (which have a very low probability of occurrence). Notwithstanding, the lodging model indicated that there is a potential to increase the root lodging velocities up to 14.8m/s by targeting the root diameter and depth.

7.3. Recommendations for further work

1. In this research, the probability of lodging in future climate conditions was derived from integrating the joint probability density functions in conditions that lodging is likely to happen. The lodging velocities in the procedure were determined based on current agronomic

values. Nevertheless, plant factors associated with lodging might be affected by environmental conditions, e.g. temperature, sunshine, air/soil moisture, plant diseases, pests, etc. (Berry et al., 2002; Berry et al., 2004). The contribution of these environmental parameters as well as the effect of climate change on the conditions can be considered in the future when more data is available.

2. This study identified the probability of lodging for oats based on experiments that were undertaken in Carlow, Ireland. Although the CDF functions used in the probabilistic framework can be considered representative for the regions where oats are grown in the British Isles, more research is recommended to study the variation of plant parameters in various sites and in different years. Moreover, the representative CDF functions were suggested based on evaluating farmlands in which oats are commercially grown, and in the peak lodging period for oats. A similar approach can be followed to find representative CDFs to evaluate the lodging probability for other crops/countries.

3. The experimental results pertaining to the anchorage system were in keeping with previous findings, i.e., this parameter was difficult to measure and the value of the constant relating the lodging moment to the ratio R_s/SLd^2 was found to be considerably low (~0.1) which suggests that the adopted model might be simplistic. Moreover, the lodging model showed that despite the higher average root diameter and depth for oats (Table 4.8) in comparison to wheat ($d \cong L \cong$40mm), oats are more susceptible to root lodging than wheat due to lower γ value. Thus, further research is required to study other parameters that can be potentially influential on the root system resistance.

4. The experiments to evaluate the dynamic/aerodynamic parameters were developed in natural conditions. Nevertheless, when a plant/canopy is lodged it would be more exposed to the wind, the drag coefficient and the wind induced force might increase, which consequently make other crops to lodge. This needs appropriate modelling and further experiments to be studied.

8.References

Agriculture, forestry and fisheries. (2020). Oats Production guideline. Available from http://www.nda.agric.za/docs/Brochures/Oats.pdf. Last accessed on 19/12/2020.

Allen, R., Pereira, L., Raes, D., Martin Smith, M. (1998). Crop evapotranspiration - Guidelines for computing crop water requirements, FAO - Food and Agriculture Organization of the United Nations.

Aly, M.A. 2014, Influence of Turbulence, Orientation, and Site Configuration on the Response of Buildings to Extreme Wind, The Scientific World Journal, Article ID 178465, 15 page. https://doi.org/10.1155/2014/178465

AntiLog RS232 Data Logging System User Guide. (2017) Available from: https://sirway.fi/st-lucia/docs/Antilog.pdf. Last accessed on 12/12/2017

AR4 Climate Change. (2007). IPCC's 4th assessment report. Available at: www.ipcc.ch/report/ar4/syr. Last accessed on 10/12/2018.

Baker, C. J. (1995). The development of a theoretical model for the windthrow of plants. Journal of Theoretical Biology, 175, 355-372.

Baker, C. J., Berry, P. M., Spink, J. H., Sylvester-Bradley, R., Griffin, J., Scott, R. K., Clare, R. (1998). A method for the assessment of the risk of wheat lodging. Journal of Theoretical Biology, 194, 587–603.

Baker, C. J., Sterling, M., Berry, P.M. (2014). A generalised model of crop lodging. Journal of Theoretical Biology, 363, 1-12.

Baldocchi, D.D., Meyers, T.P. (1988). A spectral and lag-correlation analysis of turbulence in a deciduous forest canopy. Boundary-Layer Meteorology, 45, 31–58.

Barger, V. and Olsson, M. (1973) Classical Mechanics, A Modern Perspective, McGraw-Hill.

Benedict, L.H, Gould, R.D. (1998). Concerning Time and Length Scale Estimates Made from Burst-Mode LDA Autocorrelation Measurement. Experiments in Fluid, 24, 246-253.

Berry, P. M., Sterling, M., Mooney, S. J. (2006). Development of a Model of Lodging for Barley. Journal Agronomy and Crop Science. 192, 151-158.

Berry, P., Spink, J., Sylvester-Braley, R., Pickett, A., Sterling, M., Baker, C., Cameroni, N. (2002). Lodging control through variety choice and management. HGCA conference: Agronomic intelligence: the basis for profitable production.

Berry, P., Sterling, M., Baker, C. J., Spink, J. H., Sparkes, D. L. (2003). A calibrated model of wheat lodging compared with field measurements. Agricultural and Forest Meteorology, 119, 167-180.

Berry, P.M. (1998). Predicting Lodging in Wheat. Ph.D. Thesis. The University of Nottingham, UK.

Berry, P.M., Griffin, J. M., Sylvester-Braley, R., Scott, R. K., Spink, J. H., Baker, C., Clare, R. W. (2000). Controlling plant form through husbandry to minimise lodging in wheat. Field Crops Research, 67, 59–81.

Berry, P.M., Spink, J. (2012). Predicting yield losses caused by lodging in wheat. Field Crops Research, 137, 19–26, http://dx.doi.org/10.1016/j.fcr.2012.07.019.

Berry, P.M., Sterling, M., Spink, J.H., Baker, C.J., Sylvester–Bradley, R., Monney, S.J., Tams, A.R., Ennos, A.R., Donald, L.S. (2004). Understanding and reducing lodging in cereals. Advances in Agronomy, 84, 217–271.

Brunet, Y. Turbulent Flow in Plant Canopies: Historical Perspective and Overview. Boundary-Layer Meteorology 177, 315–364 (2020). https://doi.org/10.1007/s10546-020-00560-7

Brunet, Y., Irvine, M. R. (2000). The Control of Coherent Eddies in Vegetation Canopies: Streamwise Structure Spacing, Canopy Shear Scale and Atmospheric Stability. Boundary-Layer Meteorology, 94, 1, 139–163.

CEDA (Centre for Environmental data Analysis) Archive. (2016). Retrieved from: data.ceda.ac.uk, last accessed on 10/12/2016.

Clough, R. W. , Penzien, J. (1993). Dynamics of Structures. McGraw-Hill Education

Crook, M. J. and Ennos, R. (1993). The Mechanics of Root Lodging in Winter Wheat, Triticum aestivum L., Journal of Experimental Botany, 44, 264, 1219-1224.

DAFM, Winter cereal recommended list. (2019). Crops Evaluation and Certification Division, Department of Agriculture, Food and the Marine. https://www.agriculture.gov.ie/media/migration/publications/2018/WinterCerealRecommendedLists2019140918.pdf. Last accessed on 28th May 2019.

De Langre, E. (2008). Effects of wind on plants. annual review of fluid mechanics, 40,141-168

Easson, D. J., White, E. M., Pickles, S. J. (1993). The effects of weather seed rate and cultivar on lodging and yield in winter wheat. The Journal of Agricultural Science, 121, 145-156.

European commission website, (2021) Available from https://ec.europa.eu/info/sites/default/files/food-farming-fisheries/farming/documents/agri-statistical-factsheet-ie_en.pdf. Last accessed on 07/04/2021

Finnigan, J., (2000).Turbulence in plant canopies. Annual Review of Fluid Mechanics, 32, 519–571.

Finnigan, J.J. (1979). Turbulence in waving wheat. Boundary-Layer Meteorology 16, 213–236. https://doi.org/10.1007/BF02350512.

Flint-Garcia S., C. Jampatong, L.L. Darrah, McMullen, M. (2003). Quantitative trait locus analysis of stalk strength in four maize populations. Crop Science, 43, 13-22.

Ferrero, A., Petri, D., Carbone, P., and Catelani, M. (Eds.). (2015). Modern measurements : Fundamentals and applications. Wiley-IEEE Press.

Fung, F., Bett, P., Maisey, P., Lowe, J., McSweeney, C., Mitchell, J.F.B., Murphy, J., Rostron, J., Sexton, D., Yamazaki, K. (2018). UKCP18 Factsheet: Wind. Met Office Hadley Centre, Exeter.

Gardiner BA. (1994). Wind and wind forces in a plantation spruce forest. Boundary-Layer Meteorology, 67,161–86.

Gardiner, B., Berry, P., Moulia, B. (2016). Review: Wind impacts on plant growth, mechanics and damage. plant science, 245, 94-118.

Garratt, J. R. (1994). Review: the atmospheric boundary layer. Earth-Science Reviews, 37, 89-134.

Gill manual (2019). Gill Instruments: R3-50 3-Axis Ultrasonic Anemometer. Available at http://www.gillinstruments.com/. Last accessed 02/10/2019.

Gillespie, G., Brennan, L., Burke, J, Forristal, D. (2016). Oats: Food and Crop Products CROPQUEST, Available from https://www.teagasc.ie/media/website/crops/crops/Oats-food-and-Crop products.pdf.

Gohari, A., Eslamian, S., Abedi-Koupaei, J., Massah Bavani, A., Wang, D., Madani, K. (2013). Climate change impacts on crop production in Iran's Zayandeh-Rud River Basin. Science of total environment, 442, 405-419.

Goodman, A. M., Crook, M. J. and Ennos, A. R. (2001) 'Anchorage Mechanics of the Tap Root System of Winter-sown Oilseed Rape (Brassica napus L.)', Annals of Botany, vol. 87, no. 3, pp. 397–404 . DOI: 10.1006/anbo.2000.1347.

Google Map. (2019). Available at https://www.google.com/maps.

Griffin, J. (1998). Assessing lodging risk in winter wheat PhD Thesis University of Nottingham.

Hennessy, T. (2010). The impact of climate change on Irish farming. Teagasc report.

Hill, R. (1996) Corrections to Taylor's frozen turbulence approximation. Atmospheric Research, 40(2–4), pp. 153–175.

Holmes, J.D. (2001). Wind Loading of Structures. London: Spon Press.

Jellum, M.D. (1962). Relationships between lodging resistance and certain culm characters in oats Crop Science, 2, 263–267.

Jenkins, G., Peery, M., Prior, J., 2009. The climate of the United Kingdom and recent trends, UK climate projections report. Met office, Hadley Centre, Exeter.

Kaimal J.C., Finnigan J.J. (1994). Atmospheric Boundary Layer Flows: Their Structure and Measurement. New York: Oxford University Press. 289.

Kendall, S., Holmes, H., White, C., Clarke, C., Berry, P. (2017). Quantifying lodging-induced yield losses in oilseed rape. Field Crops Research, 211, 106-113.

Klaver (1996) actions on structures-wind loads, Technical University Delft, Department of Civil Engineering available at: https://www.irbnet.de/daten/iconda/CIB14442.pdf.

Kline S.J., Reynolds W.C., Schraub F.A., Runstadler P.W. (1967). The structure of turbulent boundary layers. Journal of Fluid Mechanics. 30, 741–73.

Lockhart, J., Wieseman, A. (1983) Introduction to Crop Husbandry Book, Fifth Edition.

Lorex user guide (2017) Available at: https://www.lorextechnology.com/downloads/wireless-home-monitors/LW2770-Series/LW2770_SERIES_MANUAL_EN_R1.pdf

Magness, J. R., Markle, G. M., Compton, C.C. (1971) Food and Feed Crops of the United States, Interregional Research Project IR-4.

Maisey, P., Fung, F., Harris, G., Lowe, J., Mc Sweeney, C., Mitchell, J.F.B., Murphy, J., Rostron, J., Sexton, D., Yamazaki, K. (2018). UKCP18 Factsheet: Precipitation. Met Office Hadley Centre, Exeter.

Marshall, B. (1998). Wind Flow Structures and Wind Forces in Forests PhD Thesis University of Oxford.

Martinez Vazquez, P. (2016). Crop lodging induced by wind and rain. Agricultural and Forest Meteorology. 228–229, 265–275.

Masud, M.B., Mc Allister, T., Cordeiro M.R.C., Faramarzi M. (2017). Modelling future water footprint of barley production in Alberta, Canada: Implications for water use and yields to 2064. Science of the Total Environment. 616-617, 208-222.

MATLAB help (2021) available from https://www.mathworks.com/help. Last accessed on 07/08/2021

Mc Elwain, L., Sweeney, J. (2007). Key Meteorological Indicators of Climate Change in Ireland. Environmental Research Centre Report. Environmental protection agency.

Met Éireann, National Irish meteorological service. (2019). Available from: www.met.ie. Last accessed on 10/01/2019.

Meteorological Office, the United Kingdom's national weather service website. (2019). Available from: https://www.metoffice.gov.uk. Last accessed on 07/04/2019.

Mohammadi, M., Baker, C., Sterling, M., Finnan, J. (2018). A study on meteorological parameters in oat lodging. 13th UK Conference on Wind Engineering, Leeds, UK.

Mohammadi, M., Finnan, J., Baker, C., Sterling, M. (2020a). The potential impact of climate change on oat lodging in the UK and Republic of Ireland, Advances in Meteorology, Volume 2020.

Mohammadi, M., Finnan, J., Sterling, M., Baker, C. (2020b). A calibrated oat lodging model compared with agronomic measurements, Field Crops Research, Volume 255, 107784.

Murphy, J.M., Harris, G.R., Sexton, D.M.H., Kendon, E.J., Bett, P.E., Clark, R.T., Eagle, K.E., Fosser, G., Fung, F., Lowe, J.A., McDonald, R.E., Mc Innes, R.N., Mc Sweeney, C.F., Mitchell, J.F.B., Rostron, J.W., Thornton, H.E., Tucker, S., Yamazaki, K. (2018). UKCP18 Land Projections: Science Report. Met Office Hadley Centre, Exeter.

National Oceanic and Atmospheric Administration (2021) Available from https://www.climate.gov/maps-data/primer/climate-models. Last accessed on 07/08/2021.

NIST/SEMATECH (2020) Handbook of Statistical Methods, available at http://www.itl.nist.gov/div898/handbook/

Nolan, P. (2015). EPA Report: Ensemble of Regional Climate Model Projections for Ireland. EPA climate change research report. No. 159. EPA: Wexford.

Nolan, P., O'Sullivan, J., McGrath, R. (2017). Impacts of climate change on mid-twenty-first-century rainfall in Ireland: a high-resolution regional climate model ensemble approach. International Journal of Climatology. https://doi.org/10.1002/joc.509.

OMC-270 Precipitation Monitor. (2017). Installation and technical user manual available at :

OM-CP SERIES Data Logger and Software Available from:, https://www.omega.com/Manuals/manualpdf/M3667.pdf. Last accessed on 7/9/2017.

Panofsky, H. and Dutton, J. (1984) Atmospheric Turbulence. John Wiley and Sons.

Parker, M.J. (2009) Appendix I: Student's t-Test—Analysis of Variance of Two Samples, in Just-About-Right (JAR) Scales: Design, Usage, Benefits, and Risks, West Conshohocken, PA: ASTM International, 42-43

Pinera-Chavez, F. (2016). Identifying traits and developing genetic sources for increase lodging resistance in elite high yielding wheat cultivars. PhD Thesis University of Nottingham.

Polikar, R. (2006). The wavelet tutorial. Available at http://users.rowan.edu/~polikar/WAVELETS/WTpart1.html. Last accessed on 09/01/2019.

Py, C., Langre, E., Moulia, B. (2006). A frequency lock-in mechanism in the interaction between wind and crop canopies. Journal of Fluid Mechanics, 568, 435-449.

Rasane, P., Jha, A., Sabikhi, L., Kumar, A., Unnikrishnan, V.S. (2015). Nutritional advantages of oats and opportunities for its processing as value added foods–a review. Journal of Food Technology, 52, 662–675.

Raupach M.R., Coppin P.A., Legg B.J. (1986). Experiments on scalar dispersion within a model plant canopy. Part I: The turbulence structure. Boundary-Layer Meteorology. 35, 21–52.

Raupach M.R., Finnigan J.J., Brunet Y. (1996). Coherent eddies and turbulence in vegetation canopies: the mixing layer analogy. Boundary-Layer Meteorology, 78, 351–82.

Raupach, M. R., Thom, A. S. (1981). Turbulence in and above Plant Canopies. Annual Review of Fluid Mechanics, 13, 97-129.

Saboohi, R., Soltani, S., Khodagholi, M. (2012). Trend analysis of temperature parameters in Iran. Theoretical and Applied Climatology, 109, 3-4.

Shaw, R.H., Tavanger, J., Ward, D.P. (1983). Structure of the Reynolds stress in a canopy layer. Journal of Applied Meteorology and Climatology, 22, 1922–31.

Soltani, S., Saboohi, R., Yaghmaei, L. (2012). Rainfall and rainy days trend in Iran. Climatic Change, 110, 187–213.

Sposaro, M., Berry, P., Sterling, M., Hall, A., Chimenti, A. (2008). Development and validation of a model of lodging for sunflower. Proceeding of 17th International Sunflower Conference, Córdoba, Spain.

Sposaro, M., Berry, P., Sterling, M., Hall, A., Chimenti, A. (2010). Modelling root and stem lodging in sunflower. Field crops research, 19, 1, 125-134.

Sterling, M., Baker, C.J., Berry, P.M., Wade, A. (2003).An experimental investigation of the lodging of wheat. Agriculture for Meteorology, 119, 149–165.

Stephen B. (2000) Turbulent Flows, Cambridge University Press.

Sutton, O. G. 1953. Micrometeorology. p. 76. https://doi.org/10.1002/qj.49707934125

Teagasc - The Agriculture and Food Development Authority, the Irish Agriculture and Food Development Authority website. (2021). Available from https://www.teagasc.ie/crops/crops/cereal-crops/. Last accessed on 07/04/2021.

Tennekes H., Lumley J.L. (1972) A First Course in Turbulence. The MIT Press.

The Intergovernmental Panel on Climate Change's latest 5th assessment report. (2018). Available at: www.ipcc.ch, last accessed on 10/12/2018.

Tillage Sector Development Plan, 2012. Teagasc Tillage Crop Stakeholder Consultative Group.

Trush, A., Pospisil, S., Kozmar, H. (2020) comparison of turbulence integral length scale determination methods, advances in fluid mechanics, Volume 128, 113 – 123.

Tsinober, A. (2009). Methods of Describing and Studying Turbulent Flows. An Informal Conceptual Introduction to Turbulence. Fluid Mechanics and Its Applications, 92. Springer, Dordrecht.

UK climate projections website, 2018. Retrieved from: ukclimateprojections.metoffice.gov.uk. Last accessed on 10/12/2018.

United Nations Information Portal, 2021. Retrieved from: https://www.informea.org/en/terms/plant-variety. Last accessed on 4/6/2021.

Van Heerden, P., Singelsab, A., Paraskevopoulos, A., Rosslerab, R. (2015). Negative effects of lodging on irrigated sugarcane productivity— An experimental and crop modelling assessment. Field Crops Research, 180, 135-142.

Vining, K.C. (1990). Effects of weather on agricultural crops and livestock: an overview, International Journal of Environmental Studies, 36,1-2, 27-39.

Wallace, J.M. (2016). Quadrant Analysis in Turbulence Research: History and Evolution Annual Review of Fluid Mechanics, 48, 131-158.

Whelpdale, D.M. (1967) Hot-wire; and sonic anemometry a description and comparison, Atmosphere, Taylor and Francis, 5, 20-27.

White, E.M., Mc Garel, A.S.L. and Ruddle, O. (2003). The influence of variety, year, disease control and plant growth regulator application on crop damage, yield and quality of winter oats (Avena sativa). The Journal of agricultural science, 140, 1, 31-42.

Wilson, J.D., Ward, D.P., Thurtell G.W., Kidd G.E. (1982). Statistics of atmospheric turbulence within and above a corn canopy. Boundary-Layer Meteorology. 24, 495–519.

Wu, W., Huang, J., Cui, K., Nie, L., Wang, Q., Yang, F., Shah, F., Yao, F., Peng, S. (2012). Sheath blight reduces stem breaking resistance and increases lodging susceptibility of rice plants. Field Crops Research. 128, 101–108.

Wu, W., Ma, B. (2019). Erect–leaf posture promotes lodging resistance in oat plants under high plant population. European Journal of Agronomy, 103, 175–187.

Wu, W., Ma, B.L. (2016). A new method for assessing plant lodging and the impact of management options on lodging in canola crop production. Science Report, 6, 31890. https://doi.org/10.1038/srep31890.

Yara website. (2019). Available from https://www.yara.co.uk/crop-nutrition/oats/oat-growth-and-development. Last accessed on 19/1/2019.

Zhang, J., Li, G., Song, Y., Liu, Z., Yang, C., Tang, S., Zheng, C., Wang, S., Ding, Y. (2014). Lodging resistance characteristics of high yielding rice populations. Field Crops Research, 161, 64–74.

Zotarelli, L., Dukes, M., Romero, C., Migliaccio, K., Morgan, K. (2010). Step by Step Calculation of the Penman-Monteith Evapotranspiration (FAO-56 Method), Agricultural and Biological Engineering Department, UF/IFAS Extension.

Zwillinger, D. (1995).CRC Standard Mathematical Tables and Formulae. Boca Raton, FL: CRC Press.

Appendix A. Deriving the lodging/no lodging curve

Based on Baker et al. (2014), the following equations were presented in Chapter 2:

$$\bar{M} = \frac{\left(1+\omega_n^2\left(\frac{X}{g}\right)\right)(0.5\rho A C_F X)\left(\cos\left(\alpha\frac{x}{l}\right)-cot\alpha\sin\left(\alpha\frac{x}{l}\right)\right)}{\omega_n^2\left(\frac{X}{g}\right)}\ \bar{U}^2 \quad (2\text{-}2)$$

$$\widehat{M} = \bar{M} + ((g_{MB}\sigma_{MB})^2 + (g_{MR}\sigma_{MR})^2)^{0.5} \quad (2\text{-}4)$$

$$g_{MB} = 0.42I\ln(\frac{3600}{\tau}) \quad (2\text{-}5)$$

$$g_{MR} = (2\ln(3600f_n))^{0.5} + \frac{0.577}{(2\ln(3600f_n))^{0.5}} \quad (2\text{-}6)$$

$$\sigma_{MR}^2 = \bar{M}^2 I^2(\frac{\pi}{4\theta}) \quad (2\text{-}7)$$

$$\sigma_{MB}^2 = 4\bar{M}^2 I^2 \quad (2\text{-}8)$$

As mentioned in Chapter 2, Sterling et al. (2003) showed root lodging typically occurs over a period of minute. Consequently, Baker et al. (2014) assumed the resonant component of bending moment fluctuations is not relevant to root lodging. Assuming I=1 and τ=60s in equation 2-3 the broad band peak factor would be $g_{MB} = 1.72$. Consequently, equation 2-4 will be written as:

$$\widehat{M} = \bar{M}(1 + 3.44I) \quad (A\text{-}1)$$

Root lodging happens if $\widehat{M} > R_s$, where

$$R_s = \gamma S d^3 \tag{2-10}$$

Thus

$$\bar{M}(1 + 3.44I) > \gamma S d^3 \tag{A-2}$$

Replacing the value of $\bar{M}$ in the above equation:

$$\frac{\left(1+\omega_n^2\left(\frac{X}{g}\right)\right)(0.5\rho A_{CF} X)\left(\cos\left(\alpha\frac{x}{l}\right)-cot\alpha\,\sin\left(\alpha\frac{x}{l}\right)\right)}{\omega_n^2\left(\frac{X}{g}\right)}\,\bar{U}^2\,(1 + 3.44I) > \gamma S d^3 \tag{A-3}$$

Or

$$\frac{\left(1+\omega_n^2\left(\frac{X}{g}\right)\right)(0.5\rho A C_F X)\left(\cos\left(\alpha\frac{x}{l}\right)-cot\alpha\,\sin\left(\alpha\frac{x}{l}\right)\right)}{\omega_n^2\left(\frac{X}{g}\right)}\,\bar{U}^2\,(1 + 3.44I) > \gamma S d^3 \tag{A-4}$$

Where *S* can be found from the expression suggested by Baker (1995) and Baker et al. (1998) as follows:

$$S = S_D - \frac{i}{\left(\frac{\rho_s}{\rho_w}\right)(w_f - w)L}(S_D - S_w) \tag{A-5}$$

Where ρ_s and ρ_w are soil and water density,w_f is the water content at field capacity, w is the water content at wilting point and L is the root depth. Moreover, S_D and S_w are the soil shear strength for dry and wet soil respectively and can be derived as follows (Baker et al., 1998):

$$s_w = 1484e^{-5w_f/c}\,(2.2 - 0.24v)(4.82c - 0.30) \quad \text{(A-6)}$$

$$s_D = 1125e^{-5w/c}\,(2.2 - 0.24v)(4.82c - 0.30) \quad \text{(A-7)}$$

Where c is the clay content and v is a visual score measuring soil compaction.

$$i > 1 - \left(\frac{\left(1+\omega_n^2\left(\frac{X}{g}\right)\right)(0.5\rho A_{CF}X)\left(\cos\left(\alpha\frac{x}{l}\right) - cot\alpha\sin\left(\alpha\frac{x}{l}\right)\right)}{\omega_n^2\left(\frac{X}{g}\right)\gamma d^3 S_D}\left(\frac{\left(\frac{\rho_s}{\rho_w}\right)(w_f - w)L}{1-1.32e^{-\frac{5(w_f-w)}{c}}}\right)(1 + 3.44I)\right)\bar{U}^2 \quad \text{(A-8)}$$

The reference rainfall intensity i_0, at zero wind speed and a velocity at which root lodging occurs is defined as:

$$i_0 = \left(\frac{\left(\frac{\rho_s}{\rho_w}\right)(w_f - w)l}{1-1.32e^{-\frac{5(w_f-w)}{c}}}\right) \quad \text{(A-9)}$$

$$\bar{U}_{LR} = \left(\frac{R_s}{\frac{\left(\left(1+\omega_n^2\left(\frac{X}{g}\right)\right)\right)}{\omega_n^2\left(\frac{X}{g}\right)}(0.5\rho AC_F X)(1+3.44I)}\right)^{0.5} \quad \text{(A-10)}$$

Thus

$$i > \left(1 - \frac{\bar{U}^2}{U_{LR}^2}\right)i_0 \quad \text{(A-11)}$$

Which gives the equation 2-16 for the margin of lodging/no lodging conditions:

$$i = (1 - \frac{\bar{U}^2}{\bar{U}_{LR}^2}) i_0 \qquad (2\text{-}16)$$

Appendix B. Statistical approach to determine the number of samples for stem strength measurements

The sample size required to measure a parameter in a population can be determined based on the statistical parameters from similar measurements undertaken on another population as follows:

$$z = \frac{t-value^2 S_d^2}{E^2} \quad \text{(B-1)}$$

Where $t - value$ is confidence level value, s_d is the standard deviation and E is the acceptable error. Berry et al. (2003) has done similar test on wheat and has reported S_d =2.5 *MPa.* Moreover, the $z - value$ =1.96 for 95% confidence and the acceptable error for the stem yield stress is E~0.5MPa (such an error causes 0.01 fractional uncertainty and Section 4-7 shows such an error is negligible in the uncertainty of the stem lodging velocity). Substituting the above value is equation B-1 gives z=100.

Appendix C. Video tracking MATLAB codes

This appendix presents two codes used in the video tracking method. The first one considers the video and checks if the target is detectable. The second code analysis the video and generates a trajectory of the target in Excel format. Some the notes in the code are quoted from (MATLAB help, 2021).

MATLAB code 1: Checking if the target is detectable

```
% This code checks if the crop is detectable
%If the target is detectable the second code can be used

%  Cleaning the work space
clc;   %Providing a clean screen in MATLAB
clear; %Removing all previous items from the workspace
close all;  %Deleting all figures remaining from last code runs
imtool close all; %imtool is the Image Viewer app, this line closes all the open image viewers

%Format style configuration
workspace; %Opening workspace browser
format long g;
format compact;
fontSize = 15;

% inserting the video into the code
%identifying the current folder
Currentfolder = pwd;

% The video file name must be changed each time a new video is processed

FileName = '160554-2.ASF'; %This is just an example file
FinalFileName = fullfile (Currentfolder, FileName);

%Creating object to read video files
video = VideoReader(FinalFileName);

% number of frames
nFrames = video.NumberOfFrame;

%Setting up the thresholds to detect the target.

%Hue: Value from 0 to 1 that corresponds to the colour's position on a colour wheel. As hue increases from 0 to 1, the colour transitions from red to orange, yellow, green, cyan, blue, magenta, and finally back to red.

%Saturation: Amount of hue or departure from neutral. 0 indicates a neutral shade, whereas 1 indicates maximum saturation.
%Value: Maximum value among the red, green, and blue components of a specific colour.

hThresholds = [0, 0.008]; %hue threshold
sThresholds = [0.1, 1.7];% saturation threshold
vThresholds = [20, 250];%Value threshold

% Read frames one by one and find the target in each frame
```

```
for z = 1 : nFrames

    % Reading one frame in RGB
    thisFrame=read(video,z);


    %Converting RGB colourmap to HSV colourmap
    hsv = rgb2hsv(double(thisFrame));
    hue=hsv(:,:,1);
    sat=hsv(:,:,2);
    val=hsv(:,:,3);

    %detecting the pixels within the range of threshold
    binaryH = hue >= hThresholds(1) & hue <= hThresholds(2);
    binaryS = sat >= sThresholds(1) & sat <= sThresholds(2);
    binaryV = val >= vThresholds(1) & val <= vThresholds(2);


    % identifying the pixels which are in the all three threshold ranges.
    Filter = binaryH & binaryS & binaryV;
    %This line filter out possible small blobs detected due to reflection
    Filter = bwareaopen (Filter, 500);

    % Filling the holes in the image
    Filter = imfill (Filter, 'holes');

    [labeledImage, Regions_number] = bwlabel (Filter);

    if Regions_number >= 1

       %regionprops measures properties of image regions
       stats = regionprops(labeledImage, 'BoundingBox', 'Centroid');%Calculates centroids

       imshow(thisFrame);%This line shows the original frame
       axis on;
       hold on;
       caption = sprintf('%d blobs found in frame #%d 0f %d', Regions_number, z, nFrames);
       title(caption, 'FontSize', fontSize);

       %This loop is written to draw the target in a rectangle
       for r = 1 : Regions_number
          % Find location for this blob.
          blobloc = stats(r).BoundingBox;
          thisCentroid = stats(r).Centroid;
          hRect(r) = rectangle('Position', blobloc, 'EdgeColor', 'r', 'LineWidth', 2);
          hSpot = plot(thisCentroid(1), thisCentroid(2), 'y+', 'MarkerSize', 10, 'LineWidth', 2);
          hText(r) = text(blobloc(1), blobloc(2)-20, strcat('X: ', num2str(round(thisCentroid(1))), 'Y: ',
num2str(round(thisCentroid(2)))));
          set(hText(r), 'FontName', 'Timesnewroman', 'FontSize', 14, 'Color', 'yellow');
       end
       hold off
       drawnow;
    end
       end

 msgbox('Done.');
```

MATLAB code 2: producing the trajectory of the target

```
%This code produces a trajectory of the target
% it is assumed that the target is red
%For each recorded video the name of input and output file must be changed

% cleaning the work space
clc;   %Providing a clean screen in MATLAB
clear; %Removing all previous items from the workspace
close all;  %Deleting all figures remaining from last code runs
imtool close all; %imtool is the Image Viewer app, this line closes all open image viewers

%Format style configuration
workspace; %Opening workspace browser to manage workspace
format long g;
format compact;
fontSize = 15;


% inserting the video into the code

% Insert the exact date and time for the start of the video
D = datenum('20170615 17:48:24.000','yyyymmdd HH:MM:SS.FFF');

Currentfolder = pwd;%Identifies current folder

%this is a sample file and must be renamed for each video file name
FileName = '160554-2.ASF';
FinalFileName = fullfile(Currentfolder, FileName);

%Create object to read video files
video = VideoReader(FinalFileName);

% other factors
nFrames = video.NumberOfFrame;


%Setting up the thresholds to detect the target.
%Hue: Value from 0 to 1 that corresponds to the colour's position on a colour wheel. As hue increases from 0 to
1, the colour transitions from red to orange, yellow, green, cyan, blue, magenta, and finally back to red.

%Saturation: Amount of hue or departure from neutral. 0 indicates a neutral shade, whereas 1 indicates
maximum saturation.
%Value: Maximum value among the red, green, and blue components of a specific colour.

hThresholds = [0, 0.008]; %hue threshold
sThresholds = [0.1, 1.7];% saturation threshold
vThresholds = [20, 250];%Value threshold

%camera calibration correction
IntrinsicMatrix = [667.3396 0 0; 0 666.0677 0; 353.5067 265.4693 1];
radialDistortion = [-0.43796 0.23624];

cameraParams = cameraParameters('IntrinsicMatrix', IntrinsicMatrix, 'RadialDistortion', radialDistortion);

tr=1; % This is an index for tracking



% Read frames one by one and find the target in each frame
```

```
for z = 1 : nFrames

    % Reading one frame in RGB
    thisFrame=read(video,z);
    %applying the camera corrections
    thisFrame = undistortImage(thisFrame, cameraParams);

    %Converting RGB colour map to HSV colourmap
    hsv = rgb2hsv(double(thisFrame));
    hue=hsv(:,:,1);
    sat=hsv(:,:,2);
    val=hsv(:,:,3);

    %detecting the pixels within the range of threshold
    binaryH = hue >= hThresholds(1) & hue <= hThresholds(2);
    binaryS = sat >= sThresholds(1) & sat <= sThresholds(2);
    binaryV = val >= vThresholds(1) & val <= vThresholds(2);

    % Identifying the pixels which are in the all three threshold ranges.
    Filter = binaryH & binaryS & binaryV;
    % This line filter out possible small blobs detected due to reflection
    Filter = bwareaopen(Filter, 500);
    % Filling holes
    Filter = imfill(Filter, 'holes');

    [labeledImage, Regions_number] = bwlabel(Filter);


if Regions_number == 1

      %regionprops measures properties of image regions
      stats = regionprops(labeledImage, 'BoundingBox', 'Centroid');

for r = 1 : Regions_number
          % Find location for the centroid.

          Centroid = stats(r).Centroid;

            %producing a time seri
            D=(D+1/24/60/60/30); % generates time stamp if 1 blob is found
            XZ(tr,1)=D;
            %trajectory
            XZ(tr,2)=Centroid(1); %
            XZ(tr,3)=Centroid(2); %
            tr=tr+1;
end
end

% If multiple blobs were detected in one of the frames:
%going back to the previous reading and using the value
if Regions_number > 1
            D=(D+1/24/60/60/30);
            XZ(tr,1)=D;
            XZ(tr,2)=XZ(tr-1,2);
            XZ(tr,3)=XZ(tr-1,3);
            tr=tr+1;
end
% If no blob was detected in one the frames:
%going back to the previous reading and using the value
```

```
if Regions_number < 1
            D=(D+1/24/60/60/30);
            XZ(tr,1)=D;
            XZ(tr,2)=XZ(tr-1,2);
            XZ(tr,3)=XZ(tr-1,3);
            tr=tr+1;
end

end


Outputfilename = 'Reza.csv'; % this needs to be changed for each video
fname='174824-1'; % this needs to be changed for each video


% writing an excel output file
dlmwrite(Outputfilename, XZ, 'delimiter', ',', 'precision', 16);
```

Appendix D. The measured parameters of studied target plants

Table D.1 shows the agronomic factor of studied targets. Comparing these values with the values in Table 4.8 shows the parameters are near mean values in each year and the plants are 'typical' samples.

Table D. 1. Agronomic parameters of studied targets

Target number	*a (cm)*	*t (cm)*	*X (cm)*	*l (cm)*	*d (cm)*	*L (cm)*
2017-1	0.33	0.092	69.5	147.3	5.03	7.07
2017-2	0.31	0.091	68.8	148.4	4.95	7.1
2017-3	0.32	0.097	69.6	145.9	5.13	7.17
2018-1	0.29	0.093	60.9	114.7	5.36	5.42
2018-2	0.305	0.099	61.4	106.5	5.33	5.55
2018-3	0.22	0.090	61.7	115.0	5.37	5.52
2018-4	0.32	0.093	60.4	113.5	5.23	5.37
2018-5	0.28	0.090	61.3	112.2	5.27	5.24
2018-6	0.27	0.087	60.8	114.5	5.33	5.36
2018-7	0.32	0.098	61.5	106.7	5.33	5.58

Table D.2, D.3 and D.4 show the statistics of the damping ratio results, i,e. mean, standard deviation, random uncertainty and number of recordings. As the table shows in each day the results are at the same range of uncertainty, and consequently the results presented in Chapter 4 are not dependent on the target selection.

Table D. 2. Damping ratio results from transfer function method

Test date: 31 May 2018				
Target tag	mean	S_d	δ (±)	Number of recordings
2018-1	0.059	0.008	0.004	3
2018-2	0.05	0.01	0.006	3
2018-3	0.053	0.006	0.003	3
Test date: 13 June 2018				
2018-1	0.135	0.009	0.005	3
2018-4	0.128	0.007	0.004	3
2018-5	0.133	0.007	0.004	3
Test date: 18 June 2018				
2018-1	0.137	0.006	0.004	3
2018-6	0.131	0.004	0.002	3
Test date: 19 June 2018				
2018-1	0.134	0.001	0.001	3
2018-7	0.132	0.01	0.006	3

Table D.3. Damping ratio results from logarithmic decrement method for different plant targets in different days

Test date: 31 May 2018				
Target tag	mean	S_d	δ (±)	Number of recordings
2018-1	0.051	0.02	0.006	10
2018-2	0.053	0.019	0.006	10
2018-3	0.045	0.017	0.005	10
Test date: 13 June 2018				
2018-1	0.121	0.032	0.01	10
2018-4	0.126	0.004	0.001	10
2018-5	0.133	0.006	0.002	10
Test date: 18 June 2018				
2018-1	0.137	0.025	0.008	10
2018-6	0.132	0.008	0.003	10
Test date: 19 June 2018				
2018-1	0.142	0.024	0.008	10
2018-7	0.127	0.007	0.002	10

Table D. 4. Natural frequency results for different plant targets in different days

Test date: 31 May 2018				
Target tag	mean (*Hz*)	Sd	δ (±)	Number of recordings
2018-1	1.28	0.03	0.02	3
2018-2	1.29	0.06	0.033	3
2018-3	1.29	0.01	0	3
Test date: 13 June 2018				
2018-1	1.09	0.04	0.02	3
2018-4	1.1	0.05	0.029	3
2018-5	1.08	0.02	0.01	3
Test date: 18 June 2018				
2018-1	1.03	0.01	0.01	3
2018-6	1	0.05	0.026	3
Test date: 19 June 2018				
2018-1	0.96	0.03	0.01	3
2018-7	1.01	0.02	0.01	3

Appendix E. Calculating the uncertainty of the velocity components

$$u = (u_{North}cos\theta + u_{west}sin\theta)cos\varphi + u_{up}sin\varphi \quad (3\text{-}11)$$

$$v = -u_{North}sin\theta + u_{west}cos\theta \quad (3\text{-}12)$$

$$w = u_{up}cos\varphi - (u_{North}cos\theta + u_{west}sin\theta)sin\varphi \quad (3\text{-}13)$$

$$\frac{\delta u}{u} = \left(\frac{\partial u}{\partial u_{North}}\right)\delta u_{North} + \left(\frac{\partial u}{\partial u_{west}}\right)\delta u_{west} + \left(\frac{\partial u}{\partial u_{up}}\right)\delta u_{up} + \left(\frac{\partial u}{\partial \theta}\right)\delta\theta + \left(\frac{\partial u}{\partial \varphi}\right)\delta\varphi \quad (E\text{-}1)$$

$$\frac{\delta u}{u} = |cos\theta\ cos\varphi|\ \delta u_{North} + |sin\theta\ sin\varphi|\ \delta u_{west} + |sin\varphi|\ \delta u_{up} + |(-u_{North}cos\varphi \sin\theta + u_{west}\cos\varphi\ cos\theta)|\ \delta\theta + \left|(-u_{North}cos\theta \sin\varphi - u_{west}\sin\varphi\ sin\theta + u_{up}\cos\varphi)\right|\ \delta\varphi \quad (E\text{-}2)$$

$$\frac{\delta v}{v} = \left(\frac{\partial v}{\partial u_{North}}\right)\delta u_{North} + \left(\frac{\partial v}{\partial u_{west}}\right)\delta u_{west} + \left(\frac{\partial v}{\partial \theta}\right)\delta\theta \quad (E\text{-}3)$$

$$\frac{\delta v}{v} = |-sin\theta\ |\ \delta u_{North} + |(-u_{North}cos\,\theta - u_{west}\ sin\theta)|\ \delta\theta + |cos\theta\ |\ \delta u_{west} \quad (E\text{-}4)$$

$$\frac{\delta w}{u} = \left(\frac{\partial w}{\partial u_{North}}\right)\delta u_{North} + \left(\frac{\partial w}{\partial u_{west}}\right)\delta u_{west} + \left(\frac{\partial w}{\partial u_{up}}\right)\delta u_{up} + \left(\frac{\partial w}{\partial \theta}\right)\delta\theta + \left(\frac{\partial w}{\partial \varphi}\right)\delta\varphi \quad (E\text{-}5)$$

$$\frac{\delta w}{u} = |-cos\theta\ sin\varphi|\ \delta u_{North} + |-sin\theta\ sin\varphi|\ \delta u_{west} + |cos\varphi|\ \delta u_{up} + \left|(-u_{North}cos\theta\cos\varphi - u_{west}\cos\varphi\ sin\theta - u_{up}\sin\varphi)\right|\ \delta\varphi + |(u_{North}sin\varphi \sin\theta - u_{west}\sin\varphi\ cos\theta)|\ \delta\theta \quad (E\text{-}6)$$

As δu_{North}, δu_{west}, δu_{up}, $\delta\theta$ and $\delta\varphi$ are all an order of 10^{-2}, sin and cos are an order of 10^{-1} and velocity components are an order of 10^{0} , the fractional uncertainty in all three direction (and consequently the mean streamwise velocity) is an order of 10^{-3}.

Appendix F. Velocity fluctuations in different averaging times

Figure F.1, F.2 and F.3 show the distribution of normalized velocity fluctuations at oat crop height for 10 minutes, 30 minutes and 1 hour respectively. Additionally, Figure F.4 shows the ratio of ejections and sweeps in the total recoded velocity fluctuations in different averaging times. These figures demonstrate the results presented in Section 4.2.1 are consistent from 10 minutes to 1 hour averaging times and an averaging time of 10 minutes is sufficient to capture the general distribution of velocity fluctuations.

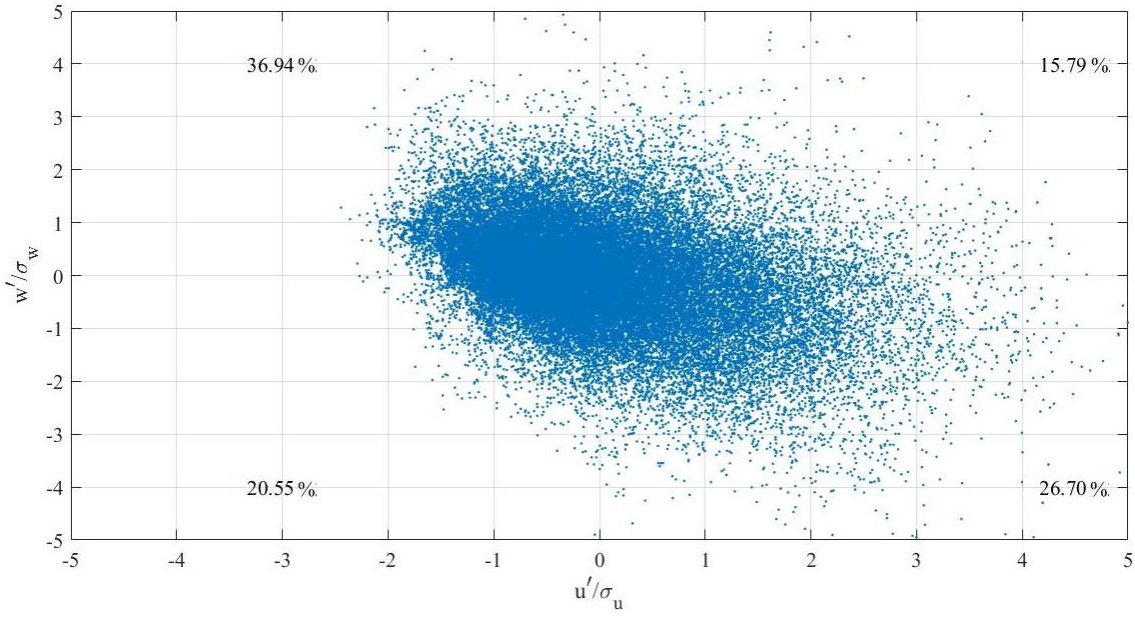

Figure F.1.The distribution of normalized velocity fluctuations at oat crop height (1.5m) for 10 minutes recording time

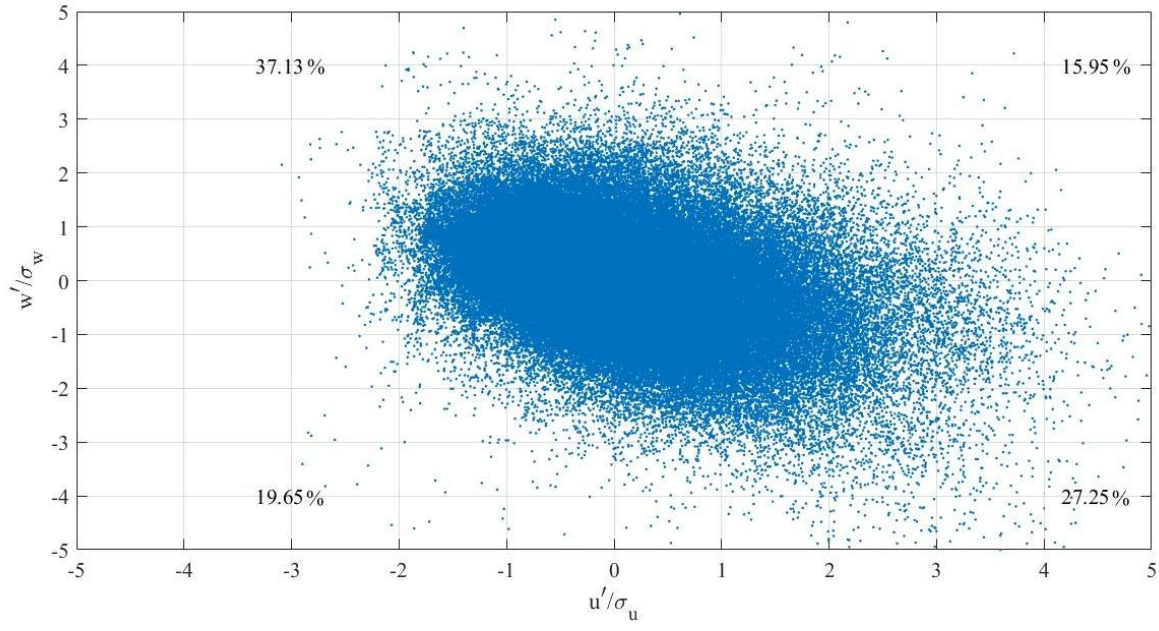

Figure F. 2. The distribution of normalized velocity fluctuations at oat crop height (1.5m) for 30 minutes recording time

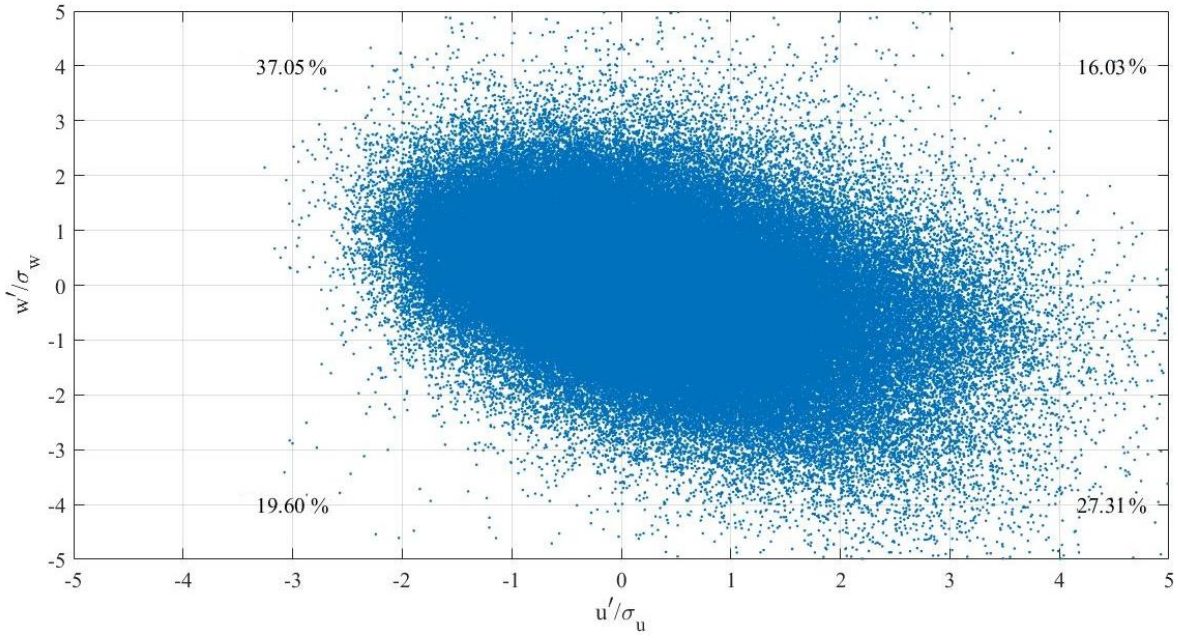

Figure F.3. The distribution of normalized velocity fluctuations at oat crop height (1.5m) for 60 minutes recording time

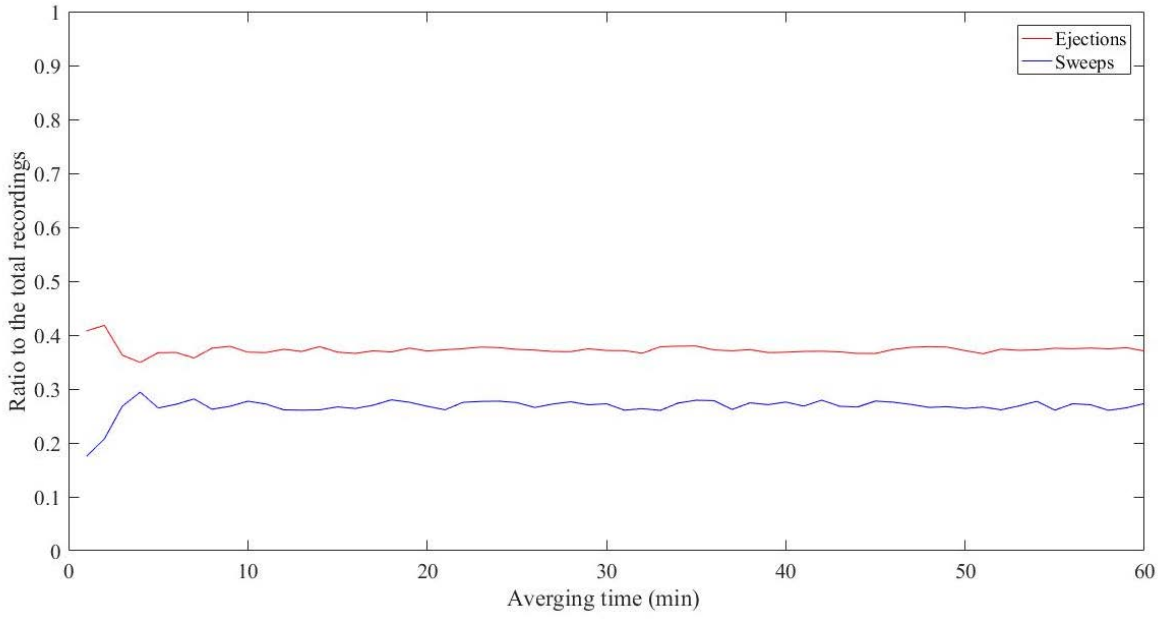

Figure F.4. The ratio of ejections and sweeps in the total recoded velocity fluctuations in different averaging times

Appendix G. Turbulence intensity variation in different averaging times

Figure G.1 shows the turbulence intensity in streamwise, lateral, and vertical directions in different time periods for an hour record on 15th June 2017. As the figure shows, the turbulence intensity values have a large fluctuation when a small time period is considered however, the values are consistent from 10 minutes to one-hour records.

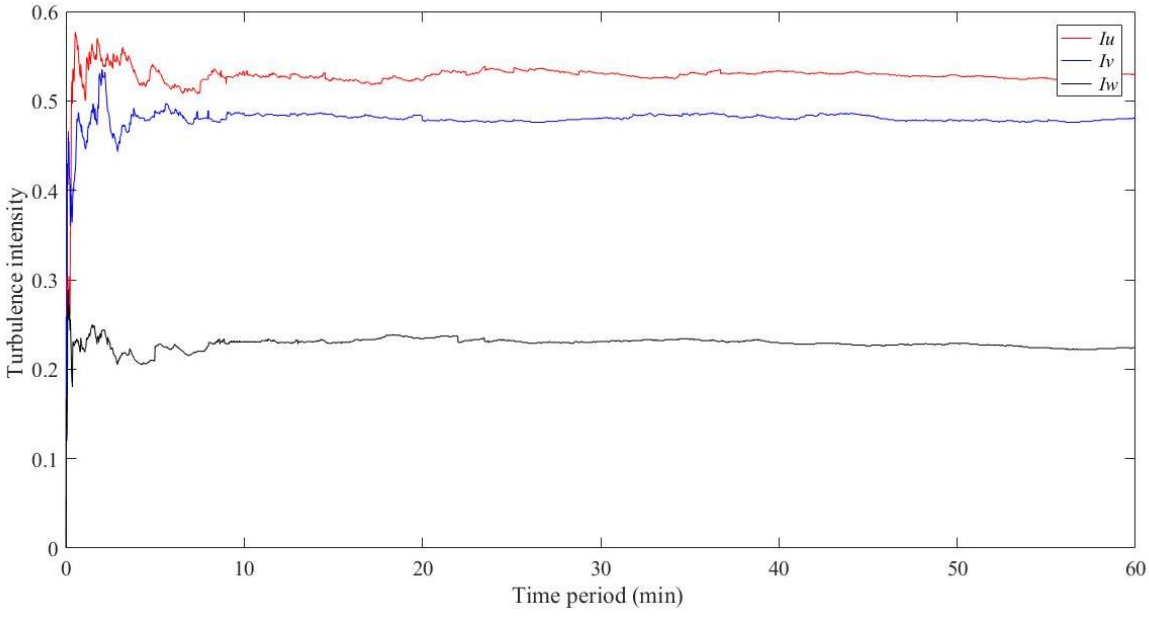

Figure G.1. The turbulence intensities in the three orthogonal directions in different time periods

Appendix H. The effect of sample size on damping ratio results

Table H.1. Mean, standard deviation and random uncertainty of damping ratio results for different sample sizes using logarithmic decrement method

	Number of datasets	mean	S_d	δ (±)
31 May 2018	10 recording	0.051	0.02	0.007
	15 recording	0.053	0.018	0.005
	20 recording	0.05	0.017	0.004
1 June 2018	10 recording	0.053	0.019	0.006
	15 recording	0.053	0.017	0.005
	20 recording	0.052	0.017	0.004

Appendix I. The equivalent mass at the top of the plant (μ) calculation

Figure I.1 shows the two assumptions for application of weight on the stem, where figure I.1.a shows a condition where the weight is applied at the centre of gravity, and Figure I.1.b assumes the weight is distributed between different nodes.

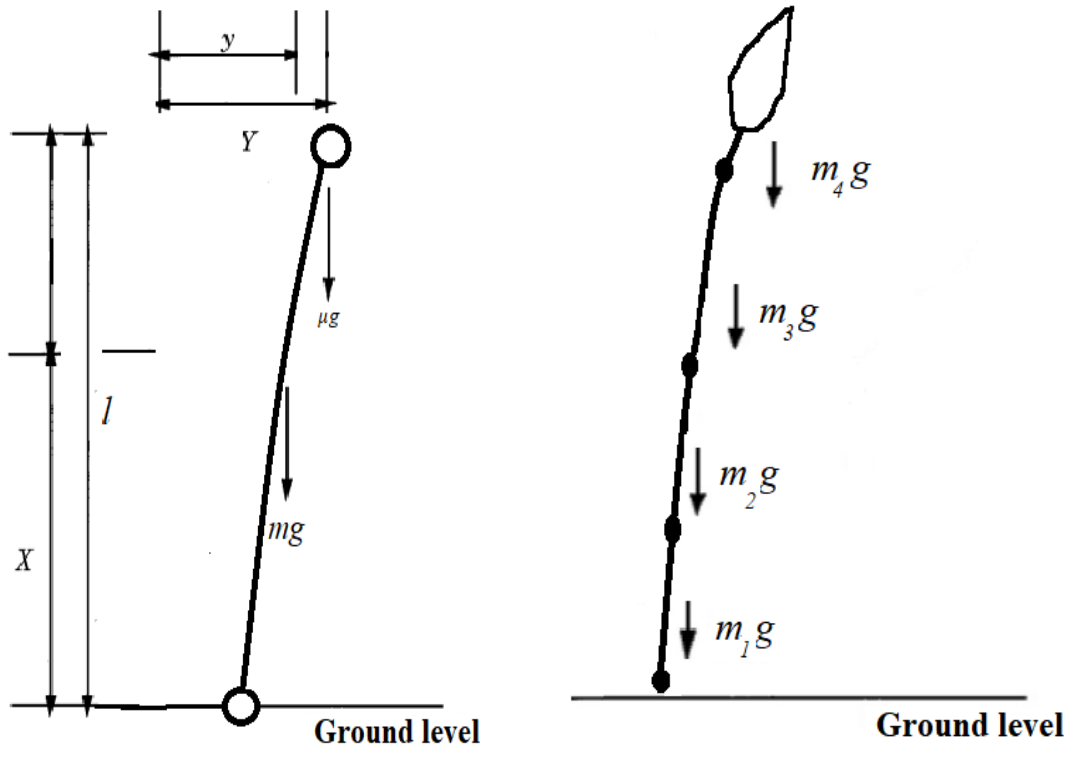

(a) Plant weight applied on the centre of gravity (b) Plant weight distributed across the stem

Figure I.1. A schematic of plant weight application on the plant

Assuming the plant weight is applied at the centre of gravity

$$\mu g Y = mgy \quad \text{(I-1)}$$

$$Y = l \,/\tan(\theta_1) \quad \text{(I-2)}$$

$$y = X/\tan(\theta_2) \quad \text{(I-3)}$$

$$\tan(\theta_1) \cong \tan(\theta_2) \tag{I-4}$$

$$\mu = \frac{mX}{l} \tag{I-5}$$

Which is the same as equation 4-15. Assuming the plant weight is equally distributed across the stem with four nodes:

$$\left[\frac{l}{8} + \left(\frac{l}{8} + \frac{l}{4}\right) + \left(\frac{l}{8} + \frac{2l}{4}\right) + \left(\frac{l}{8} + \frac{3l}{4}\right)\right] m_{node} = \mu\, l \tag{I-6}$$

Where m_{node} is the weight if each node.

$$\mu = 2m_{node} \tag{I-7}$$

$$m = m_{node}/4 \tag{I-8}$$

$$\mu = \frac{m}{2} \tag{I-9}$$

Which is the same as equation 4-16. Assuming the plant weight is equally distributed across the stem with five nodes:

$$\left[\frac{l}{10} + \left(\frac{l}{10} + \frac{l}{5}\right) + \left(\frac{l}{10} + \frac{2l}{5}\right) + \left(\frac{l}{10} + \frac{3l}{5}\right) + \left(\frac{l}{10} + \frac{4l}{5}\right)\right] m_{node} = \mu\, l \tag{I-10}$$

$$\mu = 2.5\, m_{node} \tag{I-11}$$

$$m = m_{node}/5 \tag{I-12}$$

$$\mu = m/2 \tag{I-13}$$

Which is the same as equation 4-16.

Appendix J. T-distribution

The degree of freedom in a sample population means when the average value of the data is determined, z-1 data points can take any value, so $df=z-1$ for one sample population and $df=z-2$ for two sample populations, where z is the number of data points. Table J.1 show the T distribution which is used in the t test and to determine the confidence intervals.

Table J. 1. T-distribution table (NIST/SEMATECH, 2020)

	Confidence Level										
	0%	50%	60%	70%	80%	90%	95%	98%	99%	99.8%	99.9%
df											
1	0.000	1.000	1.376	1.963	3.078	6.314	12.71	31.82	63.66	318.31	636.62
2	0.000	0.816	1.061	1.386	1.886	2.920	4.303	6.965	9.925	22.327	31.599
3	0.000	0.765	0.978	1.250	1.638	2.353	3.182	4.541	5.841	10.215	12.924
4	0.000	0.741	0.941	1.190	1.533	2.132	2.776	3.747	4.604	7.173	8.610
5	0.000	0.727	0.920	1.156	1.476	2.015	2.571	3.365	4.032	5.893	6.869
6	0.000	0.718	0.906	1.134	1.440	1.943	2.447	3.143	3.707	5.208	5.959
7	0.000	0.711	0.896	1.119	1.415	1.895	2.365	2.998	3.499	4.785	5.408
8	0.000	0.706	0.889	1.108	1.397	1.860	2.306	2.896	3.355	4.501	5.041
9	0.000	0.703	0.883	1.100	1.383	1.833	2.262	2.821	3.250	4.297	4.781
10	0.000	0.700	0.879	1.093	1.372	1.812	2.228	2.764	3.169	4.144	4.587
11	0.000	0.697	0.876	1.088	1.363	1.796	2.201	2.718	3.106	4.025	4.437
12	0.000	0.695	0.873	1.083	1.356	1.782	2.179	2.681	3.055	3.930	4.318
13	0.000	0.694	0.870	1.079	1.350	1.771	2.160	2.650	3.012	3.852	4.221
14	0.000	0.692	0.868	1.076	1.345	1.761	2.145	2.624	2.977	3.787	4.140
15	0.000	0.691	0.866	1.074	1.341	1.753	2.131	2.602	2.947	3.733	4.073
16	0.000	0.690	0.865	1.071	1.337	1.746	2.120	2.583	2.921	3.686	4.015
17	0.000	0.689	0.863	1.069	1.333	1.740	2.110	2.567	2.898	3.646	3.965
18	0.000	0.688	0.862	1.067	1.330	1.734	2.101	2.552	2.878	3.610	3.922
19	0.000	0.688	0.861	1.066	1.328	1.729	2.093	2.539	2.861	3.579	3.883
20	0.000	0.687	0.860	1.064	1.325	1.725	2.086	2.528	2.845	3.552	3.850
21	0.000	0.686	0.859	1.063	1.323	1.721	2.080	2.518	2.831	3.527	3.819
22	0.000	0.686	0.858	1.061	1.321	1.717	2.074	2.508	2.819	3.505	3.792
23	0.000	0.685	0.858	1.060	1.319	1.714	2.069	2.500	2.807	3.485	3.768
24	0.000	0.685	0.857	1.059	1.318	1.711	2.064	2.492	2.797	3.467	3.745
25	0.000	0.684	0.856	1.058	1.316	1.708	2.060	2.485	2.787	3.450	3.725
26	0.000	0.684	0.856	1.058	1.315	1.706	2.056	2.479	2.779	3.435	3.707
27	0.000	0.684	0.855	1.057	1.314	1.703	2.052	2.473	2.771	3.421	3.690
28	0.000	0.683	0.855	1.056	1.313	1.701	2.048	2.467	2.763	3.408	3.674
29	0.000	0.683	0.854	1.055	1.311	1.699	2.045	2.462	2.756	3.396	3.659
30	0.000	0.683	0.854	1.055	1.310	1.697	2.042	2.457	2.750	3.385	3.646
40	0.000	0.681	0.851	1.050	1.303	1.684	2.021	2.423	2.704	3.307	3.551
60	0.000	0.679	0.848	1.045	1.296	1.671	2.000	2.390	2.660	3.232	3.460
80	0.000	0.678	0.846	1.043	1.292	1.664	1.990	2.374	2.639	3.195	3.416
100	0.000	0.677	0.845	1.042	1.290	1.660	1.984	2.364	2.626	3.174	3.390
1000	0.000	0.675	0.842	1.037	1.282	1.646	1.962	2.330	2.581	3.098	3.300

Appendix K. Author's publications

Mohammadi, M., Finnan, J., Sterling, M., Baker, C. (2020b) A calibrated oat lodging model compared with agronomic measurements, Field Crops Research, Volume 255, 107784.

Mohammadi, M., Finnan, J., Baker, C., Sterling, M. (2020a) The potential impact of climate change on oat lodging in the UK and Republic of Ireland, Advances in Meteorology, Volume 2020

Joseph, G., Mohammadi, M., Sterling, M., Baker, C., Gillmeier, S., Soper, D., Jesson, M., Blackburn, G., Whyatt, J., Gullick, D., Murray, P., Berry, P., Hatley, D., J. Finnan, J. (2020) Determination of crop dynamic and aerodynamic parameters for lodging prediction, Journal of Wind Engineering and Industrial Aerodynamics.

Sterling, M., Baker, C., Joseph, G., Gillmeier, S., Mohammadi, M., Blackburn, G., Wyatt, D., Gullick, D., Berry, P., Hatley, D., Spink, J., Finnan, J., Miao, Y., Thanda, D., Sonder, K. (2018). Mitigating yield losses due to lodging of cereal crops. International Workshop on Wind-Related Disasters and Mitigation Tohoku University, Sendai, Japan.

New Approaches to Old Problems: Integrating Disciplines to Understand Lodging in Oats, 2018, https://sciencetrends.com/new-approaches-to-old-problems-integrating-disciplines-to-understanding-lodging-in-oats/.

Mohammadi, M., Baker, C., Sterling, M., Finnan, J. 2018. A study on meteorological parameters in oat lodging. 13th UK Conference on Wind Engineering, Leeds, UK.

Mohammadi, M., Baker, C., Sterling, M., Finnan, J. 2019. Calibration of a model for predicting wind induced failure of oats. The International Conference on Wind Engineering (ICWE), Beijing, China.